

THE DUAL RECIPROCITY BOUNDARY ELEMENT SOLUTION OF
HELMHOLTZ-TYPE EQUATIONS IN FLUID DYNAMICS

A THESIS SUBMITTED TO
THE GRADUATE SCHOOL OF NATURAL AND APPLIED SCIENCE
OF
MIDDLE EAST TECHNICAL UNIVERSITY

BY

NAGEHAN ALSOY-AKGÜN

IN PARTIAL FULFILLMENT OF THE REQUIREMENTS
FOR
THE DEGREE OF PHILOSOPHY OF DOCTORATE
IN
MATHEMATICS

FEBRUARY 2013

Approval of the thesis:

**THE DUAL RECIPROCITY BOUNDARY ELEMENT SOLUTION OF
HELMHOLTZ-TYPE EQUATIONS IN FLUID DYNAMICS**

submitted by **NAGEHAN ALSOY-AKGÜN** in partial fulfillment of the requirements for the degree of **Philosophy of Doctorate in Mathematics Department, Middle East Technical University** by,

Prof. Dr. Canan Özgen
Dean, Graduate School of **Natural and Applied Sciences**

Prof. Dr. Mustafa Korkmaz
Head of Department, **Mathematics**

Prof. Dr. Münevver Tezer-Sezgin
Supervisor, **Mathematics Department**

Examining Committee Members:

Prof. Dr. Bülent Karasözen
Mathematics Department, METU

Prof. Dr. Münevver Tezer-Sezgin
Mathematics Department, METU

Prof. Dr. I. Hakan Tarman
Engineering Sciences Department, METU

Prof. Dr. Kemal Leblebicioğlu
Electrical Engineering Department, METU

Prof. Dr. Tanıl Ergenç
Mathematics Department, Atılım University

Date:

I hereby declare that all information in this document has been obtained and presented in accordance with academic rules and ethical conduct. I also declare that, as required by these rules and conduct, I have fully cited and referenced all material and results that are not original to this work.

Name, Last Name: NAGEHAN ALSOY-AKGÜN

Signature :

ABSTRACT

THE DUAL RECIPROCITY BOUNDARY ELEMENT SOLUTION OF HELMHOLTZ-TYPE EQUATIONS IN FLUID DYNAMICS

ALSOY-AKGÜN, NAGEHAN

Ph.D., Department of Mathematics

Supervisor : Prof. Dr. Münevver Tezer-Sezgin

February 2013, 173 pages

In this thesis, the two-dimensional, unsteady, laminar and incompressible fluid flow problems governed by partial differential equations are solved by using dual reciprocity boundary element method (DRBEM). First, the governing equations are transformed to the inhomogeneous modified Helmholtz equations, and then the fundamental solution of modified Helmholtz equation is used for obtaining boundary element method (BEM) formulation. Thus, all the terms in the equation except the modified Helmholtz operator are considered as inhomogeneity. All the inhomogeneity terms are approximated by using suitable radial basis functions, and corresponding particular solutions are derived by using the annihilator method. Transforming time dependent partial differential equations to the form of inhomogeneous modified Helmholtz equations in DRBEM application enables us to use more information from the original governing equation. These are the main original parts of the thesis. In order to obtain modified Helmholtz equation for the time dependent partial differential equations, the time derivatives are approximated at two time levels by using forward finite difference method. This also eliminates the need of another time integration scheme, and diminishes stability problems.

Stream function-vorticity formulations are adopted in physical fluid dynamics problems in DRBEM by using constant elements. First, the procedure is applied to the lid-driven cavity flow and results are obtained for Reynolds number values up to 2000. The natural convection flow is solved for Rayleigh numbers between 10^3 to 10^6 when the energy equation is added to the Navier-Stokes equations. Then, double diffusive mixed convection flow problem defined in three different physical domains is solved by using the same procedure. Results are obtained for various values of Richardson and Reynolds numbers, and buoyancy ratios. Behind these, DRBEM is used for the solution of natural convection flow under a magnetic

field by using two different radial basis functions for both vorticity transport and energy equations. The same problem is also solved with differential quadrature method using the form of Poisson type stream function and modified Helmholtz type vorticity and energy equations. DRBEM and DQM results are obtained for the values of Rayleigh and Hartmann numbers up to 10^6 and 300, respectively, and are compared in terms of accuracy and computational cost. Finally, DRBEM is used for the solution of inverse natural convection flow under a magnetic field using the results of direct problem for the missing boundary conditions.

Keywords: DRBEM, DQM, Navier-Stokes equations, natural and mixed convection, inverse problems.

ÖZ

HELMHOLTZ TİPİNDEKİ AKIŞKANLAR MEKANIĞI DENKLEMLERİNİN KARŞILIKLI SINIR ELEMANLARI YÖNTEMİ İLE ÇÖZÜMÜ

ALSOY-AKGÜN, NAGEHAN

Doktora, Matematik Bölümü

Tez Yöneticisi : Prof. Dr. Münevver Tezer-Sezgin

Şubat 2013, 173 sayfa

Bu tezde, kısmi diferansiyel denklemlerle tanımlanmış iki boyutlu, zamana bağlı, katmanlı ve sıkıştırılmayan akışkan problemleri, karşılıklı sınır elemanları yöntemi ile çözülmüştür. İlk önce, denklemler homojen olmayan modifiye edilmiş Helmholtz denklemlerine dönüştürülmüş ve sonra sınır elemanları yöntemi formülasyonu modifiye edilmiş Helmholtz denkleminin temel çözümü kullanılarak elde edilmiştir. Böylece, modifiye edilmiş Helmholtz operatörü dışındaki bütün terimler sağ taraf terimi olarak değerlendirilmiştir. Bütün homojen olmayan terimler uygun radyal kökenli fonksiyonlar kullanılarak yaklaşık olarak hesaplanmıştır, ve buna bağlı özel çözümler annihilatör yöntemi kullanılarak elde edilmiştir. Karşılıklı sınır elemanları metodu uygulamasında, zamana bağlı kısmi diferansiyel denklemlerin homojen olmayan modifiye edilmiş Helmholtz denklemlerine dönüştürülmesi, orijinal dekleme ait daha fazla bilginin kullanılmasını sağlamıştır. Bu çalışmalar bu tezin orijinal bölümünü oluşturmaktadır. Zamana bağlı kısmi diferansiyel denklemler yerine modifiye edilmiş Helmholtz denklemlerini elde etmek için, denklemin zaman türevleri ileri sonlu farklar yöntemi kullanılarak iki zaman düzeyinde açılmıştır. Bu yöntem ayrıca zaman türevi için farklı bir yöntem kullanma ve buna bağlı olarak sayısal kararlılık analizi yapma gereksinimini ortadan kaldırmıştır.

Fiziksel akışkanlar mekaniği problemlerinin sabit elemanların kullanıldığı karşılıklı sınır elemanları metodu uygulamasında stream fonksiyon-vortisite formülasyonu kullanılmıştır. İlk önce bu yöntem hareketli kapaklı kanal akımları için kullanılmış ve sonuçlar Reynolds sayısı 2000'e kadar elde edilmiştir. Enerji denkleminin Navier-Stokes denklemlerine eklenmesi ile oluşan doğal konveksiyon akım problemi, 10^3 'den 10^6 'a kadarki Rayleigh sayıları için çözülmüştür. Daha sonra üç farklı fiziksel bölgede tanımlanmış çift difüzyonlu karışık konveksiyon problemi aynı yöntem kullanılarak çözülmüştür. Sonuçlar çeşitli Richardson ve Reynolds sayıları, ve hareketlilik oranları için verilmiştir. Bunun yanı sıra, aynı method

manyetik alana maruz bırakılmış doğal konveksiyon probleminin çözümünde, vortisite taşıma ve enerji denklemlerinin her ikisi için de iki farklı radyal kökenli fonksiyonlar kullanılarak uygulanmıştır. Poisson tipi stream fonksiyon ve modifiye edilmiş Helmholtz tipi vortisite ve enerji denklemleri formundaki aynı problem diferansiyel kareleme yöntemi ile de çözülmüştür. Sonuçlar her iki yöntem ile Rayleigh ve Hartmann sayıları için sırasıyla 10^6 'ya ve 300'e kadar elde edilmiştir. İki yöntemin mukayesesi elde edilen sonuçların doğruluğu ve hesaplama bedeli karşılaştırılarak yapılmıştır. Son olarak, karşılıklı sınır elemanları yöntemi, manyetik alana maruz bırakılmış, doğal konveksiyon probleminin ters çözümünde kullanılmıştır. Eksik olan sınır koşulları direkt problemin çözümlerinden elde edilmiştir.

Anahtar Kelimeler: Karşılıklı sınır elemanları yöntemi, diferansiyel kareleme yöntemi, Navier-Stokes denklemleri, doğal ve karışık konveksiyon, ters problemler.

*To my husband, Yasin,
my parents, Gülhanım and Turgut
and my son*

ACKNOWLEDGMENTS

I would like to express my sincere appreciation to the following people for their contribution to the completion of my thesis.

First, I would like to express my deep gratitude to Prof. Dr. Münevver Tezer-Sezgin, my research supervisors, for her patient guidance, enthusiastic encouragement and useful critiques of this research work. Her willingness to give her time so generously has been very much appreciated. Her great motivation and understanding makes this study possible for me. I shall never forget her patience and helpful advices for both academic research and social life.

My thanks are extended to the members of my defense committee Prof. Dr. Hakan Tarman, Prof. Dr. Bülent Karasözen, Prof. Dr. Kemal Leblebicioğlu and Prof. Dr. Tanıl Ergenç for their guidance and valuable suggestions.

I am particularly grateful for the assistance given by Prof. Dr. Daniel Lesnic for his valuable and constructive suggestions during my research visitor period at the University of Leeds.

I am very thankful for the financial support of The Scientific and Technical Research Council of Turkey (TUBİTAK).

I am deeply indebted to my friends whose assistance and encouragement made this work possible towards the end.

I offer my special thanks to my father Turgut and my mother Gülhanım for their love and support that provide me success and happiness in my life. I also thank my older brother Volkan for encouragement during my research. Of course my special thanks go to my younger brothers Murat and Fatih for making my life more colorful.

I want to show my deepest heartfelt gratitude to my husband Yasin for his patience, encouragements and supports in all the stages of this research period. He was always with me and sharing all difficulties of the life with me. I am thankful for his continuous motivation and understanding.

TABLE OF CONTENTS

ABSTRACT	v
ÖZ	vii
ACKNOWLEDGMENTS	x
TABLE OF CONTENTS	xi
LIST OF TABLES	xiv
LIST OF FIGURES	xv
NOMENCLATURE	xix
CHAPTERS	
1 INTRODUCTION	1
1.1 Diffusion Equation	3
1.2 Convection-diffusion-reaction Equation	4
1.3 Navier-Stokes Equations	5
1.3.1 Primitive Variable Formulation (u, v, p)	5
1.3.2 Stream Function-Vorticity Formulation ($\psi-w$)	6
1.4 Natural Convection Flow	7
1.5 Double Diffusive Mixed Convection Flow	10
1.6 Natural Convection Flow under a Magnetic Field	12
1.7 Literature Survey	14
1.8 Contributions in the Thesis	21
1.9 Plan of the Thesis	21
2 THE DUAL RECIPROCITY BOUNDARY ELEMENT METHOD	23
2.1 DRBEM Solution of Poisson Equation $\nabla^2 u = b_1(x, y)$	24
2.1.1 Boundary Integral Equation for the Poisson Equation	24
2.1.2 DRBEM for the Poisson Equation	26

2.2	DRBEM Solution of Inhomogeneous Modified Helmholtz Equation $\nabla^2 u - \tau^2 u = b_2(x, y)$	32
2.2.1	Boundary Integral Equation for Homogeneous Modified Helmholtz Equation	32
2.2.2	DRBEM for the Inhomogeneous Modified Helmholtz Equa- tion	34
2.2.3	DRBEM Solution for the Equation $\nabla^2 u - \tau^2 u = b_2(x, y, u_x, u_y)$	38
2.2.4	Different \bar{f} Expansions for Modified Helmholtz Operator .	39
2.2.4.1	Polynomial Form of \bar{f} Expansion	39
2.2.4.2	Thin Plate Splines for \bar{f} Expansion	40
2.3	DRBEM for Inverse Problem	47
2.3.1	DRBEM Solution of Poisson Equation for an Inverse Prob- lem	50
2.3.2	DRBEM Solution of Modified Helmholtz Equation for an Inverse Problem	51
3	DIFFERENTIAL QUADRATURE METHOD	53
3.1	Polynomial-based Differential Quadrature Method	53
3.2	Typical Grid Point Distribution	58
3.2.1	Chebyshev-Gauss-Lobatto Grid (CGL Points)	58
3.2.2	The Roots of Chebyshev Polynomial	58
3.3	DQM Solution of Poisson Equation $\nabla^2 u = b_1(x, y)$	59
3.4	DQM Solution of Modified Helmholtz Equation $\nabla^2 u - \tau^2 u = b_2(x, y)$	61
4	APPLICATION OF DRBEM AND DQM TO THE NATURAL AND MIXED CONVECTION FLOWS	65
4.1	Choice of \bar{f} Expansions for DRBEM Solution of Modified Helmholtz Equations	66
4.1.1	Example 1: Modified Helmholtz Equation	66
4.1.2	Example 2: Diffusion Equation	69
4.1.3	Example 3: Convection-Diffusion Equation	71
4.1.4	Example 4: Modified Helmholtz Equation	73
4.2	DRBEM Solution of Lid-Driven and Natural Convection Flow Prob- lems in Cavities	75
4.2.1	Lid-Driven Cavity Flow	75

	4.2.1.1	Numerical Results	78
	4.2.2	Natural Convection in a Square Cavity	84
	4.2.2.1	Numerical Results	86
4.3		DRBEM Solution of the Thermo-Solutal Buoyancy Induced Mixed Convection Flow	89
	4.3.1	Thermo-solutal Mixed Convection in a Lid-driven Cavity .	93
	4.3.2	Thermo-solutal Mixed Convection in a Lid-Driven Cavity with a Square Blockage	101
	4.3.3	Thermo-solutal Mixed Convection Flow in Backward-facing Step Horizontal Channel	106
4.4		DRBEM and DQM Solutions of Natural Convection Flow in a Cavity under a Magnetic Field	118
	4.4.1	Numerical Results	123
4.5		Application of DRBEM for the Inverse Problems	135
	4.5.1	Natural Convection Flow under a Magnetic Field	135
	4.5.2	Numerical Results	136
	4.5.2.1	Example 1	136
	4.5.2.2	Example 2	154
5		CONCLUSION	161
		REFERENCES	163
		VITA	171

LIST OF TABLES

TABLES

Table 2.1 Particular solutions for modified Helmholtz equation in \mathbf{R}^2 with inhomogeneity \bar{f} , [68].	47
Table 4.1 Polynomial \bar{f} functions and particular solutions \widehat{u}	67
Table 4.2 Dependence of wave number τ^2	68
Table 4.3 Results for diffusion problem with several \bar{f} functions for $\theta = 1/2$ and $\theta = 2/3$	70
Table 4.4 Results for convection-diffusion equation with $d = 5$, $t = 1.0$, $K = 60$, $L = 49$ at $y = 0.6$	72
Table 4.5 Results for convection-diffusion equation with $d = 40$, $t = 1.0$, $K = 100$, $L = 144$ at $y = 0.6$	72
Table 4.6 Results for Example 4 with higher order splines	73
Table 4.7 The number of iteration with corresponding θ_w for $Re = 500$, $N = 92$, $\Delta t = 0.1$	79
Table 4.8 Δt variations for thermo-solutal mixed convection in a lid-driven cavity . . .	94
Table 4.9 Number of iterations with different θ_w and θ_T in DRBEM using $\bar{f} = r^2 \log r$, $Ra = 10^4$	124
Table 4.10 Number of iterations with different θ_w and θ_T in DQM, $Ra = 10^4$	124
Table 4.11 Δt values in DRBEM using $\bar{f} = r^2 \log r$ and $\bar{f} = 1 + r^2 + r^3 - \tau^2(\frac{r^2}{4} + \frac{r^4}{16} + \frac{r^5}{25})$ for $Ha = 50$	125
Table 4.12 The comparison of maximum value of the stream function in magnitude and its location for $Ha = 100$	126
Table 4.13 The comparison of maximum value of the stream function in magnitude and its location for $Ra = 10^4$	126

LIST OF FIGURES

FIGURES

Figure 4.1 DRBEM solution of Example 4 with higher order splines and polynomial \bar{f} at $y = 0.4$	74
Figure 4.2 Boundary conditions for the lid-driven flow in a square cavity	79
Figure 4.3 Lid-driven cavity flow, $Re = 50$	80
Figure 4.4 Lid-driven cavity flow, $Re = 500$	81
Figure 4.5 Lid-driven cavity flow, $Re = 1000$	82
Figure 4.6 Lid-driven cavity flow, $Re = 2000$	83
Figure 4.7 Boundary conditions for the natural convection flow in a square cavity . . .	86
Figure 4.8 Natural convection in a square cavity: $Ra = 10^3$, $Ra = 10^4$, $Ra = 10^5$ and $Ra = 10^6$ from top to bottom	88
Figure 4.9 Boundary conditions for thermo-solutal mixed convection lid-driven cavity flow	93
Figure 4.10 The effect of the buoyancy forces on streamlines for different Ri at $Re = 100$ and $Pr = Sc = 1$	97
Figure 4.11 The effect of the buoyancy forces on vorticity for different Ri at $Re = 100$ and $Pr = Sc = 1$	98
Figure 4.12 The effect of the buoyancy forces on temperature and concentration for different Ri at $Re = 100$ and $Pr = Sc = 1$	99
Figure 4.13 u -velocity profile along vertical line ($x = 0.5$) for $Re = 500$, $Gr_T = Gr_C = 100$ and $Le = 2$	100
Figure 4.14 The effect of the buoyancy forces on the hot wall, Average Nusselt numbers for $Re = 100$ and $Pr = Sc = 1$	100
Figure 4.15 Boundary conditions for lid-driven square cavity with a square blockage placed at the bottom wall	101
Figure 4.16 The effect of the buoyancy forces for $Ri = 0.01$, $Re = 100$	103
Figure 4.17 The effect of the buoyancy forces for $Ri = 0.1$, $Re = 100$	104
Figure 4.18 The effect of the buoyancy forces for $Ri = 0.01$, $Re = 200$	105
Figure 4.19 Backward-facing step channel flow	106
Figure 4.20 Effect of Richardson number on the streamline for $Re = 200$, $N = 1$, $Pr = Sc = 1$, from top to bottom $Ri = 0.1$, $Ri = 0.5$, $Ri = 1$, $Ri = 3$, $Ri = 5$ and $Ri = 10$	109
Figure 4.21 Effect of Richardson number on the vorticity for $Re = 200$, $N = 1$, $Pr = Sc = 1$, from top to bottom $Ri = 0.1$, $Ri = 0.5$, $Ri = 1$, $Ri = 3$, $Ri = 5$ and $Ri = 10$	110

Figure 4.22 Effect of Richardson number on the temperature and concentration for $Re = 200$, $N = 1$, $Pr = Sc = 1$, from top to bottom $Ri = 0.1$, $Ri = 0.5$, $Ri = 1$, $Ri = 3$, $Ri = 5$ and $Ri = 10$	111
Figure 4.23 u -velocity profile along vertical line ($x = 5$) for $Re = 200$, $N = 1$, $Ri = 0.01$ and $Le = 1$	112
Figure 4.24 Effect of buoyancy ratio on the vorticity for $Re = 200$, $Ri = 0.1$, $Pr = Sc = 1$, for $N = -10$, $N = -5$, $N = 1$, $N = 5$ and $N = 10$	113
Figure 4.25 Effect of Reynolds number on the streamline for $Ri = 1$, $N = 1$, $Pr = Sc = 1$, from top to bottom $Re = 10$, $Re = 30$, $Re = 50$, $Re = 100$, $Re = 150$ and $Re = 200$	114
Figure 4.26 Effect of Reynolds number on the vorticity for $Ri = 1$, $N = 1$, $Pr = Sc = 1$, from top to bottom $Re = 10$, $Re = 30$, $Re = 50$, $Re = 100$, $Re = 150$ and $Re = 200$	115
Figure 4.27 Effect of Reynolds number on temperature and concentration for $Ri = 1$, $N = 1$, $Pr = Sc = 1$, from top to bottom $Re = 10$, $Re = 30$, $Re = 50$, $Re = 100$, $Re = 150$ and $Re = 200$	116
Figure 4.28 (a)Effect of buoyancy ratio for various Richardson numbers on the step: average Nusselt number, (b)Effect of buoyancy ratio for various Richardson numbers on top wall: average Sherwood number,	117
Figure 4.29 Natural convection flow in a square cavity under a magnetic field	123
Figure 4.30 Temperature, vorticity and streamline contours with DRBEM using $\bar{f} = r^2 \log r$ for $Ha = 50, 100, 200, 300$ from top to bottom with $Ra = 10^5$	128
Figure 4.31 Temperature, vorticity and streamline contours with DQM for $Ha = 50, 100, 200, 300$ from top to bottom with $Ra = 10^5$	129
Figure 4.32 Temperature, vorticity and streamline contours with DRBEM using $\bar{f} = r^2 \log r$ for $Ra = 10^3, 10^4, 10^5, 10^6$ from top to bottom with $Ha = 50$	130
Figure 4.33 Temperature, vorticity and streamline contours with DQM for $Ra = 10^3, 10^4, 10^5, 10^6$ from top to bottom with $Ha = 50$	131
Figure 4.34 Temperature, vorticity and streamline contours with DRBEM using $\bar{f} = 1 + r^2 + r + 3 - \tau^2(\frac{r^2}{4} + \frac{r^4}{16} + \frac{r^5}{25})$ for $Ra = 10^3, 10^4, 10^5$, from top to bottom with $Ha = 50$	132
Figure 4.35 Horizontal and vertical velocity profiles at the mid-plane of the cavity for $Ra = 10^4$ and $Ha = 50$	133
Figure 4.36 Horizontal and vertical velocity profiles at the mid-plane of the cavity for $Ra = 10^4$	133
Figure 4.37 Horizontal and vertical velocity profiles at the mid-plane of the cavity for $Ra = 10^4$	134
Figure 4.38 Inverse problem for the natural convection flow in a square cavity under a magnetic field.	136
Figure 4.39 Isotherm patterns at the time $t = 30\Delta t_{ref}$ for the direct problem with $Ha = 0$, $\Delta t = \frac{\Delta t_{ref}}{200}$, $K = 44$ and $L_1 = 25$	141
Figure 4.40 Isotherm patterns at the time $t = 30\Delta t_{ref}$ for the direct problem with $Ha = 0$, $\Delta t = \frac{\Delta t_{ref}}{200}$, $K = 84$ and $L_1 = 100$	142

Figure 4.41 Isotherm patterns at the time $t = 30\Delta t_{ref}$ for the direct problem with $Ha = 0$, $\Delta t = \frac{\Delta t_{ref}}{200}$, $K = 164$ and $L_1 = 400$	143
Figure 4.42 Isotherms at boundary $x = 0$ for the direct problem with $Ha = 0$, $\Delta t = \frac{\Delta t_{ref}}{200}$, $K = 84$ and $L_1 = 100$	144
Figure 4.43 Isotherms at boundary $x = 1$ for the direct problem with $Ha = 0$, $\Delta t = \frac{\Delta t_{ref}}{200}$, $K = 84$ and $L_1 = 100$	145
Figure 4.44 Isotherm patterns at the time $t = 30\Delta t_{ref}$ for the inverse problem with $Ha = 0$, $\lambda = 10^{-6}$, $\Delta t = \frac{\Delta t_{ref}}{200}$, $K = 84$ and $L_2 = 90$	146
Figure 4.45 Effect of the Rayleigh number on the heat flux $q(0.5, t)$ for $Ha = 0$, $K = 84$, $L_2 = 90$, $\lambda = 10^{-6}$, and $\Delta t = \frac{\Delta t_{ref}}{200}$	147
Figure 4.46 Effect of the time step on the heat flux $q(0.5, t)$ for $Ra = 500$, $Ha = 0$, $K = 84$, $L_2 = 90$ and $\lambda = 10^{-6}$	147
Figure 4.47 Effect of noise on the boundary temperature $T(0, 0.5, t)$ for $Ra = 500$, $Ha = 0$, $K = 84$, $L_2 = 90$, $\lambda = 10^{-6}$ and $\Delta t = \frac{\Delta t_{ref}}{200}$	148
Figure 4.48 Effect of noise on the heat flux $q(0.5, t)$ for $Ra = 500$, $Ha = 0$, $K = 84$, $L_1 = 100$, $L_2 = 90$, $\lambda = 10^{-6}$ and $\Delta t = \frac{\Delta t_{ref}}{200}$	148
Figure 4.49 Effect of regularization parameter λ on the heat flux $q(0.5, t)$ for $Ra = 500$, $K = 84$, $L_1 = 100$, $L_2 = 90$, $\rho = 4\%$ and $\Delta t = \frac{\Delta t_{ref}}{200}$	149
Figure 4.50 Isotherm patterns at the time $t = 30\Delta t_{ref}$ for the direct and inverse ($\lambda = 10^{-6}$) problems with $Ra = 500$, $Ha = 0$, $\Delta t = \frac{\Delta t_{ref}}{200}$, $K = 84$, $L_1 = 100$ and $L_2 = 90$	150
Figure 4.51 Isotherm patterns at the time $t = 60\Delta t_{ref}$ for the direct and inverse ($\lambda = 10^{-6}$) problems with $Ra = 500$, $Ha = 0$, $\Delta t = \frac{\Delta t_{ref}}{200}$, $K = 84$, $L_1 = 100$ and $L_2 = 90$	151
Figure 4.52 Effect of the Hartmann number on the heat flux $q(0.5, t)$ for $Ra = 500$, $K = 84$, $L_2 = 90$, $\lambda = 10^{-6}$, $\rho = 0$ and $\Delta t = \frac{\Delta t_{ref}}{200}$	152
Figure 4.53 Isotherms (top row), streamlines (middle row) and vorticity lines (bottom row) at the time $t = 30\Delta t_{ref}$ for the inverse problem with $Ra = 500$, $\lambda = 10^{-6}$, $\rho = 0$, $\Delta t = \frac{\Delta t_{ref}}{200}$, $K = 84$ and $L_2 = 90$	153
Figure 4.54 Effect of noise on the heat flux $q(0.5, t)$ for $Ra = 500$, $Ha = 100$, $K = 84$, $L_2 = 90$, $\lambda = 10^{-6}$, and $\Delta t = \frac{\Delta t_{ref}}{200}$	154
Figure 4.55 Inverse problem for the natural convection flow under a magnetic field with isothermal vertical walls	155
Figure 4.56 The heat flux $q_1(y, t) := \frac{\partial T}{\partial x}(1, y, t)$ at the boundary $x = 1$ for the direct problem with $Ra = 10^5$, $K = 84$, $L_1 = 100$ and $\Delta t \in \{2 \times 10^{-3}, 5 \times 10^{-4}, 3 \times 10^{-4}\}$ for $Ha \in \{100, 200, 300\}$, respectively.	156

Figure 4.57 The heat flux $q(y, t) := \frac{\partial T}{\partial x}(0, y, t)$ at the boundary $x = 0$ for the direct problem with $Ra = 10^5$, $K = 84$, $L_1 = 100$ and $\Delta t \in \{2 \times 10^{-3}, 5 \times 10^{-4}, 3 \times 10^{-4}\}$ for $Ha \in \{100, 200, 300\}$, respectively. 157

Figure 4.58 The numerically retrieved temperature $T(0, y, t)$ at the boundary $x = 0$ for the inverse problem with $Ra = 10^5$, $K = 84$, $L_2 = 90$, $\lambda = 10^{-6}$, $\rho = 2\%$ and $\Delta t \in \{2 \times 10^{-3}, 5 \times 10^{-4}, 3 \times 10^{-4}\}$ for $Ha \in \{100, 200, 300\}$, respectively. 158

Figure 4.59 The numerically retrieved temperature $q(y, t)$ at the boundary $x = 0$ for the inverse problem with $Ra = 10^5$, $K = 84$, $L_2 = 90$, $\lambda = 10^{-6}$, $\rho = 2\%$ and $\Delta t \in \{2 \times 10^{-3}, 5 \times 10^{-4}, 3 \times 10^{-4}\}$ for $Ha \in \{100, 200, 300\}$, respectively. 159

NOMENCLATURE

SYMBOLS

a_{ij}, b_{ij}	weighting coefficients for the first and second order derivatives in DQM
b_1, b_2	right hand side functions of Poisson and modified Helmholtz equation
B	magnetic field
c	specific heat
C	concentration
C_h, C_c	high and low concentration
D	binary diffusivity coefficient
f, \bar{f}	radial basis functions for Poisson and modified Helmholtz equation
$\mathbf{F}, \bar{\mathbf{F}}$	coordinate matrices for Poisson and modified Helmholtz equation
$\widehat{\mathbf{F}}$	body force
g	gravitational acceleration
Gr_T, Gr_C	Grashof numbers due to the mass and thermal diffusivity
H	characteristic channel length in Chapter 4
H_1, H_2	dimensions of cavity in Chapter 3
$\overline{\mathbf{H}}, \mathbf{H}, \mathbf{G}$	BEM matrices for Poisson equation
$\overline{\mathbf{H}'}, \mathbf{H}', \mathbf{G}'$	BEM matrices for modified Helmholtz equation
Ha	Hartmann number
J	current density
k	thermal conductivity coefficient
k_x, K_x	diffusivity or dispersion coefficient
K, L	the number of boundary and internal nodes in DRBEM
L_0	reference length
L_1, L_2	the number of internal nodes for the direct and inverse problems
Le	Lewis number
L_x	dimension of square cavity in Chapter 1
N	buoyancy ratio
N_1, N_2	the numbers of discretization points x and y directions in DQM
Nu_{av}	average Nusselt number
p	nondimensional pressure
Pr	Prandtl number
r	distance between source and field points
Ra	Rayleigh number
Re	Reynolds number
Ri	Richardson number
Sc	Schmidt number
Sh_{av}	average Sherwood number

t	nondimensional time variable
T	temperature
T_h, T_c	high and low temperature
u, v	nondimensional components of fluid velocity
u^*, q^*	fundamental solution and its normal derivative
\widehat{u}, \widehat{q}	particular solution and its normal derivative
U	reference velocity
\mathbf{V}	velocity vector
w	vorticity
x, y	nondimensional space variables
$\alpha, \bar{\alpha}$	unknown coefficients for Poisson and modified Helmholtz equations
α'	thermal diffusivity coefficient
β	thermal expansion coefficient
β_T, β_C	volumetric expansion coefficient for temperature and concentration
Γ	boundary of Ω
Δt	time step
ΔT	temperature difference
ΔC	concentration difference
$\Delta^i(x)$	Dirac delta function
$\theta, \theta_w, \theta_T, \theta_C,$	relaxation parameters
λ	Tikhonov regularization parameter
μ	dynamic viscosity coefficient
ν	kinematic viscosity coefficient
ρ	percentage of the noise
$\widehat{\rho}$	fluid density
ρ_0	reference density
σ	electrical conductivity
$\tau, \tau_w, \tau_T, \tau_C,$	wave numbers
ϕ	angle of the magnetic field with respect to x -axis
χ	random variable in $[-1, 1]$
ψ	stream function
Ω	two-dimensional domain

CHAPTER 1

INTRODUCTION

The mathematical model of physical or engineering problems can be represented by using partially differential equations (PDEs) with suitable boundary conditions. Generally, to obtain the close-form solution of these equations cannot be possible. Therefore, the approximate solutions can be obtained by using different numerical methods. There are several numerical solution techniques such as finite difference method (FDM), finite element method (FEM), differential quadrature method (DQM), boundary element method (BEM) and dual reciprocity boundary element method (DRBEM). The differences of the methods occur with the type of the approximation of the variables, and with the discretization of the domain where the problems are defined.

Finite difference method describes the derivative of the unknowns by using the truncated Taylor series expansions. Replacing the derivatives of the governing equations with the finite differences and using the boundary conditions, one can obtain a system of algebraic equations. Finite difference approximations can be used easily for the internal discretization but main difficulties of the method are caused by the curve boundaries and insertion of the boundary conditions. Also, for the regular boundaries, fictitious external points should be used for the boundary conditions which contain derivatives. Since, finite difference codes require a simple procedure to obtain an algebraic equation, it is still preferred for the solution of many fluid dynamic problems.

In contrast to the finite difference method, finite element method gives a better representation of the geometry of the domain and facilitates the insertion of the boundary conditions. This method divides the domain into small parts which are called elements. Then, the variables of the governing equations are approximated using the polynomial interpolation functions over the small parts of the domain. So, for each element, the influence matrices which contain the properties of each elements are obtained. After assembling these influence matrices by considering the properties of continuum, a global matrix is obtained for the equations. The insertion of boundary conditions can be done by evaluating the boundary integrals. This is easier way for the insertion of boundary conditions than the finite difference method. Behind this, for the discretization of the domain in the FEM it is necessary to use large amount of information. So, the size of the system increases and this causes high computational cost. Also, the method is not suitable for the problems which are defined in an infinite region or having moving boundaries.

Another finite domain discretization method is the differential quadrature method which is introduced by Bellman et al. [21]. DQM describes the derivative of the function as a linear weighted sum of the functional values at each mesh points. Shu [88] generalized all the cur-

rent methods for determination of weighting coefficients by using the properties of a linear vector space. Since DQM is based on interpolation of solution and its derivatives by polynomials, it is quite simple. Although, DQM is preferred and found to be simple in terms of computation, it is a domain discretization method where the domain must be rectangular.

The boundary element method is a numerical technique which has important advantages over the domain discretization methods mentioned above. The main idea of the method is the transformation of the differential equation defined in a domain to an integral equation defined on its boundary. The boundary integral equation contains only the values of unknown and their normal derivatives on the boundary. Since it needs just discretization of the boundary, the problem becomes a one-dimensional problem and it gives a smaller system of equations. After solving the system one can obtain all the unknown values and their normal derivatives at the boundary. Also, using these boundary values, the solution at the interior nodes can be obtained with a simple computation. Besides these, BEM can be used for the solution of the problems which are defined in the infinite regions or having moving boundaries.

BEM was introduced by small group of researchers in the 1960's. They studied on the applications of boundary integral equations to the potential flow and stress analysis. Later, the method became a perfect alternative to the finite element method for the solution of problems. The current form of the method was constructed by Brebbia in [22] and his research group [23, 24]. BEM is an excellent numerical method if the fundamental solution of the governing PDE is available. However, after obtaining the boundary integral equation there may be still domain integrals due to some force and convection-reaction terms, and these require an extra domain discretization. Thus, this extra discretization destroys the advantage of the method. Nonhomogeneous and nonlinear terms of the governing equation also cause the domain integral and extra domain discretization for the solution. Therefore, it is necessary to use another approach when the domain discretization is required. There are several methods proposed by different persons such as analytical integration of the domain integrals, the use of Fourier expansions, Galerkin vector technique, the multiple reciprocity method and the dual reciprocity boundary element method.

The dual reciprocity boundary element method is the main numerical solution procedure used in this thesis. It was introduced by Nardini and Brebbia [69] and extended by Brebbia, Wrobel and Partridge [72, 74]. DRBEM is a numerical technique which uses a fundamental solution corresponding to a simpler equation, and to treat the remaining terms as an inhomogeneous term of the differential equation. Thus, it is an efficient method for the solution of inhomogeneous, nonlinear and time-dependent problems. The important idea is to determine simpler form of the differential equation where the corresponding fundamental solution is available. Generally, when the DRBEM is used as a solution method, all the terms except the Laplacian term of the differential equation are considered as inhomogeneity. Then, the fundamental solution of Laplace equation can be used for the obtained Poisson equation. Also, it is important that, the inhomogeneous term of the governing equation should be kept as simple as possible. Therefore, one can reduce the interpolation error to a minimum. An alternative is to reduce the given PDE to an inhomogeneous modified Helmholtz equation, and then to use its fundamental solution in DRBEM formulation.

DRBEM can be applied to the modified Helmholtz equation, since its fundamental solution is available. In this case, on the left hand side of the equation, one will be left with more terms than the Laplacian case. Thus, it is possible to use more information about the original governing equation. By using some approximations for the time derivative, convection or

reaction terms, a modified Helmholtz equation can be obtained for the differential equation for which the fundamental solution is complicated to obtain in its original form. But, in the DRBEM application to inhomogeneous modified Helmholtz equation the problem lies in obtaining corresponding particular solutions for the radial basis function approximation of the inhomogeneity. For some radial basis functions \bar{f}_j , corresponding particular solutions \widehat{u}_j in $(\nabla^2 - \tau)\widehat{u}_j = \bar{f}_j$ are available [28, 68]. In this thesis, a list of particular solutions are obtained for radial basis functions in the form of polynomials, logarithmic functions and some of these combinations. A general approach for obtaining particular solutions is provided.

In this thesis, some fluid dynamics problems such as lid-driven cavity flow, natural convection flow in enclosures, double diffusive mixed convection flow and natural convection flow under a magnetic field are solved by using DRBEM. All the governing equations are transformed first to the form of inhomogeneous modified Helmholtz equations by discretizing time derivative terms first. Since the governing equations of these physical problems are diffusion or convection-diffusion-reaction equations type, this reduction to inhomogeneous modified Helmholtz equation is performed on these equations first, and then generalized to the physical problems considered. Then, the DRBEM applications are carried with the fundamental solution of modified Helmholtz equation. This forms the original core part of the thesis when it is combined with the general derivation of particular solutions for some mostly used radial basis functions in DRBEM. The obtained numerical results are deeply discussed in terms of graphics with the physical behaviors of the problems concerned.

1.1 Diffusion Equation

The fundamental concept of the fluid mechanics is the *diffusion* which is the transport caused by the random motions of the fluid particles from high concentration to low concentration. The diffusion equation represents the change in the concentration of the fluid over time at a point. The usual form of two-dimensional diffusion equation is

$$\begin{aligned} \nabla^2 u &= \frac{1}{k_x} \frac{\partial u}{\partial t} & 0 < x, y < L_x, \quad t > 0 \\ u &= 0 & \text{at } x, y = 0, L_x \end{aligned} \quad (1.1)$$

where k_x is the dispersion coefficient. The exact solution of this diffusion problem is [73]

$$u(x, y, t) = \sum_{n=1}^{\infty} \sum_{m=1}^{\infty} A_{nm} \sin\left(\frac{n\pi x}{L_x}\right) \sin\left(\frac{m\pi y}{L_x}\right) \exp\left[-\left(\frac{k_x n^2 \pi^2}{L_x^2} + \frac{k_x m^2 \pi^2}{L_x^2}\right)t\right] \quad (1.2)$$

and

$$A_{nm} = \frac{4u_0}{nm\pi^2} [(-1)^n - 1][(-1)^m - 1] \quad (1.3)$$

where L_x is the dimension of the square region, and u_0 is the initial value of u .

Since this diffusion problem has the exact solution it can be used as a test problem to control the efficiency of our method. For this aim, the diffusion equation should be written in the form of a modified Helmholtz equation.

If the time derivative is approximated using forward finite difference, diffusion equation takes the form

$$\nabla^2 u = \frac{1}{k_x} \left(\frac{u^{(n+1)} - u^{(n)}}{\Delta t} \right) \quad (1.4)$$

where $u^{(n+1)}$ and $u^{(n)}$ represent the values of u at the advance and current time levels, respectively, and Δt is the time increment. Relaxing the solution u also at these two time levels with a parameter $0 < \theta < 1$

$$\nabla^2 \left(\theta u^{(n+1)} + (1 - \theta) u^{(n)} \right) = \frac{1}{k_x} \left(\frac{u^{(n+1)} - u^{(n)}}{\Delta t} \right) \quad (1.5)$$

it can be put in the form of modified Helmholtz equation for $u^{(n+1)}$

$$\nabla^2 u^{(n+1)} - \frac{1}{k_x \Delta t \theta} u^{(n+1)} = - \left(\frac{1 - \theta}{\theta} \right) \nabla^2 u^{(n)} - \frac{1}{k_x \Delta t \theta} u^{(n)} \quad (1.6)$$

in which the inhomogeneity contains $u^{(n)}$ from previous time level.

It is rewritten as

$$\nabla^2 u^{(n+1)} - \tau^2 u^{(n+1)} = - \left(\frac{1 - \theta}{\theta} \right) \nabla^2 u^{(n)} - \tau^2 u^{(n)} \quad (1.7)$$

where $\tau^2 = \frac{1}{k_x \Delta t \theta}$.

Now, obtained inhomogeneous modified Helmholtz equation can be solved with any numerical method, iteratively in the time direction.

1.2 Convection-diffusion-reaction Equation

In the nature, the transport is occurred due to both the random and the bulk motion of the fluid. Thus, the transport caused by the bulk fluid motion is called *convection*. *Reaction* is caused by a term containing some powers of the solution. Therefore, the convection-diffusion-reaction equation is used for the transport of the fluid particles due to both random and bulk motions.

A two-dimensional convection-diffusion-reaction equation is governed by

$$\nabla^2 u = \frac{1}{K_x} \left(\frac{\partial u}{\partial t} + c_x \frac{\partial u}{\partial x} + c_y \frac{\partial u}{\partial y} + du \right), \quad (1.8)$$

and some suitable boundary conditions as

$$\begin{aligned} u(0, y, t) &= 300 & u(1, y, t) &= 10, \\ q(x, 0, t) &= 0 & q(x, 1, t) &= 0 \end{aligned} \quad (1.9)$$

with the values

$$\begin{aligned} K_x &= 1, \\ c_y &= 0, \\ c_x &= dx + \log \frac{10}{300} - \frac{d}{2} \end{aligned} \quad (1.10)$$

may be given. u is the concentration of the physical quantities, c_x and c_y are the velocity components, K_x is the dispersion coefficient and d is the coefficient of the chemical reactor. The exact solution of this convection-diffusion-reaction equation is [75]

$$u(x, y, t) = 300 \exp \left(\frac{d}{2} x^2 + \log \frac{10}{300} x - \frac{d}{2} x \right). \quad (1.11)$$

Using the similar idea with the diffusion equation, the time derivative is approximated by using forward finite difference

$$\frac{\partial u}{\partial t} = \frac{u^{(n+1)} - u^{(n)}}{\Delta t} \quad (1.12)$$

and the solution u in the Laplace term is approximated with a relaxation parameter θ between zero and one, as

$$u^{(n+1)} = \theta u^{(n+1)} + (1 - \theta)u^{(n)}. \quad (1.13)$$

Substituting these approximations (1.12) and (1.13) into the equation (1.8), and taking all the terms at n -th time level to the right hand side, a modified Helmholtz equation is obtained as

$$\nabla^2 u^{(n+1)} - \tau^2 u^{(n+1)} = -\left(\frac{1-\theta}{\theta}\right)\nabla^2 u^{(n)} - \tau^2 u^{(n)} + \frac{1}{K_x \theta} \left(c_x \frac{\partial u^{(n)}}{\partial x} + c_y \frac{\partial u^{(n)}}{\partial y} + du^{(n)} \right) \quad (1.14)$$

where the wave number is $\tau^2 = \frac{1}{K_x \theta \Delta t}$, and the inhomogeneity contains previous solution $u^{(n)}$.

1.3 Navier-Stokes Equations

The Navier-Stokes equations are the basic governing equations describing the motion of Newtonian or non-Newtonian fluid particles (liquids like water and gases like air). Using these equations, the modeling of many engineering problems such as industrial channel flow and ocean currents can be done. Navier-Stokes equations considered here are the two-dimensional vector equations which are obtained under the assumption of constant density and constant viscosity. They give the relations between the velocity, pressure and density of a moving fluid. The continuity equation (mass conservation) and the momentum equations (Newton's second law) are coupled through these variables. Momentum equations are coupled nonlinear partial differential equations, and their nonlinearity is caused by the convective acceleration. Thus, numerical methods have to be used for obtaining solution of Navier-Stokes equations.

The Navier-Stokes equations are usually written using different dependent variables such as velocity-pressure formulation (primitive variables formulation), vorticity-stream function formulation and fourth-order stream function equation. In the primitive variables formulation, the governing equations have three dependent variables which are velocity components u , v and the pressure p . Also, there is no boundary condition for the pressure. However, in the stream function-vorticity formulation of the two-dimensional problem, we can eliminate the pressure term introducing the stream function variable. Therefore, final system have two dependent variables which are the stream function ψ and vorticity w . Unknown boundary conditions for the vorticity must be derived using another numerical approach. In this thesis, stream function-vorticity formulation is used in all the computations and the derivation of this formulation is given.

1.3.1 Primitive Variable Formulation (u, v, p)

The vector form of the Navier-Stokes equations can be written as [96]

$$\nabla \mathbf{V} = 0 \quad (1.15)$$

and

$$\widehat{\rho} \frac{\partial \mathbf{V}}{\partial t} + \widehat{\rho} \mathbf{V} \cdot \nabla \mathbf{V} = -\nabla p + \mu \nabla^2 \mathbf{V} \quad (1.16)$$

with continuity and momentum equations, respectively. Here, \mathbf{V} is the velocity vector, $\widehat{\rho}$ is the fluid density, p is the pressure and μ is the dynamic viscosity.

In two-dimensions, the Navier-Stokes equations in non-dimensional form become

$$\frac{\partial u}{\partial x} + \frac{\partial v}{\partial y} = 0 \quad (1.17)$$

$$\begin{aligned} \frac{\partial u}{\partial t} + u \frac{\partial u}{\partial x} + v \frac{\partial u}{\partial y} &= -\frac{\partial p}{\partial x} + \frac{1}{Re} \left(\frac{\partial^2 u}{\partial x^2} + \frac{\partial^2 u}{\partial y^2} \right) \\ \frac{\partial v}{\partial t} + u \frac{\partial v}{\partial x} + v \frac{\partial v}{\partial y} &= -\frac{\partial p}{\partial y} + \frac{1}{Re} \left(\frac{\partial^2 v}{\partial x^2} + \frac{\partial^2 v}{\partial y^2} \right) \end{aligned} \quad (1.18)$$

where the dimensionless parameter

$$Re = \frac{\widehat{\rho} U L_0}{\mu}$$

is the Reynolds number which changes the characteristic behavior of the fluid [96], and $\mathbf{V} = (u, v)$. Re gives the ratio between the fluid inertial forces caused by the fluid density to the viscous forces. When the Reynolds number takes low values ($Re \leq 2100$), the viscous force dominates the system and the fluid is called *laminar* flow. In this case, the fluid motion can be described as smooth and constant. When the Reynolds number takes high values, the fluid inertial force dominates the system and the fluid is called *turbulent* flow. In this case, the fluid has the chaotic behavior.

1.3.2 Stream Function-Vorticity Formulation (ψ - w)

In this section, we will give stream function-vorticity formulation of the two-dimensional Navier Stokes equations. The idea is to eliminate the pressure and introduce an equation for vorticity. Time-dependent stream function $\psi(t, x, y)$ is defined by [96]

$$\frac{\partial \psi}{\partial x} = -v \quad \frac{\partial \psi}{\partial y} = u \quad (1.19)$$

satisfying the continuity equation automatically.

The fluid vorticity is obtained taking the curl of two-dimensional velocity vector as

$$w = \frac{\partial v}{\partial x} - \frac{\partial u}{\partial y} \quad (1.20)$$

which is related to the stream function by the Poisson equation

$$w = -\nabla^2 \psi. \quad (1.21)$$

Differentiating x -momentum equation with respect to y and y -momentum equation with respect to x , and subtracting one can arrive at vorticity transport equation as

$$\frac{1}{Re} \nabla^2 w = \frac{\partial w}{\partial t} + u \frac{\partial w}{\partial x} + v \frac{\partial w}{\partial y}. \quad (1.22)$$

Finally, the stream function-vorticity form of the Navier Stokes equations are

$$\nabla^2 \psi = -w \quad (1.23)$$

$$\frac{1}{Re} \nabla^2 w = \frac{\partial w}{\partial t} + u \frac{\partial w}{\partial x} + v \frac{\partial w}{\partial y} \quad (1.24)$$

and time-dependent vorticity equation now can be transformed to modified Helmholtz equation.

The time derivative in the vorticity transport equation is approximated using the forward difference approximation

$$\frac{\partial w}{\partial t} = \frac{w^{(n+1)} - w^{(n)}}{\Delta t} \quad (1.25)$$

where $w^{(n)} = w(x, y, t_n)$, $t_n = n\Delta t$, Δt is the time step and the solution w in the Laplace term is also approximated using relaxation parameter, $0 < \theta_w < 1$ as

$$w^{(n+1)} = \theta_w w^{(n+1)} + (1 - \theta_w) w^{(n)} \quad (1.26)$$

which smooths the values of vorticity between two consecutive time levels. Inserting the equations (1.25), (1.26) and (1.19) into the equation (1.24) and rearranging one can obtain an inhomogeneous modified Helmholtz equation for the vorticity. The iterative form of the governing equations are

$$\nabla^2 \psi^{(n+1)} = -w^n \quad (1.27)$$

$$\nabla^2 w^{(n+1)} - \tau_w^2 w^{(n+1)} = -\frac{(1 - \theta_w)}{\theta_w} \nabla^2 w^{(n)} - \tau_w^2 w^{(n)} + \frac{Re}{\theta_w} \left(\frac{\partial \psi^{(n+1)}}{\partial y} \frac{\partial w^{(n)}}{\partial x} - \frac{\partial \psi^{(n+1)}}{\partial x} \frac{\partial w^{(n)}}{\partial y} \right) \quad (1.28)$$

where $\tau_w^2 = \frac{Re}{\theta_w \Delta t}$, and n represents the iteration number. These coupled equations now are going to be solved by using DRBEM.

1.4 Natural Convection Flow

Heat transfer is a fundamental subject in the fluid dynamic problems. The importance of the heat transfer is caused by the usage of it in many areas of the industry. The mathematical modeling is done by adding the energy equation to the Navier-Stokes equations. The energy equation comes from the conservation of the energy which is called the first law of thermodynamics [52].

The heat transfer between the fluid molecules is called *convection heat transfer* or briefly *convection*, and it can be produced by two different mechanisms. If the energy transfer occurs with random molecular motion and there is no bulk motion, then the convection is called *conduction (diffusion)*. The conduction generally is caused by the temperature difference between the fluid molecules. In the conduction, energy transfer occurs from the more energetic molecules to the low energetic ones [52]. If the energy transfer is caused by the bulk motion, in this case, the convection is called *advection*. Therefore convection term represents the heat transfer caused by both the bulk motion and random molecular motion [52].

There are two types of convection which are called *forced* and *natural (free)* convections. If the convection occurs when external forces effect the system then it is called forced convection. As an example, the fans which are used for cooling the electronic items make an

external force for the system. Although there is not any external force on the system, still heat convection can occur due to the temperature difference of the fluid medium. As a result of the temperature difference, the density gradient occurs in the fluid. Then, the buoyancy forces caused by the density gradient effect the system and produce fluid motion in the system. Therefore, since it naturally occurs it is called *natural* or *free* convection. If these two types of convection occur at the same time, then it is called *mixed* convection [52].

The vector form of the governing equations for the natural convection flow are given with continuity, momentum and energy equation [96]

$$\nabla \mathbf{V} = 0 \quad (1.29)$$

$$\widehat{\rho} \frac{\partial \mathbf{V}}{\partial t} + \widehat{\rho} \mathbf{V} \cdot \nabla \mathbf{V} = -\nabla p + \mu \nabla^2 \mathbf{V} + \widehat{\rho} \widehat{\mathbf{F}} \quad (1.30)$$

$$\widehat{\rho} c \frac{\partial T}{\partial t} + \widehat{\rho} c \mathbf{V} \cdot \nabla T = k \nabla^2 T. \quad (1.31)$$

Here, $\widehat{\mathbf{F}}$ is the body force, c is the specific heat, T is the temperature and k is the coefficient of the thermal conductivity.

Nondimensional natural convection flow equations in two-dimensional Cartesian coordinates are

$$\frac{\partial u}{\partial x} + \frac{\partial v}{\partial y} = 0 \quad (1.32)$$

$$\begin{aligned} \frac{\partial u}{\partial t} + u \frac{\partial u}{\partial x} + v \frac{\partial u}{\partial y} &= -\frac{\partial p}{\partial x} + Pr \left(\frac{\partial^2 u}{\partial x^2} + \frac{\partial^2 u}{\partial y^2} \right) \\ \frac{\partial v}{\partial t} + u \frac{\partial v}{\partial x} + v \frac{\partial v}{\partial y} &= -\frac{\partial p}{\partial y} + Pr \left(\frac{\partial^2 v}{\partial x^2} + \frac{\partial^2 v}{\partial y^2} \right) - \frac{Pr Ra}{\beta \Delta T} (1 - \beta T \Delta T) \end{aligned} \quad (1.33)$$

and

$$\frac{\partial T}{\partial t} + u \frac{\partial T}{\partial x} + v \frac{\partial T}{\partial y} = \frac{\partial^2 T}{\partial x^2} + \frac{\partial^2 T}{\partial y^2} \quad (1.34)$$

where the dimensionless parameters are

$$Pr = \frac{\nu}{\alpha} = \frac{\mu c}{k}, \quad \text{and} \quad Ra = \frac{g \beta L_0^3 \Delta T}{\alpha \nu}, \quad \beta = -\frac{1}{\widehat{\rho}} \left(\frac{\partial \widehat{\rho}}{\partial T} \right)_p$$

the Prandtl and Rayleigh number, respectively. β is the thermal expansion coefficient, $\nu = \frac{\mu}{\rho_0}$ is the kinematic viscosity with the reference density ρ_0 , $\alpha = \frac{k}{\rho_0 c}$ is the thermal diffusivity, and $\Delta T = T_h - T_c$ is the temperature difference between hot and cold walls.

The Prandtl number is only related to the fluid property. It does not contain any length or velocity scales of the fluid. It gives the ratio between the fluid viscosity and thermal diffusivity. Prandtl number gives a relation between thermal and velocity boundary layers by comparing their thickness. Each fluid has different Prandtl number. As an example, for liquid metal such as mercury $Pr \ll 1$, for gases $Pr < 1$, for light liquids $Pr > 1$ and for oils Prandtl number is very large [96].

The Rayleigh number which is used only for buoyancy driven flow gives an information about what kind of heat transfer occur in the fluid. If the Rayleigh number is less than the critical

value of the fluid then the type of the heat transfer is called conduction, and if it is higher than the critical value of the fluid, then the heat transfer is called convection.

The body force appears in the y -direction of the momentum equation with the Boussinesq approximation

$$\widehat{\rho} = \rho_0[1 - \beta(T - T_c)].$$

Similar to Navier-Stokes equations given in Section 1.3, natural convection flow equations are transformed to stream function-vorticity-temperature form as

$$\nabla^2 \psi = -w \quad (1.35)$$

$$Pr \nabla^2 w = \frac{\partial w}{\partial t} + u \frac{\partial w}{\partial x} + v \frac{\partial w}{\partial y} - Pr Ra \frac{\partial T}{\partial x} \quad (1.36)$$

$$\nabla^2 T = \frac{\partial T}{\partial t} + u \frac{\partial T}{\partial x} + v \frac{\partial T}{\partial y}. \quad (1.37)$$

Now, the time derivatives in the vorticity transport and energy equations are approximated again by using finite difference

$$\frac{\partial w}{\partial t} = \frac{w^{(n+1)} - w^{(n)}}{\Delta t} \quad \text{and} \quad \frac{\partial T}{\partial t} = \frac{T^{(n+1)} - T^{(n)}}{\Delta t} \quad (1.38)$$

where $w^{(n)} = w(x, y, t_n)$, $T^{(n)} = T(x, y, t_n)$, and $t_n = n\Delta t$.

Vorticity and temperature in Laplace terms are relaxed as

$$w^{(n+1)} = \theta_w w^{(n+1)} + (1 - \theta_w) w^{(n)} \quad \text{and} \quad T^{(n+1)} = \theta_T T^{(n+1)} + (1 - \theta_T) T^{(n)} \quad (1.39)$$

with $0 < \theta_w, \theta_T < 1$. Thus, vorticity transport and energy equations are put in the form of inhomogeneous modified Helmholtz equations to give the iteration

$$\nabla^2 \psi^{(n+1)} = -w^{(n)} \quad (1.40)$$

$$\begin{aligned} \nabla^2 w^{(n+1)} - \tau_w^2 w^{(n+1)} = & -\frac{(1 - \theta_w)}{\theta_w} \nabla^2 w^{(n)} - \tau_w^2 w^{(n)} \\ & + \frac{1}{Pr \theta_w} \left(\frac{\partial \psi^{(n+1)}}{\partial y} \frac{\partial w^{(n)}}{\partial x} - \frac{\partial \psi^{(n+1)}}{\partial x} \frac{\partial w^{(n)}}{\partial y} \right) - \frac{Ra}{\theta_w} \frac{\partial T^{(n)}}{\partial x} \end{aligned} \quad (1.41)$$

$$\begin{aligned} \nabla^2 T^{(n+1)} - \tau_T^2 T^{(n+1)} = & -\frac{(1 - \theta_T)}{\theta_T} \nabla^2 T^{(n)} - \tau_T^2 T^{(n)} \\ & + \frac{1}{\theta_T} \left(\frac{\partial \psi^{(n+1)}}{\partial y} \frac{\partial T^{(n)}}{\partial x} - \frac{\partial \psi^{(n+1)}}{\partial x} \frac{\partial T^{(n)}}{\partial y} \right) \end{aligned} \quad (1.42)$$

between the equations where $\tau_w^2 = \frac{1}{Pr \theta_w \Delta t}$, $\tau_T^2 = \frac{1}{\theta_T \Delta t}$, and n represents the iteration number. Now, the equations are ready to be treated with DRBEM which uses fundamental solution of modified Helmholtz equation.

1.5 Double Diffusive Mixed Convection Flow

The mixed convection has been studied due to its importance in many engineering areas. If the two types of convective heat transfer namely forced and natural convection occur in the system then it is called mixed convection. In other words, if the motion of the fluid is occurred by external force and by itself then it is named as mixed convection [19].

Double diffusive convection, which is also known thermo-solutal convection, is important heat transfer mechanism. The convection is occurred due to at least two different density variations. As an example, in oceanography, heat and dissolved salt make two different density gradients in the fluid.

In this section, double diffusive convection due to the combination of thermal and solutal buoyancy forces is analyzed. Also, the fluid motion is influenced by the external forces. Then, the flow is called double diffusive mixed convection flow.

The vector form of the governing equations are [57]

$$\nabla \mathbf{V} = 0 \quad (1.43)$$

$$\widehat{\rho} \frac{\partial \mathbf{V}}{\partial t} + \widehat{\rho} \mathbf{V} \cdot \nabla \mathbf{V} = -\nabla p + \mu \nabla^2 \mathbf{V} + \widehat{\rho} \widehat{\mathbf{F}} \quad (1.44)$$

$$\frac{\partial T}{\partial t} + \mathbf{V} \cdot \nabla T = \alpha \nabla^2 T \quad (1.45)$$

$$\frac{\partial C}{\partial t} + \mathbf{V} \cdot \nabla C = D \nabla^2 C \quad (1.46)$$

where \mathbf{V} is the velocity, $\widehat{\rho}$ is the density, p is the pressure, μ is the dynamic viscosity, $\widehat{\mathbf{F}}$ is the body force, T is the temperature, α is the thermal diffusivity, C is the concentration of the species and D is the binary diffusivity coefficient.

Nondimensional governing equations in two-dimensional Cartesian coordinates are the continuity, momentum, energy and concentration equations

$$\frac{\partial u}{\partial x} + \frac{\partial v}{\partial y} = 0 \quad (1.47)$$

$$\frac{\partial u}{\partial t} + u \frac{\partial u}{\partial x} + v \frac{\partial u}{\partial y} = -\frac{\partial p}{\partial x} + \frac{1}{Re} \left(\frac{\partial^2 u}{\partial x^2} + \frac{\partial^2 u}{\partial y^2} \right) \quad (1.48)$$

$$\frac{\partial v}{\partial t} + u \frac{\partial v}{\partial x} + v \frac{\partial v}{\partial y} = -\frac{\partial p}{\partial y} + \frac{1}{Re} \left(\frac{\partial^2 v}{\partial x^2} + \frac{\partial^2 v}{\partial y^2} \right) - \frac{gL_0}{U^2} [1 - \beta_T T \Delta T - \beta_C C \Delta C]$$

$$\frac{\partial T}{\partial t} + u \frac{\partial T}{\partial x} + v \frac{\partial T}{\partial y} = \frac{1}{RePr} \left(\frac{\partial^2 T}{\partial x^2} + \frac{\partial^2 T}{\partial y^2} \right) \quad (1.49)$$

$$\frac{\partial C}{\partial t} + u \frac{\partial C}{\partial x} + v \frac{\partial C}{\partial y} = \frac{1}{ReSc} \left(\frac{\partial^2 C}{\partial x^2} + \frac{\partial^2 C}{\partial y^2} \right) \quad (1.50)$$

where $Re = \frac{UL_0}{\nu}$, $Pr = \frac{\nu}{\alpha}$ and $Sc = \frac{D}{\alpha}$ are Reynolds, Prandtl and Schmidt numbers, respectively. Schmidt number gives a relation between viscous diffusion and mass diffusion.

Also, $Ri = \frac{Gr_T}{Re^2}$, $N = \frac{\beta_C \Delta C}{\beta_T \Delta T}$, $Gr_T = \frac{g\beta_T \Delta T L_0^3}{\nu^2}$, and $Gr_C = \frac{g\beta_C \Delta C L_0^3}{\nu^2}$ are Richardson

number, buoyancy ratio and Grashof number due to the mass and thermal diffusivity, respectively, where $\Delta C = C_h - C_c$ is the difference between high and low concentration values. $\beta_T = -\frac{1}{\rho} \left(\frac{\partial \rho}{\partial T} \right)_{p,C}$, $\beta_C = -\frac{1}{\rho} \left(\frac{\partial \rho}{\partial C} \right)_{p,T}$ are the volumetric expansion coefficients with temperature and solutal concentration, respectively. U and L_0 are reference velocity and reference length, respectively, and g is the gravitational acceleration.

Richardson number shows the influence of the thermal buoyancy forces over the fluid inertial force [55]. The value of the Richardson number gives an information about the type of the convection. When $Ri < 0.1$ force convection is dominant and when $Ri > 10$ natural convection is dominant in the fluid medium. But if the Richardson number takes the values between 0.1 and 10, then both of them influence the convective heat transfer. Buoyancy ratio gives a relation between the thermal and solutal buoyancy forces. Grashof numbers are the characteristic numbers for the double diffusive mixed convection flows. The volumetric thermal expansion coefficient β_T is always positive but the volumetric solutal concentration expansion coefficient β_C can be either positive or negative depending on the species concentration. Therefore, thermal Grashof number (Gr_T) is always positive and solutal Grashof number (Gr_C) can be either positive or negative. The sign of the Gr_C has an importance over the behavior of the buoyancy forces depending on the its sign, thermal and solutal buoyancy forces can oppose or aid each other.

Now, in order to eliminate the pressure terms and obtain one equation for the vorticity, the same procedure which is done for the Navier-Stokes and natural convection equations is going to be applied for the equations (1.47)-(1.50). This procedure gives the governing equations

$$\nabla^2 \psi = -w \quad (1.51)$$

$$\frac{1}{Re} \nabla^2 w = \frac{\partial w}{\partial t} + u \frac{\partial w}{\partial x} + v \frac{\partial w}{\partial y} - Ri \left(\frac{\partial T}{\partial x} + N \frac{\partial C}{\partial x} \right) \quad (1.52)$$

$$\frac{1}{RePr} \nabla^2 T = \frac{\partial T}{\partial t} + u \frac{\partial T}{\partial x} + v \frac{\partial T}{\partial y} \quad (1.53)$$

$$\frac{1}{ReSc} \nabla^2 C = \frac{\partial C}{\partial t} + u \frac{\partial C}{\partial x} + v \frac{\partial C}{\partial y}. \quad (1.54)$$

Now, the time derivatives of vorticity, temperature and concentration and the unknowns in the Laplacian terms in equations (1.52)-(1.54) can be approximated as

$$\frac{\partial A}{\partial t} = \frac{A^{(n+1)} - A^{(n)}}{\Delta t}, \quad (1.55)$$

$$A^{(n+1)} = \theta A^{(n+1)} + (1 - \theta) A^{(n)} \quad (1.56)$$

with θ denoting θ_w , θ_T or θ_C in $(0, 1)$, and A denotes w , T or C .

Then, the following iterative equations can be written for thermo-solutal buoyancy induced

mixed convection flow

$$\begin{aligned}
\nabla^2 \psi^{(n+1)} &= -w^{(n)} \\
\nabla^2 w^{(n+1)} - \tau_w^2 w^{(n+1)} &= -\frac{(1-\theta_w)}{\theta_w} \nabla^2 w^{(n)} - \tau_w^2 w^{(n)} \\
&\quad + \frac{Re}{\theta_w} \left(\frac{\partial \psi^{(n+1)}}{\partial y} \frac{\partial w^{(n)}}{\partial x} - \frac{\partial \psi^{(n+1)}}{\partial x} \frac{\partial w^{(n)}}{\partial y} \right) \\
&\quad - \frac{Re Ri}{\theta_w} \left(\frac{\partial T^{(n)}}{\partial x} + N \frac{\partial C^{(n)}}{\partial x} \right) \\
\nabla^2 T^{(n+1)} - \tau_T^2 T^{(n+1)} &= -\frac{(1-\theta_T)}{\theta_T} \nabla^2 T^{(n)} - \tau_T^2 T^{(n)} \\
&\quad + \frac{Re Pr}{\theta_T} \left(\frac{\partial \psi^{(n+1)}}{\partial y} \frac{\partial T^{(n)}}{\partial x} - \frac{\partial \psi^{(n+1)}}{\partial x} \frac{\partial T^{(n)}}{\partial y} \right) \\
\nabla^2 C^{(n+1)} - \tau_C^2 C^{(n+1)} &= -\frac{(1-\theta_C)}{\theta_C} \nabla^2 C^{(n)} - \tau_C^2 C^{(n)} \\
&\quad + \frac{Re Sc}{\theta_C} \left(\frac{\partial \psi^{(n+1)}}{\partial y} \frac{\partial C^{(n)}}{\partial x} - \frac{\partial \psi^{(n+1)}}{\partial x} \frac{\partial C^{(n)}}{\partial y} \right)
\end{aligned} \tag{1.57}$$

where $\tau_w^2 = \frac{Re}{\Delta t \theta_w}$, $\tau_T^2 = \frac{Re Pr}{\Delta t \theta_T}$, and $\tau_C^2 = \frac{Re Sc}{\Delta t \theta_C}$, and n indicates iteration number.

1.6 Natural Convection Flow under a Magnetic Field

Natural convection flow problem is explained in the previous section (Section 1.4). Now, it will be extended to the natural convection flow under a magnetic field. Several forces can effect the natural convection. One of these forces is the Lorentz force which is the total force caused by the influence of the electric and magnetic fields on the fluid. Therefore, both buoyancy and Lorentz forces effect the system as a body force. Natural convection flow under a magnetic field is used in material manufacturing as a control mechanism.

The vector form of the continuity, momentum and energy equations are [39]

$$\nabla \mathbf{V} = 0 \tag{1.58}$$

$$\widehat{\rho} \frac{\partial \mathbf{V}}{\partial t} + \widehat{\rho} \mathbf{V} \cdot \nabla \mathbf{V} = -\nabla p + \mu \nabla^2 \mathbf{V} + \widehat{\rho} \widehat{\mathbf{F}} + \mathbf{J} \times \mathbf{B} \tag{1.59}$$

$$\widehat{\rho} c \frac{\partial T}{\partial t} + \widehat{\rho} c \mathbf{V} \cdot \nabla T = k \nabla^2 T. \tag{1.60}$$

Here, \mathbf{V} is the velocity, $\widehat{\rho}$ is the fluid density, p is the pressure, $\widehat{\mathbf{F}}$ is the body force, c is the specific heat, T is the temperature, k is the coefficient of the thermal conductivity, \mathbf{B} is the magnetic field, \mathbf{J} is the current density given as

$$\mathbf{J} = \sigma (\mathbf{V} \times \mathbf{B}) \tag{1.61}$$

where σ is the electrical conductivity of the fluid. The electric field and the induced magnetic field in the fluid are assumed to be negligible. Two-dimensional governing equations of

natural convection flow under an applied magnetic field are given in nondimensional form as

$$\frac{\partial u}{\partial x} + \frac{\partial v}{\partial y} = 0 \quad (1.62)$$

$$\frac{\partial u}{\partial t} + u \frac{\partial u}{\partial x} + v \frac{\partial u}{\partial y} = -\frac{\partial p}{\partial x} + Pr \left(\frac{\partial^2 u}{\partial x^2} + \frac{\partial^2 u}{\partial y^2} \right) \quad (1.63)$$

$$\begin{aligned} \frac{\partial v}{\partial t} + u \frac{\partial v}{\partial x} + v \frac{\partial v}{\partial y} &= -\frac{\partial p}{\partial y} + Pr \left(\frac{\partial^2 v}{\partial x^2} + \frac{\partial^2 v}{\partial y^2} \right) - Ha^2 Pr v + Ra Pr T \\ \frac{\partial T}{\partial t} + u \frac{\partial T}{\partial x} + v \frac{\partial T}{\partial y} &= \frac{\partial^2 T}{\partial x^2} + \frac{\partial^2 T}{\partial y^2} \end{aligned} \quad (1.64)$$

where the dimensionless parameters

$$Pr = \frac{\nu}{\alpha}, \quad Ra = \frac{g\beta\Delta TL_0^3}{\alpha\nu}, \quad Ha = B_0 L_0 \sqrt{\frac{\sigma}{\rho_0 \nu}}$$

are Prandtl, Rayleigh and Hartmann numbers, respectively. Hartmann number gives a ratio of electromagnetic force to viscous force. B_0 is the intensity of the applied external magnetic field.

After using the same procedure in the natural convection equation to obtain the vorticity transport equation without pressure term, the governing equations take the form

$$\nabla^2 \psi = -w \quad (1.65)$$

$$Pr \nabla^2 w = \frac{\partial w}{\partial t} + u \frac{\partial w}{\partial x} + v \frac{\partial w}{\partial y} + Ha^2 Pr \frac{\partial v}{\partial x} - Ra Pr \frac{\partial T}{\partial x} \quad (1.66)$$

$$\nabla^2 T = \frac{\partial T}{\partial t} + u \frac{\partial T}{\partial x} + v \frac{\partial T}{\partial y}. \quad (1.67)$$

In order to obtain modified Helmholtz equations for the vorticity transport and energy equations, we use the same approximations given in (1.38) and (1.39) for the time derivatives, and vorticity and temperature terms which are located in the Laplace terms in (1.66) and (1.67). Finally, the governing equations for the natural convection flow under a magnetic field contain modified Helmholtz equation for vorticity and temperature, and are given in an iterative procedure as

$$\nabla^2 \psi^{(n+1)} = -w^n \quad (1.68)$$

$$\begin{aligned} \nabla^2 w^{(n+1)} - \tau_w^2 w^{(n+1)} &= -\frac{(1-\theta_w)}{\theta_w} \nabla^2 w^{(n)} - \tau_w^2 w^{(n)} \\ &+ \frac{1}{Pr\theta_w} \left(\frac{\partial \psi^{(n+1)}}{\partial y} \frac{\partial w^{(n)}}{\partial x} - \frac{\partial \psi^{(n+1)}}{\partial x} \frac{\partial w^{(n)}}{\partial y} \right) - \frac{Ha^2}{\theta_w} \frac{\partial \psi^{(n+1)}}{\partial x^2} - \frac{Ra}{\theta_w} \frac{\partial T^{(n)}}{\partial x} \end{aligned} \quad (1.69)$$

$$\begin{aligned} \nabla^2 T^{(n+1)} - \tau_T^2 T^{(n+1)} &= -\frac{(1-\theta_T)}{\theta_T} \nabla^2 T^{(n)} - \tau_T^2 T^{(n)} \\ &+ \frac{1}{\theta_T} \left(\frac{\partial \psi^{(n+1)}}{\partial y} \frac{\partial T^{(n)}}{\partial x} - \frac{\partial \psi^{(n+1)}}{\partial x} \frac{\partial T^{(n)}}{\partial y} \right) \end{aligned} \quad (1.70)$$

where $\tau_w^2 = \frac{1}{Pr\theta_w\Delta t}$, $\tau_T^2 = \frac{1}{\theta_T\Delta t}$, and n represents the iteration number. DRBEM solution procedure will be used for ψ using the fundamental solution of Laplace equation, and for w and T using the fundamental solution of modified Helmholtz equation, respectively.

1.7 Literature Survey

The Navier-Stokes equations have attracted the attention of the scientific computational community. Actually, it is one of the most studied subject in the computational fluid dynamics field. So, there are many studies on the numerical solutions of the equations by using different numerical methods.

The steady-state incompressible Navier-Stokes equations in the primitive variable formulation are solved with an automatic adaptive refinement technique which has been coupled to multi-grid approach to obtain efficient and stable solution strategy [90]. The test problems are defined in a driven cavity and in a horizontal channel with a backward-facing step. The computational results are given for Reynolds number up to 5000 and 800, respectively. Incompressible fluid motion given by the Navier-Stokes equations is studied by Skerget *et.al* in [86]. Velocity-vorticity form of Navier-Stokes equations is solved with a boundary-domain integral method and the solutions are given for several Benchmark problems. Sahin and Owens [83], used a novel implicit cell-vertex finite volume method for the solution of Navier-Stokes equations. In the study, multiplying the momentum equations with the unit normal vector, they eliminate the pressure term from the momentum equations. This way, they get rid of the difficulties caused by the pressure or vorticity boundary conditions. The computational results are obtained for Reynolds numbers up to 10000 for both steady and unsteady two dimensional lid-driven cavity problem.

Wu and Shao [98], solved two-dimensional near-incompressible steady lid-driven cavity flows by using the Lattice Boltzmann method using MRT (multi-relaxation-time) and SRT (single-relaxation-time). The results are given by comparing these two methods and previous simulation data using the same flow conditions. A new messless scheme which is combined with the radial basis functions method is given for solving unsteady incompressible Navier-Stokes equations in vorticity-stream function formulation in [99]. The efficiency and accuracy of the method are shown by giving some numerical examples. Wong and Chan [97] presented a study for unsteady incompressible Navier-Stokes equations with the Dirichlet type boundary conditions using the consistent splitting scheme. The efficiency of the method is analyzed by using the problems which have exact solutions, and solving several two-dimensional double lid-driven cavity problems. A lattice Boltzmann model (LBM) for the solution of two-dimensional unsteady incompressible flow in vorticity-stream function formulation is given by Chen *et.al* in [29]. They examined their model by solving several benchmark problems and claimed that their model was simpler and more efficient than LBMs which are used with the primitive variables formulation. Erturk [40] made a study about the two-dimensional driven cavity flow by considering its physical, mathematical and numerical situations. In his study, also a literature review is done for the driven cavity flow problem.

Natural convection flow in enclosures plays an important role in many engineering applications such as nuclear reactor insulation, cooling of electronic components, solar energy collection, building heating and cooling systems, and crystal growth in liquids. Two-dimensional, steady, laminar fluid motion caused by the temperature gradient in an enclosed cavity is described first by De Vahl Davis [34]. Forward and central difference approximations are used as a numerical method with the primitive variable formulation and the results are given for Rayleigh numbers up to 2×10^5 , and aspect ratio up to 5. Bejan and Tien [20], examined the heat transfer by free convection in a horizontal channel with adiabatic walls and differentially heated end walls. They developed three methods for the heat transfer mechanism in a cavity

with the aspect ratio less than one, which are the intermediate and boundary layer regimes as $Ra \rightarrow 0$.

A comprehensive study for the natural convection in a square cavity is done in [36]. In the study, they summarized and discussed several contributions by comparing their accuracy for the benchmark solutions. In the computations, they used finite difference method for stream function-vorticity formulation of the problem. Forward difference and second order central difference are used for the time derivative and all the space derivatives, respectively. Another study for the natural convection of air in a square cavity is done in [35]. In this study, again the stream function-vorticity formulation is used with the same combination of the forward and central difference approximations. The results are obtained for values of Rayleigh number between $10^3 \leq Ra \leq 10^6$ by using mesh refinement and extrapolation. Natural and forced convective heat transfer in a liquid thermal storage tank is studied by Guo and Wu in [47]. Stream function-vorticity formulation is used for the two-dimensional unsteady problem. The results are obtained for very large Grashof and Reynolds numbers for the first time by using the alternating direction implicit (ADI) scheme.

A numerical study on natural convection flow inside a right-angled cavity formed by a hot vertical and a cold horizontal wall is presented by Kimura and Bejan [53]. In the study, there are the scale analysis, numerical simulation and an asymptotic solution in the $Ra \rightarrow 0$ limit. The stream function-vorticity equations are solved with Allen-Southwell finite difference scheme with the combination of point iterative method. November and Nansteel [70] investigated an analytical and numerical study on steady natural convection flow in a square water-filled enclosure heated from below and cooled from one side. Expansions of the variables ($\psi - w - T$) for low Reynolds number are obtained to order Ra^2 , and finite difference solutions are given for $0 \leq Ra \leq 10^6$. A comprehensive article on this subject is given in [43]. The aim of the study is to inform the reader what has been accomplished and what remains to be investigated about the laminar flows in a rectangular cavity.

The study of Barakos *et.al* [16] represented a numerical simulation for the benchmark problem of natural convection flow in a square cavity. In their study, the control volume method is used to solve governing equations for laminar and turbulent flows, and the results are obtained for the Rayleigh number values up to 10^{10} . Also, in order to accelerate the convergence, a mixed technique is used for the solution of final algebraic equations which are alternating direction implicit (ADI), and strongly implicit (SIP) methods. A numerical study on steady natural convection in a rectangular enclosure heated from below and symmetrically cooled from both sides is conducted by Ganzarolli and Milanez [44]. The Allen-Southwell finite difference scheme is used as a numerical method for the stream function-vorticity formulation. The computational results are obtained for $10^3 \leq Ra \leq 10^7$ by taking the $Pr = 0.7$, $Pr = 7.0$, and the aspect ratio is varied from 1 to 9. Aydin *et al.* [14, 15] investigated the heat transfer characteristics in two-dimensional enclosure heated from one side and cooled from above. The computational results are obtained using finite difference method in a range $10^3 \leq Ra \leq 10^7$. The effects of Rayleigh number are examined by changing inclination angle in the range $0^\circ - 360^\circ$ in [14], and the aspect ration in the range 0.25 – 4.0 in [15].

In another study, the diffusion-convective transport problems are solved with a mixed boundary element formulation (the boundary domain integral method using subdomains) by Ramsak and Skerget in [79]. The method is given for incompressible unsteady Navier-Stokes equations in a velocity-vorticity formulation. Numerical results are given for the driven cavity problem with $Re = 100, 400$ and 1000 , and for the natural and forced convection in a cavity

in the range $10^3 \leq Ra \leq 10^6$. Moshkin [66] presented a numerical study for the natural convection in a rectangular enclosure filled with two immiscible fluids. The numerical results are obtained using finite difference method and compared with the laboratory experiments. Another study with the finite difference method is done by Volgin *et.al* [95] for the unsteady ion transfer under the conditions of natural convection problem. They used an implicit difference scheme to calculate the distribution of electrolyte species concentrations. Therefore, efficient results are obtained at large Schmidt numbers where large Schmidt number is a typical characteristic of electrochemical system. Two-dimensional natural convection in an enclosure is solved by means of two different software packages based on Galerkin finite element method, and results are obtained for Rayleigh numbers in the range $10^3 \leq Ra \leq 10^5$ by Barletta *et.al* [17]. From the study one can conclude that, an elliptical wall increases the mean Nusselt number and dimensionless kinetic energy of the fluid.

Mixed convective heat and solutal transport play an important role in many engineering applications such as plasma spray coating, nuclear waste disposal, crystal growth and oceanography. In simulation of a real problem of continuous removal of pollutants generated at the bottom wall of a cavity by the moving top lid, the interaction between fluid inertial force and thermosolutal buoyancy forces on convective heat and mass transfer becomes important. Alleborn *et al.* [6] concerned with heat and mass transfer of steady two-dimensional flow in a shallow lid-driven cavity with a moving heated bottom lid, and a cooled top lid moving with a different constant velocity. Stream function- vorticity formulation of governing equations are discretized with second order finite difference scheme. In their study an analytical solution for limiting situations, like different cavity orientation and limiting values of parameters, is given. Aydin [13] conducted a numerical study to investigate the transport mechanism of laminar mixed convection in a shear- and buoyancy-driven cavity where the left wall is moving across the cavity from bottom to top at a uniform velocity. Control volume-based finite difference method was used in the computations. The aiding and opposing effects of buoyancy forces were characterized by considering two different implementations of the thermal boundary conditions.

Deng *et al.* [37] numerically studied laminar double-diffusive mixed convection in a two-dimensional ventilated enclosure with discrete heat and contaminant sources by investigating the effects of Grashof number, buoyancy ratio, Reynolds number and ventilation mode. Computational results which are obtained using finite volume method showed that the indoor air, heat and contaminant transport are caused by the interaction between fluid inertial force and external forces. Al-Amiri *et al.* [5] numerically investigated steady mixed convection in a square cavity under the combined buoyancy effects of thermal and mass diffusion by using the Galerkin's weighted residual finite element method. In this study, they obtained the results with a wider range of Richardson number. Maiti *et al.* [64] presented a numerical study about heat and mass transfer of two-dimensional, unsteady and laminar flow in a square cavity with a moving top lid. Because of the defined boundary conditions for the temperature and concentration on the top lid and bottom wall, vertical temperature and concentration gradients occur on the flow. The computational results are obtained from the finite volume method. The influence of solutal and thermal buoyancy forces on the flow, and the effect of shearing of the top lid are analyzed by different situations.

The velocity-vorticity form of Navier-Stokes equations was used for the analysis of the double-diffusive mixed convection in a lid-driven cavity in [54], in a lid-driven cavity with a heated blockage at the bottom wall of the cavity in [57, 58]. In these studies the Galerkin's weighted residual finite element method is used as a numerical procedure. Kumar *et al.* [54] exam-

ined deeply the interaction between fluid inertial force and thermo-solutal buoyancy forces on convective heat transfer by using various values of Richardson number (Ri), Reynolds number (Re) and buoyancy ratio (N). In [57], first the same problem with [5] (the double-diffusive mixed convection in a lid-driven cavity) is solved, and the results are compared to determine the mesh sensitivity of the method. Then, method is used to solve the problem in a lid-driven cavity with a heated square blockage at the bottom wall of the cavity, and the results are given for the values of N between -100 to 100 . In [58], the problem is defined in a lid-driven cavity with a heated square blockage at different aspect ratio, and numerical results are obtained by changing the variables Ri , N , Re and aspect ratio.

In addition, convective heat transfer in flow through channels with backward-facing step (BFS) is important in engineering applications such as heat exchanger devices, electronic cooling and turbine blade cooling. The recirculation region effects the convection heat transfer characteristics of the system. Therefore, it is important to understand the mechanisms of heat transfer. A numerical analysis is carried for two-dimensional, steady and incompressible flow to investigate the heat transfer and the characteristics of the flow by Abu-Nada et al. in [4]. Under the effect of suction and blowing, which are implemented on the bottom wall, the reattachment length and the length of the top secondary recirculation bubble are computed by using the finite volume method. Velazquez et al. [94] presented the effect of forced flow pulsation on heat transfer for incompressible laminar flow in two-dimensional channel with backward facing step. Finite-point formulation which was developed by themselves is used to solve the problem. The influence of fluid recirculation on heat transfer in BFS with porous floor segments placed after the step is presented in [2, 30]. Abu-Hijleh [2] used finite element method with nonuniform rectangular mesh, and investigated the effect of additional porous floor segment in the forced convection heat transfer characteristics of the flow field. Chen et al. [30] used SIMPEC method in the numerical computations, and different from the one-domain approach of Abu-Hijleh [2] they preferred to use two-domain approach in their computations. A review study about the single-phase, laminar mixed convection flow over vertical, horizontal, inclined backward/forward facing steps is presented by Abu-Mulaweh in [3]. The intent of the study is to summarize the literature by analyzing the effect of the parameters such as Re , Pr , buoyancy force, freestream, inclination angle, step height, expansion ratio and temperature difference between the walls.

Brown and Lai [25] investigated the problem of combined heat and mass transfer for horizontal channel with an open cavity heated on the bottom wall. In the computations, numerical results are obtained by using different values of buoyancy ratio, Lewis number and Reynolds number to obtain the correlations of combined heat and mass transfer by mixed convection. Another study for two-dimensional, steady heat transfer and fluid flow in a vertical pipe with downward and upward flow is given by Teamah et al. [89]. Parametric conditions are analyzed by giving graphical results. In these last two studies, finite difference method was used as a numerical technique.

In the BFS channel problems both the solutal buoyancy force and the thermal buoyancy force contributions must be taken into consideration on the flow field variation and heat transfer. The density gradients, which are generated by the solutal concentration and temperature difference gradients, develop the solutal and thermal buoyancy forces. At the channel entry, the fluid inertial forces are dominant but when the fluid moves between the walls, the thermo-solutal buoyancy forces influence the flow field structure. If the convective heat transfer contains the thermo-solutal buoyancy forces, then it is called double diffusive mixed convection. When the temperature and solutal concentration boundary conditions are changed,

the thermal and solutal buoyancy forces can oppose or aid each other. There are studies on the changes in recirculatory flow behavior because of the thermo-solutal buoyancy forces in a BFS horizontal channel in [55, 56], and Galerkin's finite element method was used to obtain the numerical results.

In material manufacturing industry, in cooling of nuclear reactors, the important phenomena is the external magnetic field. The Lorentz force caused by the magnetic field is used as a control mechanism to obtain good quality product in the manufacturing process. Since Lorentz force reduces the velocity, it affects the rate of heat and mass transport in the fluid. Therefore, the characteristic of the transport has attracted the attention in computational fluid dynamics field. A numerical study is presented for the effect of magnetic field on natural convection flow in a rectangular enclosure by Rudraiah *et.al* [82]. Numerical results of the stream function-vorticity formulation of the problem are given for a wide range of Grashof and Hartmann number using a finite difference scheme with the combination of ADI and SLOR (Successive Line Over Relaxation) methods. Al-Najem *et.al* [7] used the finite volume method to analyze the effect of magnetic field on the natural convection flows in the tilted enclosures. ADI method is used to accelerate the solutions towards steady-state.

Oztop *et.al* [71] studied magnetohydrodynamic (MHD) buoyancy driven heat transfer and fluid flow in a non-isothermally heated square enclosure. The finite volume method is used to solve primitive variable formulation of the governing equations. They analyzed the effect of Rayleigh number (Ra), Hartmann number (Ha) and amplitude of sinusoidal function (n) on temperature and flow fields. In the study, it is concluded that when Ra or n increases, the heat transfer increases but when Ha increases the heat transfer decreases. So, Hartmann number can be used as a control parameter for the heat transfer of the fluid. The thermal lattice Boltzmann scheme is used to solve the incompressible natural convection flow under a magnetic field for three different cases in [32]. These cases are classified with respect to location of the zones of the magnetic field. Also, Sheikhzadeh *et.al* [87] presented a study for the tilted cavity with the control volume based finite volume method. The effect of magnetic field is analyzed by changing the aspect ratio, inclination angle and the location of the partially tilted thermal walls. The results show that, together with the magnitude of the Hartmann number all the variables affect the heat transfer of the fluid.

The differential quadrature method (DQM), introduced by Bellman and Casti in [21], gives an efficient discretization technique to obtain accurate numerical solutions. The applications of DQ method has been implemented for solving engineering problems in [88]. Lo *et al.* [62] solved the benchmark problem of 2D unsteady natural convection flow in a cavity by using DQM. In their solution method, second order finite difference approximation is used for the time derivative. They obtained the results for $10^3 \leq Ra \leq 10^7$ and aspect ratios changing from 1 to 3. Ece and Büyük [39] uses DQM in the solution of steady natural convection flow under a magnetic field in an inclined rectangular enclosure heated and cooled on adjacent walls with various Grashof and Hartmann numbers. Their results showed that strength and direction of the magnetic field, the inclination angle and the aspect ratio affect the convection heat transfer and the characteristic of the fluid.

Dual reciprocity boundary element method (DRBEM) is a numerical solution technique which can treat the nonlinearities in the partial differential equations by taking them as right hand side functions [73]. In DRBEM, only a boundary integral equation is obtained for inhomogeneous, nonlinear or time dependent problems by eliminating the domain integral through the BEM formulation. Sarler and Kuhn [84] studied DRBEM solution of two-dimensional

Navier-Stokes equations using the primitive variable formulation. Numerical results are given for the lid-driven cavity flow problem for $Re = 100$. The DRM subdomain decomposition approach is used for the solution of two-dimensional Navier-Stokes equations by Power and Mingo in [77]. In this approach the original domain is divided into several subdomains and in each subdomain the integral representation is given. The numerical results are given for lid-driven cavity and backward facing step flow for different Reynolds numbers. The subdomain decomposition method also is used for the Navier-Stokes equations in [41] and [42]. Florez and Power [41], Florez *et.al* [42] used this method by obtaining small quadrilateral elements which have isoparametric linear continuous or discontinuous boundary elements. The thin plate splines ($r^2 \log r$) are used in the integral representation of the subdomains. DRBEM is used for two-dimensional unsteady incompressible Navier-Stokes equations by Choi and Balaras in [33]. A fractional step algorithm is utilized for the time advancement, and Adam-Bashforth scheme is used for the nonlinear convective terms. The numerical results are obtained for Taylor-Green vortex and lid-driven cavity flows, and compared with the analytical solution and the results in the literature, respectively. Ghadimi and Dashtimanesh [45] presented a new coupled method for solving the stream function-vorticity formulation of the Navier-Stokes equations. They used finite difference method for the solution of vorticity transport equation, and DRBEM for the solution of stream function equation. They compared the numerical results with a benchmark problem.

Steady natural convection in Darcy-Brinkman porous media in a two-dimensional differentially heated rectangular cavity is solved by Sarler *et.al* in [85] with DRBEM. The method is based on augmented scaled thin plate splines and numerical results are obtained using constant, linear and quadratic boundary elements with different mesh size, uniform and non-uniform mesh arrangement. Gümüş and Tezer-Sezgin [48, 49] numerically investigated the unsteady natural convection of nanofluids and micropolar fluids, respectively. In [48], the problem is solved with DRBEM and implicit Euler scheme is used for the time derivative. Also vorticity boundary conditions are obtained using the Taylor series expansion of stream function. In [49], they again used DRBEM for the solution of the problem but in this case vorticity boundary conditions are obtained using the DRBEM coordinate matrix. Bozkaya and Tezer-Sezgin [26] solved the natural convection flow in differentially heated enclosure by using the coupling of the DRBEM in space with the DQM in time. They solved three test problem which are two-dimensional Navier-Stokes equations including a force term, lid-driven cavity flow and natural convection flow in a square cavity. The results are given for $500 \leq Re \leq 2000$, $100 \leq Re \leq 1000$ and $10^3 \leq Ra \leq 10^5$, respectively.

Alsoy-Akgün and Tezer-Sezgin [9] used DRBEM procedure in the solution of the natural convection and lid-driven flow problems in cavities. The results are obtained for Navier-Stokes equations in a lid-driven cavity with Re values up to 2000, and $Ra = 10^6$ is achieved for natural convection flow in enclosures. In another study of Alsoy-Akgün and Tezer-Sezgin [10] natural convection in a cavity under a magnetic field is solved by using DRBEM. Results are obtained again up to Ra values of 10^6 , and Hartmann number $Ha = 300$. In both problems, stream function-vorticity formulation is used. The vorticity and energy equations are transformed to modified Helmholtz equations by utilizing forward difference with relaxation parameters for the time derivatives before discretization in space direction is performed. This procedure eliminates the need of another time integration scheme in vorticity transport and energy equations. The resulting modified Helmholtz equations are solved by DRBEM using the fundamental solution $K_0(x)$ whereas in the stream function Poisson's equation $\ln(x)$ is made use of. The inhomogeneities are approximated by using coordinate functions $f = 1 + r$

in the stream function equation, and $f = r^2 \log r$ or $f = 1 + r^2 + r^3 - \lambda \left(\frac{r^2}{4} + \frac{r^4}{16} + \frac{r^5}{25} \right)$ in the vorticity and energy equations. Also, natural convection flow problem is solved by DQM by transforming the vorticity transport and energy equations to the modified Helmholtz equation. The results obtained from DRBEM and DQM are compared in terms of accuracy and computational cost.

Alsoy-Akgün and Tezer-Sezgin [11, 12] presented the DRBEM solution of the two-dimensional thermo-solutal buoyancy-driven flow problems. The mixed convective heat and solutal transport in a lid-driven cavity and in a horizontal channel with backward-facing step are given in [11], and in a lid-driven square cavity with a square blockage placed at the bottom wall is given in [12]. In all problems, stream function, vorticity, temperature and concentration variables are used. The vorticity, energy and concentration equations are transformed to modified Helmholtz equations by using the same procedure in [9, 10]. The inhomogeneities are approximated by using coordinate functions $f = 1 + r$ in the stream function equation and $f = r^2 \log r$ in the vorticity, energy and concentration equations.

There are many applications in heat and mass transfer, e.g. re-entry of vehicles into the atmosphere, combustion chamber processes, in which high temperatures/ high pressures prevent the measurement, or the prescription of known boundary conditions on the hostile portion of the surface of a specimen. Instead, measurements of both temperature and heat flux may be available on the remaining friendly portion of the surface, or even internal temperature values may be more conveniently measured. This gives rise to an inverse problem and many efforts have been devoted in the past for solving the inverse heat conduction problem for the temperature satisfying the heat equation only, see the excellent book by Beck *et al.* [18].

Later on, inverse convection-diffusion problems received the attention of several researchers. Moutsoglou [67] investigated the steady inverse natural-convection between vertical parallel plates, whilst Huang and Ozisik [51] solved an inverse forced-convection problem in a channel. Cauchy inverse problems for convection-diffusion equation have been investigated in [81, 59, 80], whilst for advection-diffusion and reaction-diffusion equations in [60, 65], respectively. In all these papers the coupling between the fluid velocity and the temperature was not taken into account. However, the main difficulty in the inverse convection problem arises when the flow and temperature equations are coupled nonlinearly. This coupling was taken into account in [61].

Alsoy-Akgün and Lesnic [8] extended the analysis to inverse natural magneto-convection problems. The inclusion of the magnetic field acting on the fluid results in the Lorentz force interacting with the buoyancy force in the equations governing the fluid flow and temperature field. This way the Lorentz force suppresses the convection currents by reducing velocities. The direct problem was solved with DRBEM by Alsoy-Akgün and Tezer-Sezgin in [10] and the numerical results were given for various values of Ra and Ha . These results are used as missing boundary conditions for DRBEM solution of the inverse problem, and the numerical results represented stable and reasonably accurate approximation to desired direct problem heat flux output.

1.8 Contributions in the Thesis

In this thesis, some physically important time-dependent fluid dynamics problems such as lid-driven cavity flow, natural convection flow in enclosures, double diffusive mixed convection flow, and natural convection flow under a magnetic field are solved by using dual reciprocity boundary element method. The previously known dual reciprocity boundary element method applications are always for the Poisson type differential equations. In this thesis, the governing equations containing time derivatives are transformed first to the form of inhomogeneous modified Helmholtz equations by discretizing time derivatives using the forward finite difference approximation. Thus, the formulation of dual reciprocity boundary element method is given for inhomogeneous modified Helmholtz equations with the fundamental solution $\frac{1}{2\pi}K_0(r)$ of modified Helmholtz equation. Since, the inhomogeneity of the modified Helmholtz equation is approximated by using radial basis functions the corresponding particular solution must be derived. In this thesis, corresponding particular solutions and their normal derivatives for polynomial radial basis functions are obtained starting from particular solutions. For the thin plate splines the annihilator method is used for obtaining particular solutions. These form the original core part of the thesis. Behind these, dual reciprocity boundary element method is used for the solution of time-dependent, inverse natural convection flow in the presence of a magnetic field in the form of inhomogeneous modified Helmholtz equation [8]. This is achieved for the first time in the literature. Numerical experiments are carried for two test problems, accurate and stable results are obtained for the temperature and heat flux with various Hartmann and Rayleigh numbers.

1.9 Plan of the Thesis

The thesis aims to apply dual reciprocity boundary element method to some fluid dynamics problems such as lid-driven cavity flow, natural convection and mixed convection flows in enclosures, either in direct or inverse formulations. For this, governing equations are transformed first to the modified Helmholtz equations, and DRBEM is used with its fundamental solution capturing more information from the dominating operator. Particular solutions corresponding to radial basis functions used in the approximation of inhomogeneities are derived. These are the main contributions made in the thesis for using DRBEM in the physical problems considered. The thesis is organized as follows.

Chapter 2 presents the derivation of the dual reciprocity boundary element method for Poisson and inhomogeneous modified Helmholtz equations giving the corresponding boundary integral equations. The fundamental solution $\ln(x)$ of Laplace equation is used for the Poisson equation, and the fundamental solution $K_0(x)$ of modified Helmholtz equation is used for the inhomogeneous modified Helmholtz equation. The discretization of the boundary for both problems is done by using constant boundary elements, and the resulting system of algebraic equations are obtained. The DRBEM solution of unsteady partial differential equations by transforming them to the modified Helmholtz equations is the main idea of this thesis. Thus, partial differential equations governing unsteady physical problems such as Navier-Stokes equations and equations of natural convection, mixed convection flows are all transformed first to the form of modified Helmholtz equations. The inhomogeneity term of the modified Helmholtz equation is approximated by using several radial basis functions, and corresponding particular solutions and their normal derivatives are obtained by using annihilator method

for each case. In the last part of the chapter, dual reciprocity boundary element method is explained for the inverse problem defined by the modified Helmholtz equation. Thus, the method is made available for the solutions of both direct and inverse problems of any partial differential equation.

Chapter 3 presents the application of the polynomial-based differential quadrature method for the modified Helmholtz equation which is the transformed form of the partial differential equation defining a physical fluid dynamics problem. Typical nonuniform grid point distributions which give more stable numerical results for the differential quadrature method are described for the domain discretization. The discretization and insertion of the Dirichlet and Neumann type boundary conditions in differential quadrature method is explained at the end of the chapter.

Chapter 4 emphasizes on the solution of direct and inverse partial differential equations using DRBEM and DQM. At the beginning of the chapter, the validity of the DRBEM using fundamental solution of modified Helmholtz equation, and efficiency of different radial basis functions are tested with some problems by comparing obtained numerical results with the exact solutions. DRBEM is used for the solution of physical problems which are Navier-Stokes equations, natural convection flow, double diffusive mixed convection flow and natural convection flow under a magnetic field. The governing equations are solved with constant elements using the stream function-vorticity formulation. Since vorticity, temperature and concentration equations are transformed to the modified Helmholtz equations, resulting equations are solved by DRBEM using the fundamental solution $K_0(x)$ whereas stream function Poisson equation is solved by DRBEM using the fundamental solution $\ln(x)$. The inhomogeneity of stream function equation is approximated with the coordinate function (radial basis function) $f = 1 + r$, and the inhomogeneities of vorticity, temperature and concentration equations are approximated with coordinate function $\bar{f} = r^2 \log r$. In addition, natural convection flow under a magnetic field is solved by DRBEM with the fundamental solution of modified Helmholtz equation using $\bar{f} = 1 + r^2 + r^3 - \tau \left(\frac{r^2}{4} + \frac{r^4}{16} + \frac{r^5}{25} \right)$ as a coordinate function. Natural convection flow under a magnetic field which is in the form of Poisson type stream function and modified Helmholtz type vorticity and energy equations is also solved with DQM. Results obtained from DRBEM and DQM procedures are compared in terms of accuracy and computational effort. Finally, the inverse problem is described for the natural convection flow under a magnetic field. Then, the application of the DRBEM with the fundamental solution of modified Helmholtz equation is explained for the inverse problem. The computational results are obtained for two problems with different boundary conditions which are solved before as direct problems using DRBEM.

CHAPTER 2

THE DUAL RECIPROCITY BOUNDARY ELEMENT METHOD

Many engineering and physical problems are represented with differential equations and very few of them can be solved analytically. So, for the solution of these equations it is necessary to find accurate and efficient numerical solution method. In the literature, for this aim there are several numerical methods which have different advantages or disadvantages. Classical methods such as finite element method (FEM) or finite difference method (FDM) discretize the domain of the problem by using a number of elements or cells and these methods are called domain methods. The use of these type of solution techniques causes to obtain large discretized systems and needs extra computational effort.

Boundary element method (BEM) can be used as an alternative numerical method for the solution of the differential equations. It transforms a differential equation defined in a domain to an integral equation defined on its boundary. Therefore, it is enough to discretize only the boundary instead of all the domain. BEM is very suitable technique for the solution of homogeneous differential equations. However, when the method is used for the inhomogeneous differential equations, the inhomogeneity results in a domain integral. So, the method loses its advantage. Also, in the process of obtaining a boundary integral equation it is necessary to use the fundamental solution of the original differential equation. In some physical problems involving time dependence, convection terms or nonlinearity it cannot be possible to find a fundamental solution for the governing differential equation. This emerges the need of modifications on BEM for treating inhomogeneities, nonlinearities and time dependence in the differential equation.

Dual reciprocity boundary element method (DRBEM) is a useful method to overcome these problems. In the DRBEM, a boundary formulation is obtained for inhomogeneous, nonlinear and time dependent problems by eliminating the domain integral. The basic idea of the DRBEM is to treat all these terms as the inhomogeneity (forcing term) in the differential equation, and then is to approximate forcing term by a series of radial basis functions. Thus, BEM formulation can be carried out with the fundamental solution of mostly known differential equation as Laplace or biharmonic equation. Also, it is important that, the forcing term of the governing equation be kept as simple as possible so that the interpolation error can be reduced to a minimum. This is achieved by leaving convection terms or reaction terms on the left hand side (in the governing differential operator) for which the corresponding fundamental solution is still available. Fundamental solution of Laplace, biharmonic and convection diffusion equations are already known and given in [22, 73]. Reaction terms are generally result in modified Helmholtz equation in which corresponding fundamental solution is rather

complicated to obtain.

In this chapter, the basic theory of DRBEM is given for two cases. The first case is DRBEM formulation for Poisson equation, and the second case is DRBEM formulation for inhomogeneous modified Helmholtz equation which are explained in Section 2.1 and Section 2.2, respectively. Modified Helmholtz equation can also be obtained when a time derivative is discretized at two time levels at the beginning of the solution procedure. In this thesis, the partial differential equations are put in the form of modified Helmholtz equations discretizing the time derivative first, and applying DRBEM to the modified Helmholtz operator. Corresponding particular solutions for the radial basis functions used in the approximation of inhomogeneities are derived. This forms the main original part of the thesis.

Obtaining a particular solution analytically for the Laplace operator $L = \nabla^2$ and the biharmonic operator $L = \nabla^4$ can be possible done by repeated integrations [46, 28, 73]. For that reason most of the differential operators were restricted to the form $\nabla^2 u = b(x, y, u, u_x, u_y)$ when the DRBEM was used [73]. We have arranged the differential equations in the form $\nabla^2 u - \tau^2 u = b(x, y, u, u_x, u_y)$, and approximated the function b by using several radial basis functions for which corresponding particular solutions are also obtained in Section 2.2.

Generally, DRBEM is used as a solution technique for the direct problems, but it can also be used for an inverse problem. We explain the use of DRBEM for the solution of the inverse problem which is again defined with modified Helmholtz operator in Section 2.3 indicating some advantages of the method.

2.1 DRBEM Solution of Poisson Equation $\nabla^2 u = b_1(x, y)$

DRBEM is also a boundary only solution method which transforms domain integrals into equivalent boundary integrals, and gives the solution at required interior points at the same time. The solutions are obtained by using less computational time and data preparation effort since it discretizes boundary only. As a difference from the BEM, it does not need to use the fundamental solution of the original equation.

In this part, the DRBEM will be discussed for the Poisson equation where the right hand side function contains only space variables by giving the derivation of boundary integral equations.

2.1.1 Boundary Integral Equation for the Poisson Equation

Dual reciprocity boundary element method is going to be explained by constructing the boundary integral equation as in [22, 73]. Let us consider the following two dimensional Poisson equation

$$\nabla^2 u = b_1(x, y) \quad , \quad (x, y) \in \Omega \quad (2.1)$$

with the Dirichlet and/or Neumann boundary conditions

$$\begin{aligned} u(x, y) &= \bar{u}(x, y) \quad , \quad (x, y) \in \Gamma_1 \\ q(x, y) &= \frac{\partial u}{\partial n} = \bar{q}(x, y) \quad , \quad (x, y) \in \Gamma_2 \end{aligned} \quad (2.2)$$

where ∇^2 is the Laplace operator and $b_1(x, y)$ is a known function of position. n is the unit outward normal to the boundary $\Gamma = \Gamma_1 + \Gamma_2$ of the region Ω , $\bar{u}(x, y)$ and $\bar{q}(x, y)$ are the prescribed functions for u and q , respectively.

The aim of this section is to obtain a boundary integral equation corresponding to Poisson equation. Multiplying equation (2.1) with the fundamental solution of Laplace equation, in which r is the distance between the source and the field points

$$u^* = \frac{1}{2\pi} \ln\left(\frac{1}{r}\right) \quad (2.3)$$

and integrating over the domain Ω one can obtain a domain integral equation (weighted residual statement)

$$\int_{\Omega} (\nabla^2 u - b_1) u^* d\Omega = 0. \quad (2.4)$$

Application of Divergence theorem leads

$$\int_{\Omega} (u \nabla^2 u^* - b_1 u^*) d\Omega + \int_{\Gamma} \frac{\partial u}{\partial n} u^* d\Gamma - \int_{\Gamma} \frac{\partial u^*}{\partial n} u d\Gamma = 0. \quad (2.5)$$

Insertion of boundary conditions (2.2) gives

$$\int_{\Omega} u \nabla^2 u^* d\Omega - \int_{\Omega} b_1 u^* d\Omega = - \int_{\Gamma_2} \bar{q} u^* d\Gamma - \int_{\Gamma_1} q u^* d\Gamma + \int_{\Gamma_2} u q^* d\Gamma + \int_{\Gamma_1} \bar{u} q^* d\Gamma \quad (2.6)$$

where $q^* = \frac{\partial u^*}{\partial n}$ is the normal derivative of the fundamental solution.

The fundamental solution u^* satisfies Laplace equation as

$$\nabla^2 u^* + \Delta^i = 0 \quad (2.7)$$

where Δ^i is Dirac delta function and defined as follow

$$\Delta^i(x) = \begin{cases} 0 & \text{if } x \neq x_i \\ \infty & \text{if } x = x_i \end{cases} \quad (2.8)$$

The integral of Δ^i over the domain is equal to one, and with the integral property of Dirac delta function one can obtain

$$\int_{\Omega} u \nabla^2 u^* d\Omega = \int_{\Omega} u (-\Delta^i) u^* d\Omega = -c_i u_i \quad (2.9)$$

where $u_i = u(x_i, y_i)$, c_i is a constant which depends on the geometry of boundary as

$$c_i = \begin{cases} \frac{\theta_i}{2\pi}, & \text{if } i \in \Gamma \\ 1, & \text{if } i \in \Omega/\Gamma. \end{cases} \quad (2.10)$$

Here θ_i represents the internal angle at the point i . Using equation (2.9) and grouping all the terms together in equation (2.6) give the boundary integral equation at the point i

$$c_i \tilde{u}_i + \int_{\Omega} b_1 u^* d\Omega + \int_{\Gamma} \tilde{u} q^* d\Gamma = \int_{\Gamma} \tilde{q} u^* d\Gamma \quad (2.11)$$

where the notations \tilde{u} and \tilde{q} are used as

$$\tilde{u} = \begin{cases} u, & \text{on } \Gamma_2 \\ \bar{u}, & \text{on } \Gamma_1 \end{cases} \quad (2.12)$$

and

$$\tilde{q} = \begin{cases} q, & \text{on } \Gamma_1 \\ \bar{q}, & \text{on } \Gamma_2 \end{cases} . \quad (2.13)$$

In equation (2.11) there is still a domain integral which contains the known function $b_1(x, y)$ and dual reciprocity boundary element method will be used to transform this domain integral also to a boundary integral.

2.1.2 DRBEM for the Poisson Equation

In the previous section, a corresponding integral equation is obtained for the Poisson equation. Due to the right hand side function $b_1(x, y)$ there is still a domain integral in (2.11), and it can be transformed to a boundary integral by using the dual reciprocity boundary element method. In this section, DRBEM is explained for the Poisson equation (2.1) following the reference [73].

The solution to equation (2.1) can be expressed as

$$u = u' + \hat{u} \quad (2.14)$$

where u' is the solution of Laplace equation and \hat{u} is a particular solution which satisfies the governing equation (2.1)

$$\nabla^2 \hat{u} = b_1(x, y). \quad (2.15)$$

Actually, it is not easy to find a particular solution \hat{u} satisfying the equation (2.15). The DRBEM recommended a series of particular solutions \hat{u}_j instead of a single function \hat{u} . Thus, the inhomogeneity function $b_1(x, y)$ is expanded with the approximating functions as

$$b_1 \approx \sum_{j=1}^{K+L} \alpha_j f_j \quad (2.16)$$

where K and L are the number of boundary and internal nodes, α_j are initially unknown coefficients, and f_j are the approximating functions. Also, there is a relation between the particular solutions \hat{u}_j and f_j such as

$$\nabla^2 \hat{u}_j = f_j. \quad (2.17)$$

After substituting equation (2.17) into equation (2.16) one can obtain a new approximation for the right hand side function b_1

$$b_1 = \sum_{j=1}^{K+L} \alpha_j \nabla^2 \hat{u}_j. \quad (2.18)$$

Substitution of b_1 into the Poisson equation (2.1) gives the following equation

$$\nabla^2 u = \sum_{j=1}^{K+L} \alpha_j \nabla^2 \widehat{u}_j. \quad (2.19)$$

Now, the Laplace operator appears to be in both sides. Multiplying equation (2.19) with the fundamental solution of the Laplace equation and integrating over the domain one obtains

$$\int_{\Omega} (\nabla^2 u) u^* d\Omega = \sum_{j=1}^{K+L} \alpha_j \int_{\Omega} (\nabla^2 \widehat{u}_j) u^* d\Omega. \quad (2.20)$$

Integrating equation (2.20) by parts and applying Green's theorem twice for the Laplace term produces the following integral equation for each source node i

$$c_i \widehat{u}_i + \int_{\Gamma} \widehat{u} q^* d\Gamma - \int_{\Gamma} \widehat{q} u^* d\Gamma = \sum_{j=1}^{K+L} \alpha_j \left[c_i \widehat{u}_{ij} + \int_{\Gamma} \widehat{u}_j q^* d\Gamma - \int_{\Gamma} \widehat{q}_j u^* d\Gamma \right] \quad (2.21)$$

where $\widehat{u}_{ij} = \widehat{u}_j(x_i, y_i)$, and \widehat{q}_j is the normal derivative of \widehat{u}_j defined as

$$\widehat{q}_j = \frac{\partial \widehat{u}_j}{\partial n} = \frac{\partial \widehat{u}_j}{\partial x} \frac{\partial x}{\partial n} + \frac{\partial \widehat{u}_j}{\partial y} \frac{\partial y}{\partial n}. \quad (2.22)$$

For simplicity of the notation, \sim will be dropped in u and q in the rest of the formulation.

Now the equation (2.21) contains only boundary integrals and the next step is to obtain a system of equations by discretizing the boundary of the domain. Each part of the boundary is called as *boundary element*, and the points which are located on the boundary elements are called as *nodes*. The type of the boundary elements is changed depending on the number of nodes on the possession. If the nodes are placed at the center of each element, the elements are called *constant elements*. If an element has two nodes placed at the ends, it is a *linear element*. Similarly, the number of the nodes can be increased to obtain higher order boundary elements. In this thesis, the discretization of the boundary is done by using constant elements.

The boundary is divided into K constant boundary elements by taking the nodes in the middle of each element. In the case of the constant element the boundary is always smooth and thus u and q are assumed to be constant over the element. The values of u and q at any point on the element can be defined in terms of their nodal values as

$$\begin{aligned} u &\approx u_k \\ q &\approx q_k \end{aligned} \quad (2.23)$$

on the k -th boundary element Γ_k , (k -th node also), $k = 1, 2, \dots, K$. Discretization of the boundary Γ in (2.21) gives an expression

$$c_i u_i + \sum_{k=1}^K \int_{\Gamma_k} u q^* d\Gamma - \sum_{k=1}^K \int_{\Gamma_k} q u^* d\Gamma = \sum_{j=1}^{K+L} \alpha_j \left[c_i \widehat{u}_{ij} + \sum_{k=1}^K \int_{\Gamma_k} \widehat{u}_j q^* d\Gamma - \sum_{k=1}^K \int_{\Gamma_k} \widehat{q}_j u^* d\Gamma \right]. \quad (2.24)$$

The constant values of u and q can be taken out of the integrals and equation (2.24) becomes

$$c_i u_i + \sum_{k=1}^K u_k \int_{\Gamma_k} q^* d\Gamma - \sum_{k=1}^K q_k \int_{\Gamma_k} u^* d\Gamma = \sum_{j=1}^{K+L} \alpha_j \left[c_i \widehat{u}_{ij} + \sum_{k=1}^K \widehat{u}_{kj} \int_{\Gamma_k} q^* d\Gamma - \sum_{k=1}^K \widehat{q}_{kj} \int_{\Gamma_k} u^* d\Gamma \right]. \quad (2.25)$$

Integration of u^* and q^* over each boundary element results in the system of equations

$$c_i u_i + \sum_{k=1}^K \bar{H}_{ik} u_k - \sum_{k=1}^K G_{ik} q_k = \sum_{j=1}^{K+L} \alpha_j \left[c_i \widehat{u}_{ij} + \sum_{k=1}^K \bar{H}_{ik} \widehat{u}_{kj} - \sum_{k=1}^K G_{ik} \widehat{q}_{kj} \right] \quad (2.26)$$

where the index k is used for the boundary nodes, and the components of \bar{H} and G matrices are

$$\begin{aligned} \bar{H}_{ik} &= \int_{\Gamma_k} q^* d\Gamma_k = \frac{1}{2\pi} \int_{\Gamma_k} \frac{(\mathbf{r} - \mathbf{r}_i) \cdot \mathbf{n}}{|\mathbf{r} - \mathbf{r}_i|^2} d\Gamma_k \quad i \neq k, \\ G_{ik} &= \int_{\Gamma_k} u^* d\Gamma_k = \frac{1}{2\pi} \int_{\Gamma_k} \ln \frac{1}{|\mathbf{r} - \mathbf{r}_i|} d\Gamma_k \quad i \neq k. \end{aligned} \quad (2.27)$$

where $\mathbf{r} = (x, y)$ and $\mathbf{r}_i = (x_i, y_i)$ are the field and source points, respectively. \mathbf{n} is the outward unit vector on the boundary Γ_k .

When $i = k$, there are singularities in \bar{H}_{ii} and G_{ii} but they can be calculated analytically for a constant element. Since normal \mathbf{n} and distance $(\mathbf{r} - \mathbf{r}_i)$ vectors are always perpendicular to each other, \bar{H}_{ii} components are identically zero. The G_{ii} components are [22]

$$G_{ii} = \frac{1}{2\pi} \left(\ln \frac{1}{l} + 1 \right) \quad (2.28)$$

where l is the length of the element.

Since all the boundary elements are straight lines the angle θ_i can be taken as π and for the constant element c_i is

$$c_i = \begin{cases} \frac{1}{2}, & \text{if } i \in \Gamma \\ 1, & \text{if } i \in \Omega/\Gamma \end{cases}. \quad (2.29)$$

Thus, the equation (2.26) becomes for K nodes on the boundary

$$\frac{1}{2}u_i + \sum_{k=1}^K \bar{H}_{ik}u_k - \sum_{k=1}^K G_{ik}q_k = \sum_{j=1}^{K+L} \alpha_j \left[\frac{1}{2}\widehat{u}_{ij} + \sum_{k=1}^K \bar{H}_{ik}\widehat{u}_{kj} - \sum_{k=1}^K G_{ik}\widehat{q}_{kj} \right] \quad (2.30)$$

where $i = 1, \dots, K$. After rearranging the coefficient matrices, equations (2.30) take the form

$$\mathbf{H}\mathbf{u} - \mathbf{G}\mathbf{q} = \sum_{j=1}^{K+L} \alpha_j (\mathbf{H}\widehat{\mathbf{u}}_j - \mathbf{G}\widehat{\mathbf{q}}_j) \quad (2.31)$$

where

$$H_{ik} = \bar{H}_{ik} + \frac{1}{2}\delta_{ik} \quad (2.32)$$

and δ is the Kronecker delta function defined as

$$\delta_{ik} = \begin{cases} 1, & \text{if } i = k \\ 0, & \text{if } i \neq k \end{cases} \quad (2.33)$$

for $i, k = 1, 2, \dots, K$.

In equation (2.31) each vector, $\widehat{\mathbf{u}}_j$ and $\widehat{\mathbf{q}}_j$ is considered to be one column of the matrices $\widehat{\mathbf{U}}$ and $\widehat{\mathbf{Q}}$ respectively. Thus, equation (2.31) results in

$$\mathbf{H}\mathbf{u} - \mathbf{G}\mathbf{q} = (\mathbf{H}\widehat{\mathbf{U}} - \mathbf{G}\widehat{\mathbf{Q}})\boldsymbol{\alpha} \quad (2.34)$$

where the matrices \mathbf{H} and \mathbf{G} are of size $K \times K$, the matrices $\widehat{\mathbf{U}}$ and $\widehat{\mathbf{Q}}$ have the size $K \times (K+L)$, the vectors \mathbf{u} and \mathbf{q} are of size $K \times 1$, and the vector $\boldsymbol{\alpha}$ has the size $(K+L) \times 1$ which contains unknown coefficients α_j .

In equation (2.34) all the coefficients $c_i = \frac{1}{2}$'s are located on the main diagonal of the matrix \mathbf{H} , and the solution of equation (2.34) gives the unknown boundary values where i ranges from 1 to K . The values at any interior point i can be calculated from equation (2.26) with $c_i = 1$ as

$$u_i = - \sum_{k=1}^K \bar{H}_{ik}u_k + \sum_{k=1}^K G_{ik}q_k + \sum_{j=1}^{K+L} \alpha_j \left[\widehat{u}_{ij} + \sum_{k=1}^K \bar{H}_{ik}\widehat{u}_{kj} - \sum_{k=1}^K G_{ik}\widehat{q}_{kj} \right] \quad (2.35)$$

where L is the number of the interior points, and i ranges from 1 to L . Thus, equation (2.35) can be written in a matrix-vector form

$$\mathbf{I}\mathbf{u}^i = \mathbf{G}\mathbf{q} - \mathbf{H}\mathbf{u} + [\widehat{\mathbf{U}}^i + \mathbf{H}\widehat{\mathbf{U}} - \mathbf{G}\widehat{\mathbf{Q}}]\boldsymbol{\alpha} \quad (2.36)$$

where \mathbf{u}^i is a vector of size $L \times 1$ which contains the computed values of interior points. Here, \mathbf{H} and \mathbf{G} matrices are of size $L \times K$, $\widehat{\mathbf{U}}$ and $\widehat{\mathbf{Q}}$ matrices have the size $K \times (K+L)$, $\widehat{\mathbf{U}}^i$ has the size $L \times (K+L)$, and \mathbf{I} is a $L \times L$ identity matrix. The vectors \mathbf{u} and \mathbf{q} contain the known values of boundary points which have the size $K \times 1$, and the vector $\boldsymbol{\alpha}$ is of size $(K+L) \times 1$.

Now, systems (2.34) and (2.36) can be combined in a one system by enlarging the matrices [73] as

$$\begin{aligned} & \begin{bmatrix} \mathbf{H}^b_{K \times K} & \mathbf{0}_{K \times L} \\ \mathbf{H}^i_{L \times K} & \mathbf{I}_{L \times L} \end{bmatrix} \begin{Bmatrix} \mathbf{u}^b_{K \times 1} \\ \mathbf{u}^i_{L \times 1} \end{Bmatrix} - \begin{bmatrix} \mathbf{G}^b_{K \times K} & \mathbf{0}_{K \times L} \\ \mathbf{G}^i_{L \times K} & \mathbf{0}_{L \times L} \end{bmatrix} \begin{Bmatrix} \mathbf{q}^b_{K \times 1} \\ \mathbf{0}_{L \times 1} \end{Bmatrix} \\ & = \left(\begin{bmatrix} \mathbf{H}^b_{K \times K} & \mathbf{0}_{K \times L} \\ \mathbf{H}^i_{L \times K} & \mathbf{I}_{L \times L} \end{bmatrix} \begin{bmatrix} \widehat{\mathbf{U}}^b_{K \times (K+L)} \\ \widehat{\mathbf{U}}^i_{L \times (K+L)} \end{bmatrix} - \begin{bmatrix} \mathbf{G}^b_{K \times K} & \mathbf{0}_{K \times L} \\ \mathbf{G}^i_{L \times K} & \mathbf{0}_{L \times L} \end{bmatrix} \begin{bmatrix} \widehat{\mathbf{Q}}^b_{K \times (K+L)} \\ \mathbf{0}_{L \times (K+L)} \end{bmatrix} \right) \{\boldsymbol{\alpha}_{(K+L) \times 1}\} \end{aligned} \quad (2.37)$$

where b and i refer to the boundary and interior nodes, and \mathbf{I} and $\mathbf{0}$ are identity and zero matrices, respectively. So, the enlarged system (2.37) can be written in a compact form

$$\mathbf{H}\mathbf{u} - \mathbf{G}\mathbf{q} = (\mathbf{H}\widehat{\mathbf{U}} - \mathbf{G}\widehat{\mathbf{Q}})\boldsymbol{\alpha}. \quad (2.38)$$

In the above system all the matrices are of size $(K + L) \times (K + L)$, and all the vectors have the size $(K + L) \times 1$. For simplicity, the same notations with the equation (2.34) are used for the enlarged system.

Now, the $\boldsymbol{\alpha}$ vector can be computed by using the approximation (2.16) with the value of b_1 at $(K + L)$ different points which gives a matrix form as

$$\mathbf{b}_1 = \mathbf{F}\boldsymbol{\alpha} \quad (2.39)$$

where \mathbf{F} is the coordinate matrix of size $(K + L) \times (K + L)$, \mathbf{b}_1 is the vector containing values of b_1 function at $(K + L)$ points. In the \mathbf{F} matrix f_j are consisted of columns which contain the value of function f_j at $(K + L)$ points. Thereby, $\boldsymbol{\alpha}$ vector can be obtained by inverting the equation (2.39)

$$\boldsymbol{\alpha} = \mathbf{F}^{-1}\mathbf{b}_1. \quad (2.40)$$

Inserting equation (2.40) into equation (2.38) one can get the system

$$\mathbf{H}\mathbf{u} - \mathbf{G}\mathbf{q} = (\mathbf{H}\widehat{\mathbf{U}} - \mathbf{G}\widehat{\mathbf{Q}})\mathbf{F}^{-1}\mathbf{b}_1 \quad (2.41)$$

in which the right hand side of the equation (2.41) can be calculated by using known values of \mathbf{H} , \mathbf{G} , $\widehat{\mathbf{U}}$, $\widehat{\mathbf{Q}}$, \mathbf{F}^{-1} and \mathbf{b}_1 . Using the given boundary conditions and rearranging the equation (2.41) one can obtain the usual linear system of algebraic equations

$$\mathbf{A}\mathbf{x} = \mathbf{y} \quad (2.42)$$

where \mathbf{x} is the vector of K unknown boundary values u or q , and L unknown interior values of u , \mathbf{y} contains all known values at the boundary points, and both \mathbf{x} and \mathbf{y} have the size $(K + L) \times 1$.

It is necessary to choose suitable f_j function to obtain \mathbf{F} , $\widehat{\mathbf{U}}$ and $\widehat{\mathbf{Q}}$ matrices. Several type of functions can be used for f_j but it should be chosen in such a way that resulting matrix \mathbf{F} should be nonsingular. Therefore, usually polynomials in terms of the distance function r with the constant term which are simplest and accurate alternatives for f_j are preferred.

Let us define f in a polynomial form as in [73]

$$f = 1 + r + r^2 + \dots + r^m \quad (2.43)$$

where r is the distance between source and field points. This f function should satisfy the equation

$$\nabla^2 \widehat{u} = f \quad (2.44)$$

which is equal to in polar coordinates with the definition of f

$$\frac{1}{r} \frac{\partial}{\partial r} \left(r \frac{\partial \widehat{u}}{\partial r} \right) = 1 + r + r^2 + \dots + r^m. \quad (2.45)$$

Corresponding \widehat{u} and \widehat{q} functions can be obtain by using equation (2.45) in the form

$$\widehat{u} = \frac{r^2}{4} + \frac{r^3}{9} + \dots + \frac{r^{m+2}}{(m+2)^2} \quad (2.46)$$

$$\widehat{q} = \left(r_x \frac{\partial x}{\partial n} + r_y \frac{\partial y}{\partial n} \right) \left(\frac{1}{2} + \frac{r}{3} + \dots + \frac{r^m}{(m+2)} \right) \quad (2.47)$$

with the definitions

$$r^2 = r_x^2 + r_y^2 \quad (2.48)$$

and

$$\frac{\partial r}{\partial n} = \frac{1}{r} \left(r_x \frac{\partial r_x}{\partial n} + r_y \frac{\partial r_y}{\partial n} \right) \quad (2.49)$$

where $\mathbf{r} = (r_x, r_y)$ and r is the length of the vector \mathbf{r} .

Actually, one can use any combination of terms from equation (2.43) but there is not much of a difference between the results. So, for simplicity $f = 1 + r$ is used in the solution of the Poisson equation. Also, different kind of radial basis functions can be used for Laplace operator which results in corresponding particular solution \widehat{u} and \widehat{q} ($\widehat{q} = \frac{\partial \widehat{u}}{\partial n}$) functions as

$$f = r^2 \ln r, \quad \widehat{u} = \frac{r^4}{16} \left(\ln r - \frac{1}{2} \right), \quad \widehat{q} = \left(\frac{r^3}{4} \ln r - \frac{r^3}{16} \right) \frac{\partial r}{\partial n} \quad (2.50)$$

$$f = \frac{2c - r}{(r + c)^4}, \quad \widehat{u} = -\frac{c + 2r}{2(r + c)^2}, \quad \widehat{q} = \frac{r}{(r + c)^3} \frac{\partial r}{\partial n} \quad (2.51)$$

$$f = \exp(-r^2), \quad \widehat{u} = \frac{1}{4} (\ln r^2 + E_1(r^2)), \quad \widehat{q} = \frac{1}{2r} (1 - \exp(-r^2)) \frac{\partial r}{\partial n} \quad (2.52)$$

where c is an arbitrary constant and E_1 is the exponential integral represented by [100]

$$E_1(X) = \int_X^\infty \frac{\exp(-t)}{t} dt. \quad (2.53)$$

2.2 DRBEM Solution of Inhomogeneous Modified Helmholtz Equation $\nabla^2 u - \tau^2 u = b_2(x, y)$

DRBEM which is available in the literature is basically the boundary element technique treating both sides of inhomogeneous partial differential equations with the fundamental solution of Laplace equation [73]. Thus, the domain integral resulting from inhomogeneous term in the BEM formulation is also transformed to a boundary integral. This current section presents the dual reciprocity boundary element method application to the inhomogeneous modified Helmholtz equation. For this aim, mathematical development of DRBEM will be modified for the inhomogeneous modified Helmholtz equations. This means that the fundamental solution of modified Helmholtz equation will be used in the formulation.

2.2.1 Boundary Integral Equation for Homogeneous Modified Helmholtz Equation

In this Section, we first describe boundary integral equation for the homogeneous modified Helmholtz equation since it forms a basis for the DRBEM solution of inhomogeneous modified Helmholtz equation. Let us consider the homogeneous modified Helmholtz Equation in two-dimensional domain

$$\nabla^2 u - \tau^2 u = 0 \quad , \quad (x, y) \in \Omega \quad (2.54)$$

with the following Dirichlet and Neumann boundary conditions

$$\begin{aligned} u(x, y) &= \bar{u}(x, y) \quad , \quad (x, y) \in \Gamma_1 \\ q(x, y) &= \frac{\partial u}{\partial n} = \bar{q}(x, y) \quad , \quad (x, y) \in \Gamma_2 \end{aligned} \quad (2.55)$$

where ∇^2 is the Laplace operator. Here n is unit outward normal to the boundary $\Gamma = \Gamma_1 + \Gamma_2$, $\bar{u}(x, y)$ and $\bar{q}(x, y)$ are the prescribed functions for u and q , respectively.

In order to obtain an integral equation for the modified Helmholtz equation (2.54), we multiply with the fundamental solution of modified Helmholtz equation and integrate over the domain to obtain weighting residual statement

$$\int_{\Omega} (\nabla^2 u - \tau^2 u) u^* d\Omega = \int_{\Gamma_2} (q - \bar{q}) u^* d\Gamma - \int_{\Gamma_1} (u - \bar{u}) q^* d\Gamma \quad (2.56)$$

where $q = \frac{\partial u}{\partial n}$ and $q^* = \frac{\partial u^*}{\partial n}$.

Applying Green's theorem twice for the left hand side of equation (2.56) we obtain the following equation

$$\int_{\Omega} (\nabla^2 u^* - \tau^2 u^*) u d\Omega = - \int_{\Gamma_2} \bar{q} u^* d\Gamma - \int_{\Gamma_1} q u^* d\Gamma + \int_{\Gamma_2} u q^* d\Gamma + \int_{\Gamma_1} \bar{u} q^* d\Gamma \quad (2.57)$$

or

$$\int_{\Omega} (\nabla^2 u^* - \tau^2 u^*) u d\Omega - \int_{\Gamma} \bar{u} q^* d\Gamma + \int_{\Gamma} \bar{q} u^* d\Gamma = 0 \quad (2.58)$$

where \tilde{u} and \tilde{q} contain all known and unknown boundary values.

The weighting function u^* satisfies the differential equation (2.58) in the Dirac delta sense, then

$$\int_{\Gamma} \tilde{q} u^* d\Gamma - \int_{\Gamma} \tilde{u} q^* d\Gamma = 0. \quad (2.59)$$

The fundamental solution of the modified Helmholtz equation is $u^* = K_0(\tau r)$, second kind modified Bessel function of order zero, where r is the distance from an arbitrary point i to a point on the boundary [92, 69].

Substitution of u^* in equation (2.59) becomes (using u and q for \tilde{u} and \tilde{q} for convenience)

$$\int_{\Gamma} \left(\frac{\partial u}{\partial n} K_0(\tau r) - u \frac{\partial K_0(\tau r)}{\partial n} \right) d\Gamma = 0. \quad (2.60)$$

In order to take this integral, the singularities must be removed in the region as ($r \rightarrow 0$). So, the singularity can be handled by integrating around the circle of radius ε containing the singularity [92]

$$\int_{\Gamma} \left(\frac{\partial u}{\partial n} K_0(\tau r) - u \frac{\partial K_0(\tau r)}{\partial n} \right) d\Gamma + \int_0^{2\pi} \left(\frac{\partial u}{\partial n} K_0(\tau \varepsilon) - u \frac{\partial K_0(\tau \varepsilon)}{\partial n} \right) \varepsilon d\theta = 0 \quad (2.61)$$

where θ increases counterclockwise when the integral along $d\Gamma$ is taken in a clockwise direction.

Let us take the both side limits when $\varepsilon \rightarrow 0$. Since K_0 function has the asymptotic behavior, like $-\log(\tau \varepsilon)$ for small argument and $\lim_{\varepsilon \rightarrow 0} \varepsilon \log(\tau \varepsilon) = 0$, we have

$$\int_0^{2\pi} \frac{\partial u}{\partial n} K_0(\tau \varepsilon) \varepsilon d\theta = 0 \quad (2.62)$$

$$\int_0^{2\pi} u \frac{\partial K_0(\tau \varepsilon)}{\partial n} \varepsilon d\theta = \int_0^{2\pi} u \frac{\partial(-\log(\varepsilon))}{\partial n} \varepsilon d\theta = \int_0^{2\pi} u \left(\frac{1}{\varepsilon} \right) \varepsilon d\theta = 2\pi u. \quad (2.63)$$

After substituting equation (2.62) and equation (2.63) into the equation (2.61), we arrive at the boundary integral equation

$$u_i = \frac{1}{2\pi} \int_{\Gamma} \left(\frac{\partial u}{\partial n} K_0(\tau r) - u \frac{\partial K_0(\tau r)}{\partial n} \right) d\Gamma. \quad (2.64)$$

Thus, evaluating the above integral for any point i in the interior of the domain, u values can be found by just using the boundary points.

To remove the singularities which occur on the boundary as ($r \rightarrow 0$), the integration is taken around a semi-circular path Γ_{ε} of radius ε [92],

$$\int_{\Gamma - \Gamma_{\varepsilon}} \left(\frac{\partial u}{\partial n} K_0(\tau r) - u \frac{\partial K_0(\tau r)}{\partial n} \right) d\Gamma + \int_0^{\pi} \left(\frac{\partial u}{\partial n} K_0(\tau \varepsilon) - u \frac{\partial K_0(\tau \varepsilon)}{\partial n} \right) \varepsilon d\theta = 0 \quad (2.65)$$

Taking limit as $\varepsilon \rightarrow 0$, we get the boundary integral for i at the boundary, which gives a u and $\frac{\partial u}{\partial n}$ values on the boundary

$$u_i = \frac{1}{\pi} \int_{\Gamma} \left(\frac{\partial u}{\partial n} K_0(\tau r) - u \frac{\partial K_0(\tau r)}{\partial n} \right) d\Gamma. \quad (2.66)$$

After combining equations (2.64) and (2.66) one can obtain a boundary integral equation

$$c_i u_i = \frac{1}{2\pi} \int_{\Gamma} \left(\frac{\partial u}{\partial n} K_0(\tau r) - u \frac{\partial K_0(\tau r)}{\partial n} \right) d\Gamma \quad (2.67)$$

where

$$c_i = \begin{cases} \frac{1}{2}, & \text{if } i \in \Gamma \\ 1, & \text{if } i \in \Omega/\Gamma \end{cases}. \quad (2.68)$$

2.2.2 DRBEM for the Inhomogeneous Modified Helmholtz Equation

In this part, the dual reciprocity BEM method will be developed for the inhomogeneous modified Helmholtz equation by using the same idea with the reference [73]. Consider the inhomogeneous modified Helmholtz equation in two-dimensional domain

$$\nabla^2 u - \tau^2 u = b_2(x, y). \quad (2.69)$$

We need a simple way to solve the equation (2.69) without computing any domain integral. As is done for Poisson equation, solution is written as

$$u = u' + \widehat{u} \quad (2.70)$$

where u' is the solution of the homogeneous equation and \widehat{u} is a particular solution of the Modified Helmholtz equation

$$\nabla^2 \widehat{u} - \tau^2 \widehat{u} = b_2. \quad (2.71)$$

Similarly the DRBEM proposes a series of particular solutions \widehat{u}_j instead of a single function \widehat{u} . There will be $K + L$ values of \widehat{u}_j if there are K boundary nodes and L interior nodes.

In addition, the DRBEM proposes an approximation for b_2 as

$$b_2 \approx \sum_{j=1}^{K+L} \bar{\alpha}_j \bar{f}_j \quad (2.72)$$

where the \bar{f}_j are approximating functions and $\bar{\alpha}_j$ are coefficients which are initially unknown. There is a relation between \widehat{u}_j and \bar{f}_j functions such that

$$\nabla^2 \widehat{u}_j - \tau^2 \widehat{u}_j = \bar{f}_j. \quad (2.73)$$

If the equation (2.73) is substituted into the equation (2.72) it gives

$$b_2 = \sum_{j=1}^{K+L} \bar{\alpha}_j (\nabla^2 \widehat{u}_j - \tau^2 \widehat{u}_j) \quad (2.74)$$

and then the right hand side of equation (2.69) becomes

$$\nabla^2 u - \tau^2 u = \sum_{j=1}^{K+L} \bar{\alpha}_j (\nabla^2 \hat{u}_j - \tau^2 \hat{u}_j). \quad (2.75)$$

Multiplying the equation (2.75) with the fundamental solution u^* of modified Helmholtz equation, and integrate over the domain (weighting with u^* over Ω)

$$\int_{\Omega} (\nabla^2 u - \tau^2 u) u^* d\Omega = \sum_{j=1}^{K+L} \bar{\alpha}_j \int_{\Omega} (\nabla^2 \hat{u}_j - \tau^2 \hat{u}_j) u^* d\Omega. \quad (2.76)$$

Integrating by parts the *Laplacian* terms on both sides and inserting the fundamental solution, we obtain the following integral equation for each source node i (either on the boundary or inside)

$$c_i u_i - \frac{1}{2\pi} \int_{\Gamma_k} u \frac{\partial Ko(\tau r_i)}{\partial n} d\Gamma_k + \frac{1}{2\pi} \int_{\Gamma_k} \frac{\partial u}{\partial n} Ko(\tau r_i) d\Gamma_k = \sum_{j=1}^{K+L} \bar{\alpha}_j \left[c_i \hat{u}_{ij} - \frac{1}{2\pi} \int_{\Gamma_k} \hat{u}_j \frac{\partial Ko(\tau r_i)}{\partial n} d\Gamma_k + \frac{1}{2\pi} \int_{\Gamma_k} \hat{q}_j Ko(\tau r_i) d\Gamma_k \right] \quad (2.77)$$

where $\hat{q}_j = \frac{\partial \hat{u}_j}{\partial n}$, n is the unit outward normal to Γ , and r_i is the distance from the source node i to field point k . Note that equation (2.77) involves no domain integrals. The constant c_i takes the values given in (2.68) according to the position of the source point i .

Discretizing equation (2.77) by using constant boundary elements gives for a source node i the expression

$$\frac{1}{2} u_i + \sum_{k=1}^K \bar{H}'_{ik} u_k + \sum_{k=1}^K G'_{ik} q_k = \sum_{j=1}^{K+L} \bar{\alpha}_j \left(\frac{1}{2} \hat{u}_{ij} + \sum_{k=1}^K \bar{H}'_{ik} \hat{u}_{kj} + \sum_{k=1}^K G'_{ik} \hat{q}_{kj} \right) \quad (2.78)$$

where index k is used for the boundary nodes which are field points and the entries of \bar{H}' and G' matrices are

$$\begin{aligned} \bar{H}'_{ik} &= -\frac{1}{2\pi} \int_{\Gamma_k} \frac{\partial Ko(\tau r_i)}{\partial n} d\Gamma_k & i \neq k, \\ G'_{ik} &= \frac{1}{2\pi} \int_{\Gamma_k} Ko(\tau r_i) d\Gamma_k & i \neq k. \end{aligned} \quad (2.79)$$

When the Γ_k contains the point i , the integrals in \bar{H}'_{ii} and G'_{ii} contain singularities, so these integrals need different algorithm. For the case of $i = k$ since the direction cosine is zero, the diagonal entries become

$$\bar{H}'_{ii} = 0. \quad (2.80)$$

When the G matrix is calculated for the case $i = k$, the equation (2.79) is not useful to take the integral. So, the integration formula given in [63] is used

$$G'_{ii} = \frac{1}{2\pi} \int_{\Gamma_i} K_0(\tau r_i) d\Gamma \approx \frac{1}{\pi} \sum_{l=0}^6 (d_l \beta^{2l+1} - \log \beta c_l \beta^{2l+1}) / \tau \quad (2.81)$$

where $\beta = (\tau \Delta \xi_i) / 4$ and the values of d_l and c_l are given in [63], (page:64).

For the case $i \neq k$, the coefficients are [92, 1]

$$\overline{H'}_{ik} = -\frac{1}{2\pi} \int_{\Gamma_k} \frac{\partial K_0(\tau r_i)}{\partial n} d\Gamma = \frac{1}{2\pi} \int_{\Gamma_k} \tau K_1(\tau r_i) \frac{\partial r_i}{\partial n} d\Gamma = \frac{1}{2\pi} \tau \Delta \xi_j K_1(\tau r_i) \frac{\partial r_i}{\partial n} \quad (2.82)$$

where $K_1(x)$ is a modified Bessel function of second kind and of order one, and $\frac{\partial r_i}{\partial n}$ is the normal derivative of r defined in equation (2.48), and evaluated at the point i .

Similarly, for the G matrix, we have

$$G'_{ik} = \frac{1}{2\pi} \int_{\Gamma_k} K_0(\tau r_i) d\Gamma \approx \frac{1}{2\pi} \Delta \xi_k \left[K_0(\tau r_i |_{k-1/2}) + 4K_0(\tau r_i) + K_0(\tau r_i |_{k+1/2}) \right] / 6 \quad (2.83)$$

where the term $r_i |_{k-1/2}$ and $r_i |_{k+1/2}$ are the distance between the point i and the end points of the k -th elements, [92].

In equation (2.78) \widehat{u} and \widehat{q} are known functions when \overline{f} function is defined. If the same procedure is used for every source node $i, i = 1, \dots, K$ (discretization with K constant boundary elements), equation (2.78) can be expressed in matrix-vector form as

$$\mathbf{H}' \mathbf{u} + \mathbf{G}' \mathbf{q} = \sum_{j=1}^{K+L} \overline{\alpha}_j (\mathbf{H}' \widehat{\mathbf{u}}_j + \mathbf{G}' \widehat{\mathbf{q}}_j). \quad (2.84)$$

If each of the vectors $\widehat{\mathbf{u}}_j$ and $\widehat{\mathbf{q}}_j$ is considered to be one column of the matrices $\widehat{\mathbf{U}}$ and $\widehat{\mathbf{Q}}$ respectively, the equation (2.84) becomes a matrix-vector equation for the unknown vectors \mathbf{u} and \mathbf{q} defined on Γ

$$\mathbf{H}' \mathbf{u} + \mathbf{G}' \mathbf{q} = (\mathbf{H}' \widehat{\mathbf{U}} + \mathbf{G}' \widehat{\mathbf{Q}}) \overline{\boldsymbol{\alpha}}. \quad (2.85)$$

The terms $c_i = \frac{1}{2}$ have been incorporated onto the principle diagonal of \mathbf{H}' such that

$$H'_{ik} = \overline{H'}_{ik} + c_i \delta_{ik} \quad (2.86)$$

and $\overline{\boldsymbol{\alpha}}$ is vector containing $\overline{\alpha}_j$ values from 1 to $K + L$.

Since this system involves the discretization of the boundary only, the location of the interior points is not important. These nodes can be defined at the locations desired by the user. The values at any interior point i can be calculated from equation (2.77) with $c_i = 1$ as

$$u_i = - \sum_{k=1}^K \overline{H'}_{ik} u_k - \sum_{k=1}^K G'_{ik} q_k + \sum_{j=1}^{K+L} \overline{\alpha}_j \left[\widehat{u}_{ij} + \sum_{k=1}^K \overline{H'}_{ik} \widehat{u}_{kj} + \sum_{k=1}^K G'_{ik} \widehat{q}_{kj} \right] \quad (2.87)$$

where L is the number of the interior points, and i ranges from 1 to L . Thus, equation (2.87) can be written in a matrix-vector form

$$\mathbf{I}u^i = -\mathbf{H}'\mathbf{u} - \mathbf{G}'\mathbf{q} + [\mathbf{I}\widehat{\mathbf{U}}^i + \mathbf{H}'\widehat{\mathbf{U}} + \mathbf{G}'\widehat{\mathbf{Q}}]\bar{\alpha} \quad (2.88)$$

where u^i is a vector with the size $L \times 1$ which contains the computed values of interior points, \mathbf{H}' and \mathbf{G}' matrices have the size $L \times K$, $\widehat{\mathbf{U}}$ and $\widehat{\mathbf{Q}}$ matrices are of size $K \times (K + L)$, $\widehat{\mathbf{U}}^i$ has the size $L \times (K + L)$, and \mathbf{I} is a $L \times L$ identity matrix. The vector $\bar{\alpha}$ has size $(K + L) \times 1$ and the vectors \mathbf{u} and \mathbf{q} contain the known values of boundary points which are of the size $K \times 1$.

By using equations (2.85) and (2.88) a global scheme may be obtained which is valid for both boundary and interior points [73] as

$$\begin{aligned} & \begin{bmatrix} \mathbf{H}'^b_{K \times K} & \mathbf{0}_{K \times L} \\ \mathbf{H}'^i_{L \times K} & \mathbf{I}_{L \times L} \end{bmatrix} \begin{Bmatrix} u^b_{K \times 1} \\ u^i_{L \times 1} \end{Bmatrix} + \begin{bmatrix} \mathbf{G}'^b_{K \times K} & \mathbf{0}_{K \times L} \\ \mathbf{G}'^i_{L \times K} & \mathbf{0}_{L \times L} \end{bmatrix} \begin{Bmatrix} q^b_{K \times 1} \\ \mathbf{0}_{L \times 1} \end{Bmatrix} \\ &= \left(\begin{bmatrix} \mathbf{H}'^b_{K \times K} & \mathbf{0}_{K \times L} \\ \mathbf{H}'^i_{L \times K} & \mathbf{I}_{L \times L} \end{bmatrix} \begin{bmatrix} \widehat{\mathbf{U}}^b_{K \times (K+L)} \\ \widehat{\mathbf{U}}^i_{L \times (K+L)} \end{bmatrix} + \begin{bmatrix} \mathbf{G}'^b_{K \times K} & \mathbf{0}_{K \times L} \\ \mathbf{G}'^i_{L \times K} & \mathbf{0}_{L \times L} \end{bmatrix} \begin{bmatrix} \widehat{\mathbf{Q}}^b_{K \times (K+L)} \\ \mathbf{0}_{L \times (K+L)} \end{bmatrix} \right) \{\bar{\alpha}_{(K+L) \times 1}\} \end{aligned} \quad (2.89)$$

where b and i refer to the boundary and interior nodes, \mathbf{I} and $\mathbf{0}$ are identity and zero matrices, respectively. So, the enlarged system (2.89) can be written in a compact form as

$$\mathbf{H}'\mathbf{u} + \mathbf{G}'\mathbf{q} = (\mathbf{H}'\widehat{\mathbf{U}} + \mathbf{G}'\widehat{\mathbf{Q}})\bar{\alpha}. \quad (2.90)$$

In the above system all the matrices have the size $(K + L) \times (K + L)$, and all the vectors have the size $(K + L) \times 1$. The same notations with the equation (2.85) are used for the enlarged system also.

The $\bar{\alpha}$ vector can be computed by using the approximation (2.72). If the right hand side term $b_2(x, y)$ is a known function of space, one can obtain the values of $b_2(x, y)$ at $(K + L)$ different points which gives a matrix form as

$$b_2 = \bar{\mathbf{F}}\bar{\alpha} \quad (2.91)$$

where the $\bar{\mathbf{f}}_j$ are approximating functions and $\bar{\mathbf{F}}$ is the coordinate matrix which has the size $(K + L) \times (K + L)$. In the $\bar{\mathbf{F}}$ matrix $\bar{\mathbf{f}}_j$ are consisted as columns which contain the value of function $\bar{\mathbf{f}}_j$ at $(K + L)$ points. Thus, $\bar{\alpha}$ vector can be obtained by inverting the equation (2.91)

$$\bar{\alpha} = \bar{\mathbf{F}}^{-1} b_2 \quad (2.92)$$

and is inserted back into equation (2.90) to arrive at

$$\mathbf{H}'\mathbf{u} + \mathbf{G}'\mathbf{q} = (\mathbf{H}'\widehat{\mathbf{U}} + \mathbf{G}'\widehat{\mathbf{Q}})\bar{\mathbf{F}}^{-1} b_2 \quad (2.93)$$

in which the right hand side can be obtained by using known values of \mathbf{H}' , \mathbf{G}' , $\widehat{\mathbf{U}}'$, $\widehat{\mathbf{Q}}'$, $\overline{\mathbf{F}}^{-1}$ and $b_2(x, y)$.

2.2.3 DRBEM Solution for the Equation $\nabla^2 u - \tau^2 u = b_2(x, y, u_x, u_y)$

If the right hand side function is in the form $b(x, y, u_x, u_y)$ then a different idea should be used for the terms u_x and u_y . Let the inhomogeneous term be a combination of space derivatives such as

$$b_2(x, y, u_x, u_y) = \frac{\partial u}{\partial x} + \frac{\partial u}{\partial y}. \quad (2.94)$$

Now, the basic approximation of the DRBEM can be done for the right hand side function $b_2(x, y, u_x, u_y)$, i.e.

$$\mathbf{b}_2 = \overline{\mathbf{F}}\overline{\boldsymbol{\alpha}}. \quad (2.95)$$

A similar idea can be written for the function u

$$\mathbf{u} = \overline{\mathbf{F}}\boldsymbol{\beta} \quad (2.96)$$

where $\boldsymbol{\beta} \neq \overline{\boldsymbol{\alpha}}$. Differentiation (2.96) with respect to x and y , gives

$$\frac{\partial \mathbf{u}}{\partial x} = \frac{\partial \overline{\mathbf{F}}}{\partial x} \boldsymbol{\beta} \quad (2.97)$$

and

$$\frac{\partial \mathbf{u}}{\partial y} = \frac{\partial \overline{\mathbf{F}}}{\partial y} \boldsymbol{\beta}, \quad (2.98)$$

respectively. Inverting equation (2.96), $\boldsymbol{\beta}$ is obtained as

$$\boldsymbol{\beta} = \overline{\mathbf{F}}^{-1} \mathbf{u} \quad (2.99)$$

then equations (2.97) and (2.98) become

$$\frac{\partial \mathbf{u}}{\partial x} = \frac{\partial \overline{\mathbf{F}}}{\partial x} \overline{\mathbf{F}}^{-1} \mathbf{u} \quad (2.100)$$

and

$$\frac{\partial \mathbf{u}}{\partial y} = \frac{\partial \overline{\mathbf{F}}}{\partial y} \overline{\mathbf{F}}^{-1} \mathbf{u}, \quad (2.101)$$

respectively. Therefore, the right hand side function (2.94) is

$$\mathbf{b}_2(x, y, u_x, u_y) = \left(\frac{\partial \overline{\mathbf{F}}}{\partial x} \overline{\mathbf{F}}^{-1} + \frac{\partial \overline{\mathbf{F}}}{\partial y} \overline{\mathbf{F}}^{-1} \right) \mathbf{u}. \quad (2.102)$$

Substituting equation (2.102) into equation (2.93) one can obtain

$$\mathbf{H}' \mathbf{u} + \mathbf{G}' \mathbf{q} = \mathbf{d} \quad (2.103)$$

where

$$\mathbf{d} = (\mathbf{H}'\widehat{\mathbf{U}}' + \mathbf{G}'\widehat{\mathbf{Q}}')\overline{\mathbf{F}}^{-1} \left(\frac{\partial \overline{\mathbf{F}}}{\partial x} \overline{\mathbf{F}}^{-1} + \frac{\partial \overline{\mathbf{F}}}{\partial y} \overline{\mathbf{F}}^{-1} \right) \mathbf{u}. \quad (2.104)$$

Therefore, \mathbf{d} vector can be obtained directly by multiplying known vector and matrices except the solution \mathbf{u} . Defining

$$\mathbf{S} = (\mathbf{H}'\widehat{\mathbf{U}}' + \mathbf{G}'\widehat{\mathbf{Q}}')\overline{\mathbf{F}}^{-1} \left(\frac{\partial \overline{\mathbf{F}}}{\partial x} \overline{\mathbf{F}}^{-1} + \frac{\partial \overline{\mathbf{F}}}{\partial y} \overline{\mathbf{F}}^{-1} \right) \quad (2.105)$$

equation (2.103) becomes

$$\mathbf{H}'\mathbf{u} + \mathbf{G}'\mathbf{q} = \mathbf{S}\mathbf{u} \quad (2.106)$$

where the calculation of the matrix \mathbf{S} can be done by multiplying known vector and matrices. Collecting the terms for \mathbf{u} on the left hand side one can obtain

$$(\mathbf{H}' - \mathbf{S})\mathbf{u} + \mathbf{G}'\mathbf{q} = \mathbf{0}. \quad (2.107)$$

After inserting the boundary conditions, this equation reduces to the form

$$\mathbf{A}\mathbf{x} = \mathbf{y} \quad (2.108)$$

where \mathbf{x} is a vector of unknown boundary values of \mathbf{u} and \mathbf{q} , and \mathbf{y} is obtained by multiplying the corresponding columns of \mathbf{H}' or \mathbf{G}' by the known values of \mathbf{u} and \mathbf{q} . This linear system of equation is solved for \mathbf{x} by using any direct solution method and all the boundary values will be known. The coefficient matrix \mathbf{A} does not show a special form. It contains lots of scattered zeros but still in the form of a full matrix.

2.2.4 Different \overline{f} Expansions for Modified Helmholtz Operator

A coordinate function \overline{f} in terms of radial distance r is used for approximating the inhomogeneity $b_2(x, y)$ in the differential equation (2.69),

$$b_2 = \sum_{j=1}^{K+L} \overline{\alpha}_j \overline{f}_j. \quad (2.109)$$

It is also used for obtaining the $\overline{\mathbf{F}}$ matrix in (2.95) and (2.96) which must be non-singular. So, we cannot choose \overline{f} function arbitrarily. Usually polynomials in terms of the distance r are taken but some other definitions of \overline{f} are used for computing corresponding particular solutions \widehat{u} , and its normal derivative \widehat{q} by using $(\nabla^2 - \tau^2)\widehat{u} = \overline{f}$.

2.2.4.1 Polynomial Form of \overline{f} Expansion

We start by taking particular solution \widehat{u} also as a polynomial in r

$$\widehat{u} = a_0 + a_1 r + a_2 r^2 + a_3 r^3 + \dots + a_m r^m \quad (2.110)$$

where a_k is a set of coefficients. This particular solution \widehat{u} satisfies the modified Helmholtz equation

$$\nabla^2 \widehat{u} - \tau^2 \widehat{u} = \bar{f} \quad (2.111)$$

or in the cylindrical coordinates

$$\frac{1}{r} \frac{\partial}{\partial r} \left(r \frac{\partial \widehat{u}}{\partial r} \right) - \tau^2 \widehat{u} = \bar{f}. \quad (2.112)$$

Thus, approximation for \widehat{u} gives

$$\nabla^2 \widehat{u} - \tau^2 \widehat{u} = \frac{a_1}{r} + 4a_2 + 9a_3 r + \dots + m^2 a_m r^{m-2} - \tau^2 (a_0 + a_1 r + a_2 r^2 + a_3 r^3 + \dots + a_m r^m). \quad (2.113)$$

Taking $a_0 = 0$ and $a_1 = 0$, the \bar{f} and \widehat{u} functions are

$$\bar{f} = 4a_2 + 9a_3 r + \dots + m^2 a_m r^{m-2} - \tau^2 (a_2 r^2 + a_3 r^3 + \dots + a_m r^m) \quad (2.114)$$

$$\widehat{u} = a_2 r^2 + a_3 r^3 + \dots + a_m r^m. \quad (2.115)$$

The normal derivative \widehat{q} function is computed as

$$\widehat{q} = \frac{\partial \widehat{u}}{\partial n} = \frac{\partial \widehat{u}}{\partial x} \frac{\partial x}{\partial n} + \frac{\partial \widehat{u}}{\partial y} \frac{\partial y}{\partial n} \quad (2.116)$$

or

$$\widehat{q} = \frac{\partial \widehat{u}}{\partial n} = \frac{\partial \widehat{u}}{\partial r} \frac{\partial r}{\partial n}. \quad (2.117)$$

In the two-dimensional case the distance of the vector $\mathbf{r} = (r_x, r_y)$ is

$$r^2 = r_x^2 + r_y^2 \quad (2.118)$$

and

$$\frac{\partial r}{\partial n} = \frac{1}{r} \left(r_x \frac{\partial r_x}{\partial n} + r_y \frac{\partial r_y}{\partial n} \right). \quad (2.119)$$

So, using definitions (2.115) and (2.116) we arrive at

$$\widehat{q} = (2a_2 + 3a_3 r + \dots + m a_m r^{m-2}) \left(r_x \frac{\partial x}{\partial n} + r_y \frac{\partial y}{\partial n} \right). \quad (2.120)$$

2.2.4.2 Thin Plate Splines for \bar{f} Expansion

Other than the polynomial form of \bar{f} functions there is a different way to obtain a suitable function which satisfies the modified Helmholtz equation. Chen and Rashed [28], obtained a closed form expression for \widehat{u} , and \bar{f} was a linear combination of thin plate splines (TPS) but systematic derivation was not given. Then Muleskov, Golberg and Chen [68] generalized these results by using the annihilator method which is used to obtain particular solutions for ordinary differential equations.

Annihilator Method:

Let P be a linear partial differential operator and

$$Pu = b_2(x, y) \quad (2.121)$$

where

$$b_2 = \sum_{j=1}^{K+L} \bar{\alpha}_j \bar{f}_j \quad \text{and} \quad P\widehat{u}_j = \bar{f}_j. \quad (2.122)$$

Suppose that there is a differential operator M satisfying

$$M\bar{f}_j = 0 \quad (2.123)$$

and commutes with P such that $MP = PM$. Using operator M for equation (2.122), we get

$$M(P\widehat{u}_j) = M\bar{f}_j = 0 = P(M\widehat{u}_j). \quad (2.124)$$

Let $V = \{v : Pv = 0\}$ and $W = \{w : Mw = 0\}$ are finite and disjoint sets and $\{\beta_k\}$ and $\{\gamma_k\}$ are bases for V and W , respectively. Then, a particular solution can be written as

$$\widehat{u}_j = \sum_{k=1}^s b_k \beta_k + \sum_{k=1}^t c_k \gamma_k \quad (2.125)$$

where the coefficients $\{b_k\}$ and $\{c_k\}$ are determined by equation (2.122). Thus, \widehat{u}_j satisfies equation (2.124) as

$$\begin{aligned} MP\widehat{u}_j &= MP \left(\sum_{k=1}^s b_k \beta_k + \sum_{k=1}^t c_k \gamma_k \right) \\ &= MP \left(\sum_{k=1}^s b_k \beta_k \right) + MP \left(\sum_{k=1}^t c_k \gamma_k \right) \\ &= 0. \end{aligned} \quad (2.126)$$

Assigning now P as modified Helmholtz operator ($P = \nabla^2 - \tau^2$) and M as biharmonic operator ($M = \nabla^4$), we can use the annihilator method for solving

$$(\nabla^2 - \tau^2)\widehat{u}_j = r_j^2 \log r_j, \quad j = 1, \dots, K + L. \quad (2.127)$$

Thus, it is enough to solve

$$\frac{1}{r} \frac{d}{dr} \left(r \frac{d(\widehat{u}(r))}{dr} \right) - \tau^2 \widehat{u}(r) = r^2 \log r \quad (2.128)$$

where

$$\nabla^2 u(r) = \frac{1}{r} \frac{d}{dr} \left(r \frac{d(\widehat{u}(r))}{dr} \right). \quad (2.129)$$

Also, it is equivalent to solving

$$\nabla^4(\nabla^2 - \tau^2)\widehat{u}(r) = 0 \quad (2.130)$$

where biharmonic operator and modified Helmholtz operator commute. In order to find a solution for equation (2.130), we must find finite and disjoint solution sets for $\nabla^4 w = 0$ and $(\nabla^2 - \tau^2)v = 0$. Biharmonic operator is a fourth order Euler operator and its characteristic polynomial is $p^2(p - 2)^2$. So, its solution can be written as

$$w(r) = a + b \log r + cr^2 + dr^2 \log r. \quad (2.131)$$

Also, modified Helmholtz equation is a Bessel operator and its solution can be written as

$$v(r) = AI_0(\tau r) + BK_0(\tau r) \quad (2.132)$$

where I_0 and K_0 are the first and second kind modified Bessel functions of order zero. Therefore, the solution of equation (2.130) is

$$\widehat{u}(r) = AI_0(\tau r) + BK_0(\tau r) + a + b \log r + cr^2 + dr^2 \log r. \quad (2.133)$$

All the coefficients in equation (2.133) can be determined by using the equation (2.128). Since

$$(\nabla^2 - \tau^2)I_0(\tau r) = (\nabla^2 - \tau^2)K_0(\tau r) = 0 \quad (2.134)$$

we can take

$$\begin{aligned} (\nabla^2 - \tau^2)\widehat{u}(r) &= (\nabla^2 - \tau^2)(a + b \log r + cr^2 + dr^2 \log r) \\ &= r^2 \log r. \end{aligned} \quad (2.135)$$

Solution of this equation gives

$$a = b = -\frac{4}{\tau^4}, \quad c = 0 \quad \text{and} \quad d = -\frac{1}{\tau^2}. \quad (2.136)$$

Thus,

$$\widehat{u}(r) = AI_0(\tau r) + BK_0(\tau r) - \frac{4}{\tau^4} - \frac{4}{\tau^4} \log r - \frac{1}{\tau^2} r^2 \log r. \quad (2.137)$$

But there is a singularity in (2.133) at $r = 0$. So we need to choose B to cancel the 'log r ' term at $r = 0$. If $K_0(\tau r)$ is expanded for small argument [46], we have

$$K_0(\tau r) \rightarrow -\gamma - \log\left(\frac{\tau r}{2}\right) \quad \text{as} \quad r \rightarrow 0 \quad (2.138)$$

where $\gamma = 0.5772156649015328$ is known as Euler's constant [1]. Thus, for $B = -\frac{4}{\tau^4}$, we obtain a particular solution which is continuous at $r = 0$. Also, since particular solutions are not unique, we can consider $A = 0$. Therefore, we obtain

$$\begin{aligned} \widehat{u}(r) &= -\frac{4}{\tau^4} - \frac{4 \log r}{\tau^4} - \frac{r^2 \log r}{\tau^2} - \frac{4K_0(\tau r)}{\tau^4}, \quad r \neq 0 \\ \widehat{u}(r) &= -\frac{4}{\tau^4} + \frac{4\gamma}{\tau^4} + \frac{4}{\tau^4} \log\left(\frac{\tau}{2}\right), \quad r = 0. \end{aligned} \quad (2.139)$$

In general, we can use higher order splines as [68]

$$(\nabla^2 - \tau^2)\widehat{u}_j = r_j^{2n} \log r_j, \quad j = 1, \dots, K + L. \quad (2.140)$$

This differential equation can be solved now by taking $M = (\nabla^2)^{(n+1)}$ and using the annihilator method where $(n + 1)$ denotes $(n + 1)$ -th derivative of the ∇^2 .

Now, using the fact that

$$(\nabla^2)^{(n+1)}r^{2n} \log r = 0, \quad r > 0, \quad (2.141)$$

\widehat{u} can be obtained by solving

$$(\nabla^2)^{(n+1)}(\nabla^2 - \tau^2)\widehat{u}(r) = 0. \quad (2.142)$$

Thus, its solution can be written as

$$\widehat{u} = v + w \quad (2.143)$$

where

$$(\nabla^2)^{(n+1)}w = 0, \quad (\nabla^2 - \tau^2)v = 0. \quad (2.144)$$

The solution for v is given in (2.132). It will be enough to solve $\nabla^{2(n+1)}w = 0$. $\nabla^{2(n+1)}$ is the multiple of the Euler operator where its characteristic polynomial is $p^2(p-2)^2 \dots (p-2n)^2 = 0$ and characteristic exponents are $p = 0, 2, 4, \dots, 2n$. Its solution can be written as

$$w(r) = \sum_{k=1}^{n+1} c_k r^{2k-2} \log r + \sum_{k=1}^{n+1} d_k r^{2k-2}. \quad (2.145)$$

Thus, the solution of equation (2.142) is

$$\widehat{u} = AI_0(\tau r) + BK_0(\tau r) + w(r). \quad (2.146)$$

The coefficients of equation (2.146) can be determined by using the equation

$$(\nabla^2 - \tau^2)\widehat{u} = r^{2n} \log r. \quad (2.147)$$

In [1] K_0 is define as

$$K_0(\tau r) = \sum_{k=0}^{\infty} \mu_k r^{2k} - \sum_{k=0}^{\infty} \frac{\tau^{2k}}{2^{2k}(k!)^2} r^{2k} \log r \quad (2.148)$$

where

$$\mu_0 = \log\left(\frac{2}{\tau}\right) - \gamma \quad (2.149)$$

and

$$\mu_k = \left[\log\left(\frac{2}{\tau}\right) - \gamma + \sum_{j=1}^k \left(\frac{1}{j}\right) \right] \frac{\tau^{2k}}{2^{2k}(k!)^2}, \quad k \geq 1. \quad (2.150)$$

But, it has a singularity at $r = 0$. So, if we choose c_k 's in (2.145) as

$$c_{k+1} = \frac{B\tau^{2k}}{2^{2k}(k!)^2}, \quad 0 \leq k \leq n, \quad (2.151)$$

then we can cancel the $\log r$ terms in (2.148).

By using the equation (2.147), we can determine the d_k 's in (2.145). Since

$$(\nabla^2 - \tau^2)I_0(\tau r) = (\nabla^2 - \tau^2)K_0(\tau r) = 0 \quad (2.152)$$

and it suffices to solve

$$(\nabla^2 - \tau^2)w = r^{2n} \log r. \quad (2.153)$$

Thus, we have

$$\begin{aligned} (\nabla^2 - \tau^2)w(r) &= \sum_{k=1}^n (4k^2 c_{k+1} - \tau^2 c_k) r^{2k-2} \log r - \tau^2 c_{n+1} r^{2n} \log r \\ &+ \sum_{k=1}^n (4k c_{k+1} - \tau^2 d_k + 4k^2 d_{k+1}) r^{2k-2} - \tau^2 d_{n+1} r^{2n} \end{aligned} \quad (2.154)$$

where

$$\nabla^2(r^{2k} \log r) = 4k^2 r^{2k-2} \log r + 4k r^{2k-2} \quad (2.155)$$

and

$$\nabla^2(r^{2k}) = 4k^2 r^{2k-2}. \quad (2.156)$$

In order to obtain the whole coefficients, we use the assumptions

$$\begin{aligned} 4k^2 c_{k+1} - \tau^2 c_k &= 0, & (i) \\ -\tau^2 c_{n+1} &= 1, & (ii) \\ 4k c_{k+1} - \tau^2 d_k + 4k^2 d_{k+1} &= 0, & (iii) \\ -\tau^2 d_{n+1} &= 0, & (iv) \end{aligned} \quad (2.157)$$

$k=1,2,\dots,n$. By using equation (2.151) and (i) we have

$$4k^2 c_{k+1} - \tau^2 c_k = \frac{4k^2 B \tau^{2k}}{2^{2k}(k!)^2} - \frac{\tau^2 B \tau^{2k-2}}{2^{2k-2}((k-1)!)^2} = 0. \quad (2.158)$$

Conditions (ii), and (iv) give

$$c_{n+1} = -\frac{1}{\tau^2} \quad \text{and} \quad d_{n+1} = 0. \quad (2.159)$$

From (2.151) and (2.159) the constant B becomes

$$B = -\frac{2^{2n}(n!)^2}{\tau^{2n+2}} \quad (2.160)$$

and then the coefficients c_k 's

$$c_k = -\frac{2^{2n}(n!)^2}{2^{2k-2}((k-1)!)^2} \tau^{2k-2n-4}. \quad (2.161)$$

Substituting (2.161) into condition (iii) in the equation (2.157) and multiplying by $\frac{2^{2k-2}(k-1)!^2}{\tau^{2k+2}}$ it becomes

$$-\frac{2^{2n}(n!)^2}{\tau^{2n+4}k} - \frac{2^{2k-2}((k-1)!)^2 d_k}{\tau^{2k}} + \frac{2^{2k}(k!)^2 d_{k+1}}{\tau^{2k+2}} = 0. \quad (2.162)$$

If we take

$$\delta_k = \frac{2^{2k-2}((k-1)!)^2 d_k}{\tau^{2k}}, \quad 1 \leq k \leq n+1, \quad (2.163)$$

then (2.162) can be written

$$-\frac{2^{2n}(n!)^2}{\tau^{2n+4}k} - \delta_k + \delta_{k+1} = 0 \quad (2.164)$$

where from (2.159), $\delta_{n+1} = 0$. So,

$$\delta_k = \delta_{n+1} + \sum_{j=k}^n (\delta_j - \delta_{j+1}), \quad 1 \leq k \leq n. \quad (2.165)$$

Thus,

$$\delta_k = -\frac{2^{2n}(n!)^2}{\tau^{2n+4}} \sum_{j=k}^n \left(\frac{1}{j}\right) \quad (2.166)$$

and

$$d_k = -\frac{2^{2n}(n!)^2}{2^{2k-2}((k-1)!)^2} \tau^{2k-2n-4} \sum_{j=k}^n \left(\frac{1}{j}\right), \quad 1 \leq k \leq n. \quad (2.167)$$

Finally, from (2.161) and (2.167)

$$d_k = c_k \sum_{j=k}^n \left(\frac{1}{j}\right), \quad 1 \leq k \leq n. \quad (2.168)$$

Also, since particular solutions are not unique, we can consider $A = 0$. Therefore, we obtain [68]

$$\widehat{u}(r) = AI_0(\tau r) + BK_0(\tau r) + \sum_{k=1}^{n+1} c_k r^{2k-2} \log r + \sum_{k=1}^n d_k r^{2k-2} \quad (2.169)$$

where

$$\left\{ \begin{array}{l} B = -\frac{2^{2n}(n!)^2}{\tau^{2n+2}} \\ c_k = -\frac{2^{2n}(n!)^2}{2^{2k-2}((k-1)!)^2} \tau^{2k-2n-4}, \quad 1 \leq k \leq n+1 \\ d_k = c_k \sum_{j=k}^n \left(\frac{1}{j}\right), \quad 1 \leq k \leq n. \end{array} \right. \quad (2.170)$$

A list of particular solutions \widehat{u} explicitly for modified Helmholtz equation for the two-dimensional case with corresponding \bar{f} is shown in Table (2.1).

Table 2.1: Particular solutions for modified Helmholtz equation in \mathbf{R}^2 with inhomogeneity \bar{f} , [68].

\bar{f}	\widehat{u}
<p>Case I</p> <p>$\bar{f} = r^2 \log r$</p>	$-\frac{4}{\tau^4}(K_0(\tau r) + \log r) - \frac{r^2 \log r}{\tau^2} - \frac{4}{\tau^4}, \quad r > 0$ $\frac{4}{\tau^4}(\gamma + \log(\frac{\tau}{2})) - \frac{4}{\tau^4}, \quad r = 0$
<p>Case II</p> <p>$\bar{f} = r^4 \log r$</p>	$-\frac{64}{\tau^6}(K_0(\tau r) + \log r) - \frac{r^2 \log r}{\tau^2}(\frac{16}{\tau^2} + r^2) - \frac{8r^2}{\tau^4} - \frac{96}{\tau^6}, \quad r > 0$ $\frac{64}{\tau^6}(\gamma + \log(\frac{\tau}{2})) - \frac{96}{\tau^6}, \quad r = 0$
<p>Case III</p> <p>$\bar{f} = r^6 \log r$</p>	$-\frac{2304}{\tau^8}(K_0(\tau r) + \log r) - \frac{r^2 \log r}{\tau^2}(\frac{576}{\tau^4} + \frac{36r^2}{\tau^2} + r^4)$ $-\frac{12r^2}{\tau^4}(\frac{40}{\tau^2} + r^2) - \frac{4224}{\tau^8}, \quad r > 0$ $\frac{2304}{\tau^8}(\gamma + \log(\frac{\tau}{2})) - \frac{4224}{\tau^8}, \quad r = 0$
<p>Case IV</p> <p>$\bar{f} = r^8 \log r$</p>	$-\frac{147456}{\tau^{10}}(K_0(\tau r) + \log r) - \frac{r^2 \log r}{\tau^2}(\frac{36864}{\tau^6} + \frac{2304r^2}{\tau^4} + \frac{64r^4}{\tau^2} + r^6)$ $-\frac{r^2}{\tau^4}(\frac{39936}{\tau^4} + \frac{1344r^2}{\tau^2} + 16r^4) - \frac{307200}{\tau^{10}}, \quad r > 0$ $\frac{147456}{\tau^{10}}(\gamma + \log(\frac{\tau}{2})) - \frac{307200}{\tau^{10}}, \quad r = 0$
<p>Case V</p> <p>$\bar{f} = r^{10} \log r$</p>	$-\frac{14745600}{\tau^{12}}(K_0(\tau r) + \log r) - \frac{r^2 \log r}{\tau^2}(\frac{3686400}{\tau^8} + \frac{230400r^2}{\tau^6} + \frac{6400r^4}{\tau^4} + \frac{100r^6}{\tau^2} + r^8)$ $-\frac{r^2}{\tau^4}(\frac{4730880}{\tau^6} + \frac{180480r^2}{\tau^4} + \frac{2880r^4}{\tau^2} + 20r^6) - \frac{33669120}{\tau^{12}}, \quad r > 0$ $\frac{14745600}{\tau^{12}}(\gamma + \log(\frac{\tau}{2})) - \frac{33669120}{\tau^{12}}, \quad r = 0$

2.3 DRBEM for Inverse Problem

A direct (forward) problem which is also called a *well-posed* problem is a classical mathematical description of a physical problem with the properties of uniqueness, stability and existence of a solution of corresponding mathematical problem. A problem is called an inverse problem which consists of finding an unknown property of an object from the observation of response of this object to probing signal [78]. If a mathematical problem does not have any of the above

properties, it is called *ill-posed* problem. On the contrary to the solution of a direct problem, the solution of inverse problem is generally ill-posed. Ill-posedness is a typical property of inverse problems.

Actually direct and inverse problems are related to each other. The data of one problem can be an unknown of the other. The purpose of a direct problem is to resolve the field variables but in an inverse problem, one of the terms (boundary conditions) is not known explicitly and it should be specified from a direct problem. So, the main idea of the inverse problem is to determine the unknown variables using additional information which are usually obtained by some measured data.

For instance, in a heat conduction problem if the temperature or heat flux values on the solid surface are known as functions of time then all the temperature distributions of the solid can be obtained [18]. This problem is called a direct problem. In some cases, to obtain the temperature or heat flux values of the solid on its surface can not be measured. Sometimes the surface heat flux and temperature values are determined by using previously known interior temperature values, or transient level known boundary values. In this case the problem is called an inverse problem.

The mathematical modeling of heat transfer process is necessary for estimating the surface transient heat flux of the solid. One-dimensional temperature distribution T in a plate can be modeled as

$$\frac{\partial}{\partial x} \left(k \frac{\partial T}{\partial x} \right) = \widehat{\rho}c \frac{\partial T}{\partial t} \quad (2.171)$$

$$T(x, t) = T_0(x) \quad (2.172)$$

$$\frac{\partial T}{\partial x} = 0 \quad \text{at} \quad x = L_p \quad (2.173)$$

$$T(x_1, t_i) = Y_i \quad (2.174)$$

where k is thermal conductivity, c is the specific heat, $\widehat{\rho}$ is the density, T_0 is the known initial temperature, L_p is the thickness of the plate, and x_1 is the location of interior temperature sensor. The temperature is measured by using the sensor at discrete times t_i and the temperature measurement at time t_i is Y_i . So, in the problem the only known boundary condition is given for $x = L_p$. Using the measurement obtained from interior temperature sensor this problem can be transformed to two different problems

$$\frac{\partial}{\partial x} \left(k \frac{\partial T}{\partial x} \right) = \widehat{\rho}c \frac{\partial T}{\partial t} \quad (2.175)$$

$$T(x, t) = T_0(x) \quad (2.176)$$

$$T(x, t) = Y(t) \quad \text{at} \quad x = x_1 \quad (2.177)$$

$$\frac{\partial T}{\partial x} = 0 \quad \text{at} \quad x = L_p \quad (2.178)$$

as a direct problem, and

$$\frac{\partial}{\partial x} \left(k \frac{\partial T}{\partial x} \right) = \widehat{\rho}c \frac{\partial T}{\partial t} \quad (2.179)$$

$$T(x, t) = T_0(x) \quad (2.180)$$

$$T(x, t) = Y(t) \quad \text{at} \quad x = x_1 \quad (2.181)$$

$$q(x_1, t) = -k \frac{\partial T}{\partial x} \quad \text{at} \quad x = x_1 \quad (2.182)$$

as an inverse problem. Here, the heat flux at x_1 can be obtained from the solution of direct problem in $x \in [x_1, L_p]$.

Now, the inverse heat conduction problem is an ill-posed problem. There are many reasons for its ill-posedness. Sometimes the solution of the problem is not unique or does not depend continuously on the data, or does not exist for arbitrary data. The ill-posedness of the inverse problem is caused by the noise in the data which may give rise to some errors in the measurement. Therefore, some techniques which are known as regularization methods should be used to deal with this problem. There are two subclasses for the ill-posed problems which are due to the estimation of the data and design of automatic controls [93, 18]. The ill-posedness of inverse heat conduction problem belongs to the first subclass.

For the solution of heat conduction problem, many numerical methods such as BEM, FEM, and FDM can be used, and these methods lead to the sets of algebraic equations such as

$$\mathbf{Ax}=\mathbf{b} \quad (2.183)$$

where x contains the temperature or heat flux values. The location of the temperature measurement and small time step cause the ill conditioned system where for small changes in b would make large changes in x [18]. So, the system is ill-posed in the sense that the inverse operator \mathbf{A}^{-1} of \mathbf{A} exists but is not continuous, it has a unique solution. But, when it is solved directly, a right solution may not be obtained.

The regularization method is an modification of the least squares approach by adding the factors [18]. Several regularization methods have been developed to solve such ill-conditioned systems [50]. The most common and well known regularization method for linear ill-posed problem is the Tikhonov Regularization Method [93]. In order to get a stable solution for the system (2.183) Tikhonov Regularization Method proposes that the equation

$$(\mathbf{A}^T \mathbf{A} + \lambda \mathbf{I}) \mathbf{x} = \mathbf{A}^T \mathbf{b} \quad (2.184)$$

has a unique solution which is called *Tikhonov* solution. In equation (2.184) λ is the regularization parameter forcing $(\mathbf{A}^T \mathbf{A} + \lambda \mathbf{I})$ to be positive definite, \mathbf{A}^T is transpose matrix of \mathbf{A} , and \mathbf{I} is the identity matrix.

The numerical solution of the inverse problem consists of two parts. The first part of the problem is a numerical discretization of the equation, and the second part is a regularization procedure to stabilize the usually ill-conditioned system obtained in the first part. Therefore, various numerical methods such as BEM, FEM, and FDM can be used in the solution of the inverse problem [18, 91]. Since the solution procedure of DRBEM does not require the domain discretization, it gives a small sized discretized system than the other numerical schemes. In the calculation of the inverse problem, the size of the numerical discretization system has an important effect on the computing effort [31]. Thus, DRBEM enables a remarkable computing saving.

In this thesis, some of the problems which are solved by direct DRBEM are solved also with inverse DRBEM. For this, the governing equations of the inverse problem are discretized with DRBEM as is done with the direct problem where its derivation is given in Section 2.1 and 2.2. In the solution procedure, known variables of the inverse problem and additional

information obtained from the solution of direct problem are combined. However, at the end of the solution procedure, an ill-posed linear system is obtained caused by the noise in the data. Thus, the Tikhonov regularization method is used to deal with this ill-posedness of the problem.

2.3.1 DRBEM Solution of Poisson Equation for an Inverse Problem

In this section, DRBEM is developed for the inverse problem governed by two-dimensional Poisson equation

$$\nabla^2 u = b_1(x, y) \quad (x, y) \in \Omega \quad (2.185)$$

with the Dirichlet and Neumann boundary conditions

$$\begin{aligned} u(x, y) &= \bar{u}_1(x, y) & (x, y) \in \Gamma_1 \\ q(x, y) &= \frac{\partial u}{\partial n} = \bar{q}_2(x, y) & (x, y) \in \Gamma_2 \end{aligned} \quad (2.186)$$

where $b_1(x, y)$ is known function of position and n is the unit outward normal to the boundary $\Gamma = \Gamma_1 + \Gamma_2$. $\bar{u}_1(x, y)$ and $\bar{q}_2(x, y)$ are the prescribed functions for u at the boundary Γ_1 and q at the boundary Γ_2 , respectively.

Sometimes, one boundary can be overprescribed with both u and q given while the other boundary can be underprescribed without a condition on either u or q . These type of problems are called inverse problem and their solutions require extra attention.

As an example, a governing equation of inverse problem can be described as

$$\nabla^2 u = b_1(x, y) \quad (x, y) \in \Omega \quad (2.187)$$

with the Dirichlet and Neumann boundary conditions

$$\begin{aligned} u(x, y) &= \bar{u}_1(x, y) & q(x, y) &= \bar{q}_1(x, y) & (x, y) &\in \Gamma_1 \\ u(x, y) &= \bar{u}_2(x, y) =? & q(x, y) &= \bar{q}_2(x, y) =? & (x, y) &\in \Gamma_2 \end{aligned} \quad (2.188)$$

where the prescribed values of direct problem are regarded as unknown in the inverse problem, and the missing boundary condition of inverse problem will be obtained from the solution of the direct problem.

DRBEM derivation of Poisson equation for an inverse problem is done by using the same way with the direct problem which was explained in Section 2.1. At the end of the solution procedure one can obtain the system of algebraic equations

$$\mathbf{Ax}=\mathbf{y}. \quad (2.189)$$

This system is constructed using the known variables of the inverse problem and additional informations obtained from the direct problem. Since Γ_1 is considered as overprescribed and Γ_2 is considered as underprescribed, this system will lead to the ill-posedness of the problem. Therefore, classical DRBEM is not adequate and a regularization procedure should be used to overcome obtained ill-posed system.

2.3.2 DRBEM Solution of Modified Helmholtz Equation for an Inverse Problem

Let us consider the following two-dimensional Modified Helmholtz equation in which the right hand side is a known function $b_2(x, y)$, i.e.

$$\nabla^2 u - \tau^2 u = b_2(x, y) \quad (x, y) \in \Omega \quad (2.190)$$

with the Dirichlet and Neumann boundary conditions

$$\begin{aligned} u(x, y) &= \bar{u}_1(x, y) & (x, y) \in \Gamma_1 \\ q(x, y) &= \frac{\partial u}{\partial n} = \bar{q}_2(x, y) & (x, y) \in \Gamma_2 \end{aligned} \quad (2.191)$$

where n is the unit outward normal to the boundary $\Gamma = \Gamma_1 + \Gamma_2$, and $\bar{u}_1(x, y)$ and $\bar{q}_2(x, y)$ are the prescribed functions for u at the boundary Γ_1 and q at the boundary Γ_2 , respectively.

In the direct problem, normal derivative $\bar{q}_2(x, y)$ on the boundary Γ_2 is considered as prescribed, but in the inverse problem it will be regarded as unknown. Normal derivative $\bar{q}_1(x, y)$ at Γ_1 , which will be obtained from the solution of the direct problem will be used for the missing boundary condition at Γ_2 . Therefore, an inverse problem for modified Helmholtz equation can be defined as

$$\nabla^2 u - \tau^2 u = b_2(x, y) \quad (x, y) \in \Omega \quad (2.192)$$

with the Dirichlet and Neumann boundary conditions

$$\begin{aligned} u(x, y) &= \bar{u}_1(x, y) & q(x, y) &= \bar{q}_1(x, y) & (x, y) &\in \Gamma_1 \\ u(x, y) &= \bar{u}_2(x, y) =? & q(x, y) &= \bar{q}_2(x, y) =? & (x, y) &\in \Gamma_2. \end{aligned} \quad (2.193)$$

In the DRBEM derivation of modified Helmholtz equation, there is no difference between direct and inverse problem, and it was given for direct problem in Section 2.2. Similar with inverse Poisson equation, the DRBEM solution procedure for modified Helmholtz equation also gives an ill-posed system of algebraic equations which is obtained using the known variables of the inverse problem and additional information obtained from the direct problem as

$$\mathbf{Ax}=\mathbf{y}. \quad (2.194)$$

Therefore, the solution of inverse problem will be obtained after using Tikhonov regularization method for the ill-posed system. In the regularization procedure, the system (2.194) is written in the form [76]

$$\left(\mathbf{A}^T \mathbf{A} + \lambda \mathbf{I}\right) \mathbf{x} = \mathbf{A}^T \mathbf{b} \quad (2.195)$$

where $\lambda > 0$ is the regularization parameter to achieve positive definiteness of the coefficient matrix, and it should be chosen close to 0 but too much small choice may cause again an ill-conditioned system. Therefore, the choice of λ is an important point on the solution of the system.

CHAPTER 3

DIFFERENTIAL QUADRATURE METHOD

The differential quadrature method (DQM) is a numerical discretization technique for the approximation of derivatives which was developed by R. Bellman and his associates in the early 1970's. Bellman introduced DQM as an efficient solution technique to obtain accurate numerical solutions by using a considerably small number of mesh points [21]. In the solution procedure, a partial derivative of a function with respect to a coordinate direction can be expressed as a linear summation of all the function values along a mesh line.

The aim of the DQM is the determination of the weighting coefficients for the discretization of a partial derivative of any order. The weighting coefficients can be obtained just by using the grid point information. Thus, one can easily obtain a set of algebraic equations for any partial differential equation by using these coefficients. Shu [88] generalized all the current methods for determination of weighting coefficients by using the properties of a linear vector space. Shu [88] proposed that, in order to compute the weighting coefficients of the first order derivative, a simple algebraic formulation can be obtained without any restriction on the choice of the mesh points. Also, a recurrence relation to compute the weighting coefficients of second and higher order derivatives in terms of first order derivative weighting coefficients, are presented in [88]. If the polynomial approximation is considered as a base of DQM, then the method is called polynomial-based differential quadrature (PDQ). It is possible to approximate a function by using Fourier series, and the use of Fourier series approximation as a base results in Fourier-based differential quadrature (FDQ).

In this thesis, the partial differential equations governing the physical problems considered are transformed to the form of modified Helmholtz equations, and then they are solved with polynomial-based differential quadrature method. Non-uniform grid point distributions as the roots of Chebyshev polynomial or Chebyshev-Gauss-Lobatto points are used in the computations. In Section 3.1, the polynomial-based differential quadrature method is going to be explained in detail for the first, second and higher order derivative approximations. Then, different type of grid point distributions are given in Section 3.2. Sections 3.3 and 3.4 give applications of PDQ to Poisson and modified Helmholtz equations, respectively, with Dirichlet and Neumann boundary conditions.

3.1 Polynomial-based Differential Quadrature Method

In this section, we will explain the fundamentals of the differential quadrature method (DQM) in one-dimension when the derivatives of a function are approximated by using polynomials

following the reference [88]. Generalization to higher order dimensions follows the same idea. The main idea of the DQM is that the first order derivative of a function $f(x)$ with respect to x , at a grid point x_i can be approximated by the linear sum of all the functional values in the domain such as

$$f_x(x_i) = \frac{\partial f}{\partial x}(x_i) = \sum_{j=1}^N a_{ij}f(x_j), \quad \text{for } i = 1, 2, \dots, N \quad (3.1)$$

where a_{ij} are the weighting coefficients and N is the number of the grid points in the whole domain. DQM determines the weighting coefficients a_{ij} which are different at different grid points x_i . The function $f(x)$ is assumed to be sufficiently smooth over the one-dimensional domain in R^1 .

Generally, the solution of partial differential equations (PDEs) may not be obtained in a closed form. However, the solution of well-posed PDEs can be approximated by using higher order polynomials. High order polynomials and the Weierstrass' first Theorem form the basis of the DQM. The statement of the theorem is given bellow:

Weierstrass' first Theorem: Let $f(x)$ be a real valued continuous function defined in a closed interval $[a, b]$. Then there exists a sequence of polynomials $P_n(x)$ which converges to $f(x)$ uniformly as n goes to infinity or for every $\epsilon > 0$, there exists a polynomial $P_n(x)$ of degree $n = n(\epsilon)$ such that the inequality

$$|f(x) - P_n(x)| \leq \epsilon \quad (3.2)$$

holds through the interval $[a, b]$.

Thus, the solution of a differential equation can be approximated by a high degree polynomial of degree $N - 1$ as in [88] such that

$$f(x) \approx P_N(x) = \sum_{k=0}^{N-1} c_k x^k \quad (3.3)$$

where $f(x)$ represents the solution of differential equation and c_k 's are the coefficients. Here $P_N(x)$ sets up an N -dimensional linear vector space with the operation of vector addition and scalar multiplication.

Let suppose that there are N mesh points in a closed interval $[a, b]$ with the coordinates $a = x_1, x_2, \dots, x_n = b$. To obtain a numerical solution of a PDE one needs to find the functional values $f(x_i)$. If the function $f(x)$ is evaluated at these N different points, this gives the following equation system

$$\begin{cases} c_0 + c_1 x_1 + c_2 x_1^2 + \dots + c_{N-1} x_1^{N-1} = f(x_1) \\ c_0 + c_1 x_2 + c_2 x_2^2 + \dots + c_{N-1} x_2^{N-1} = f(x_2) \\ \dots \\ c_0 + c_1 x_N + c_2 x_N^2 + \dots + c_{N-1} x_N^{N-1} = f(x_N) \end{cases} \quad (3.4)$$

which is called *Vandermonde* matrix. Since this matrix is nonsingular, matrix equation (3.4) has a unique solution for the coefficients $c_0, c_1, c_2, \dots, c_{N-1}$. So, in order to obtain the approximate function, the coefficients must be determined. But, when N is large, the matrix can be highly ill-conditioned and in this situation to obtain its inverse is very difficult. This problem can be solved by using different sets of base functions. In this section, Lagrange interpolation polynomials are used in the derivation of coefficients in differential quadrature method which is called Shu's general approach [88].

If the Lagrange interpolation polynomials are taken as a set of base polynomials,

$$f(x) = \sum_{k=1}^N l_k(x) f(x_k) \quad (3.5)$$

is obtained where $l_k(x)$'s are Lagrange polynomials. The k -th degree Lagrange polynomial $l_k(x)$ can be written in the form

$$l_k(x) = \frac{N(x, x_k)}{M^{(1)}(x_k)} \quad (3.6)$$

with

$$\begin{aligned} M(x) &= (x - x_1)(x - x_2)\dots(x - x_N) = N(x, x_k)(x - x_k) \\ M^{(1)}(x_k) &= (x_k - x_1)\dots(x_k - x_{k-1})(x_k - x_{k+1})\dots(x_k - x_N) = \prod_{k=1, k \neq i}^n (x_k - x_i) \\ N(x_k, x_j) &= M^{(1)}(x_k) \delta_{kj} \end{aligned} \quad (3.7)$$

where δ_{kj} is the Kronecker delta function and $k = 1, \dots, N$. So, k -th degree Lagrange polynomial $l_k(x)$ in the equation (3.5) possesses the property

$$l_k(x_i) = \begin{cases} 1, & \text{when } k = i \\ 0, & \text{otherwise.} \end{cases} \quad (3.8)$$

The derivative of $f(x)$ can be obtained by just differentiating $l_k(x)$ polynomials,

$$f^{(1)}(x_i) = \sum_{k=1}^N l_k^{(1)}(x) f(x_k). \quad (3.9)$$

A practical notation is introduced for calculating the weighting coefficients by Shu [88] as

$$f^{(1)}(x_i) = \sum_{k=1}^N a_{ik} f(x_k) \quad (3.10)$$

where

$$a_{ik} = \frac{N^{(1)}(x_i, x_k)}{M^{(1)}(x_k)}. \quad (3.11)$$

If $M(x) = N(x, x_k)(x - x_k)$ is successively differentiated with respect to x , the following recurrence formulation

$$M^{(m)}(x) = N^{(m)}(x, x_k)(x - x_k) + mN^{(m-1)}(x, x_k) \quad (3.12)$$

can be achieved for $m = 1, 2, \dots, N - 1$ where $M^{(m)}(x)$ and $N^{(m)}(x, x_k)$ indicate the m th order derivative of $M(x)$ and $N(x, x_k)$, respectively. From equation (3.12), one can obtain

$$\begin{aligned} N^{(1)}(x_i, x_k) &= \frac{M^{(1)}(x_i)}{x_i - x_k}, & i \neq k \\ N^{(1)}(x_i, x_i) &= \frac{M^{(2)}(x_i)}{2}. \end{aligned} \quad (3.13)$$

Substituting equation (3.13) into equation (3.11), one can get

$$\begin{aligned} a_{ik} &= \frac{M^{(1)}(x_i)}{(x_i - x_k)M^{(1)}(x_k)}, & i \neq k, \\ a_{ii} &= \frac{M^{(2)}(x_i)}{2M^{(1)}(x_i)}. \end{aligned} \quad (3.14)$$

If x_i is given, it is easy to compute $M^{(1)}(x_i)$ and hence a_{ik} for $i \neq k$. But the calculation of a_{ii} is based on the computation of the second order derivative $M^{(2)}(x_i)$ which is not an easy task. This difficulty can be eliminated by using the set of polynomials x^{k-1} . According to the property of a linear vector space, if one set of base polynomials satisfies a linear operator, so does another set of base polynomials [88]. Therefore, the system for determination of a_{ik} derived from the Lagrange interpolation polynomials should be equivalent to that derived from another set of base polynomials $x^{k-1}, k = 1, \dots, N$. Thus, a_{ik} satisfies the following equation which is obtained by the base polynomial x^{k-1} when $k = 1$, [88]

$$\sum_{k=1}^N a_{ik} = 0 \quad \text{or} \quad a_{ii} = - \sum_{k=1, k \neq i}^N a_{ik}. \quad (3.15)$$

Thus, equations (3.14) and (3.15) are two formulations to compute the weighting coefficients a_{ii} .

For the discretization of second order derivative, we use a similar approximation given by

$$f^{(2)}(x_i) = \sum_{k=1}^N b_{ik} f(x_k) \quad (3.16)$$

for $i = 1, \dots, N$, where $f^{(2)}(x_i)$ is the second derivative of $f(x)$ at x_i , b_{ik} are the weighting coefficients for the second order derivative approximation.

Similar with the first order derivative, by taking second derivative of equation (3.6), we obtain

$$b_{ik} = \frac{N^{(2)}(x_i, x_k)}{M^{(1)}(x_k)}. \quad (3.17)$$

In addition, from the equation (3.12), we get

$$\begin{aligned} N^{(2)}(x_i, x_k) &= \frac{M^{(2)}(x_i) - 2N^{(1)}(x_i, x_k)}{x_i - x_k}, \quad i \neq k \\ N^{(2)}(x_i, x_i) &= \frac{M^{(3)}(x_i)}{3}. \end{aligned} \quad (3.18)$$

Substituting these into equation (3.17), we obtain

$$\begin{aligned} b_{ik} &= \frac{M^{(2)}(x_i) - 2N^{(1)}(x_i, x_k)}{(x_i - x_k)M^{(1)}(x_k)}, \quad i \neq k \\ b_{ii} &= \frac{M^{(3)}(x_i)}{3M^{(1)}(x_i)}. \end{aligned} \quad (3.19)$$

Therefore, by using equation (3.14) and (3.19) we get

$$b_{ik} = 2a_{ik} \left(a_{ii} - \frac{1}{x_i - x_k} \right), \quad i \neq k. \quad (3.20)$$

Similar with the first order derivative, b_{ik} satisfies the following equation which is obtained by the base polynomial x^{k-1} when $k = 1$,

$$\sum_{k=1}^N b_{ik} = 0 \quad \text{or} \quad b_{ii} = - \sum_{k=1, k \neq i}^N b_{ik}. \quad (3.21)$$

So, equations (3.19) and (3.21) are two formulations to compute the weighting coefficients b_{ii} .

For the higher order derivatives there is a generalization which is called Shu's recurrence relation formulation for high order derivatives for $m = 2, 3, \dots, N - 1$

$$\begin{aligned}
w_{ij}^{(m)} &= m \left(a_{ij} w_{ii}^{(m-1)} - \frac{w_{ij}^{(m-1)}}{x_i - x_j} \right), & i \neq j \\
w_{ii}^{(m)} &= - \sum_{j=1, i \neq j}^N w_{ij}^{(m)}, & i = j
\end{aligned} \tag{3.22}$$

where $i, j = 1, 2, \dots, N$ and a_{ij} are the weighting coefficients of the first order derivative. Now, when the coordinates of grid points x_i are known, the weighting coefficients for the discretization of derivatives can be calculated easily.

3.2 Typical Grid Point Distribution

In this section, two typical point distributions will be given which are Chebyshev-Gauss-Lobatto (CGL) grid, and a grid with coordinates chosen as the roots of Chebyshev polynomial. These point distributions enable us to take grid points close to the end points. Generally, when the other numerical methods are used, uniform grid points are preferred because of its practical use. But nonuniform grid points which give more stable numerical result than the other are suitable for DQM [88].

3.2.1 Chebyshev-Gauss-Lobatto Grid (CGL Points)

The Chebyshev polynomial of degree i is defined as

$$T_i(x) = \cos i\theta \quad \theta = \arccos x \tag{3.23}$$

and the Chebyshev-Gauss-Lobatto points are chosen as the roots of $|T_N(x)| = 1$, which are given

$$x_i = \cos \left(\frac{i\pi}{N} \right), \quad i = 0, 1, \dots, N. \tag{3.24}$$

All the points in equation (3.24) are located in the interval $[-1, 1]$. If CGL will be used for any physical domain $[a, b]$, it should be transformed to $[-1, 1]$ by using the following coordinate transformation

$$x = \frac{b-a}{2} (1 - \xi) + a. \tag{3.25}$$

This transformation maps the interval $[a, b]$ in the x -domain onto the interval $[-1, 1]$ in the ξ -domain.

3.2.2 The Roots of Chebyshev Polynomial

The roots of Chebyshev polynomial can be obtained by solving the equation $T_N(x) = 0$ which are

$$x_i = \cos \left(\frac{(2i-1)\pi}{2N} \right), \quad i = 1, 2, \dots, N. \tag{3.26}$$

The roots of Chebyshev polynomial x_i are in the domain $[x_1, x_N]$ where $x_1 = \cos\left(\frac{\pi}{2N}\right)$ and $x_N = \cos\left(\frac{(2N-1)\pi}{2N}\right) = -x_1$.

For a general domain $[a, b]$, the following transformation

$$x = \frac{b-a}{2x_1}(x_1 - \xi) + a. \quad (3.27)$$

is used to map $[a, b]$ in the x -domain onto the interval $[x_1, x_N]$ in the ξ -domain.

3.3 DQM Solution of Poisson Equation $\nabla^2 u = b_1(x, y)$

In this part, DQM will be applied to Poisson equation where the right hand side function contains only space coordinates as in [88]. Let us consider the following two dimensional Poisson equation

$$\nabla^2 u = b_1(x, y) \quad (3.28)$$

on a rectangular domain, $0 \leq x \leq H_1$, $0 \leq y \leq H_2$. Let N_1 and N_2 be the number of grid points in x - and y - directions, respectively. At any point (x_i, y_j) , (3.28) can be discretized as

$$\sum_{k=1}^{N_1} b_{ik} u_{kj} + \sum_{k=1}^{N_2} \bar{b}_{jk} u_{ik} = b_1(x_i, y_j) \quad (3.29)$$

where b_{ij} and \bar{b}_{ij} are the weighting coefficients of the second order derivatives of u with respect to x and y , respectively. u_{ij} represents the value of u at the grid point (x_i, y_j) , and $i = 1, \dots, N_1$ and $j = 1, \dots, N_2$.

Assume that Dirichlet type boundary conditions are defined at all the boundaries. Since the functional values at the boundary points are known, DQM procedure should be applied only at the interior points. Thus, equation (3.29) can be written as

$$\sum_{k=2}^{N_1-1} b_{ik} u_{kj} + \sum_{k=2}^{N_2-1} \bar{b}_{jk} u_{ik} = s_{ij} \quad (3.30)$$

for $i = 2, \dots, N_1 - 1$, $j = 2, \dots, N_2 - 1$, and the right hand side function is

$$s_{ij} = b_1(x_i, y_j) - (b_{i1} u_{1j} + b_{iN_1} u_{N_1j} + \bar{b}_{j1} u_{i1} + \bar{b}_{jN_2} u_{iN_2}). \quad (3.31)$$

Equations (3.30) give a set of algebraic equations, which can be written in a matrix form

$$\mathbf{A}\mathbf{u} = \mathbf{s} \quad (3.32)$$

where \mathbf{A} is a coefficient matrix with the dimension $(N_1 - 2)(N_2 - 2) \times (N_1 - 2)(N_2 - 2)$, \mathbf{u} is a vector of unknown values at all the interior points given by

$$\mathbf{u} = [u_{22}, u_{23}, \dots, u_{2(N_2-1)}, u_{32}, u_{33}, \dots, u_{3(N_2-1)}, \dots, u_{(N_1-1)2}, u_{(N_1-1)3}, \dots, u_{(N_1-1)(N_2-1)}]^T \quad (3.33)$$

with the dimension $(N_1 - 2)(N_2 - 2)$, and \mathbf{s} is a known vector given by

$$\mathbf{s} = [s_{22}, s_{23}, \dots, s_{2(N_2-1)}, s_{32}, s_{33}, \dots, s_{3(N_2-1)}, \dots, s_{(N_1-1)2}, s_{(N_1-1)3}, \dots, s_{(N_1-1)(N_2-1)}]^T \quad (3.34)$$

with the dimension $(N_1 - 2)(N_2 - 2)$. Thus, equation (3.32) can be solved by direct or iterative methods.

Assume that Neumann type boundary conditions are defined at all the boundaries such as

$$\begin{aligned} \frac{\partial u}{\partial x} &= c_1, & x &= 0, & 0 \leq y \leq H_2 \\ \frac{\partial u}{\partial y} &= c_2, & y &= 0, & 0 \leq x \leq H_1 \\ \frac{\partial u}{\partial x} &= c_3, & x &= H_1, & 0 \leq y \leq H_2 \\ \frac{\partial u}{\partial y} &= c_4, & y &= H_2, & 0 \leq x \leq H_1 \end{aligned} \quad (3.35)$$

where c_1, c_2, c_3 and c_4 are constants. Since Neumann type boundary conditions are defined at the boundary points, DQM procedure should be applied to both interior and boundary points. For the interior points, similar with the Dirichlet type boundary conditions, DQM gives

$$\sum_{k=2}^{N_1-1} b_{ik} u_{kj} + \sum_{k=2}^{N_2-1} \bar{b}_{jk} u_{ik} = s_{ij} \quad (3.36)$$

where $s_{ij} = b_1(x_i, y_j)$, $i = 2, \dots, N_1 - 1$ and $j = 2, \dots, N_2 - 1$. For the Neumann type boundary conditions, the first order derivatives are discretized at the boundaries as

$$\begin{aligned} \sum_{k=1}^{N_1} a_{1k} u_{kj} &= c_1, & j &= 1, \dots, N_2, \\ \sum_{k=1}^{N_2} \bar{a}_{1k} u_{ik} &= c_2, & i &= 2, \dots, N_1 - 1 \\ \sum_{k=1}^{N_1} a_{N_1k} u_{kj} &= c_3, & j &= 1, \dots, N_2, \\ \sum_{k=1}^{N_2} \bar{a}_{N_2k} u_{ik} &= c_4, & i &= 2, \dots, N_1 - 1 \end{aligned} \quad (3.37)$$

where a_{ij} and \bar{a}_{ij} are the weighting coefficients of the first order derivatives of u with respect to x and y , respectively.

Equation system (3.37) can be used to solve for $2(N_1 + N_2 - 2)$ unknown boundary points. Together with the equation (3.36) there are $N_1 N_2$ equations for $N_1 N_2$ unknowns which give a set of algebraic equations, and can be written in a matrix-vector form

$$\mathbf{A}\mathbf{u} = \mathbf{s} \quad (3.38)$$

where \mathbf{A} is a coefficient matrix with the dimension $N_1 N_2 \times N_1 N_2$, \mathbf{u} is a vector of unknown values at all the interior and boundary points given by

$$\mathbf{u} = \begin{bmatrix} u_{22}, u_{23}, \dots, u_{2(N_2-1)}, u_{32}, u_{33}, \dots, u_{3(N_2-1)}, \dots, u_{(N_1-1)2}, u_{(N_1-1)3}, \dots, u_{(N_1-1)(N_2-1)}, \\ u_{11}, u_{12}, \dots, u_{1N_2}, u_{N_11}, u_{N_12}, \dots, u_{N_1N_2}, u_{21}, u_{31}, \dots, u_{(N_1-1)1}, u_{(2N_2)}, u_{3N_2}, \dots, u_{(N_1-1)N_2} \end{bmatrix}^T \quad (3.39)$$

with the dimension N_1N_2 , and \mathbf{s} is a known vector

$$\mathbf{s} = \begin{bmatrix} s_{22}, s_{23}, \dots, s_{2(N_2-1)}, s_{32}, s_{33}, \dots, s_{3(N_2-1)}, \dots, s_{(N_1-1)2}, s_{(N_1-1)3}, \dots, s_{(N_1-1)(N_2-1)}, \\ c_1, c_1, \dots, c_1, c_3, c_3, \dots, c_3, c_2, c_2, \dots, c_2, c_4, c_4, \dots, c_4 \end{bmatrix}^T \quad (3.40)$$

with the dimension N_1N_2 . Now, equation (3.38) can be solved by direct or iterative methods.

The mixed type boundary conditions are combinations of the Dirichlet and Neumann type boundary conditions. So, they can be implemented in a similar way.

3.4 DQM Solution of Modified Helmholtz Equation $\nabla^2 u - \tau^2 u = b_2(x, y)$

In this part, DQM will be applied to inhomogeneous modified Helmholtz equation where the right hand side function contains only space coordinates as in [88]. Two dimensional nonhomogeneous modified Helmholtz equation can be written as

$$\nabla^2 u - \tau^2 u = b_2(x, y) \quad (3.41)$$

on a rectangular domain, $0 \leq x \leq H_1$, $0 \leq y \leq H_2$ where τ is the wave number. Let N_1 and N_2 be the number of grid points in x - and y - direction, respectively. At any point (x_i, y_j) , (3.41) can be discretized as

$$\sum_{k=1}^{N_1} b_{ik} u_{kj} + \sum_{k=1}^{N_2} \bar{b}_{jk} u_{ik} - \tau^2 u_{ij} = b_2(x_i, y_j) \quad (3.42)$$

where b_{ij} and \bar{b}_{ij} are the weighting coefficients of the second order derivatives of u with respect to x and y , respectively, u_{ij} represents the value of u at the grid point (x_i, y_j) , and $i = 1, \dots, N_1$ and $j = 1, \dots, N_2$.

Similar to Poisson equation insertion of Dirichlet type boundary condition results in a system of equations passing the known boundary values to the right hand side

$$\sum_{k=2}^{N_1-1} b_{ik} u_{kj} + \sum_{k=2}^{N_2-1} \bar{b}_{jk} u_{ik} - \tau^2 u_{ij} = s_{ij} \quad (3.43)$$

for $i = 2, \dots, N_1 - 1$, $j = 2, \dots, N_2 - 1$, and the right hand side function is

$$s_{ij} = b_2(x_i, y_j) - (b_{i1} u_{1j} + b_{iN_1} u_{N_1j} + \bar{b}_{j1} u_{i1} + \bar{b}_{jN_2} u_{iN_2}). \quad (3.44)$$

From the equations (3.43), a set of algebraic equations can be obtain and written in a matrix-vector form

$$\mathbf{A}\mathbf{u} = \mathbf{s} \quad (3.45)$$

where \mathbf{A} is a coefficient matrix. \mathbf{u} is a vector of unknown values at all the interior points which are given by

$$\mathbf{u} = [u_{22}, u_{23}, \dots, u_{2(N_2-1)}, u_{32}, u_{33}, \dots, u_{3(N_2-1)}, \dots, u_{(N_1-1)2}, u_{(N_1-1)3}, \dots, u_{(N_1-1)(N_2-1)}]^T. \quad (3.46)$$

\mathbf{s} can be obtained by using the known values of right hand side function and Dirichlet type boundary conditions such as

$$\mathbf{s} = [s_{22}, s_{23}, \dots, s_{2(N_2-1)}, s_{32}, s_{33}, \dots, s_{3(N_2-1)}, \dots, s_{(N_1-1)2}, s_{(N_1-1)3}, \dots, s_{(N_1-1)(N_2-1)}]^T \quad (3.47)$$

Therefore, equation (3.45) can be solved by direct or iterative methods.

Similarly, Neumann type boundary conditions are defined at all the boundaries such as

$$\begin{aligned} \frac{\partial u}{\partial x} &= c_1, & x &= 0, & 0 &\leq y \leq H_2 \\ \frac{\partial u}{\partial y} &= c_2, & y &= 0, & 0 &\leq x \leq H_1 \\ \frac{\partial u}{\partial x} &= c_3, & x &= H_1, & 0 &\leq y \leq H_2 \\ \frac{\partial u}{\partial y} &= c_4, & y &= H_2, & 0 &\leq x \leq H_1 \end{aligned} \quad (3.48)$$

where c_1, c_2, c_3 and c_4 are constants, then DQM should be applied both to the interior and boundary points. For the interior points we have

$$\sum_{k=2}^{N_1-1} b_{ik} u_{kj} + \sum_{k=2}^{N_2-1} \bar{b}_{jk} u_{ik} - \tau^2 u_{ij} = s_{ij} \quad (3.49)$$

where $s_{ij} = b_2(x_i, y_j)$, $i = 2, \dots, N_1 - 1$ and $j = 2, \dots, N_2 - 1$. Similarly, Neumann boundary conditions (3.48) are discretized as

$$\begin{aligned} \sum_{k=1}^{N_1} a_{1k} u_{kj} &= c_1, & j &= 1, \dots, N_2, \\ \sum_{k=1}^{N_2} \bar{a}_{1k} u_{ik} &= c_2, & i &= 2, \dots, N_1 - 1 \\ \sum_{k=1}^{N_1} a_{N_1k} u_{kj} &= c_3, & j &= 1, \dots, N_2, \\ \sum_{k=1}^{N_2} \bar{a}_{N_2k} u_{ik} &= c_4, & i &= 2, \dots, N_1 - 1 \end{aligned} \quad (3.50)$$

where a_{ij} and \bar{a}_{ij} are the weighting coefficients for the first order derivatives of u with respect to x and y , respectively.

For the $2(N_1 + N_2 - 2)$ unknown boundary points there are $2(N_1 + N_2 - 2)$ equations which are obtained by using the Neumann boundary conditions. Thus, equations (3.49) and (3.50) give a set of algebraic equations, and it can be expressed in a matrix-vector form

$$\mathbf{A}\mathbf{u} = \mathbf{s} \quad (3.51)$$

where \mathbf{A} is a coefficient matrix with the dimension $N_1 N_2 \times N_1 N_2$, \mathbf{u} is a vector of unknown values at all the interior and boundary points given by

$$\mathbf{u} = \begin{bmatrix} u_{22}, u_{23}, \dots, u_{2(N_2-1)}, u_{32}, u_{33}, \dots, u_{3(N_2-1)}, \dots, u_{(N_1-1)2}, u_{(N_1-1)3}, \dots, u_{(N_1-1)(N_2-1)}, \\ u_{11}, u_{12}, \dots, u_{1N_2}, u_{N_11}, u_{N_12}, \dots, u_{N_1N_2}, u_{21}, u_{31}, \dots, u_{(N_1-1)1}, u_{(2N_2)}, u_{3N_2}, \dots, u_{(N_1-1)N_2} \end{bmatrix}^T \quad (3.52)$$

with the dimension $N_1 N_2$ and \mathbf{s} is a known vector given by

$$\mathbf{s} = \begin{bmatrix} s_{22}, s_{23}, \dots, s_{2(N_2-1)}, s_{32}, s_{33}, \dots, s_{3(N_2-1)}, \dots, s_{(N_1-1)2}, s_{(N_1-1)3}, \dots, s_{(N_1-1)(N_2-1)}, \\ c_1, c_1, \dots, c_1, c_3, c_3, \dots, c_3, c_2, c_2, \dots, c_2, c_4, c_4, \dots, c_4 \end{bmatrix}^T \quad (3.53)$$

with the dimension $N_1 N_2$. Again, equation (3.51) can be solved by direct or iterative methods. Mixed type boundary conditions are discretized by using similar idea.

DQM is going to be applied to the natural convection flow in a cavity under the effect of an externally applied magnetic field. Obtained solutions will be compared with the DRBEM solution of the same problem in terms of effectiveness and computational cost.

CHAPTER 4

APPLICATION OF DRBEM AND DQM TO THE NATURAL AND MIXED CONVECTION FLOWS

DRBEM formulations for both inhomogeneous modified Helmholtz equation and Poisson equation are given in general in Chapter 2. For the modified Helmholtz equation, different type of \bar{f} expansions are derived, and related particular solutions and their normal derivatives are computed. Thus, as a starter, these \bar{f} radial basis functions are tested with four test problems which have exact solutions in the first section of this chapter. Two of these problems are inhomogeneous modified Helmholtz equations, and the remaining two problems are diffusion and convection-diffusion-reaction type equations. The efficiency of these \bar{f} expansions in DRBEM applications is analyzed using the numerical results of these four examples (Section 4.1) in terms of maximum absolute errors between the exact and the numerical solutions.

The application of DRBEM using the fundamental solution of the modified Helmholtz equation is performed on different types of fluid flow problems. In Section 4.2, lid driven cavity and natural convection flow problems are solved, and then in Section 4.3 solutions of thermosolutal buoyancy induced mixed convection flow problems are given in different type of physical domains. We have also solved natural convection flow under a magnetic field using the DRBEM and DQM, comparing the advantages and disadvantages of the two methods with the numerical results obtained, in Section 4.4.

Finally, in Section 4.5, the application of DRBEM with the fundamental solution of modified Helmholtz equation is used for the inverse problems. In this section, first we describe the inverse problem of the natural convection flow under a magnetic field, and solve the problem with two different types of boundary conditions in square cavities.

Before the DRBEM application of the fluid dynamics problems considered in the thesis, the governing equations which include the time derivatives of the unknowns are transformed to the inhomogeneous modified Helmholtz equations using forward difference approximation for the time derivatives. Then, Laplace terms are approximated also with relaxation parameters at two consecutive time levels. The results for some of the test problems are given using tables, and for the others the results are presented in terms of streamlines, vorticity contours, isotherms, concentration contours, and velocity profiles at the mid-plane of the cavity.

4.1 Choice of \bar{f} Expansions for DRBEM Solution of Modified Helmholtz Equations

In Chapter 2, different \bar{f} expansions were given for DRBEM solution of inhomogeneous modified Helmholtz equation. For the problems discussed in this section, the order of the polynomial radial function \bar{f} is selected to achieve less maximum absolute error.

In the approximation of the inhomogeneity

$$b(x, y) = \sum_{j=1}^{K+L} \bar{\alpha}_j \bar{f}_j \quad (4.1)$$

the radial basis function \bar{f} is assumed to be a polynomial in the distance r as

$$\bar{f} = 4a_2 + 9a_3r + \dots + m^2 a_m r^{m-2} - \tau^2 (a_2 r^2 + a_3 r^3 + \dots + a_m r^m). \quad (4.2)$$

4.1.1 Example 1: Modified Helmholtz Equation

Consider the Dirichlet problem defined by inhomogeneous modified Helmholtz equation in a square domain

$$\nabla^2 u - \tau^2 u = b(x, y, \tau) \quad \text{in} \quad \Omega = (0, 1) \times (0, 1) \quad (4.3)$$

$$u(x, 0) = 0 \quad u(0, y) = \sin 4\pi y \quad (4.4)$$

$$u(x, 1) = 0 \quad u(1, y) = \sin 4\pi y \quad (4.5)$$

where the exact solution is

$$u(x, y) = \cos(4\pi x) \sin(4\pi y) \quad (4.6)$$

and the right hand side function is

$$b(x, y, \tau) = -(32\pi^2 + \tau^2) \cos 4\pi x \sin 4\pi y. \quad (4.7)$$

Table 4.1: Polynomial \bar{f} functions and particular solutions \widehat{u}

Case	a_2	a_3	\widehat{u}	\bar{f}	max. abs. err.
1	$\frac{1}{4}$	$\frac{1}{9}$	$\frac{r^2}{4} + \frac{r^3}{9}$	$1 + r - \tau^2 \left(\frac{r^2}{4} + \frac{r^3}{9} \right)$	0.26587
2	$-\frac{1}{4}$	$\frac{1}{9}$	$-\frac{r^2}{4} + \frac{r^3}{9}$	$-1 + r - \tau^2 \left(-\frac{r^2}{4} + \frac{r^3}{9} \right)$	0.02649
3	$-\frac{1}{4}$	$-\frac{1}{9}$	$-\frac{r^2}{4} - \frac{r^3}{9}$	$-1 - r - \tau^2 \left(-\frac{r^2}{4} - \frac{r^3}{9} \right)$	0.26587
4	$\frac{1}{4}$	$-\frac{1}{9}$	$\frac{r^2}{4} - \frac{r^3}{9}$	$1 - r - \tau^2 \left(\frac{r^2}{4} - \frac{r^3}{9} \right)$	0.02649
5	$\frac{1}{2}$	$-\frac{1}{9}$	$\frac{r^2}{2} - \frac{r^3}{9}$	$2 - r - \tau^2 \left(\frac{r^2}{2} - \frac{r^3}{9} \right)$	0.06334
6	$\frac{1}{2}$	$\frac{1}{9}$	$\frac{r^2}{2} + \frac{r^3}{9}$	$2 + r - \tau^2 \left(\frac{r^2}{2} + \frac{r^3}{9} \right)$	38.44541
7	$-\frac{1}{8}$	$\frac{1}{9}$	$-\frac{r^2}{8} + \frac{r^3}{9}$	$-0.5 + r - \tau^2 \left(-\frac{r^2}{8} + \frac{r^3}{9} \right)$	0.01552
8	$-\frac{1}{16}$	$\frac{1}{9}$	$-\frac{r^2}{8} + \frac{r^3}{9}$	$-0.25 + r - \tau^2 \left(-\frac{r^2}{16} + \frac{r^3}{9} \right)$	0.02255
9	$-\frac{1}{4}$	$\frac{1}{18}$	$-\frac{r^2}{4} + \frac{r^3}{18}$	$-1 + \frac{r}{2} - \tau^2 \left(-\frac{r^2}{4} + \frac{r^3}{18} \right)$	0.06334
10	$-\frac{1}{4}$	$\frac{1}{3}$	$-\frac{r^2}{4} + \frac{r^3}{3}$	$-1 + 3r - \tau^2 \left(-\frac{r^2}{4} + \frac{r^3}{3} \right)$	0.01652
11	$-\frac{1}{8}$	$\frac{1}{3}$	$-\frac{r^2}{8} + \frac{r^3}{3}$	$-0.5 + 3r - \tau^2 \left(-\frac{r^2}{8} + \frac{r^3}{3} \right)$	0.03008
12	$-\frac{1}{2}$	$\frac{1}{3}$	$-\frac{r^2}{2} + \frac{r^3}{3}$	$-2 + 3r - \tau^2 \left(-\frac{r^2}{2} + \frac{r^3}{3} \right)$	0.01469
13	-1	1	$-r^2 + r^3$	$-4 + 9r - \tau^2 (-r^2 + r^3)$	0.01584

First, the problem is solved with DRBEM using \bar{f} polynomial of order 3, and keeping the wave number as $\tau^2 = 1$. From the Table 4.1 it can be seen that, the accuracy of the results depends on the coefficients a_2 and a_3 . It is observed that the best results are obtained when the coefficients a_2 and a_3 have opposite signs, and the coefficients must be reduced or enlarged together. With these constraints, the maximum absolute errors for the problem are $\varepsilon = 10^{-2}$.

Then the dependence of DRBEM solution on the wave number τ^2 is given in terms of maximum absolute errors in Table 4.2. Radial function \bar{f} is taken as $\bar{f} = 1 - r - \tau^2 \left(\frac{r^2}{4} - \frac{r^3}{9} \right)$. The minimum error is attained with a very high value of τ^2 for this particular problem since the exact solution is independent of τ .

Table 4.2: Dependence of wave number τ^2

τ^2	max. abs. err.	τ^2	max. abs. err.
1	0.026486	4900	0.000933
9	0.018987	8100	0.000531
100	0.011299	10000	0.000432
169	0.009853	40000	0.000380
400	0.006879	160000	0.000131
900	0.004424	250000	0.000087
1600	0.003149	360000	0.000062
2500	0.002102	1440000	0.000016

4.1.2 Example 2: Diffusion Equation

The diffusion equation is given as

$$\nabla^2 u = \frac{1}{k_x} \frac{\partial u}{\partial t} \quad (4.8)$$

where k_x is the dispersion or diffusivity coefficient. Consider equation (4.8) in a square plate ($0 \leq x, y \leq L_x$) initially at a temperature u_0 and cooled by the application of a thermal shock ($u = 0$ all over the boundary). The exact solution for this problem is given as [73],

$$u(x, y, t) = \sum_{n=1}^{\infty} \sum_{m=1}^{\infty} A_{nm} \sin\left(\frac{n\pi x}{L_x}\right) \sin\left(\frac{m\pi y}{L_x}\right) \exp\left[-\left(\frac{k_x n^2 \pi^2}{L_x^2} + \frac{k_x m^2 \pi^2}{L_x^2}\right)t\right] \quad (4.9)$$

where

$$A_{nm} = \frac{4u_0}{nm\pi^2} [(-1)^n - 1][(-1)^m - 1] \quad (4.10)$$

and the problem is solved with $L_x = 3$, $k_x = 1.25$, $t = 1.2$ and $u_0 = 30$.

After using the procedure to obtain a modified Helmholtz equation given in Section 1, equation (4.8) takes the form

$$\nabla^2 u^{(n+1)} - \frac{1}{k_x \theta \Delta t} u^{(n+1)} = -\left(\frac{1-\theta}{\theta}\right) \nabla^2 u^{(n)} - \frac{1}{k_x \theta \Delta t} u^{(n)} \quad (4.11)$$

where Δt is the time increment, θ is a relaxation parameter, and $(n+1)$ and (n) represent current and previous time levels, respectively. Now, equation (4.11) is inhomogeneous modified Helmholtz equation with the known values $u^{(n)}$, Δt , k_x and θ .

For the case $\theta = 1$, it reduces to a backward difference time-stepping procedure. For $\theta = 0.5$ it is called Crank-Nicolson scheme and $\theta = 2/3$ is the Galerkin scheme. These schemes are frequently preferred to backward differences. The use of these schemes implies expressing the term $\nabla^2 u^{(n)}$ in terms of known values [75]. This can be done as follows. First, equation (4.11) is written using $\theta = 1$

$$\nabla^2 u^{(n+1)} = \frac{1}{k_x \Delta t} (u^{(n+1)} - u^{(n)}) \quad (4.12)$$

and then equation (4.12) is written for $n = 0$

$$\nabla^2 u^{(1)} = \frac{1}{k_x \Delta t} (u^{(1)} - u^{(0)}) \quad (4.13)$$

Then, when $n = 1$ equation (4.11) takes the form

$$\nabla^2 u^{(2)} - \frac{1}{k_x \theta \Delta t} u^{(2)} = -\left(\frac{1-\theta}{\theta}\right) \nabla^2 u^{(1)} - \frac{1}{k_x \theta \Delta t} u^{(1)} \quad (4.14)$$

Substituting equation (4.13) into equation (4.14) gives

$$\nabla^2 u^{(2)} - \frac{1}{k_x \theta \Delta t} u^{(2)} = -\left(\frac{1-\theta}{\theta}\right) \left(\frac{u^{(1)} - u^{(0)}}{k_x \Delta t}\right) - \frac{1}{k_x \theta \Delta t} u^{(1)} \quad (4.15)$$

Therefore, equation (4.15) can be written for any time level

$$\nabla^2 u^{(n+1)} - \frac{1}{k_x \theta \Delta t} u^{(n+1)} = -\left(\frac{1-\theta}{\theta}\right) \left(\frac{u^{(n)} - u^{(n-1)}}{k_x \Delta t}\right) - \frac{1}{k_x \theta \Delta t} u^{(n)} \quad (4.16)$$

Thus, inhomogeneous modified Helmholtz equation (4.16) is going to be solved by using DRBEM which uses fundamental solution of the modified Helmholtz equation.

In the DRBEM solution of the test problem the following \bar{f} expansions are taken as

$$\begin{aligned}
 \text{Case 4} \quad \bar{f} &= 1 - r - \tau^2 \left(\frac{r^2}{4} - \frac{r^3}{9} \right) && \text{(Table 4.1)} \\
 \text{Case 14} \quad \bar{f} &= 1 - r + r^2 - \tau^2 \left(\frac{r^2}{4} - \frac{r^3}{9} + \frac{r^4}{16} \right) && (4.17) \\
 \text{Case 15} \quad \bar{f} &= 1 - r + r^2 - r^3 - \tau^2 \left(\frac{r^2}{4} - \frac{r^3}{9} + \frac{r^4}{16} - \frac{r^5}{25} \right)
 \end{aligned}$$

where $\tau^2 = \frac{1}{k_x \theta \Delta t}$ with $\widehat{u} = \frac{r^2}{4} - \frac{r^3}{9}$, $\widehat{u} = \frac{r^2}{4} - \frac{r^3}{9} + \frac{r^4}{16}$ and $\widehat{u} = \frac{r^2}{4} - \frac{r^3}{9} + \frac{r^4}{16} - \frac{r^5}{25}$, respectively.

The Crank-Nicolson and Galerkin time integration schemes are used with these \bar{f} expansions. Results for the problem are shown in Table 4.3 at three interior points. The results are obtained using 60 constant boundary elements, and 35 interior nodes. From the Table 4.3 it can be seen that Case 15 (higher order \bar{f} polynomial) with $\theta = 2/3$ (Galerkin scheme) gives the best accuracy comparing with exact solution of the diffusion problem.

Table 4.3: Results for diffusion problem with several \bar{f} functions for $\theta = 1/2$ and $\theta = 2/3$

Point		(0.6, 0.2)	(0.2, 1.3)	(0.9, 1.3)
case 4	$\theta = 2/3$	0.278	0.453	1.446
	$\theta = 1/2$	0.277	0.452	1.442
case 14	$\theta = 2/3$	0.280	0.458	1.455
	$\theta = 1/2$	0.279	0.457	1.458
case 15	$\theta = 2/3$	0.295	0.483	1.503
	$\theta = 1/2$	0.294	0.482	1.500
Exact		0.298	0.487	1.514

4.1.3 Example 3: Convection-Diffusion Equation

Two-dimensional convection-diffusion equation is given

$$K_x \frac{\partial^2 u}{\partial x^2} + K_x \frac{\partial^2 u}{\partial y^2} - c_x \frac{\partial u}{\partial x} - c_y \frac{\partial u}{\partial y} - du = \frac{\partial u}{\partial t} \quad (4.18)$$

with the boundary conditions on a square $[0, 1] \times [0, 1]$

$$\begin{aligned} u(0, y, t) &= 300 & u(1, y, t) &= 10 \\ q(x, 0, t) &= 0 & q(x, 1, t) &= 0. \end{aligned} \quad (4.19)$$

The values of the parameters are

$$\begin{aligned} K_x &= 1, \\ c_y &= 0, \\ c_x &= dx + \log \frac{10}{300} - \frac{d}{2} \end{aligned} \quad (4.20)$$

and initial condition is $u = 0$. The steady-state solution is given in [75] as

$$u(x, y, t) = 300 \exp\left(\frac{d}{2}x^2 + \log \frac{10}{300}x - \frac{d}{2}x\right). \quad (4.21)$$

The procedure of obtaining modified Helmholtz model can be applied to the convection-diffusion equation as is done in Chapter 1. Thus, following the same procedure one can obtain an inhomogeneous modified Helmholtz equation

$$\nabla^2 u^{(n+1)} - \frac{1}{K_x \theta \Delta t} u^{(n+1)} = -\left(\frac{1-\theta}{\theta}\right) \left(\frac{u^{(n)} - u^{(n-1)}}{K_x \Delta t}\right) - \frac{1}{K_x \theta \Delta t} u^{(n)} + \frac{c_x}{K_x} \frac{\partial u^{(n)}}{\partial x} + \frac{c_y}{K_x} \frac{\partial u^{(n)}}{\partial y} + \frac{d}{K_x} u^{(n)}. \quad (4.22)$$

Following the conclusion of diffusion problem 4.1.2, convection-diffusion equation is also solved by using higher order \bar{f} expansion in DRBEM as (case 15)

$$\bar{f} = 1 - r + r^2 - r^3 - \tau^2 \left(\frac{r^2}{4} - \frac{r^3}{9} + \frac{r^4}{16} - \frac{r^5}{25}\right) \quad (4.23)$$

where $\tau^2 = \frac{1}{K_x \theta \Delta t}$ for $d = 5$ and $d = 40$.

The boundary of the region is discretized using $K = 60$ and 100 constant boundary elements for the values of $d = 5$ and 40 , with $L = 49$ and 144 interior nodes, respectively. In Table 4.4 and Table 4.5 we give DRBEM solutions of the convection-diffusion problem with Galerkin and Crank-Nicolson schemes, for $d = 5$ and 40 , respectively, and these solutions are compared with the exact solutions. From these tables it can be seen that, as in the case of diffusion equation, Galerkin scheme is better than the Crank-Nicolson scheme in terms of accuracy. Also, as the coefficient of reaction term (d) increases we need to take more boundary elements due to the dominance of reaction term in the convection-diffusion equation.

Table 4.4: Results for convection-diffusion equation with $d = 5$, $t = 1.0$, $K = 60$, $L = 49$ at $y = 0.6$.

X	Exact	$\theta = 1/2$	$\theta = 2/3$
0.000	300.000	300.000	300.000
0.088	181.735	181.963	181.794
0.206	98.968	98.673	98.999
0.324	57.757	58.007	57.745
0.441	36.122	36.474	36.102
0.559	24.210	24.589	24.151
0.676	17.389	17.693	17.351
0.794	13.284	13.597	13.389
0.912	11.040	11.089	11.019
1.000	10.000	10.000	10.000

Table 4.5: Results for convection-diffusion equation with $d = 40$, $t = 1.0$, $K = 100$, $L = 144$ at $y = 0.6$.

X	Exact	$\theta = 1/2$	$\theta = 2/3$
0.000	300.000	300.000	300.000
0.220	4.588	4.675	4.538
0.300	1.622	1.731	1.680
0.460	0.437	0.515	0.459
0.700	0.416	0.501	0.485
0.860	1.449	1.492	1.479
1.000	10.000	10.000	10.000

4.1.4 Example 4: Modified Helmholtz Equation

Consider the following Dirichlet problem for the modified Helmholtz equation [27]

$$(\nabla^2 - \tau^2)u(x, y) = (e^x + e^y)(1 - \tau^2), \quad (x, y) \in D, \quad (4.24)$$

$$u(x, y) = (e^x + e^y), \quad (x, y) \in \partial D, \quad (4.25)$$

where $D \cup \partial D = \{(x, y) : 0 \leq x, y \leq 1\}$.
The exact solution of the problem is

$$u(x, y) = (e^x + e^y), \quad (x, y) \in D \cup \partial D. \quad (4.26)$$

In the DRBEM solution of the problem, higher order logarithmic splines $\bar{f} = r^{2n} \log r$ are used for \bar{f} function by taking n as 1, 2, 3, 4 and 5. $\bar{f} = 1 - r + r^2 - r^3 - \tau^2(\frac{r^2}{4} - \frac{r^3}{9} + \frac{r^4}{16} - \frac{r^5}{25})$ is also used as a 6-th case. For the DRBEM solution 56 constant boundary elements and 49 internal nodes are used, and the results for the problem are shown in Table 4.6 for cases 1-6. From the Table 4.6 it can be seen that, all orders of the spline function give results with almost the same accuracy with the exact solution, but when the order of spline functions is increased, the accuracy of the solutions are also increased. In addition, it is seen that, when $\bar{f} = 1 - r + r^2 - r^3 - \tau^2(\frac{r^2}{4} - \frac{r^3}{9} + \frac{r^4}{16} - \frac{r^5}{25})$ is used, the accuracy is almost the same with the higher order splines. In Figure 4.1 very good agreement is shown with the exact solution at $y = 0.4$ for all cases of \bar{f} expansion. Since all the higher order splines results are found to differ little from those obtained using $\bar{f} = r^2 \log r$ which is simplest alternative, it will be used in the rest of the examples.

Table 4.6: Results for Example 4 with higher order splines

X	Y	Exact	n=1	n=2	n=3	n=4	n=5	5th order \bar{f}
0.0000	0.0000	2.0000	2.0000	2.0000	2.0000	2.0000	2.0000	2.0000
0.2500	0.2500	2.5681	2.5695	2.5680	2.5684	2.5682	2.5680	2.5679
0.3214	0.3929	2.8603	2.8608	2.8602	2.8604	2.8603	2.8603	2.8602
0.3929	0.5357	3.1899	3.1903	3.1897	3.1899	3.1899	3.1899	3.1899
0.4643	0.6071	3.4261	3.4264	3.4259	3.4260	3.4261	3.4261	3.4260
0.6071	0.6071	3.6704	3.6707	3.6706	3.6703	3.6703	3.6704	3.6703
0.7500	0.6786	4.0881	4.0887	4.0883	4.0880	4.0881	4.0881	4.0879
1.0000	1.0000	5.4366	5.4366	5.4366	5.4366	5.4366	5.4366	5.4366

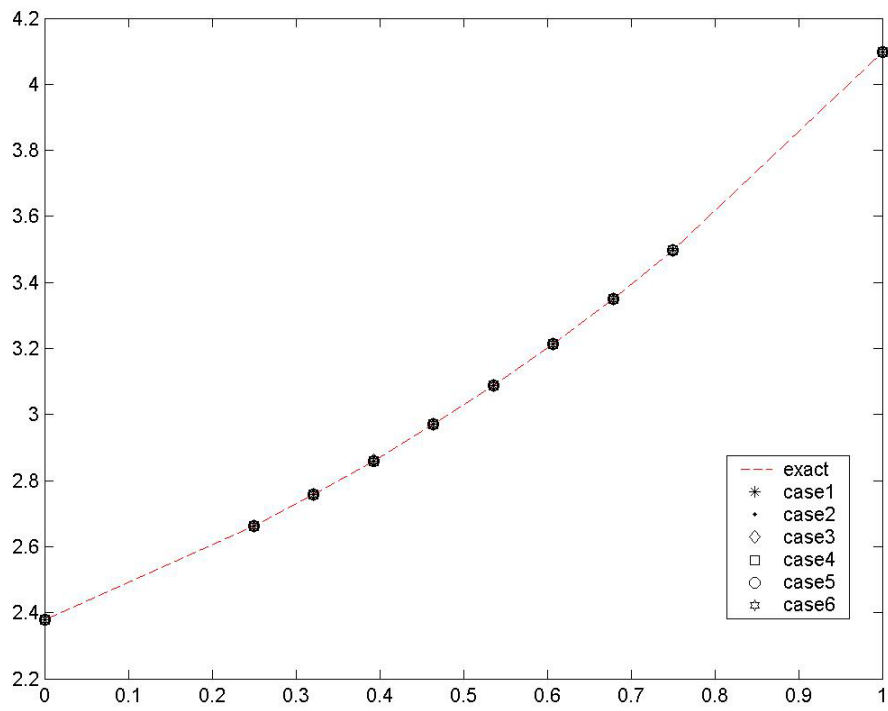


Figure 4.1: DRBEM solution of Example 4 with higher order splines and polynomial \bar{f} at $y = 0.4$

4.2 DRBEM Solution of Lid-Driven and Natural Convection Flow Problems in Cavities

In this section, DRBEM solution of two-dimensional unsteady Navier-Stokes equations in a lid-driven square cavity, and natural convection flow equations in a cavity are considered. Stream function-vorticity and temperature formulation is used, and vorticity transport and energy equations are transformed to inhomogeneous modified Helmholtz equations. The resulting modified Helmholtz equations are solved by DRBEM using the fundamental solution $\frac{1}{2\pi}K_0(x)$ of modified Helmholtz equation whereas in the stream function Poisson equation fundamental solution $\frac{1}{2\pi}\ln(x)$ of Laplace equation is made use of. The inhomogeneities are approximated by using coordinate functions $f = 1 + r$ and $\bar{f} = r^2 \ln r$ in the stream function and vorticity-energy equations, respectively.

4.2.1 Lid-Driven Cavity Flow

This is the classical two-dimensional incompressible flow problem which is defined in a square cavity $[0, 1] \times [0, 1]$ and governed by unsteady Navier-Stokes equations. Stream function-vorticity ($\psi - w$) formulation of Navier-stokes equations is given as

$$\nabla^2 \psi = -w \quad (4.27)$$

$$\frac{1}{Re} \nabla^2 w = \frac{\partial w}{\partial t} + u \frac{\partial w}{\partial x} + v \frac{\partial w}{\partial y} \quad (4.28)$$

where $Re = \frac{\widehat{\rho}UL_0}{\mu}$ is the Reynolds number of the fluid and

$$u = \frac{\partial \psi}{\partial y}, \quad v = -\frac{\partial \psi}{\partial x}, \quad w = \frac{\partial v}{\partial x} - \frac{\partial u}{\partial y} \quad (4.29)$$

are the time dependent velocity components and the vorticity, respectively.

Using the procedure for obtaining inhomogeneous modified Helmholtz equation for vorticity transport equation given in Chapter 1, the governing equations take to form

$$\begin{aligned} \nabla^2 \psi^{(n+1)} &= -w^{(n)} \\ \nabla^2 w^{(n+1)} - \tau_w^2 w^{(n+1)} &= -\left(\frac{1 - \theta_w}{\theta_w}\right) \nabla^2 w^{(n)} - \tau_w^2 w^{(n)} \\ &+ \frac{Re}{\theta_w} \left(\frac{\partial \psi^{(n+1)}}{\partial y} \frac{\partial w^{(n)}}{\partial x} - \frac{\partial \psi^{(n+1)}}{\partial x} \frac{\partial w^{(n)}}{\partial y} \right) \end{aligned} \quad (4.30)$$

where $\tau_w^2 = \frac{Re}{\Delta t \theta_w}$. Δt and θ_w are the time step and relaxation parameter $0 < \theta_w < 1$, respectively. Thus, we have Poisson (4.27) and modified Helmholtz (4.28) equations for stream function and vorticity transport equations, respectively.

The DRBEM is going to be applied now to the equations (4.30). For this, these equations are rewritten as inhomogeneous Poisson and modified Helmholtz equations

$$\nabla^2 \psi^{(n+1)} = b_1 \quad (4.31)$$

$$\nabla^2 w^{(n+1)} - \tau_w^2 w^{(n+1)} = b_2 \quad (4.32)$$

where b_1 and b_2 are the right hand sides of corresponding equations in (4.30). These functions are constructed using the values of vorticity obtained from the previous time level and stream function from the newly obtained current time level.

The DRBEM transforms the governing equations defined in a region Ω bounded by Γ , to corresponding boundary integral equations. The equations are weighted with the fundamental solutions $u_1^* = \frac{1}{2\pi} \ln r$ and $u_2^* = \frac{1}{2\pi} K_0(\tau r)$, respectively, and then the Green's second identity is applied to arrive at the equations as explained in Chapter 2

$$c_i \psi_i^{(n+1)} + \int_{\Gamma} \left(q_1^* \psi^{(n+1)} - u_1^* \frac{\partial \psi^{(n+1)}}{\partial n} \right) d\Gamma = - \int_{\Omega} b_1 u_1^* d\Omega, \quad (4.33)$$

$$c_i w_i^{(n+1)} + \int_{\Gamma} \left(q_2^* w^{(n+1)} - u_2^* \frac{\partial w^{(n+1)}}{\partial n} \right) d\Gamma = - \int_{\Omega} b_2 u_2^* d\Omega, \quad (4.34)$$

where

$$b_1 = -w^{(n)} \quad (4.35)$$

$$b_2 = - \left(\frac{1 - \theta_w}{\theta_w} \right) \nabla^2 w^{(n)} - \tau_w^2 w^{(n)} + \frac{Re}{\theta_w} \left(\frac{\partial \psi^{(n+1)}}{\partial y} \frac{\partial w^{(n)}}{\partial x} - \frac{\partial \psi^{(n+1)}}{\partial x} \frac{\partial w^{(n)}}{\partial y} \right) \quad (4.36)$$

Here, $q_1^* = \frac{\partial u_1^*}{\partial n}$ and $q_2^* = \frac{\partial u_2^*}{\partial n}$. Approximating b_1 and b_2 with the radial basis functions $f_j = 1 + r_j$ and $\bar{f}_j = r_j^2 \ln r_j$

$$b_1 = \sum_{j=1}^{K+L} \alpha_{1j} f_j \quad (4.37)$$

$$b_2 = \sum_{j=1}^{K+L} \alpha_{2j}(t) \bar{f}_j \quad (4.38)$$

where α_{1j} and $\alpha_{2j}(t)$ are coefficients which are initially unknown, r_j denotes the distance between the source and field points, K and L are the numbers of boundary and interior points, respectively. The discretization of Γ using constant boundary elements gives DRBEM matrix-vector equations

$$\mathbf{H}\psi - \mathbf{G}\mathbf{q}_\psi = (\mathbf{H}\widehat{\Psi} - \mathbf{G}\widehat{\mathbf{Q}}_\psi)\alpha_1 \quad (4.39)$$

$$\mathbf{H}'\mathbf{w} + \mathbf{G}'\mathbf{q}_w = (\mathbf{H}'\widehat{\mathbf{W}} + \mathbf{G}'\widehat{\mathbf{Q}}_w)\alpha_2$$

where \mathbf{H} , \mathbf{G} , \mathbf{H}' and \mathbf{G}' are square matrices of size $(K+L) \times (K+L)$ which are derived in Chapter 2 (equations (2.32), (2.27), (2.86) and (2.79), respectively). ψ , \mathbf{w} , and \mathbf{q}_ψ , \mathbf{q}_w are $(K+L) \times 1$ vectors containing discretized values of stream function, vorticity and their normal derivatives. $\widehat{\Psi}$, $\widehat{\mathbf{Q}}_\psi$, $\widehat{\mathbf{W}}$ and $\widehat{\mathbf{Q}}_w$ matrices are formed columnwise from the particular solutions and their normal derivatives of the equations at the nodes $j = 1, \dots, K+L$ with

$$\nabla^2 \widehat{\psi}_j = f_j = 1 + r_j \quad (4.40)$$

and

$$\nabla^2 \widehat{w}_j - \tau_w^2 \widehat{w}_j = \bar{f}_j = r_j^2 \ln r_j. \quad (4.41)$$

Collocating b_1 and b_2 in (4.37) and (4.38) at all boundary and interior nodes gives $\mathbf{b}_1 = \mathbf{F}\alpha_1$ and $\mathbf{b}_2 = \bar{\mathbf{F}}\alpha_2$, and inverting, one can get the matrix-vector equations

$$\mathbf{H}\psi - \mathbf{G}\mathbf{q}_\psi = (\mathbf{H}\widehat{\Psi} - \mathbf{G}\widehat{\mathbf{Q}}_\psi)\mathbf{F}^{-1}\mathbf{b}_1 \quad (4.42)$$

and

$$\mathbf{H}' \mathbf{w} + \mathbf{G}' \mathbf{q}_w = (\mathbf{H}' \widehat{\mathbf{W}} + \mathbf{G}' \widehat{\mathbf{Q}}_w) \overline{\mathbf{F}}^{-1} \mathbf{b}_2 \quad (4.43)$$

where \mathbf{F} and $\overline{\mathbf{F}}$ are $(K+L) \times (K+L)$ coordinate matrices and their columns are constructed using $f_j = 1 + r_j$ and $\overline{f}_j = r_j^2 \ln r_j$, $j = 1, \dots, K+L$, respectively.

In equation (4.36), the first and second order derivatives of stream function and vorticity can be approximated using DRBEM idea with the coordinate matrices as

$$\psi^{(n+1)} = \sum_{j=1}^{K+L} \beta_j \overline{f}_j \quad \text{and} \quad \mathbf{w}^{(n)} = \sum_{j=1}^{K+L} \widetilde{\beta}_j \overline{f}_j \quad (4.44)$$

where $\beta_j, \widetilde{\beta}_j$ are unknown coefficients and $\alpha_{2j}(t) \neq \beta_j$, $\alpha_{2j}(t) \neq \widetilde{\beta}_j$. These equations result in systems

$$\psi^{(n+1)} = \overline{\mathbf{F}} \boldsymbol{\beta} \quad \text{and} \quad \mathbf{w}^{(n)} = \overline{\mathbf{F}} \widetilde{\boldsymbol{\beta}} \quad (4.45)$$

which give

$$\frac{\partial \psi^{(n+1)}}{\partial x} = \frac{\partial \overline{\mathbf{F}}^{-1}}{\partial x} \boldsymbol{\beta} \psi^{(n+1)}, \quad \frac{\partial \psi^{(n+1)}}{\partial y} = \frac{\partial \overline{\mathbf{F}}^{-1}}{\partial y} \boldsymbol{\beta} \psi^{(n+1)} \quad (4.46)$$

and

$$\frac{\partial \mathbf{w}^{(n)}}{\partial x} = \frac{\partial \overline{\mathbf{F}}^{-1}}{\partial x} \widetilde{\boldsymbol{\beta}} \mathbf{w}^{(n)}, \quad \frac{\partial \mathbf{w}^{(n)}}{\partial y} = \frac{\partial \overline{\mathbf{F}}^{-1}}{\partial y} \widetilde{\boldsymbol{\beta}} \mathbf{w}^{(n)} \quad (4.47)$$

where $\boldsymbol{\beta} = \overline{\mathbf{F}}^{-1} \psi^{(n+1)}$ and $\widetilde{\boldsymbol{\beta}} = \overline{\mathbf{F}}^{-1} \mathbf{w}^{(n)}$.

Also, using the first order derivatives of the vorticity in equation (4.47), $\nabla^2 \mathbf{w}^{(n)}$ can be obtained with the help of coordinate matrix $\overline{\mathbf{F}}$ such that

$$\nabla^2 \mathbf{w}^{(n)} = \frac{\partial \overline{\mathbf{F}}^{-1}}{\partial x} \widetilde{\boldsymbol{\beta}} \left(\frac{\partial \mathbf{w}^{(n)}}{\partial x} \right) + \frac{\partial \overline{\mathbf{F}}^{-1}}{\partial y} \widetilde{\boldsymbol{\beta}} \left(\frac{\partial \mathbf{w}^{(n)}}{\partial y} \right). \quad (4.48)$$

Physically there is no boundary condition for the vorticity. But it can be obtained from (4.29) with the help of coordinate matrix $\overline{\mathbf{F}}$

$$\mathbf{w}^{(n+1)} = \frac{\partial \mathbf{v}^{(n+1)}}{\partial x} - \frac{\partial \mathbf{u}^{(n+1)}}{\partial y} = \frac{\partial \overline{\mathbf{F}}^{-1}}{\partial x} \mathbf{v}^{(n+1)} + \frac{\partial \overline{\mathbf{F}}^{-1}}{\partial y} \mathbf{u}^{(n+1)}. \quad (4.49)$$

Since the right hand sides of the equations (4.42) and (4.43) can be obtained from the previously known ψ and w values in (4.30) and, all the vectors and matrices are known, linear systems of equations are obtained as

$$\begin{aligned} \mathbf{A}_1 \mathbf{x}_1 &= \mathbf{y}_1 \\ \mathbf{A}_2 \mathbf{x}_2 &= \mathbf{y}_2 \end{aligned} \quad (4.50)$$

with \mathbf{x}_1 and \mathbf{x}_2 containing only unknown values of ψ , \mathbf{q}_ψ and w , \mathbf{q}_w , respectively.

Since the governing equations (4.27)-(4.28) are coupled in vorticity and stream functions, the system of equations (4.42)-(4.43) are also coupled in vorticity and stream function values. Thus, an iterative procedure should be used for the solution which can be given as follows:

1. Start with an initial approximation $w^{(0)} = 0$ for $n = 0$, and obtain the right hand side b_1 in (4.42).
2. Solve the stream function equation for $\psi^{(n+1)}$ using $w^{(n)}$.
3. Approximate the first derivatives of $\psi^{(n+1)}$ using (4.46), and then $u^{(n+1)}$ and $v^{(n+1)}$ velocity components from relationships (4.29).
4. Compute the vorticity boundary conditions $w^{(n+1)}$ using the equation (4.49).
5. Approximate first and second order space derivatives of $w^{(n)}$ by using the DRBEM idea with the coordinate matrix \bar{F} , and compute the right hand side b_2 of the equation (4.43).
6. Solve the vorticity transport equation (4.43) using b_2 and obtain $w^{(n+1)}$.
7. Check the stopping criteria to obtain steady-state solution as

$$\max_i |\psi^{(n+1)} - \psi^{(n)}| \leq \varepsilon \quad i = 1, \dots, K + L$$

$$\max_i |w^{(n+1)} - w^{(n)}| \leq \varepsilon \quad i = 1, \dots, K + L$$

8. Update $w^{(n)}$ values for the next iteration.
9. Continue steps 2-8 at the next time levels until the stopping criteria is satisfied.

4.2.1.1 Numerical Results

The lid-driven cavity flow problem is defined in a square domain $\Omega = [0, 1] \times [0, 1]$ shown as Figure 4.2. The non-dimensional equations in stream function-vorticity formulation in the modified Helmholtz operator form are given in equations (4.30). The no-slip boundary conditions are imposed on the vertical and bottom walls, and the upper boundary is assumed to move with the constant velocity $u = -1$. Therefore, stream function boundary conditions are considered zero. The vorticity boundary conditions are obtained using DRBEM idea with the coordinate matrix \bar{F} (equation (4.49)). The initial vorticity is taken as zero.

The problem is solved using constant boundary elements and the radial basis functions are taken as $f = 1 + r$ and $\bar{f} = r^2 \ln r$, for stream function and vorticity equations, respectively. The solutions are given at steady state where stopping criteria is taken as $\varepsilon = 10^{-4}$. For this problem, $K = 52, 92, 108$ and 140 boundary elements are used, and $\Delta t = 1.0, 0.1, 0.05$ and 0.025 are taken for the values of Reynolds number $Re = 50, 500, 1000$ and 2000 , respectively. As Re increases, we need to take more boundary elements. Although, we need to take smaller time increments as Re increases, these are still quite large time steps than the ones required in other time integration methods. This situation is expected for high Reynolds numbers which cause thin boundary layers near the walls.

From the Table 4.7, we can see that θ_w values close to one take less iterations than the other values when the corresponding K and Δt values are kept fixed. The relation between θ_w and convergence rate is due to $\tau_w^2 = \frac{Re}{\Delta t \theta_w}$. So, the behavior of $K_0(x) \rightarrow 0$ for large x , makes it possible to use large time steps, and to keep θ_w close to one.

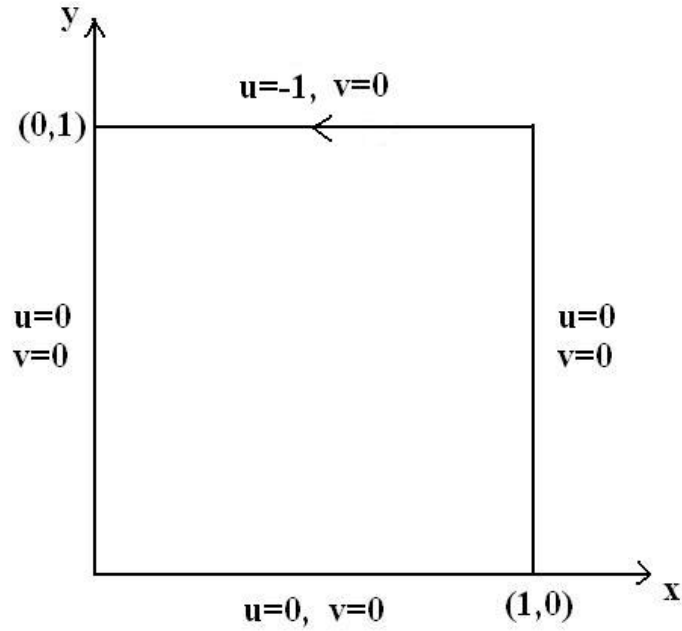


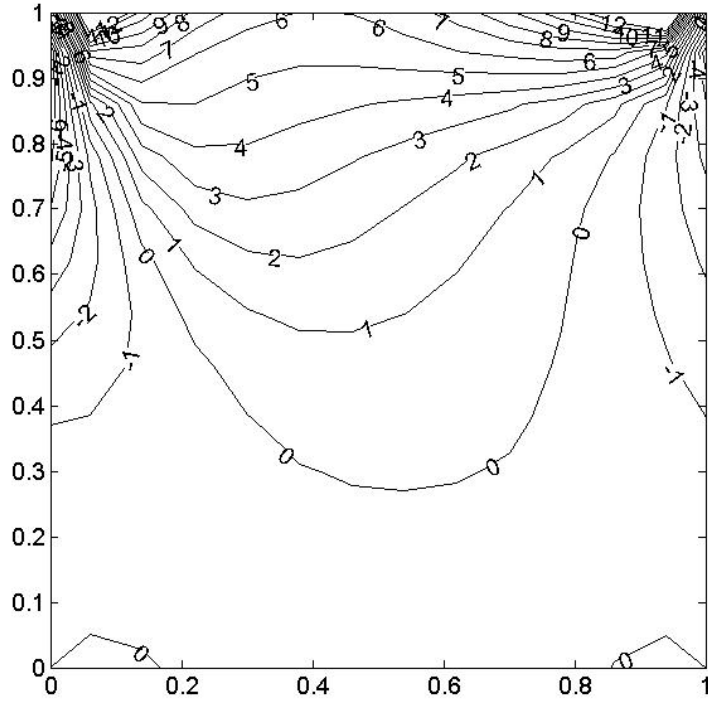
Figure 4.2: Boundary conditions for the lid-driven flow in a square cavity

Table 4.7: The number of iteration with corresponding θ_w for $Re = 500$, $N = 92$, $\Delta t = 0.1$

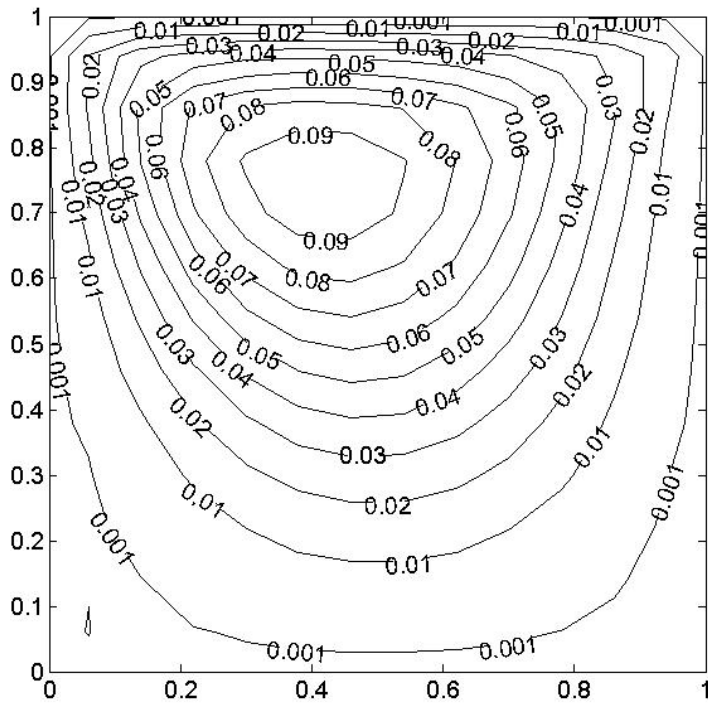
θ_w	0.1	0.2	0.3	0.4	0.5	0.6	0.7	0.8	0.9
Iterations	–	385	272	189	132	102	83	70	61

Figures 4.3-4.6 show the contour lines of ψ and w for flows $50 \leq Re \leq 2000$. At a Reynolds number of around 50 the streamline primary vortex moves toward the left-hand wall with the same direction of the movement of the lid. Also, at the left bottom corner, there is a secondary eddy which is very small and thin. When the Reynolds number takes the higher values, the primary vortex moves towards the center of the cavity. In the case of $Re = 500$, the secondary eddy at the left bottom corner enlarges, and also at the right bottom corner, a new secondary eddy starts to appear. When the Reynolds number achieves to 1000, the eddy in the right bottom corner enlarges and a new secondary eddy appears at the right upper corner. As Reynolds number increases from 1000 to 2000 the eddy at the right corner grows.

From the vorticity contour lines, as Re increases, because of the movement of the lid, there is a recirculation on the fluid towards to the left upper corner. When Re increases, the boundary layers occur at the walls, especially close to the left wall and on the top lid. The center of the cavity becomes stationary. This behavior of the fluid shows that the strong velocity gradients occur at the left wall and on the top lid. These solutions are in good agreement with the ones in [29, 83], and physically expected behaviors are obtained.

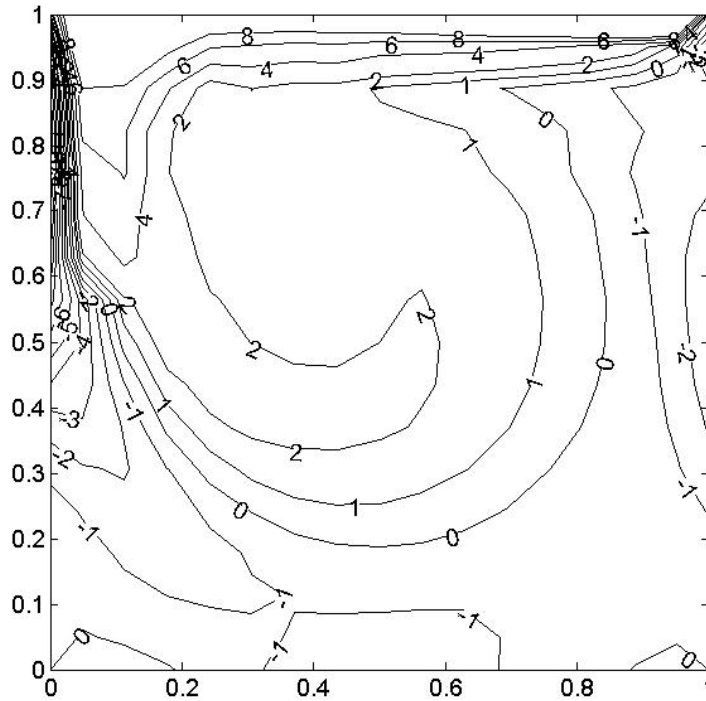


(a) Vorticity

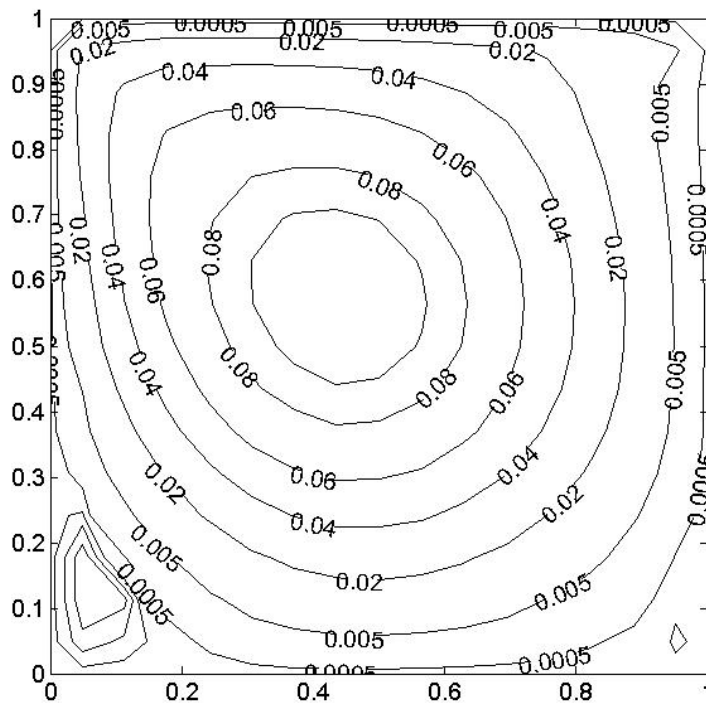


(b) Streamline

Figure 4.3: Lid-driven cavity flow, $Re = 50$.

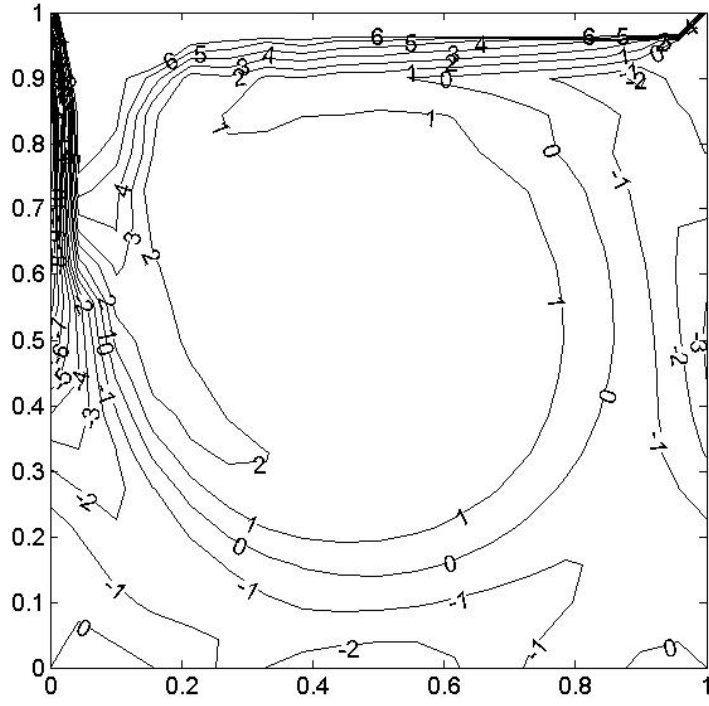


(a) Vorticity

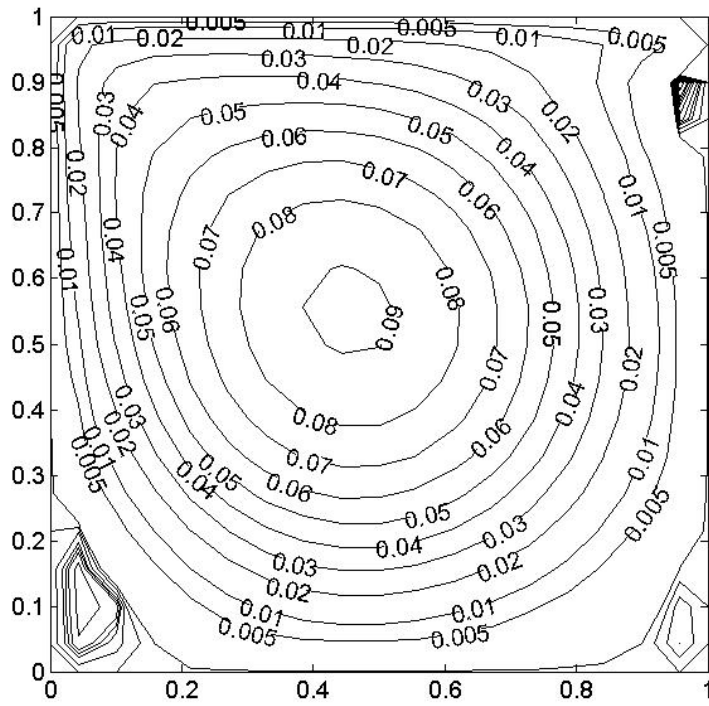


(b) Streamline

Figure 4.4: Lid-driven cavity flow, $Re = 500$.

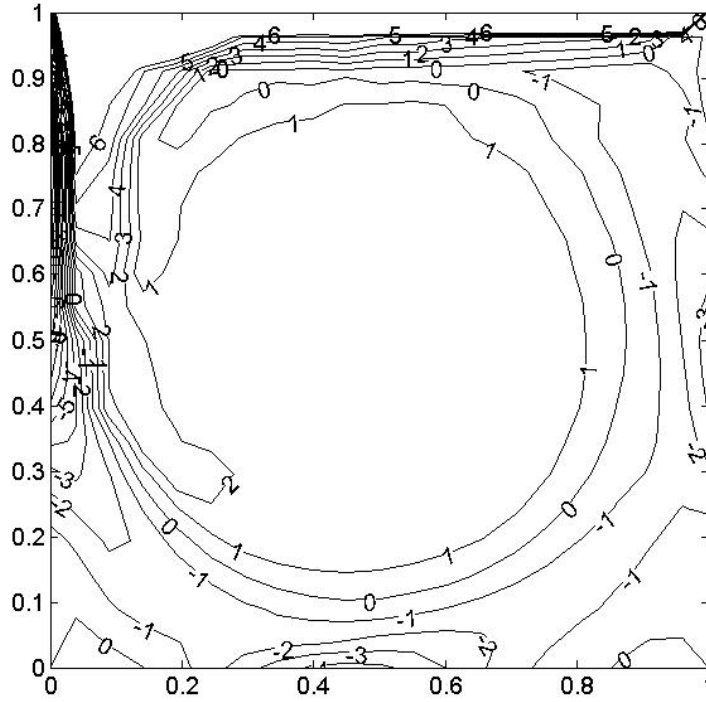


(a) Vorticity

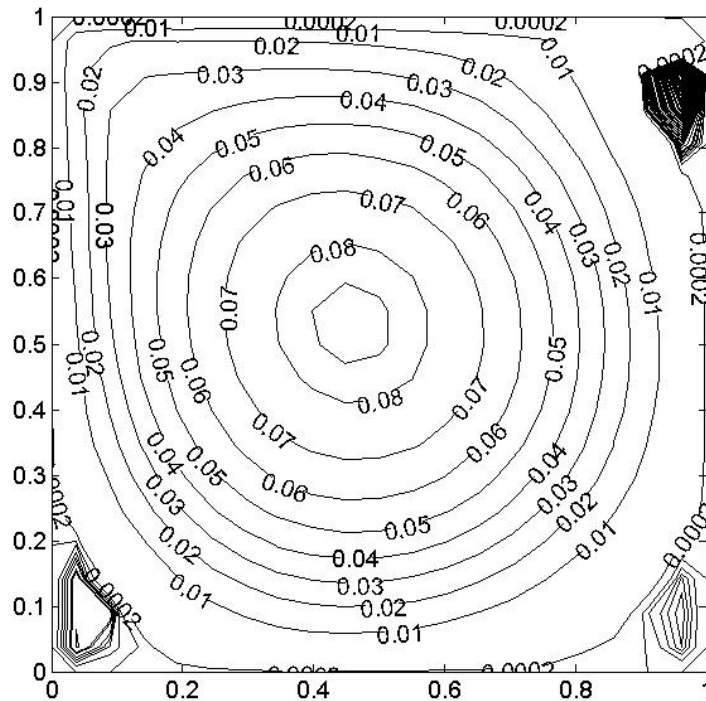


(b) Streamline

Figure 4.5: Lid-driven cavity flow, $Re = 1000$.



(a) Vorticity



(b) Streamline

Figure 4.6: Lid-driven cavity flow, $Re = 2000$.

4.2.2 Natural Convection in a Square Cavity

In this section, the application of DRBEM will be given for the natural convection flow problem. In the natural convection problems, the fluid density differences, caused by the temperature, generate the buoyancy force $RaPr\frac{\partial T}{\partial x}$ which is the dominant driving force for the system. Therefore the energy equation should be directly coupled with the momentum equations. The governing equations of the natural convection problem in the stream function-vorticity-temperature ($\psi - w - T$) formulation are obtained in Chapter 1 as

$$\nabla^2\psi = -w \quad (4.51)$$

$$Pr\nabla^2 w = \frac{\partial w}{\partial t} + u\frac{\partial w}{\partial x} + v\frac{\partial w}{\partial y} - RaPr\frac{\partial T}{\partial x} \quad (4.52)$$

$$\nabla^2 T = \frac{\partial T}{\partial t} + u\frac{\partial T}{\partial x} + v\frac{\partial T}{\partial y} \quad (4.53)$$

where Pr and Ra are Prandtl number and Rayleigh number, respectively, and

$$u = \frac{\partial\psi}{\partial y}, \quad v = -\frac{\partial\psi}{\partial x}, \quad w = \frac{\partial v}{\partial x} - \frac{\partial u}{\partial y} \quad (4.54)$$

are the time dependent velocity components and the vorticity.

After transforming the vorticity transport and energy equations to inhomogeneous modified Helmholtz equations as is done in Chapter 1, the following iteration procedure can be written for natural convection flow

$$\begin{aligned} \nabla^2\psi^{(n+1)} &= -w^{(n)} \\ \nabla^2 w^{(n+1)} - \tau_w^2 w^{(n+1)} &= -\frac{(1-\theta_w)}{\theta_w}\nabla^2 w^{(n)} - \tau_w^2 w^{(n)} \\ &\quad + \frac{1}{Pr\theta_w}\left(\frac{\partial\psi^{(n+1)}}{\partial y}\frac{\partial w^{(n)}}{\partial x} - \frac{\partial\psi^{(n+1)}}{\partial x}\frac{\partial w^{(n)}}{\partial y}\right) - \frac{Ra}{\theta_w}\left(\frac{\partial T^{(n)}}{\partial x}\right) \\ \nabla^2 T^{(n+1)} - \tau_T^2 T^{(n+1)} &= -\frac{(1-\theta_T)}{\theta_T}\nabla^2 T^{(n)} - \tau_T^2 T^{(n)} \\ &\quad + \frac{1}{\theta_T}\left(\frac{\partial\psi^{(n+1)}}{\partial y}\frac{\partial T^{(n)}}{\partial x} - \frac{\partial\psi^{(n+1)}}{\partial x}\frac{\partial T^{(n)}}{\partial y}\right) \end{aligned} \quad (4.55)$$

where $\tau_w^2 = \frac{1}{Pr\Delta t\theta_w}$ and $\tau_T^2 = \frac{1}{\Delta t\theta_T}$. So, we have a Poisson equation for stream function and two inhomogeneous modified Helmholtz equations for vorticity transport and energy equations, respectively (equations (4.52) and (4.53)).

The application of DRBEM is carried for the equations in the form

$$\nabla^2\psi^{(n+1)} = b_1 \quad (4.56)$$

$$\nabla^2 w^{(n+1)} - \tau_w^2 w^{(n+1)} = b_2 \quad (4.57)$$

$$\nabla^2 T^{(n+1)} - \tau_T^2 T^{(n+1)} = b_3 \quad (4.58)$$

where b_1 , b_2 and b_3 are the right hand sides of corresponding equations in (4.55), and they contain the values of vorticity and temperature obtained from the previous time level and stream function from the newly obtained current time level.

In the DRBEM procedure, the fundamental solutions $\frac{1}{2\pi} \ln(r)$ and $\frac{1}{2\pi} K_0(\tau r)$ are used for the Poisson and modified Helmholtz equations, respectively. The procedure for the stream function and vorticity equations is the same with the lid-driven flow problem which differs only with the term $RaPr \frac{\partial T}{\partial x}$. Thus, energy equation will also be discretized by using DRBEM, and will be included in the iteration.

Now, the DRBEM discretized system of equations become

$$\mathbf{H}\psi - \mathbf{G}\mathbf{q}_\psi = (\mathbf{H}\widehat{\Psi} - \mathbf{G}\widehat{Q}_\psi)\mathbf{F}^{-1}\mathbf{b}_1 \quad (4.59)$$

$$\mathbf{H}'\mathbf{w} + \mathbf{G}'\mathbf{q}_w = (\mathbf{H}'\widehat{W} + \mathbf{G}'\widehat{Q}_w)\overline{\mathbf{F}}^{-1}\mathbf{b}_2 \quad (4.60)$$

$$\mathbf{H}'\mathbf{T} + \mathbf{G}'\mathbf{q}_T = (\mathbf{H}'\widehat{T} + \mathbf{G}'\widehat{Q}_T)\overline{\mathbf{F}}^{-1}\mathbf{b}_3 \quad (4.61)$$

where vectors \mathbf{b}_1 , \mathbf{b}_2 , \mathbf{b}_3 are formed from

$$b_1 = -w^{(n)} \quad (4.62)$$

$$b_2 = -\left(\frac{1-\theta_w}{\theta_w}\right)\nabla^2 w^{(n)} - \tau_w^2 w^{(n)} + \frac{1}{Pr\theta_w}\left(\frac{\partial\psi^{(n+1)}}{\partial y}\frac{\partial w^{(n)}}{\partial x} - \frac{\partial\psi^{(n+1)}}{\partial x}\frac{\partial w^{(n)}}{\partial y}\right) - \frac{Ra}{\theta_w}\left(\frac{\partial T^{(n)}}{\partial x}\right) \quad (4.63)$$

and

$$b_3 = -\left(\frac{1-\theta_T}{\theta_T}\right)\nabla^2 T^{(n)} - \tau_T^2 T^{(n)} + \frac{1}{\theta_T}\left(\frac{\partial\psi^{(n+1)}}{\partial y}\frac{\partial T^{(n)}}{\partial x} - \frac{\partial\psi^{(n+1)}}{\partial x}\frac{\partial T^{(n)}}{\partial y}\right). \quad (4.64)$$

ψ and \mathbf{q}_ψ , \mathbf{w} and \mathbf{q}_w , and \mathbf{T} and \mathbf{q}_T are the vectors containing known and unknown values, and their normal derivative values at the corresponding nodes, for the stream function, vorticity and temperature, respectively. The right hand side functions b_1 is approximated using the coordinate function $f = 1 + r$ whereas b_2 and b_3 are approximated using the coordinate function $\bar{f} = r^2 \ln r$.

Space derivatives of T are also computed with the coordinate matrix $\overline{\mathbf{F}}$ as

$$\frac{\partial \mathbf{T}^{(n)}}{\partial x} = \frac{\partial \overline{\mathbf{F}}}{\partial x} \overline{\mathbf{F}}^{-1} \mathbf{T}^{(n)}, \quad \frac{\partial \mathbf{T}^{(n)}}{\partial y} = \frac{\partial \overline{\mathbf{F}}}{\partial y} \overline{\mathbf{F}}^{-1} \mathbf{T}^{(n)}. \quad (4.65)$$

The Laplacian term $\nabla^2 T^{(n)}$ is also approximated by using DRBEM idea with the coordinate matrix belonging to T as $\overline{\mathbf{F}}$, such that

$$\nabla^2 \mathbf{T}^{(n)} = \frac{\partial \overline{\mathbf{F}}}{\partial x} \overline{\mathbf{F}}^{-1} \left(\frac{\partial \mathbf{T}^{(n)}}{\partial x}\right) + \frac{\partial \overline{\mathbf{F}}}{\partial y} \overline{\mathbf{F}}^{-1} \left(\frac{\partial \mathbf{T}^{(n)}}{\partial y}\right). \quad (4.66)$$

Thus, linear system of equations are obtained after the insertion of related boundary conditions to (4.59)-(4.61)

$$\begin{aligned} \mathbf{A}_1 \mathbf{x}_1 &= \mathbf{y}_1 \\ \mathbf{A}_2 \mathbf{x}_2 &= \mathbf{y}_2 \\ \mathbf{A}_3 \mathbf{x}_3 &= \mathbf{y}_3 \end{aligned} \quad (4.67)$$

where x_1 , x_2 and x_3 contain now only unknown values of ψ , q_ψ , w , q_w and T , q_T , respectively.

In the iterative procedure for the lid-driven cavity flow, the system for energy equation will be included now with an initial $T^{(0)}$ vector, and the temperature is obtained at steady-state with the same stopping criteria in the cycle.

4.2.2.1 Numerical Results

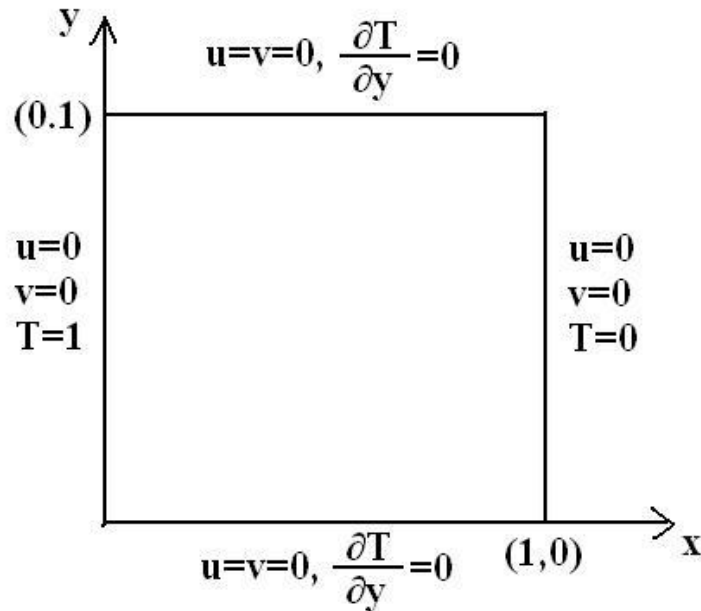


Figure 4.7: Boundary conditions for the natural convection flow in a square cavity

The boundary conditions of natural convection flow problem defined in a square cavity $\Omega = [0, 1] \times [0, 1]$ are shown in Figure 4.7. The no-slip boundary conditions are assumed on the fixed walls and boundary conditions of stream function are taken as zero at these walls. The vorticity boundary conditions are obtained from $w = \frac{\partial v}{\partial x} - \frac{\partial u}{\partial y}$ by using the coordinate matrix \bar{F} . At the left and right walls Dirichlet type boundary conditions are considered as 1 and 0 for T (walls are heated and cooled, respectively) whereas Neumann type boundary conditions $\frac{\partial T}{\partial y} = 0$ (adiabatic) are imposed on the horizontal walls.

The problem is solved iteratively using the given numerical algorithm to obtain the unknown values of stream function, vorticity and temperature. The stopping criteria for the steady-state results is taken as $\varepsilon = 10^{-4}$ for all variables. The radial basis functions are taken as $f = 1 + r$ for stream function equation and $\bar{f} = r^2 \ln r$ for vorticity and temperature equations. Computations are carried using $Ra = 10^3, 10^4, 10^5$ and 10^6 with $N = 60, 68, 100$ and 132 constant boundary elements, and $\Delta t = 0.1, 0.05, 0.01$ and 0.005 , respectively, and for every

case Pr is taken as 1. Thus, one can conclude that time increment is decreased and boundary element numbers are increased with increasing values of Rayleigh number. The choices of Δt and θ_w, θ_T are closely related with the nice behavior of $K_0(\tau r)$ since $\tau^2 = \frac{1}{\Delta t \theta}$ as in the lid-driven cavity problem. Relaxation parameters are taken close to one and not too small step size, prevent $K_0(x) \rightarrow \infty$ behavior, but $K_0(x) \rightarrow 0$ smoothly.

In Figure 4.8 we give isotherms, vorticity contours and streamlines at steady-state for $Ra = 10^3 - 10^6$ using constant boundary elements. When $Ra = 10^3$ there is not enough convection, so viscous forces are dominating in the cavity. From the figure, it is observed that the vortex of the streamlines shows a circular behavior and it takes the minimum value at the center of the cavity. The isotherms take the values 1 to 0 from left to right walls of the cavity due to the boundary conditions. Their behaviors look like a vertical line and they are perpendicular to the top and bottom walls. This is caused by the adiabatic boundary conditions obeying the physics of heat transfer in the cavity. The vorticity action occurs by forming a vortex at the center of the cavity.

As the Rayleigh number increases, in the system, convection forces start to dominate over the viscous forces. So, the circular shape of the streamlines takes the shape of an ellipse and boundary layer formation occurs near the vertical walls. Because of the high values of Rayleigh number, the vorticity values near the vertical walls increase and so boundary layers occur near the vertical walls. Also, the primary vortex starts to divide into two new vortices which move towards the left upper and the right bottom corners. Vertical shape of the isotherms becomes parallel to the bottom wall and form boundary layers closer to the vertical walls of the cavity. The central region of the cavity is almost stationary. These behaviors are in good agreement with the ones given in [62].

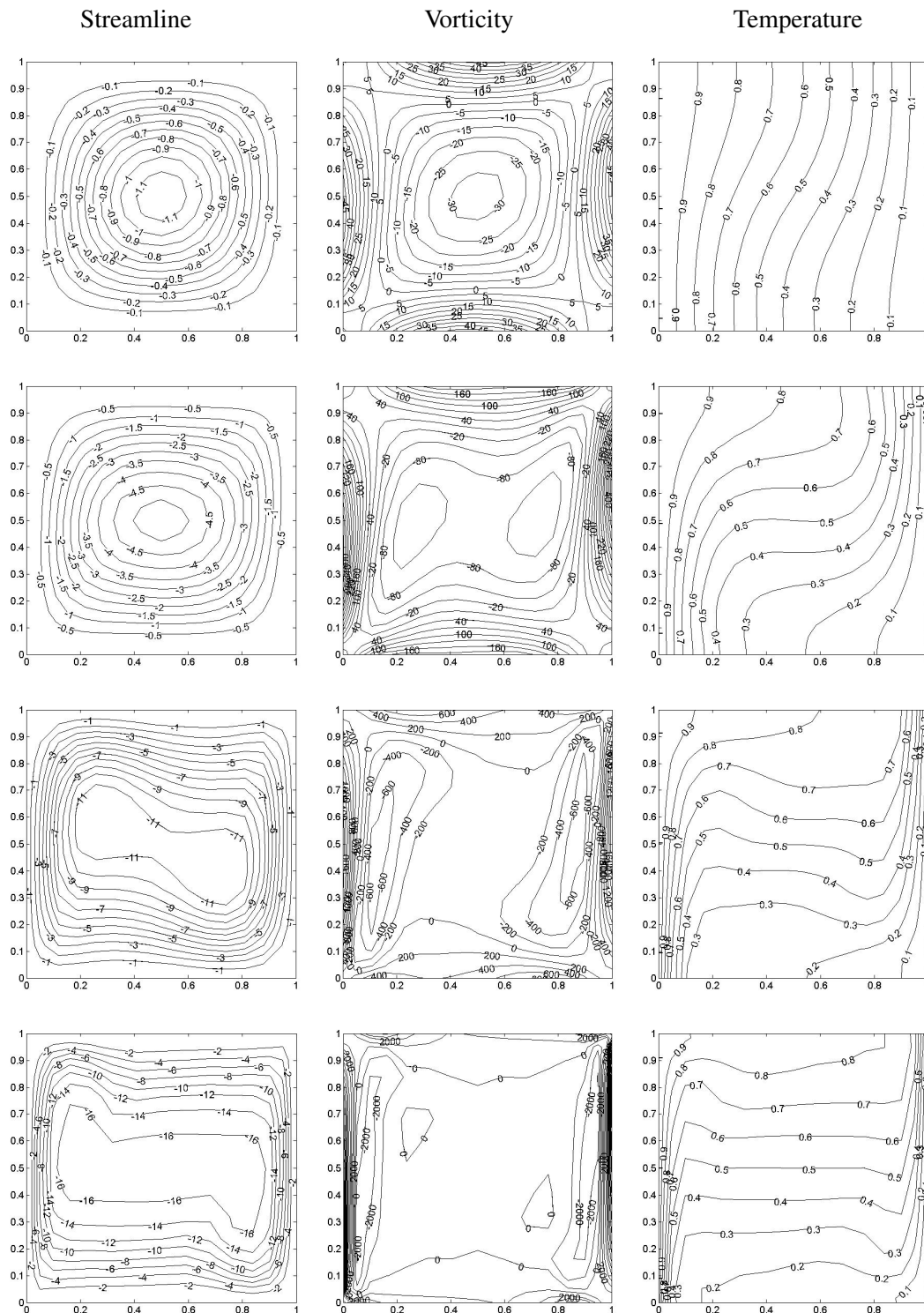


Figure 4.8: Natural convection in a square cavity: $Ra = 10^3$, $Ra = 10^4$, $Ra = 10^5$ and $Ra = 10^6$ from top to bottom

4.3 DRBEM Solution of the Thermo-Solutal Buoyancy Induced Mixed Convection Flow

The thermo-solutal buoyancy-driven flow is governed by the equations that represent conservation of mass, momentum, energy and solutal concentration. Together with the velocity-vorticity form of vorticity transport equation the governing equations are given in non-dimensional form as

$$\nabla^2 \psi = -w \quad (4.68)$$

$$\frac{1}{Re} \nabla^2 w = \frac{\partial w}{\partial t} + u \frac{\partial w}{\partial x} + v \frac{\partial w}{\partial y} - Ri \left(\frac{\partial T}{\partial x} + N \frac{\partial C}{\partial x} \right) \quad (4.69)$$

$$\frac{1}{RePr} \nabla^2 T = \frac{\partial T}{\partial t} + u \frac{\partial T}{\partial x} + v \frac{\partial T}{\partial y} \quad (4.70)$$

$$\frac{1}{ReSc} \nabla^2 C = \frac{\partial C}{\partial t} + u \frac{\partial C}{\partial x} + v \frac{\partial C}{\partial y} \quad (4.71)$$

in which velocity components u , v and vorticity w are defined as

$$u = \frac{\partial \psi}{\partial y}, \quad v = -\frac{\partial \psi}{\partial x}, \quad w = \frac{\partial v}{\partial x} - \frac{\partial u}{\partial y} \quad (4.72)$$

where ψ , w , T , and C are the stream function, vorticity, temperature, and solutal concentration, respectively. Re is the Reynolds number given by $Re = \frac{U_0 H}{\nu}$ where U_0 , H and ν are characteristic velocity, characteristic length and the kinematic viscosity, respectively. Ri is the Richardson number given by $\frac{Gr_T}{Re^2}$ where Gr_T is the Grashof number due to the thermal diffusion. N is the buoyancy ratio given by $\frac{\beta_C \Delta C}{\beta_T \Delta T}$ where β_C is the volumetric solutal concentration expansion coefficient, β_T is the volumetric thermal expansion coefficient, $\Delta C = C_h - C_c$ (C_h and C_c are high and low solutal concentrations), and $\Delta T = T_h - T_c$ (T_h and T_c are high and low temperatures).

Using the same procedure given in Chapter 1 for obtaining inhomogeneous modified Helmholtz equations for the vorticity transport, energy and concentration equations the following itera-

tive equations can be written for thermo-solutal buoyancy induced mixed convection flow

$$\begin{aligned}
\nabla^2 \psi^{(n+1)} &= -w^{(n)} \\
\nabla^2 w^{(n+1)} - \tau_w^2 w^{(n+1)} &= -\frac{(1-\theta_w)}{\theta_w} \nabla^2 w^{(n)} - \tau_w^2 w^{(n)} \\
&\quad + \frac{Re}{\theta_w} \left(\frac{\partial \psi^{(n+1)}}{\partial y} \frac{\partial w^{(n)}}{\partial x} - \frac{\partial \psi^{(n+1)}}{\partial x} \frac{\partial w^{(n)}}{\partial y} \right) \\
&\quad - \frac{Re Ri}{\theta_w} \left(\frac{\partial T^{(n)}}{\partial x} + N \frac{\partial C^{(n)}}{\partial x} \right) \\
\nabla^2 T^{(n+1)} - \tau_T^2 T^{(n+1)} &= -\frac{(1-\theta_T)}{\theta_T} \nabla^2 T^{(n)} - \tau_T^2 T^{(n)} \\
&\quad + \frac{Re Pr}{\theta_T} \left(\frac{\partial \psi^{(n+1)}}{\partial y} \frac{\partial T^{(n)}}{\partial x} - \frac{\partial \psi^{(n+1)}}{\partial x} \frac{\partial T^{(n)}}{\partial y} \right) \\
\nabla^2 C^{(n+1)} - \tau_C^2 C^{(n+1)} &= -\frac{(1-\theta_C)}{\theta_C} \nabla^2 C^{(n)} - \tau_C^2 C^{(n)} \\
&\quad + \frac{Re S c}{\theta_C} \left(\frac{\partial \psi^{(n+1)}}{\partial y} \frac{\partial C^{(n)}}{\partial x} - \frac{\partial \psi^{(n+1)}}{\partial x} \frac{\partial C^{(n)}}{\partial y} \right)
\end{aligned} \tag{4.73}$$

where $\tau_w^2 = \frac{Re}{\Delta t \theta_w}$, $\tau_T^2 = \frac{Re Pr}{\Delta t \theta_T}$, and $\tau_C^2 = \frac{Re S c}{\Delta t \theta_C}$, and n indicates iteration number.

DRBEM solutions for stream function, vorticity, temperature and concentration equations are obtained from Poisson, and modified Helmholtz equations

$$\nabla^2 \psi^{(n+1)} = b_1 \tag{4.74}$$

$$\nabla^2 w^{(n+1)} - \tau_w^2 w^{(n+1)} = b_2 \tag{4.75}$$

$$\nabla^2 T^{(n+1)} - \tau_T^2 T^{(n+1)} = b_3 \tag{4.76}$$

$$\nabla^2 C^{(n+1)} - \tau_C^2 C^{(n+1)} = b_4 \tag{4.77}$$

where b_1, b_2, b_3 and b_4 are the right hand sides of corresponding equations in (4.73), and they contain the values of vorticity, temperature and concentration obtained from the previous time level and stream function from the newly obtained current time level.

Again, the fundamental solutions $\frac{1}{2\pi} \ln(r)$ and $\frac{1}{2\pi} K_0(\tau r)$ are used for the Poisson and modified Helmholtz equations, respectively. The radial basis functions $f = 1 + r$ is used to approximate b_1 and $\bar{f} = r^2 \ln r$ is used to approximate b_2, b_3 and b_4 .

The DRBEM discretized matrix-vector equations for stream function, vorticity, temperature and concentration are

$$\mathbf{H}\psi - \mathbf{G}\mathbf{q}_\psi = (\mathbf{H}\widehat{\Psi} - \mathbf{G}\widehat{Q}_\psi)\mathbf{F}^{-1}\mathbf{b}_1 \tag{4.78}$$

$$\mathbf{H}'\mathbf{w} + \mathbf{G}'\mathbf{q}_w = (\mathbf{H}'\widehat{W} + \mathbf{G}'\widehat{Q}_w)\overline{\mathbf{F}}^{-1}\mathbf{b}_2 \tag{4.79}$$

$$\mathbf{H}'\mathbf{T} + \mathbf{G}'\mathbf{q}_T = (\mathbf{H}'\widehat{T} + \mathbf{G}'\widehat{Q}_T)\overline{\mathbf{F}}^{-1}\mathbf{b}_3 \tag{4.80}$$

$$\mathbf{H}'\mathbf{C} + \mathbf{G}'\mathbf{q}_C = (\mathbf{H}'\widehat{C} + \mathbf{G}'\widehat{Q}_C)\overline{\mathbf{F}}^{-1}\mathbf{b}_4 \tag{4.81}$$

where $\mathbf{b}_1, \mathbf{b}_2, \mathbf{b}_3$ and \mathbf{b}_4 vectors are formed collocating b_1, b_2, b_3 and b_4 from

$$b_1 = -w^{(n)} \quad (4.82)$$

$$b_2 = -\left(\frac{1-\theta_w}{\theta_w}\right)\nabla^2 w^{(n)} - \tau_w^2 w^{(n)} + \frac{Re}{\theta_w}\left(\frac{\partial\psi^{(n+1)}}{\partial y}\frac{\partial w^{(n)}}{\partial x} - \frac{\partial\psi^{(n+1)}}{\partial x}\frac{\partial w^{(n)}}{\partial y}\right) - \frac{Re Ri}{\theta_w}\left(\frac{\partial T^{(n)}}{\partial x} + N\frac{\partial C^{(n)}}{\partial x}\right) \quad (4.83)$$

$$b_3 = -\left(\frac{1-\theta_T}{\theta_T}\right)\nabla^2 T^{(n)} - \tau_T^2 T^{(n)} + \frac{Re Pr}{\theta_T}\left(\frac{\partial\psi^{(n+1)}}{\partial y}\frac{\partial T^{(n)}}{\partial x} - \frac{\partial\psi^{(n+1)}}{\partial x}\frac{\partial T^{(n)}}{\partial y}\right) \quad (4.84)$$

$$b_4 = -\left(\frac{1-\theta_C}{\theta_C}\right)\nabla^2 C^{(n)} - \tau_C^2 C^{(n)} + \frac{Re Sc}{\theta_C}\left(\frac{\partial\psi^{(n+1)}}{\partial y}\frac{\partial C^{(n)}}{\partial x} - \frac{\partial\psi^{(n+1)}}{\partial x}\frac{\partial C^{(n)}}{\partial y}\right). \quad (4.85)$$

$\bar{\mathbf{F}}$, is $(K+L) \times (K+L)$ coordinate matrix formed columnwise from the radial basis function $\bar{f}_j = r_j^2 \ln r_j$. $\psi, \mathbf{q}_\psi, \mathbf{w}, \mathbf{q}_w, \mathbf{T}, \mathbf{q}_T$, and \mathbf{C}, \mathbf{q}_C contain known and unknown values of stream function, vorticity, temperature, concentration and their normal derivatives, respectively.

First and second order space derivatives are computed with the help of coordinate matrices

$$\frac{\partial \mathbf{T}^{(n)}}{\partial x} = \frac{\partial \bar{\mathbf{F}}}{\partial x} \bar{\mathbf{F}}^{-1} \mathbf{T}^{(n)}, \quad \frac{\partial \mathbf{T}^{(n)}}{\partial y} = \frac{\partial \bar{\mathbf{F}}}{\partial y} \bar{\mathbf{F}}^{-1} \mathbf{T}^{(n)} \quad (4.86)$$

and

$$\frac{\partial \mathbf{C}^{(n)}}{\partial x} = \frac{\partial \bar{\mathbf{F}}}{\partial x} \bar{\mathbf{F}}^{-1} \mathbf{C}^{(n)}, \quad \frac{\partial \mathbf{C}^{(n)}}{\partial y} = \frac{\partial \bar{\mathbf{F}}}{\partial y} \bar{\mathbf{F}}^{-1} \mathbf{C}^{(n)}. \quad (4.87)$$

The Laplacian terms $\nabla^2 T^{(n)}$ and $\nabla^2 C^{(n)}$ in equations (4.84) and (4.85), are also computed as

$$\nabla^2 \mathbf{T}^{(n)} = \frac{\partial \bar{\mathbf{F}}}{\partial x} \bar{\mathbf{F}}^{-1} \left(\frac{\partial \mathbf{T}^{(n)}}{\partial x}\right) + \frac{\partial \bar{\mathbf{F}}}{\partial y} \bar{\mathbf{F}}^{-1} \left(\frac{\partial \mathbf{T}^{(n)}}{\partial y}\right) \quad (4.88)$$

and

$$\nabla^2 \mathbf{C}^{(n)} = \frac{\partial \bar{\mathbf{F}}}{\partial x} \bar{\mathbf{F}}^{-1} \left(\frac{\partial \mathbf{C}^{(n)}}{\partial x}\right) + \frac{\partial \bar{\mathbf{F}}}{\partial y} \bar{\mathbf{F}}^{-1} \left(\frac{\partial \mathbf{C}^{(n)}}{\partial y}\right). \quad (4.89)$$

With the insertion of related boundary conditions for $\psi, \mathbf{w}, \mathbf{T}$, and \mathbf{C} the following system of linear equations are obtained

$$\begin{aligned} \mathbf{A}_1 \mathbf{x}_1 &= \mathbf{y}_1 \\ \mathbf{A}_2 \mathbf{x}_2 &= \mathbf{y}_2 \\ \mathbf{A}_3 \mathbf{x}_3 &= \mathbf{y}_3 \\ \mathbf{A}_4 \mathbf{x}_4 &= \mathbf{y}_4 \end{aligned} \quad (4.90)$$

where $\mathbf{x}_1, \mathbf{x}_2, \mathbf{x}_3$ and \mathbf{x}_4 contain only unknown values of $\psi, \mathbf{q}_\psi, \mathbf{w}, \mathbf{q}_w, \mathbf{T}, \mathbf{q}_T$ and \mathbf{C}, \mathbf{q}_C on the walls and unknown interior values, respectively.

Solution is obtained iteratively by solving systems (4.90) with initial estimates $w^{(0)}, T^{(0)}$ and $C^{(0)}$ for $n = 0$ as

1. Solve the stream function equation for $\psi^{(n+1)}$ using $w^{(n)}$.

2. Compute first order space derivatives of $\psi^{(n+1)}$ by using coordinate matrix $\overline{\mathbf{F}}$ and compute the u and v velocity components using the equation (4.29).
3. Obtain the vorticity boundary conditions using the definition (4.49) and coordinate matrix $\overline{\mathbf{F}}$.
4. Compute first and second order space derivatives of $w^{(n)}$, $T^{(n)}$ and $C^{(n)}$ by using the DRBEM idea.
5. Compute the right hand side b_2 and solve the vorticity transport equation to obtain $w^{(n+1)}$.
6. Compute the right hand side b_3 and solve the temperature equation to obtain $T^{(n+1)}$.
7. Compute the right hand side b_4 and solve the concentration equation to obtain $C^{(n+1)}$.
8. Check the stopping criteria in order to get steady-state solution as

$$\max_i |\psi^{(n+1)} - \psi^{(n)}| \leq \varepsilon \quad i = 1, \dots, K + L$$

$$\max_i |w^{(n+1)} - w^{(n)}| \leq \varepsilon \quad i = 1, \dots, K + L$$

$$\max_i |T^{(n+1)} - T^{(n)}| \leq \varepsilon \quad i = 1, \dots, K + L$$

$$\max_i |C^{(n+1)} - C^{(n)}| \leq \varepsilon \quad i = 1, \dots, K + L$$

9. Update $w^{(n)}$, $T^{(n)}$ and $C^{(n)}$ values for the next iteration.
10. Continue the steps 1-9 for the next time levels until the stopping criteria is satisfied.

Now, the computational results for the two-dimensional, thermo-solutal mixed convection flow are given for three test problems. Thermo-solutal mixed convection in a lid-driven square cavity, and then in a lid-driven cavity with a square blockage placed at the bottom wall. As the third problem, thermo-solutal mixed convection flow is given in a horizontal channel with a step.

4.3.1 Thermo-solutal Mixed Convection in a Lid-driven Cavity

In the first example, we consider lid-driven flow problem in a square cavity $\Omega = [0, 1 \times 0, 1]$ as shown in Figure 4.9 [54]. The governing equations are given in (4.68)-(4.71) in the form of stream function, vorticity, temperature and solutal concentration. These equations are solved using DRBEM in a square cavity which has three motionless walls, where the upper lid moves with a uniform velocity $u = 1$. The adiabatic boundary conditions are imposed for both temperature and concentration on the vertical walls. The bottom wall of the cavity is heated ($T = 1$) and it is subjected to the high solutal concentration ($C = 1$), whereas the top lid is cooled ($T = 0$) and it is subjected to the low solutal concentration ($C = 0$.)

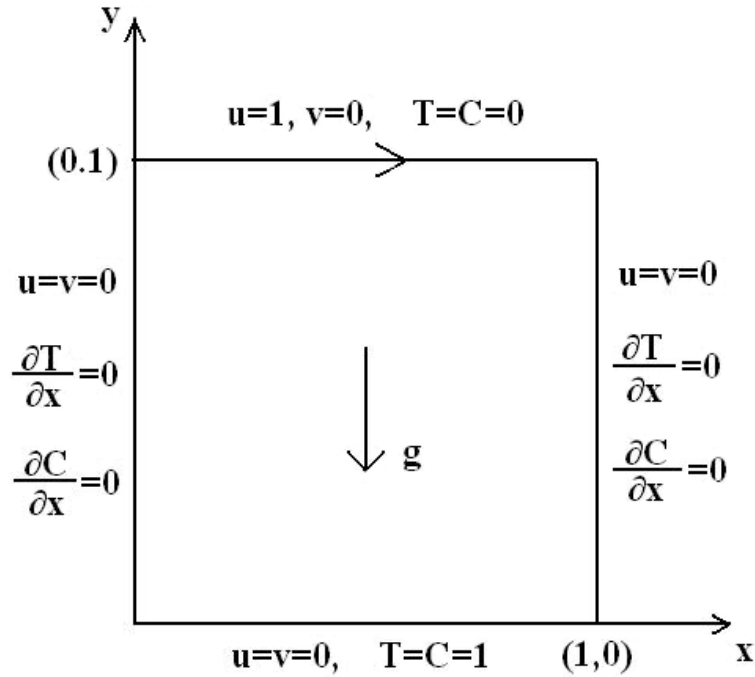


Figure 4.9: Boundary conditions for thermo-solutal mixed convection lid-driven cavity flow

At the three walls no-slip boundary conditions for the velocity are considered, thus the stream function boundary conditions are taken zero at all the walls of the cavity. Physically, there is no boundary condition for the vorticity but they can be obtained from its definition $w = \frac{\partial v}{\partial x} - \frac{\partial u}{\partial y}$ using the DRBEM idea with the help of the coordinate matrix. In all computations the results are obtained using the highest $K = 124$ constant boundary elements, and $L = 225$ interior points. Actually, as Ri , N and Re increase one needs to take more boundary elements. For achieving smooth results the highest number of boundary elements and interior nodes are preferred. The relaxation parameters $(\theta_w, \theta_T, \theta_C)$ for vorticity, temperature and solutal concentration resulted from the procedure of obtaining modified Helmholtz equation

Table 4.8: Δt variations for thermo-solutal mixed convection in a lid-driven cavity

	$N = -10$	$N = -3$	$N = 1$	$N = 3$	$N = 10$
$Ri = 0.5$	0.25	0.25	0.1	0.1	0.05
$Ri = 1$	0.1	0.1	0.05	0.05	0.03
$Ri = 3$	0.05	0.05	0.03	0.03	0.01

are taken as 0.9. This means that more contribution is used from the newly obtained solutions. Therefore one can get steady-state results using less number of iterations with a stopping criteria tolerance $\varepsilon = 10^{-5}$ for all unknowns. Table 4.8 shows time increments Δt needed for reaching steady-state solutions for several values of Richardson number and buoyancy ratio. From the table one can conclude that as N or Ri increases the time increment must decrease but these time increments are still very large compared to the ones needed for other time discretization schemes.

In the thermo-solutal buoyancy induced mixed convection flow there is a close relationship between the parameters Re , Ri and N . Reynolds number (Re) gives a measure of the ratio of fluid inertial force to viscous force, and its magnitude defines the dominance of the fluid inertial force compared with viscous force of the fluid. Richardson number (Ri) describes the relative strength of thermal buoyancy force over the inertial force of the fluid. Buoyancy ratio (N) represents the effect of solutal buoyancy force on the fluid flow. In this study, the effect of fluid inertial force is examined using the different combinations of Ri and N . There is an important relation between the boundary conditions of temperature and solutal concentration. Different situations create different results for the buoyancy forces where they may oppose or aid each other. In our case the bottom wall is heated and is subjected to the high solutal concentration whereas the top lid is cooled and is subjected to the low solutal concentration. Thus, the density due to the temperature gradient and solutal concentration near the bottom wall and top lid plays an important role in the emergence of the buoyancy forces. When N takes positive values, because of the high temperature and high concentration at the bottom wall, the fluid buoyancy forces act together and the density due to the temperature and solutal concentration gradients is lower than the density near the top lid. Therefore, the lighter fluid moves from bottom wall towards the top lid. When N takes negative values, the density due to the temperature gradient near the bottom wall is lower than the density near the top lid but the density due to solutal concentration near the bottom wall is higher than the density near the top lid. Hence, the lighter fluid caused by temperature gradient moves from bottom wall to the lid, and upward thermal buoyancy force occurs in the fluid. Thus, the heavier fluid caused by solutal concentration gradient moves from top lid to the bottom wall, and downward solutal buoyancy force occurs in the fluid. Consequently, thermal and solutal buoyancy forces oppose each other.

Figure 4.10 shows streamlines for the variations of Ri and N by assuming $Re = 100$ and $Pr = Sc = 1$. In Figure 4.10(a), $Ri = 0.5$ and N changes between -10 to 10 . When $N = 1$, the thermal and solutal buoyancy forces are equal and aid each other. In this case, there is a single fluid core in the middle of the cavity. Also a small eddy occurs at the right bottom corner. When N decreases in the negative direction, the density due to the solutal concentration gradient increases. So, the configuration of the secondary fluid circulation occurs for $N = -3$ and three fluid cells are developed when $N = -10$. These additional fluid cells cause the transport

of momentum and heat to slow down. When N increases in the positive direction, the thermal and solutal buoyancy forces aid each other. The size of the eddy increases for $N = 3$ and secondary fluid cell also occurs for $N = 10$. In the contrast to the negative values of N , these secondary fluid cells aid the fluid momentum transport from top lid to the bottom wall.

The same analysis is carried by taking $Ri = 1$ and $Ri = 3$, and results are given in Figure 4.10(b) and Figure 4.10(c), respectively. The behavior of streamlines for $Ri = 1$ is almost the same with the case $Ri = 0.5$. But in this case, the size of the secondary cells increases. In the case of $Ri = 3$, we can see the three fluid cores when $N = -10$ and $N = -3$. Also, secondary fluid cell begins to appear for $N = 1$. Further increase in N as $N = 3$ and $N = 10$ causes a small eddy at the left bottom corner. For the positive value of N , solutal and thermal buoyancy forces aid each other, and buoyancy forces become dominant in the fluid which is expected behavior reported in [54].

The effect of the buoyancy force on vorticity for different values of Ri is given in Figure 4.11. For increasing positive N values, fluid flow covers almost all parts of the cavity forming vortex at the center. As Ri increases this center vortex starts to be developed at lower values of N , and even it is divided to two vortices for $Ri = 3$. For negative values of N , the increase in Ri causes boundary layer formation close to the moving lid on the vertical walls. As N decreases a center vortex also is formed especially for small values of Ri as can be seen in Figure 4.11 ($N = 1$, $N = -3$, $N = -10$ cases).

Figure 4.12 depicts the temperature and concentration contours for different values of Ri and N by taking $Re = 100$, and $Pr = Sc = 1$. Since $Pr = Sc = 1$ is taken in the computations, the temperature and concentration contours are identical. So, both contour lines are given in the same figure. Contour lines take the values between 1 and 0 from bottom to the top walls of the cavity due to the boundary conditions. Because of the adiabatic boundary conditions which are imposed on the vertical walls, the temperature contours are perpendicular to the vertical walls. In the figures which are given for the negative values of N and all values of Ri , the smooth linear variation of the temperature can be seen clearly. The density due to the thermal gradient is less than the density due to solutal concentration for negative values of N . So, heavier fluid moves from top lid to bottom wall. Therefore, heat transfer due to the fluid convection does not occur. But when N increases in positive direction fluid behavior changes. When $N = 1$ and $N = 3$ for $Ri = 0.5$ and $Ri = 1$, the circular behavior is shown in the cavity. When $N = 10$, the magnitude of the solutal buoyancy force reaches its highest value. Also, both solutal and thermal buoyancy forces aid each other. Thus, the secondary bubble is noticed for all values of Ri . Also, this behavior can be seen when $Ri = 3$ for all positive values of N . Since the constant value of Re is used in the computations, the thermo-solutal buoyancy forces affect all behaviors of the isotherms and concentration contours. These primary and secondary bubbles increase with increasing values of N and Ri . These results are remarkably similar to the ones in [54], and the values of the contours are matching.

Figure 4.13 represents u -velocity profile along the vertical mid-plane of the cavity by taking $Le = 2$. Le is the Lewis number and it is defined as $Le = \frac{Sc}{Pr}$. The computation is done to make a comparison with reference [54] by using the same values of parameters, and it is seen that the behavior is in agreement with the behavior in [54].

The convective heat and mass transfer along the bottom wall of the cavity are calculated in

terms of average Nusselt and Sherwood numbers defined as

$$Nu_{av} = \frac{1}{H} \int_0^H \left(uT - \frac{\partial T}{\partial y} \right) dx \quad (4.91)$$

$$Sh_{av} = \frac{1}{H} \int_0^H \left(uC - \frac{\partial C}{\partial y} \right) dx \quad (4.92)$$

where H is the characteristic length of the channel.

Figure 4.14 presents Nusselt and Sherwood numbers for the bottom wall to show the effect of thermo-solutal buoyancy forces on convective heat and mass transfer. In the figure, Nusselt and Sherwood numbers are plotted for $Re = 100$ in the range $-10 \leq N \leq 10$ at different values of Ri . Although Nusselt and Sherwood numbers show a steady increase for $Ri = 0.1$ in the range $-10 \leq N \leq 10$, for the other values of Ri there is always a sharp increase in Nusselt and Sherwood numbers with a maximum value of N around 2.5. The same behavior is observed in reference [54].

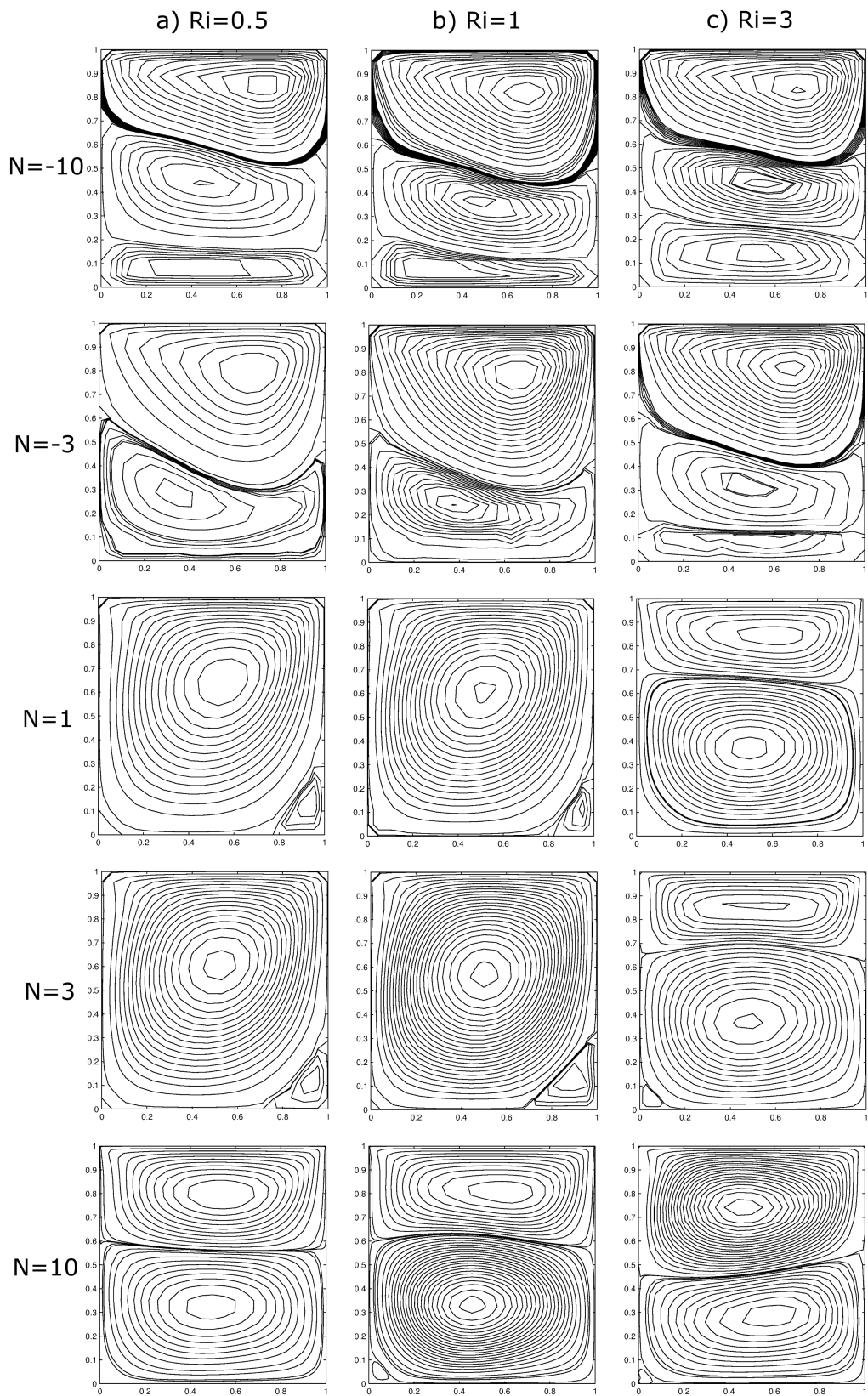


Figure 4.10: The effect of the buoyancy forces on streamlines for different Ri at $Re = 100$ and $Pr = Sc = 1$.

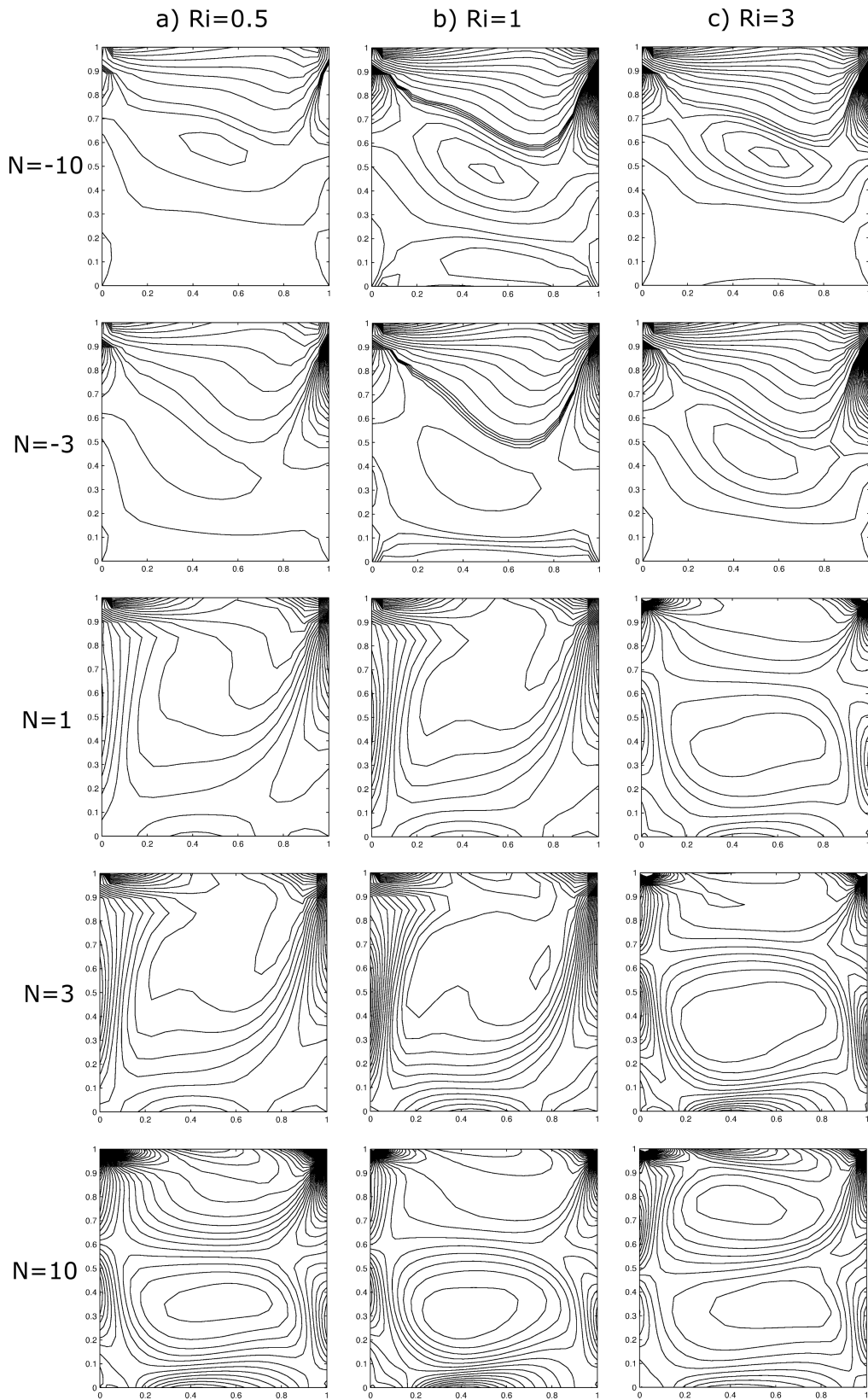


Figure 4.11: The effect of the buoyancy forces on vorticity for different Ri at $Re = 100$ and $Pr = Sc = 1$.

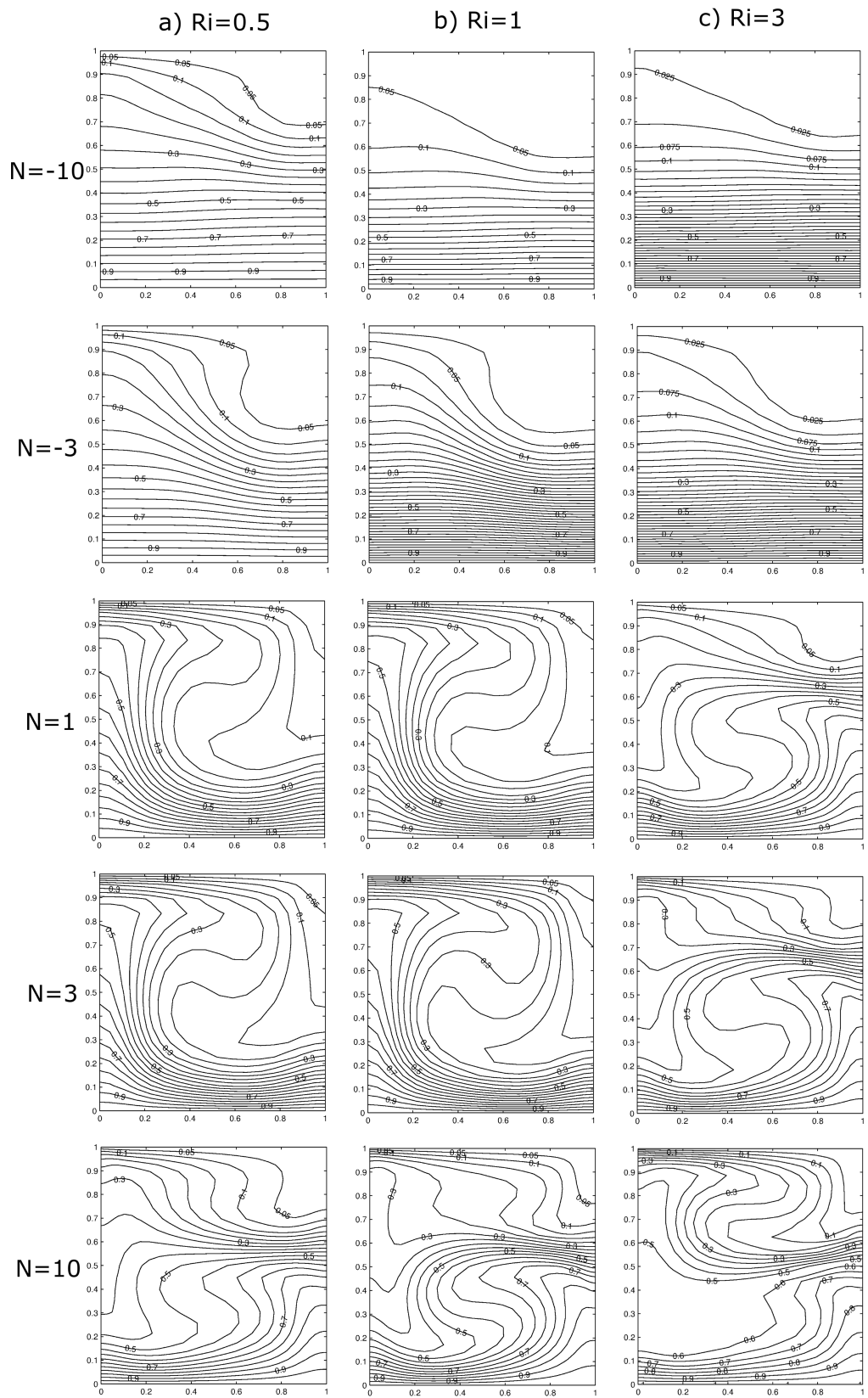


Figure 4.12: The effect of the buoyancy forces on temperature and concentration for different Ri at $Re = 100$ and $Pr = Sc = 1$.

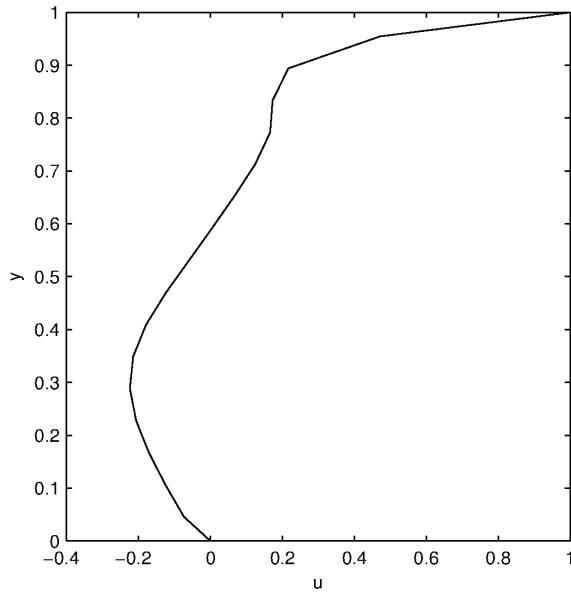


Figure 4.13: u -velocity profile along vertical line ($x = 0.5$) for $Re = 500$, $Gr_T = Gr_C = 100$ and $Le = 2$.

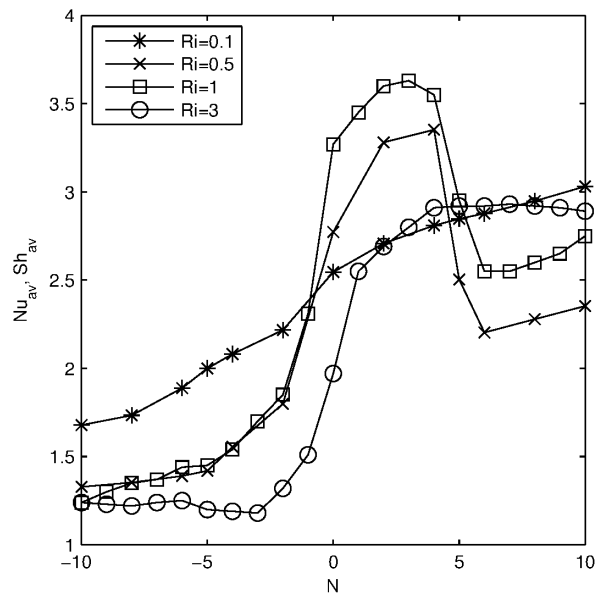


Figure 4.14: The effect of the buoyancy forces on the hot wall, Average Nusselt numbers for $Re = 100$ and $Pr = Sc = 1$.

4.3.2 Thermo-solutal Mixed Convection in a Lid-Driven Cavity with a Square Blockage

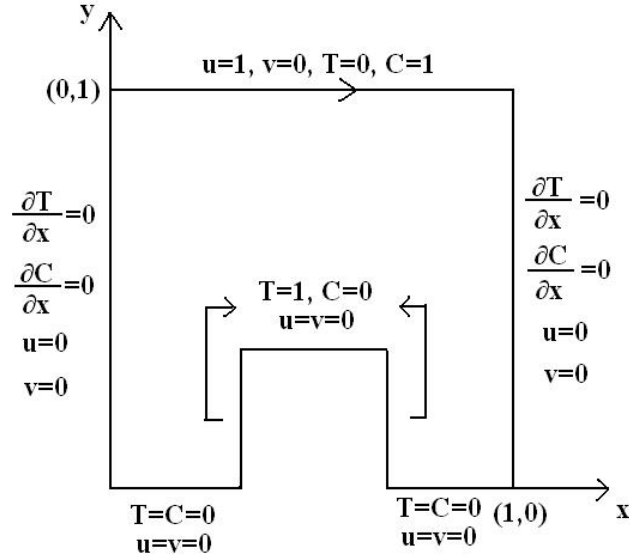


Figure 4.15: Boundary conditions for lid-driven square cavity with a square blockage placed at the bottom wall

We solve the thermal-solutal mixed convection flow in a lid-driven square cavity $\Omega = [0, 1 \times 0, 1]$ with a square blockage placed at the bottom wall. The no-slip boundary conditions for velocity are imposed on all the walls of the cavity and the square blockage with the exception of the upper lid which moves with a uniform velocity $u = 1$. The top lid assumed to be cooled ($T = 0$) with high solutal concentration ($C = 1$). The bottom wall of the cavity except the square blockage are cooled ($T = 0$) with low solutal concentration ($C = 0$). The adiabatic boundary conditions are imposed on the vertical walls for both temperature and solutal concentration. Blockage boundary conditions for T and C are 1 and 0, respectively.

Boundary conditions for stream function are taken as zero at the walls due to the Dirichlet type wall conditions of velocities, and the vorticity boundary conditions are obtained from the discretization of $w = \frac{\partial v}{\partial x} - \frac{\partial u}{\partial y}$ by using the DRBEM coordinate matrix. The boundary of the cavity is discretized by using $K = 286$ constant boundary elements, and $L = 1066$ interior points are used for obtaining the solution and drawing graphics. The pre-assigned accuracy for reaching steady-state is taken as $\epsilon = 10^{-5}$. In the numerical solution, relaxation parameters ($\theta_w, \theta_T, \theta_C$) for vorticity, temperature and solutal concentration are taken 0.9, which takes less number of iterations for reaching steady-state solution. These values of relaxation parameters indicate that more contribution is from the newly obtained solutions. The time increment $\Delta t = 0.05$ is used for reaching steady-state which is very large compared to other time discretization schemes.

First, the effect of the buoyancy ratio is given for $Ri = 0.01$, $Re = 100$ and $Pr = Sc = 1$ by using $N = -50, 0, 50$. From Figure 4.16 one can see that fluid cores occur in the cavity even around the blockage when $N = 50$. When N decreases from 50 to -50 the center of the fluid core gets shifted closer to the center of the cavity increasing the fluid convection. The vorticity which is generated by the boundaries gets diffused and convected throughout the cavity for $N = -50$, and the fluid regime gets divided for $N = 50$. These are expected behaviors since for the negative and positive values of N , buoyancy forces aid and oppose each other. We can see that remarkable temperature gradients occur only near the hot square blockage. Also, since the top lid of the cavity moves from left to right, the temperature contours are twisted towards left-hand side along the left corner of the blockage. For concentration, one can see that there is a boundary layer over the top side of the blockage. When N decrease from 50 to -50 , this boundary layer becomes thick. These results are remarkably similar to the ones in [57]. In the second case, the effect of the buoyancy ratio is given for $Ri = 0.1$, $Re = 100$ and $Pr = Sc = 1$ by using $N = -50, 0, 50$. Figure 4.17 shows a fluid core at the center of the cavity and secondary cores for $N = -50, 0$ around the blockage. But, when $N = 50$ there is a secondary fluid cell in the cavity. Vorticity behavior is similar to the first case. When N is increased to $N = 0$ and $N = 50$, boundary layers are more pronounced close to and on the top lid. When we look at temperature and concentration contours we see that for $N = -50$ and $N = 0$, the behaviors are almost the same with the previous case. When $N = 50$ temperature and concentration contours occupy almost all parts of the cavity with smooth variations. Action around the blockage is weakened. In the Figure 4.18 the effect of increase in Re is visualized. When Re is increased main fluid core is shifted through upper right corner with the movement of the upper lid. This behavior is more pronounced for $N = 50$. Vorticity forms strong boundary layers close to the upper lid and at the side walls close to the upper corners. Isotherms and concentration are not effected much with the increase of Re .

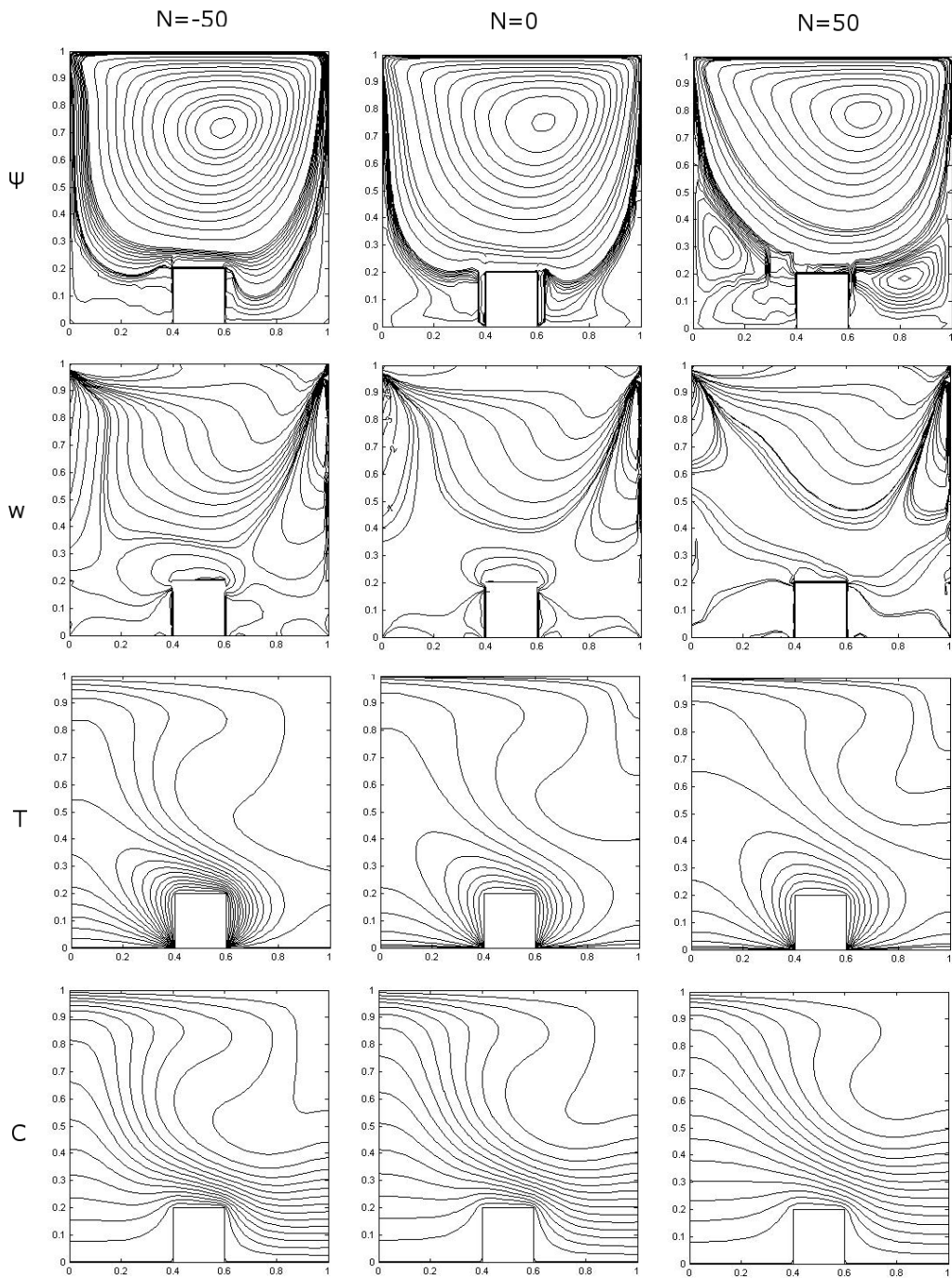


Figure 4.16: The effect of the buoyancy forces for $Ri = 0.01$, $Re = 100$

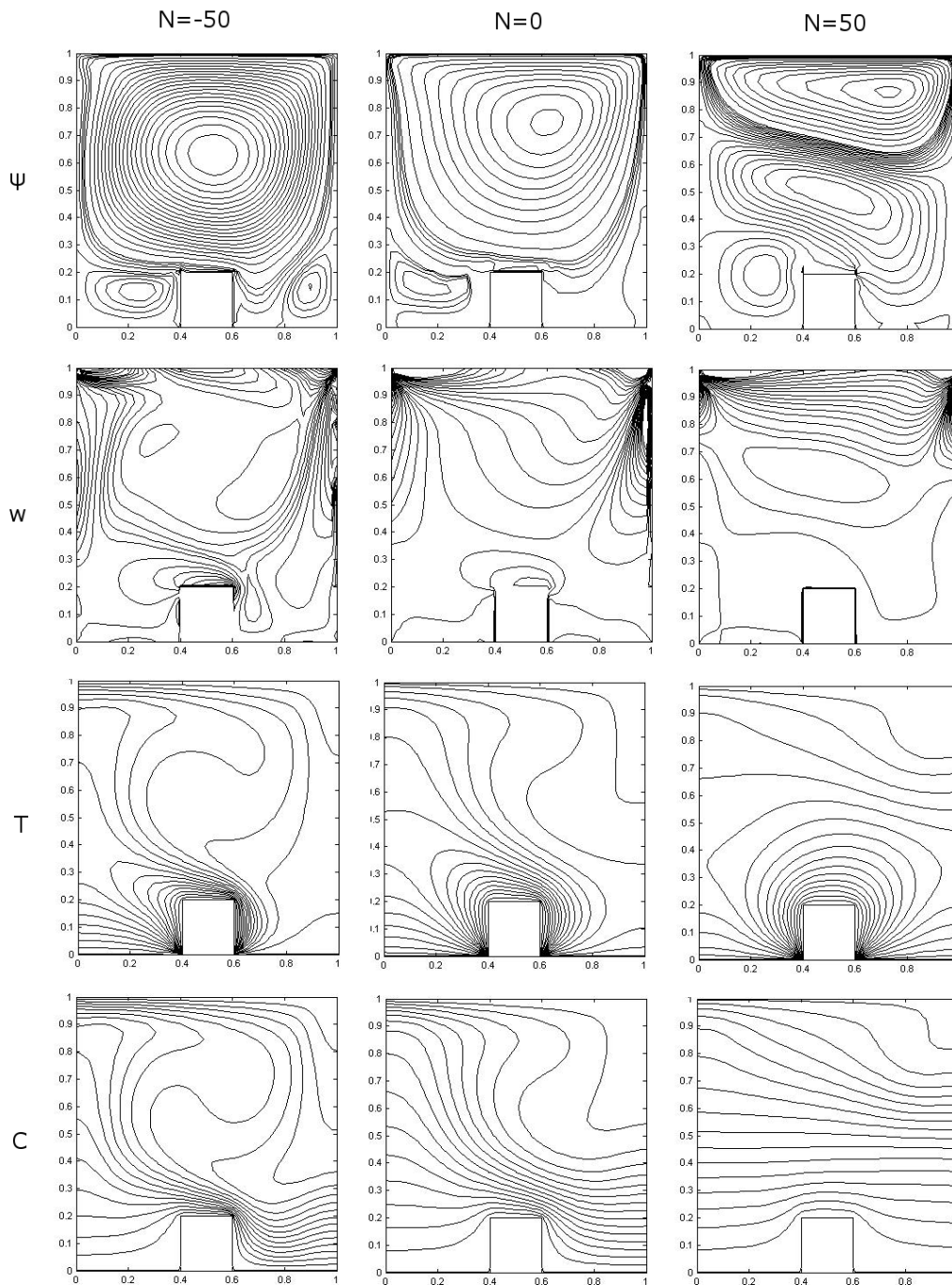


Figure 4.17: The effect of the buoyancy forces for $Ri = 0.1$, $Re = 100$

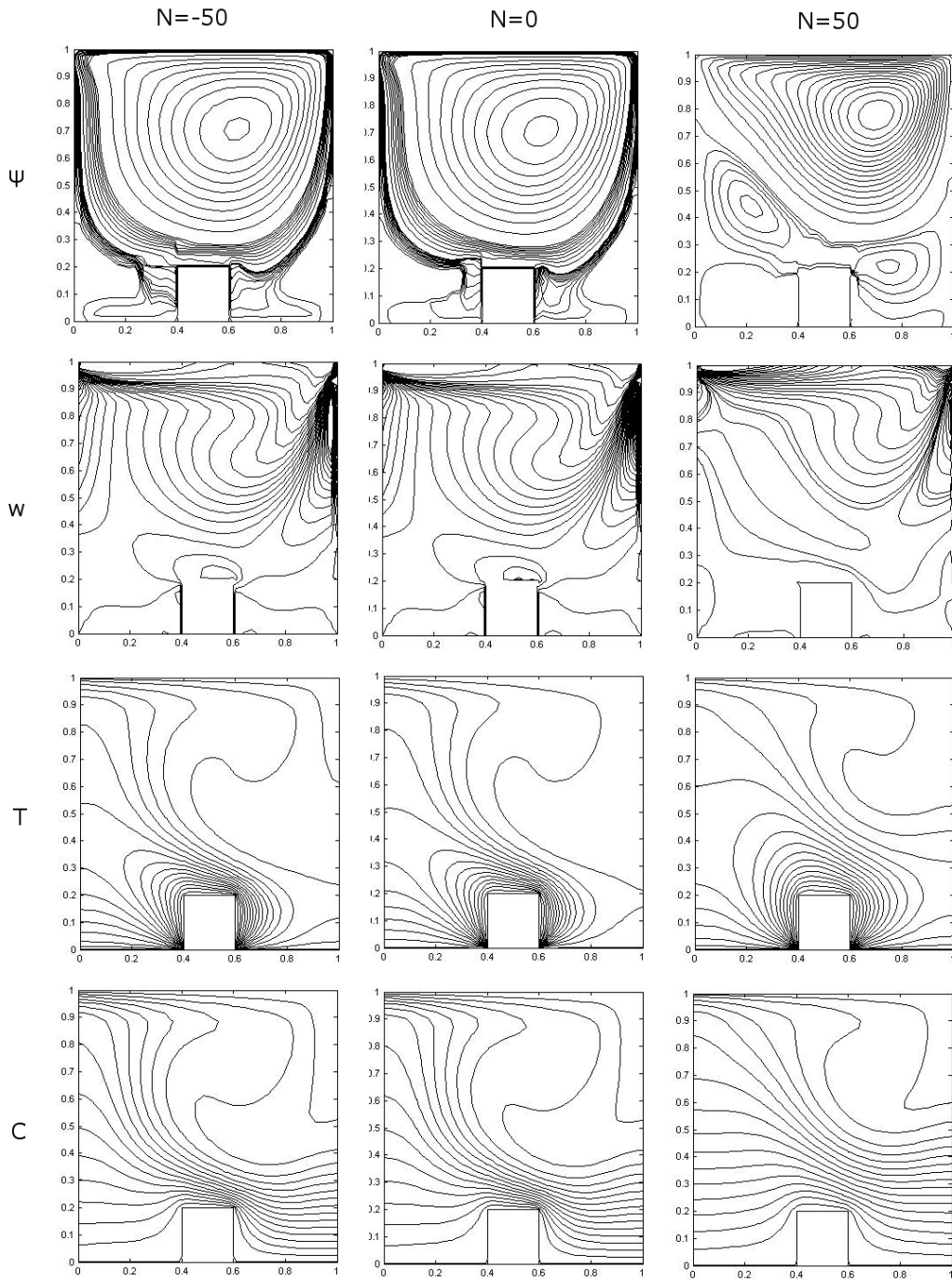


Figure 4.18: The effect of the buoyancy forces for $Ri = 0.01$, $Re = 200$

4.3.3 Thermo-solutal Mixed Convection Flow in Backward-facing Step Horizontal Channel

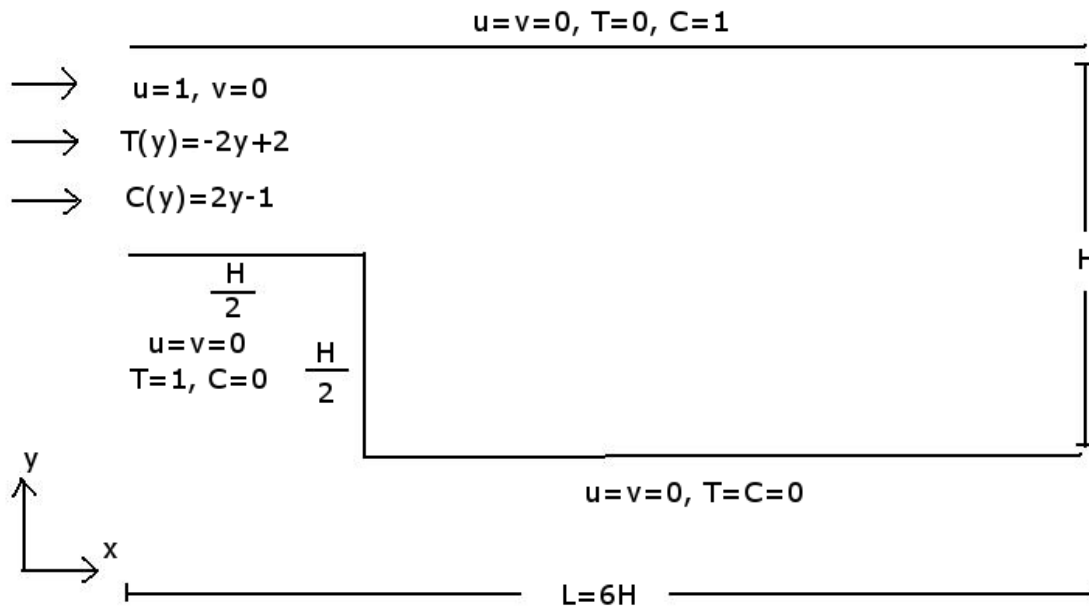


Figure 4.19: Backward-facing step channel flow

Third test problem is the backward-facing step (BFS) horizontal channel thermo-solutal mixed convection flow. Computed results are given to show the changes in the recirculatory flow pattern near the step due to the changes in the Ri , N and Re . The BFS problem is defined in a horizontal channel with step height $\frac{H}{2}$, channel height H and length $6H$ as is shown in Figure 4.19, and H is taken 1 in all computations. Boundary conditions of temperature and concentration are different over the walls and the step of the channel. The channel walls are maintained at low temperature ($T = 0$) whereas the step is at high temperature ($T = 1$). The step and bottom wall of the channel are assumed to be maintained at low solutal concentration $C = 0$ while the top wall is at high solutal concentration ($C = 1$). At the inlet, temperature and solutal concentration are linear functions as $T(y) = -2y + 2$ and $C(y) = 2y - 1$. The no-slip boundary conditions of velocity are imposed on the channel walls and the step, and at the inlet the fluid flows with constant velocity $u = 1$. Stream function is zero at the bottom wall and the step, and 0.5 at the top wall, whereas $\Psi(y) = y - 0.5$ at the inlet. The vorticity boundary conditions on the channel walls and step are obtained from the discretization of $w = \frac{\partial v}{\partial x} - \frac{\partial u}{\partial y}$ by using the DRBEM coordinate matrix, and is taken as zero at the inlet. At the exist, the exist conditions are imposed for all variables as $\frac{\partial}{\partial n} = 0$. At most $K = 212$ constant boundary elements, $L = 672$ interior nodes and $\Delta t = 0.025$ time increment are used in the application

of DRBEM in obtaining the solution for the values of $Ri = 0.1, 0.5, 1, 3, 5, 10$, $N = -10, -5, 1, 5, 10$, and $Re = 10, 30, 50, 100, 150, 200$.

The results are obtained first for $N = 1$, $Re = 200$, and Ri is changing between 0.1 to 10, and are shown in the Figures 4.20, 4.21 and 4.22. Figure 4.20 depicts streamlines for the variations of Ri . When $Ri = 0.1$, the fluid inertial forces are dominant over the thermal and solutal buoyancy forces. From the figure, the primary recirculation bubble at the downstream of the step is very clear. As Ri increases the buoyancy forces begin to dominate over the inertial force of the fluid. Because of the high concentration of the fluid near the top wall the recirculation bubble gets compressed. Also, the thermal buoyancy force originates only from the hot sides of the step, so the recirculatory fluid core gets shifted towards the heated vertical steps. Since the buoyancy ratio N is taken 1, the magnitude of the solutal buoyancy force is equal to the magnitude of the thermal buoyancy force. So, as Ri increases, both thermal and solutal buoyancy forces increase and make the bubble growth but flattened.

Figure 4.21 gives vorticity behavior for increasing Ri values. For all values of Ri , the circulations occur near the step due to the sharp drop of the fluid from the step, but when Ri increases the lengths of the circulations decrease since the fluid circulation core is concentrated in front of the step.

The temperature and concentration distributions in the channel for different values of Ri are given in Figure 4.22. From Figure 4.22(a) we see that, the thermal energy accession into the flow occurs near the hot side of the step and high temperature contour lines are located in the central core of the fluid. When Ri increases, the thermal energy convection is more in the hot stream of the fluid and less at the central core of the stream. From the Figure 4.22(b) it is concluded that, the concentration gradient is less near the hot side of the step for low values of Ri compared to high values of Ri . Results are in good agreement with the results given in [55] that the values of the contours are matching.

Figure 4.23 shows u -velocity profile along the vertical line at $x = 5$ of the channel for the same values of parameters of the reference [55]. Behavior of u is in agreement with the u -behavior in reference [55].

Figures 4.24(a) and 4.24(b) represent u -velocity and vorticity profiles at $x = 3$. From the Figure 4.24(a) it is seen that, the maximum values of velocity are changed between 0.8 and 1.0, and their locations vary between $y = 0.45$ and $y = 0.6$. Maximum values of velocity profiles decrease when N increases from -10 to 10. When we look at the Figure 4.24(b) we see that the vorticity profiles are almost the same for all values of N , and their values are changed between -3 to 5. For all cases these values decrease between $y = 0$ to $y = 0.025$.

The effect of Reynolds number on the streamline, vorticity, temperature and solutal concentration is analyzed for $Ri = 1$, $N = 1$, $Pr = Sc = 1$, and Re is changing from 10 to 200. Since $N = 1$ is taken in the analysis, thermal and solutal buoyancy forces are equal to each other. So, when Re increases, the inertial force effect becomes dominant on the solutions. Figure 4.25 shows streamlines for the variations of Re . As is shown in the figure, the recirculation bubble occurs near the step and when Re increases, reattachment length increases.

Figure 4.26 gives vorticity contours for different values of Re . Similar to the contours in Figure 4.22, the boundary layers occur at the inlet and near the channel walls, and the recirculations near the step. When Re increases from 10 to 200, the lengths of the circulations increase.

In Figures 4.21 and 4.26, some discrepancies are noticed in vorticity values near the top and bottom corners at the exit of the channel. This is not an expected physical behavior of vorticity. This may be due to the singularities in boundary conditions (passing from the Dirichlet type to the Neumann type) at the corners of the exit. These discrepancies which are far away from the step don't effect the general behavior of the flow, and can be eliminated by refining the mesh. However, the advantage of DRBEM actually lies in obtaining solutions with small number of boundary elements.

Figure 4.27 depicts the temperature and concentration distributions in the channel for different values of Re . From the Figure 4.27(a) one can see that, when Re increases, the thermal energy is convected in the fluid approximately at the central core of the stream. From the Figure 4.27(b), the concentration gradient is less near the hot side of the step for low values of Re compared to high values of Re .

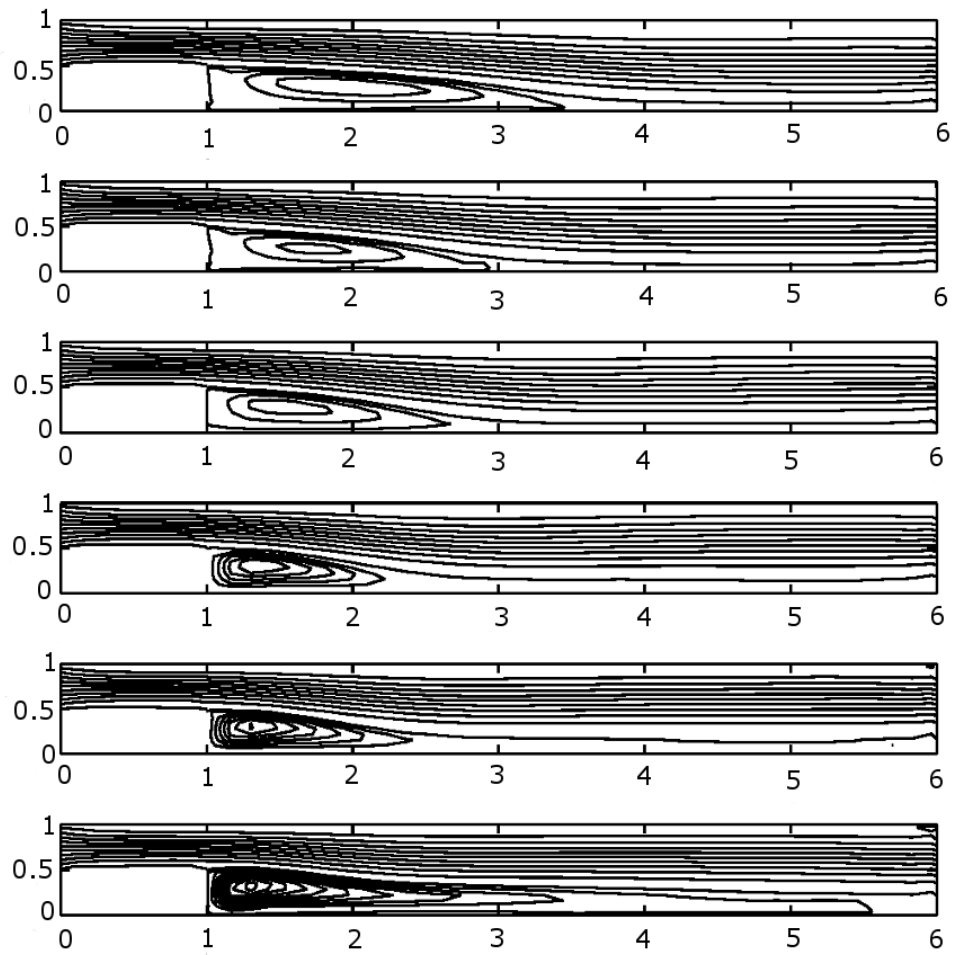


Figure 4.20: Effect of Richardson number on the streamline for $Re = 200$, $N = 1$, $Pr = Sc = 1$, from top to bottom $Ri = 0.1$, $Ri = 0.5$, $Ri = 1$, $Ri = 3$, $Ri = 5$ and $Ri = 10$.

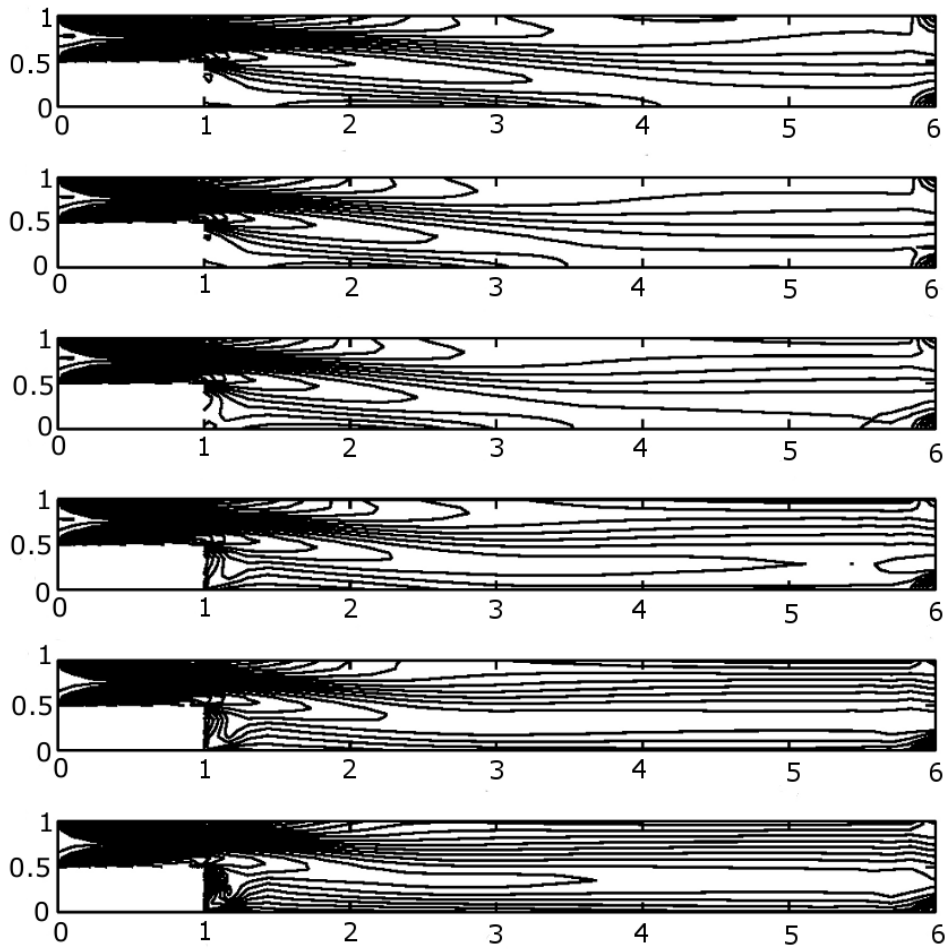


Figure 4.21: Effect of Richardson number on the vorticity for $Re = 200$, $N = 1$, $Pr = Sc = 1$, from top to bottom $Ri = 0.1$, $Ri = 0.5$, $Ri = 1$, $Ri = 3$, $Ri = 5$ and $Ri = 10$.

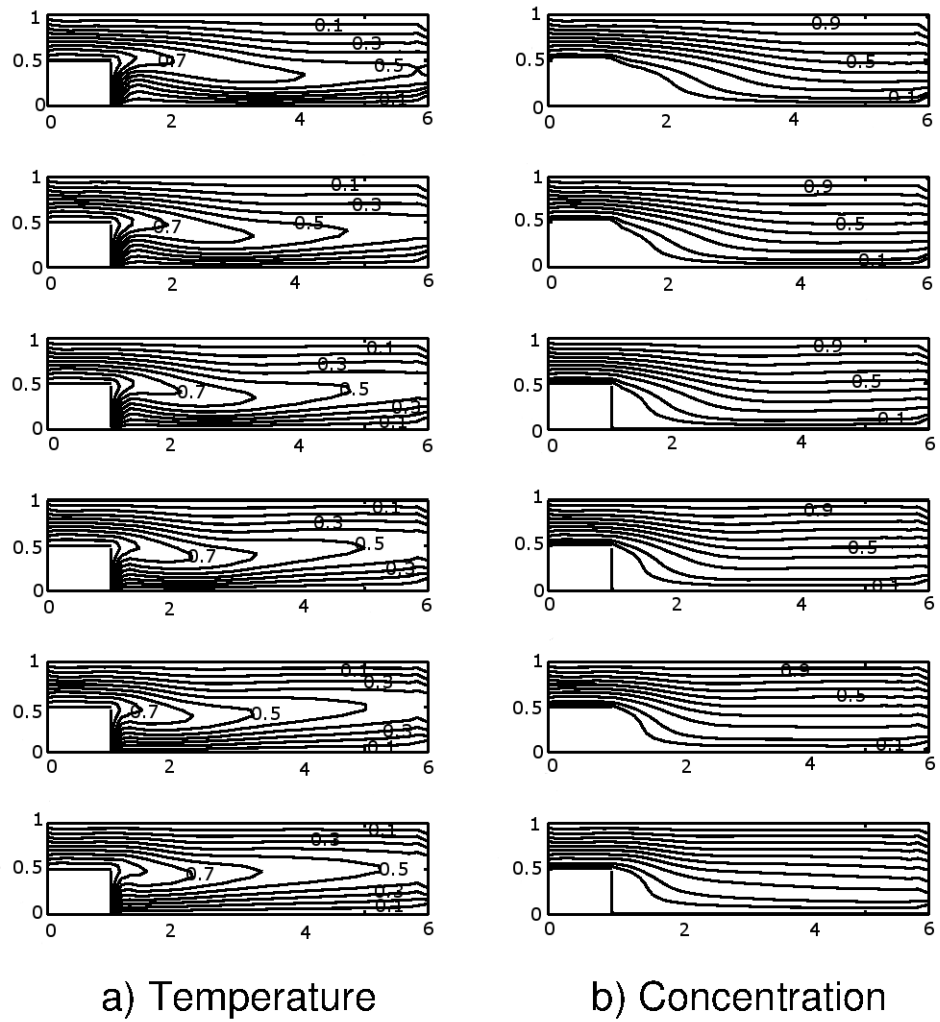


Figure 4.22: Effect of Richardson number on the temperature and concentration for $Re = 200$, $N = 1$, $Pr = Sc = 1$, from top to bottom $Ri = 0.1$, $Ri = 0.5$, $Ri = 1$, $Ri = 3$, $Ri = 5$ and $Ri = 10$.

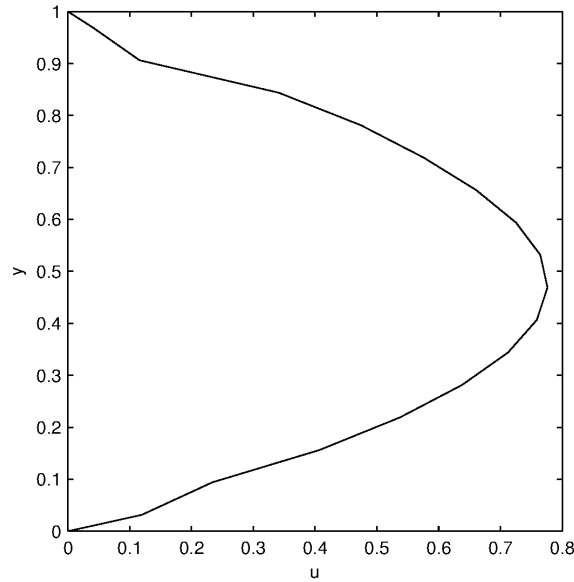


Figure 4.23: u -velocity profile along vertical line ($x = 5$) for $Re = 200$, $N = 1$, $Ri = 0.01$ and $Le = 1$

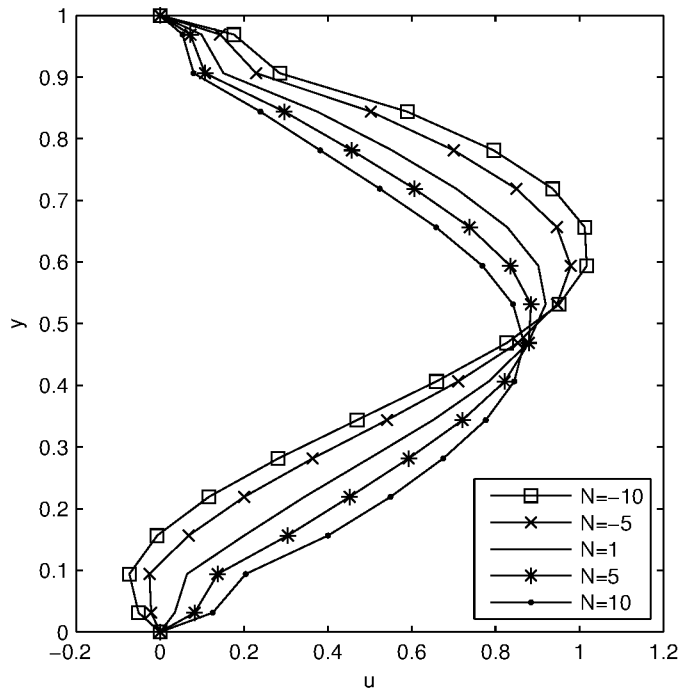
The convective heat and mass transfer are calculated in terms of average Nusselt and Sherwood numbers defined as follows

$$Nu_{av} = \frac{1}{H} \int_0^H \left(uT - \frac{\partial T}{\partial n} \right) d\Gamma \quad (4.93)$$

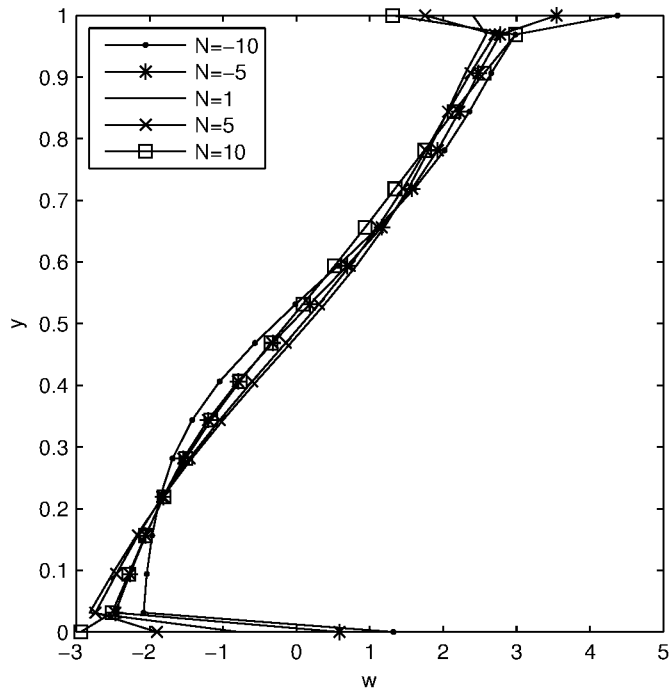
$$Sh_{av} = \frac{1}{6H} \int_0^{6H} \left(uC - \frac{\partial C}{\partial y} \right) dx \quad (4.94)$$

where H is characteristic length (width) of the channel, n is direction normal to the surface. $d\Gamma = dx$ for the horizontal side of the step and $d\Gamma = dy$ for the vertical side of the step.

The variation of average Nusselt and Sherwood numbers with buoyancy ratio at various values of Richardson number are given in Figure 4.28(a) and Figure 4.28(b). Average Nusselt numbers take the values between 3 and 5. A steady behavior is observed in the Nusselt number for $Ri = 0.1$ in the range $-10 \leq N \leq 10$. But when the Richardson number increases the Nusselt number decreases with increasing values of N , and after $N = -0.5$ the decreasing behavior becomes very fast for $Ri = 1$ and $Ri = 3$. Average Sherwood numbers have the same behavior with the average Nusselt numbers for all values of Ri , but the values of Sherwood numbers change between 1.2 and 1.45. Behavior is in agreement with the behavior in the reference [55].



(a) u -velocity profile along vertical line ($x = 3$)



(b) Vorticity profile along vertical line ($x = 3$)

Figure 4.24: Effect of buoyancy ratio on the vorticity for $Re = 200$, $Ri = 0.1$, $Pr = Sc = 1$, for $N = -10$, $N = -5$, $N = 1$, $N = 5$ and $N = 10$.

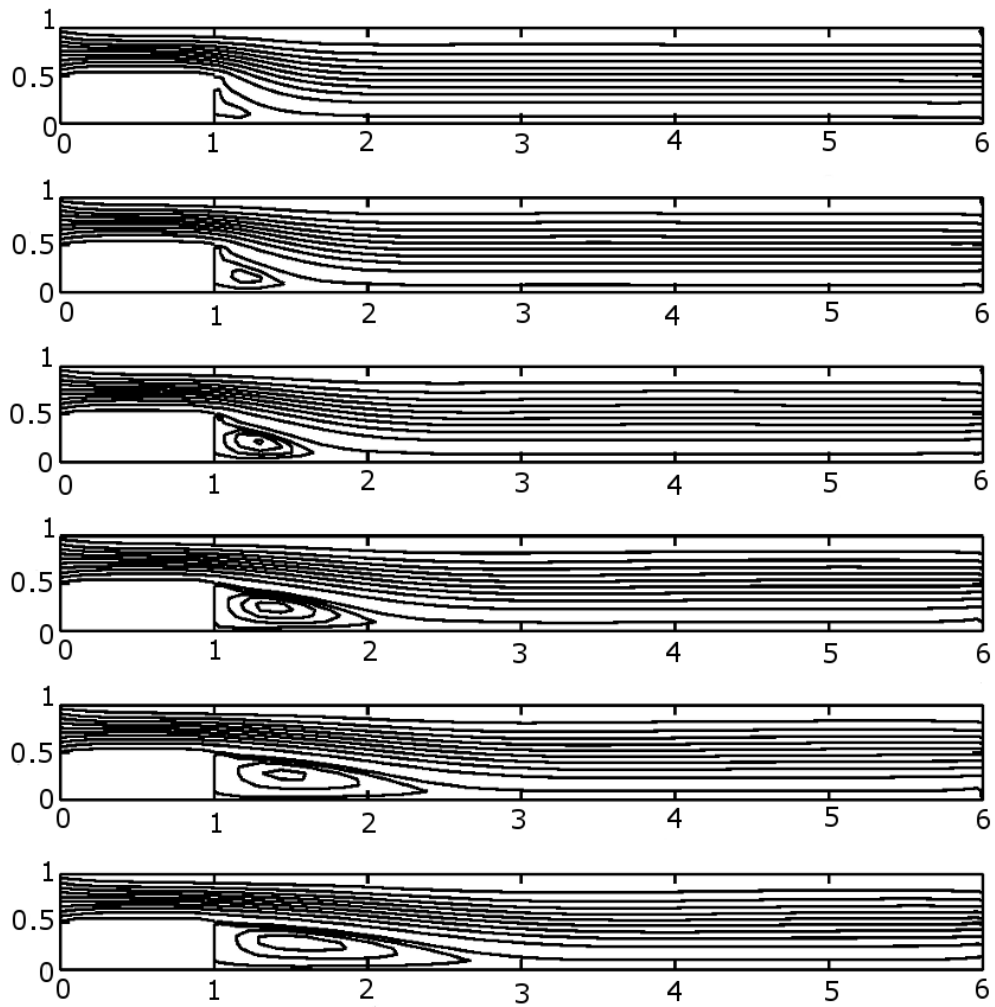


Figure 4.25: Effect of Reynolds number on the streamline for $Ri = 1$, $N = 1$, $Pr = Sc = 1$, from top to bottom $Re = 10$, $Re = 30$, $Re = 50$, $Re = 100$, $Re = 150$ and $Re = 200$.

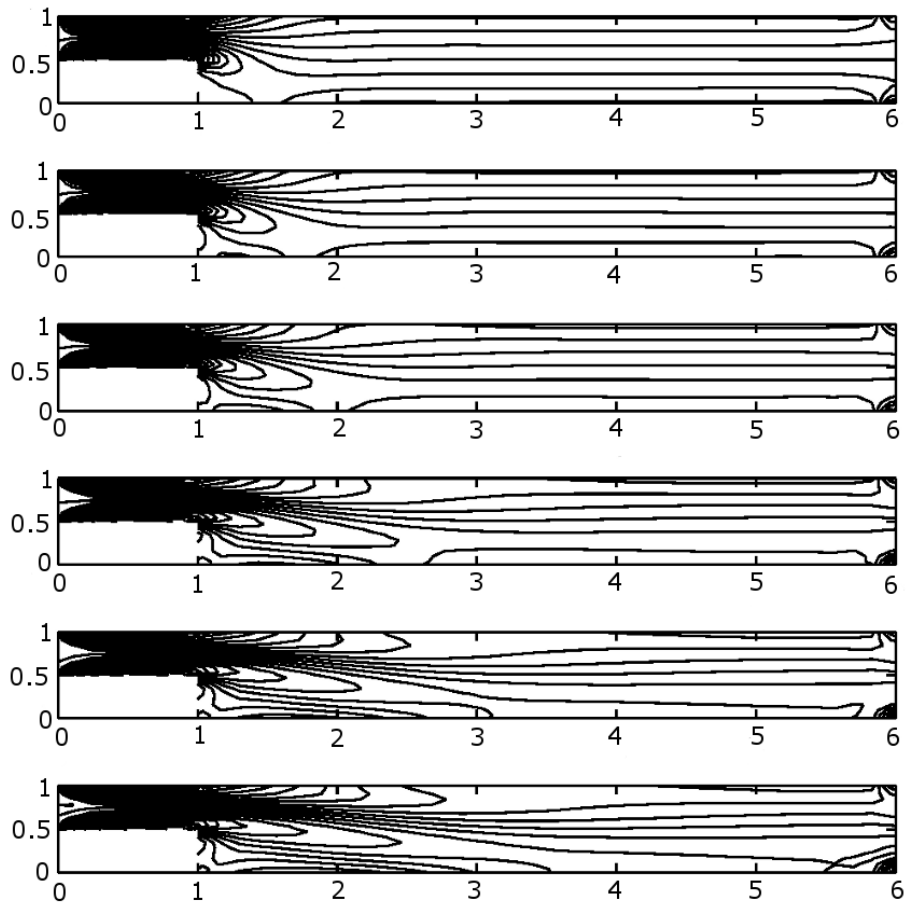


Figure 4.26: Effect of Reynolds number on the vorticity for $Ri = 1$, $N = 1$, $Pr = Sc = 1$, from top to bottom $Re = 10$, $Re = 30$, $Re = 50$, $Re = 100$, $Re = 150$ and $Re = 200$.

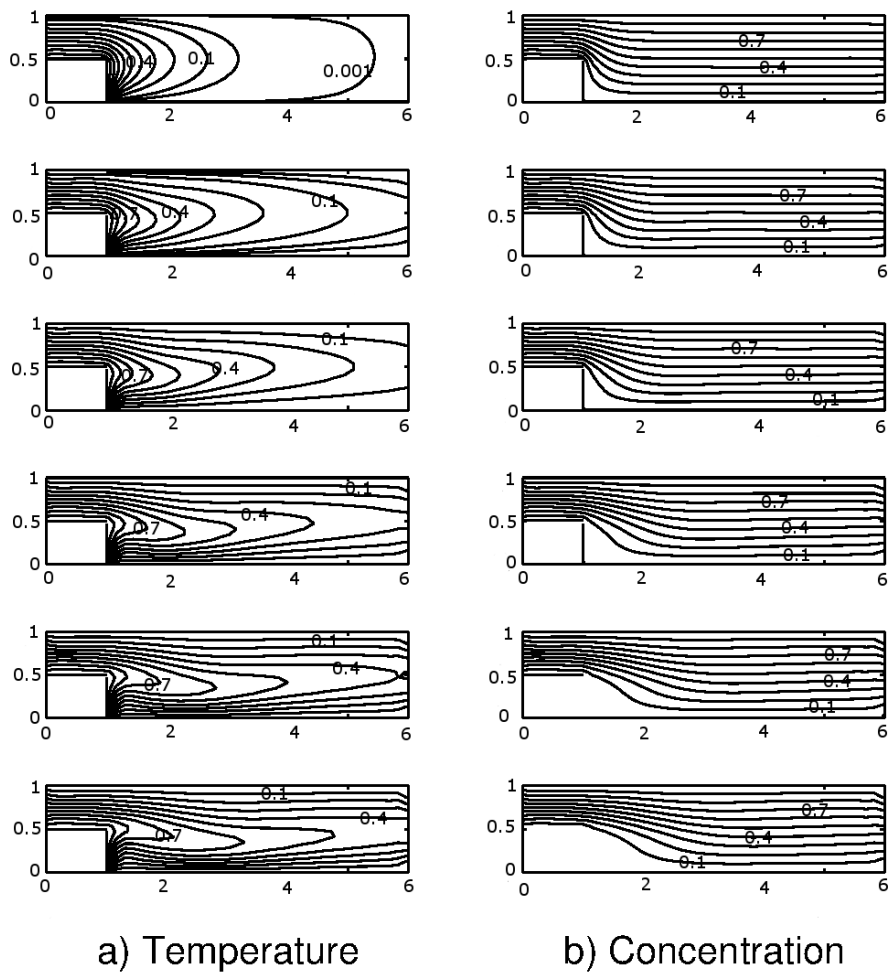
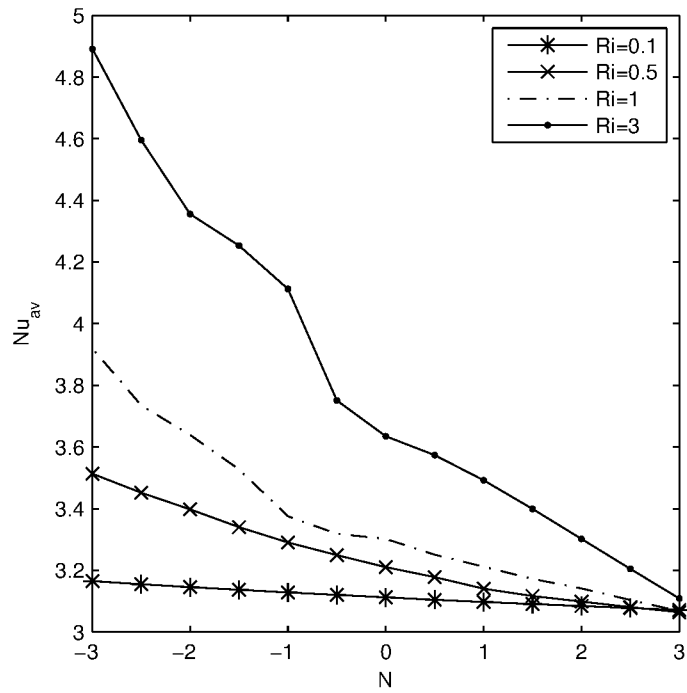
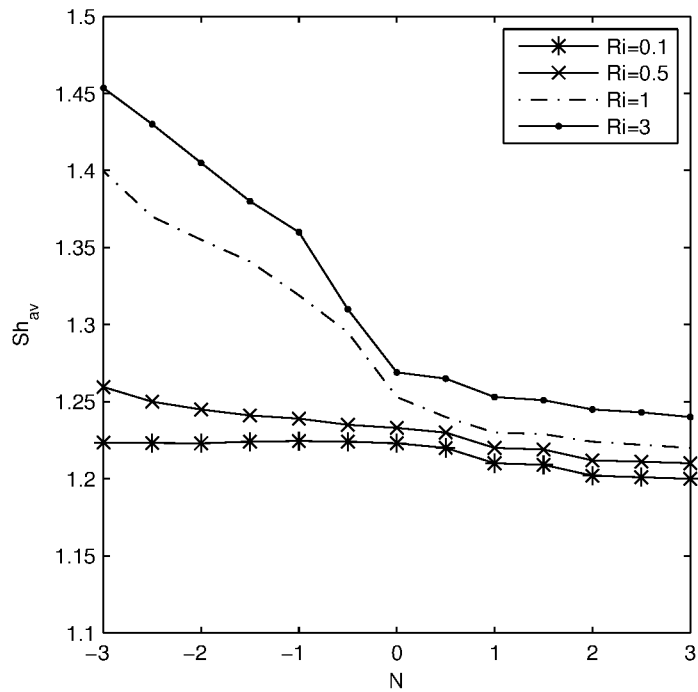


Figure 4.27: Effect of Reynolds number on temperature and concentration for $Ri = 1$, $N = 1$, $Pr = Sc = 1$, from top to bottom $Re = 10$, $Re = 30$, $Re = 50$, $Re = 100$, $Re = 150$ and $Re = 200$.



(a) Nu_{av}



(b) Sh_{av}

Figure 4.28: (a)Effect of buoyancy ratio for various Richardson numbers on the step: average Nusselt number, (b)Effect of buoyancy ratio for various Richardson numbers on top wall: average Sherwood number,

4.4 DRBEM and DQM Solutions of Natural Convection Flow in a Cavity under a Magnetic Field

In this section, we consider the numerical solution of two-dimensional unsteady natural convection flow in a square cavity under an externally applied magnetic field. Stream function-vorticity and temperature variables are used, and vorticity and energy equations are transformed to modified Helmholtz equations. The vorticity transport equation is altered due to the effects of temperature and applied magnetic field. The governing equations in the stream function-vorticity-temperature ($\psi - w - T$) formulation are given in Chapter 1 as

$$\nabla^2 \psi = -w \quad (4.95)$$

$$Pr \nabla^2 w = \frac{\partial w}{\partial t} + u \frac{\partial w}{\partial x} + v \frac{\partial w}{\partial y} + Ha^2 Pr \frac{\partial v}{\partial x} - Ra Pr \frac{\partial T}{\partial x} \quad (4.96)$$

$$\nabla^2 T = \frac{\partial T}{\partial t} + u \frac{\partial T}{\partial x} + v \frac{\partial T}{\partial y} \quad (4.97)$$

where T , Pr , and Ra are the temperature, Prandtl number and Rayleigh number, respectively,

$$u = \frac{\partial \psi}{\partial y}, \quad v = -\frac{\partial \psi}{\partial x}, \quad w = \frac{\partial v}{\partial x} - \frac{\partial u}{\partial y} \quad (4.98)$$

are the time dependent velocity components, and w is the vorticity.

As is done in all other cases the vorticity transport and energy equations are written in the form of inhomogeneous modified Helmholtz equation (Chapter 1) in $(n + 1)$ th level

$$\begin{aligned} \nabla^2 \psi^{(n+1)} &= -w^{(n)} \\ \nabla^2 w^{(n+1)} - \tau_w^2 w^{(n+1)} &= -\frac{(1 - \theta_w)}{\theta_w} \nabla^2 w^{(n)} - \tau_w^2 w^{(n)} \\ &+ \frac{1}{Pr \theta_w} \left(\frac{\partial \psi^{(n+1)}}{\partial y} \frac{\partial w^{(n)}}{\partial x} - \frac{\partial \psi^{(n+1)}}{\partial x} \frac{\partial w^{(n)}}{\partial y} \right) \\ &- \frac{Ha^2}{\theta_w} \left(\frac{\partial^2 \psi^{(n+1)}}{\partial x^2} \right) - \frac{Ra}{\theta_w} \left(\frac{\partial T^{(n)}}{\partial x} \right) \\ \nabla^2 T^{(n+1)} - \tau_T^2 T^{(n+1)} &= -\frac{(1 - \theta_T)}{\theta_T} \nabla^2 T^{(n)} - \tau_T^2 T^{(n)} \\ &+ \frac{1}{\theta_T} \left(\frac{\partial \psi^{(n+1)}}{\partial y} \frac{\partial T^{(n)}}{\partial x} - \frac{\partial \psi^{(n+1)}}{\partial x} \frac{\partial T^{(n)}}{\partial y} \right) \end{aligned} \quad (4.99)$$

where $\tau_w^2 = \frac{1}{Pr \Delta t \theta_w}$ and $\tau_T^2 = \frac{1}{\Delta t \theta_T}$. So, we have a Poisson equation for stream function and two modified Helmholtz equations for vorticity transport (4.96) and temperature equation (4.97), respectively.

As in Sections (4.2) and (4.3) for the natural convection and thermo-solutal mixed convection flows, first, the resulting modified Helmholtz equations are solved by DRBEM using the

fundamental solution $\frac{1}{2\pi}K_0(x)$ whereas in the stream function Poisson equation $\frac{1}{2\pi}\ln(x)$ is made use of. Next, they are solved by DQM using polynomial based test functions.

In order to use the DRBEM, equations (4.95)-(4.97) are written in a compact form

$$\nabla^2\psi^{(n+1)} = b_1 \quad (4.100)$$

$$\nabla^2 w^{(n+1)} - \tau_w^2 w^{(n+1)} = b_2 \quad (4.101)$$

$$\nabla^2 T^{(n+1)} - \tau_T^2 T^{(n+1)} = b_3 \quad (4.102)$$

where b_1 , b_2 and b_3 are the right hand sides of corresponding equations in (4.99), and they are constructed using the values of vorticity and temperature at the n th time level but stream function at the $(n + 1)$ th time level.

DRBEM solutions are obtained with both of the approximating functions (radial basis functions) which are $\bar{f} = r^2 \ln r$ and $\bar{f} = 1 + r^2 + r^3 - \tau^2 \left(\frac{r^2}{4} + \frac{r^4}{16} + \frac{r^5}{25} \right)$ (τ refers to τ_w and τ_T) for vorticity transport and temperature equations, respectively, for the right hand side functions b_2 and b_3 . For both cases $f = 1 + r$ is used to approximate the function b_1 . These radial basis functions are depending only on geometry.

Approximating the functions b_1 , b_2 and b_3 with radial basis functions $f = 1 + r$, and $\bar{f} = r^2 \ln r$ or $\bar{f} = 1 + r^2 + r^3 - \tau^2 \left(\frac{r^2}{4} + \frac{r^4}{16} + \frac{r^5}{25} \right)$

$$b_1 = \sum_{j=1}^{K+L} \alpha_{1j} f_j \quad (4.103)$$

$$b_2 = \sum_{j=1}^{K+L} \alpha_{2j}(t) \bar{f}_j \quad (4.104)$$

$$b_3 = \sum_{j=1}^{K+L} \alpha_{3j}(t) \bar{f}_j \quad (4.105)$$

where α_{1j} , $\alpha_{2j}(t)$ and $\alpha_{3j}(t)$ are initially unknown coefficients, r is distance between the source and field points, K and L are the the number of boundary and interior nodes, respectively.

DRBEM formulation of the governing equations (4.100)-(4.102) now give the matrix-vector equations

$$\mathbf{H}\psi - \mathbf{G}\mathbf{q}_\psi = (\mathbf{H}\widehat{\Psi} - \mathbf{G}\widehat{Q}_\Psi)\mathbf{F}^{-1}\mathbf{b}_1 \quad (4.106)$$

$$\mathbf{H}'\mathbf{w} + \mathbf{G}'\mathbf{q}_w = (\mathbf{H}'\widehat{W} + \mathbf{G}'\widehat{Q}_w)\overline{\mathbf{F}}^{-1}\mathbf{b}_2 \quad (4.107)$$

$$\mathbf{H}'\mathbf{T} + \mathbf{G}'\mathbf{q}_T = (\mathbf{H}'\widehat{T} + \mathbf{G}'\widehat{Q}_T)\overline{\mathbf{F}}^{-1}\mathbf{b}_3 \quad (4.108)$$

with the vectors \mathbf{b}_1 , \mathbf{b}_2 , \mathbf{b}_3 formed from

$$b_1 = -w^{(n)} \quad (4.109)$$

$$b_2 = -\left(\frac{1-\theta_w}{\theta_w}\right)\nabla^2 w^{(n)} - \tau_w^2 w^{(n)} + \frac{1}{Pr\theta_w}\left(\frac{\partial\psi^{(n+1)}}{\partial y}\frac{\partial w^{(n)}}{\partial x} - \frac{\partial\psi^{(n+1)}}{\partial x}\frac{\partial w^{(n)}}{\partial y}\right) - \frac{Ha^2}{\theta_w}\left(\frac{\partial^2\psi^{(n+1)}}{\partial x^2}\right) - \frac{Ra}{\theta_w}\left(\frac{\partial T^{(n)}}{\partial x}\right) \quad (4.110)$$

$$b_3 = -\left(\frac{1-\theta_T}{\theta_T}\right)\nabla^2 T^{(n)} - \tau_T^2 T^{(n)} + \frac{1}{\theta_T}\left(\frac{\partial\psi^{(n+1)}}{\partial y}\frac{\partial T^{(n)}}{\partial x} - \frac{\partial\psi^{(n+1)}}{\partial x}\frac{\partial T^{(n)}}{\partial y}\right) \quad (4.111)$$

where \mathbf{F} and $\bar{\mathbf{F}}$ are $(K+L) \times (K+L)$ coordinate matrices and their columns are constructed using $f_j = 1 + r_j$ and $\bar{f}_j = r_j^2 \ln r_j$ or $\bar{f} = 1 + r_j^2 + r_j^3 - \tau^2\left(\frac{r_j^2}{4} + \frac{r_j^4}{16} + \frac{r_j^5}{25}\right)$, respectively.

First and second order space derivatives of stream function, vorticity and temperature can be approximated using the coordinate matrix $\bar{\mathbf{F}}$ as

$$\begin{aligned} \psi^{(n+1)} &= \sum_{j=1}^{K+L} \beta_j \bar{f}_j \\ \mathbf{w}^{(n)} &= \sum_{j=1}^{K+L} \beta'_j \bar{f}_j \\ \mathbf{T}^{(n)} &= \sum_{j=1}^{K+L} \beta''_j \bar{f}_j \end{aligned} \quad (4.112)$$

where β_j, β'_j and β''_j are unknown coefficients. These result in systems

$$\begin{aligned} \psi^{(n+1)} &= \bar{\mathbf{F}}\boldsymbol{\beta} \\ \mathbf{w}^{(n)} &= \bar{\mathbf{F}}\boldsymbol{\beta}' \\ \mathbf{T}^{(n)} &= \bar{\mathbf{F}}\boldsymbol{\beta}'' \end{aligned} \quad (4.113)$$

Thus, first and second order derivatives of stream function

$$\frac{\partial\psi^{(n+1)}}{\partial x} = \frac{\partial\bar{\mathbf{F}}}{\partial x}\bar{\mathbf{F}}^{-1}\boldsymbol{\psi}^{(n+1)}, \quad \frac{\partial\psi^{(n+1)}}{\partial y} = \frac{\partial\bar{\mathbf{F}}}{\partial y}\bar{\mathbf{F}}^{-1}\boldsymbol{\psi}^{(n+1)} \quad (4.114)$$

and

$$\frac{\partial^2\psi^{(n+1)}}{\partial x^2} = \frac{\partial\bar{\mathbf{F}}}{\partial x}\bar{\mathbf{F}}^{-1}\left(\frac{\partial\psi^{(n+1)}}{\partial x}\right), \quad \frac{\partial^2\psi^{(n+1)}}{\partial y^2} = \frac{\partial\bar{\mathbf{F}}}{\partial y}\bar{\mathbf{F}}^{-1}\left(\frac{\partial\psi^{(n+1)}}{\partial y}\right). \quad (4.115)$$

Similarly,

$$\frac{\partial\mathbf{w}^{(n)}}{\partial x} = \frac{\partial\bar{\mathbf{F}}}{\partial x}\bar{\mathbf{F}}^{-1}\mathbf{w}^{(n)}, \quad \frac{\partial\mathbf{w}^{(n)}}{\partial y} = \frac{\partial\bar{\mathbf{F}}}{\partial y}\bar{\mathbf{F}}^{-1}\mathbf{w}^{(n)} \quad (4.116)$$

$$\frac{\partial\mathbf{T}^{(n)}}{\partial x} = \frac{\partial\bar{\mathbf{F}}}{\partial x}\bar{\mathbf{F}}^{-1}\mathbf{T}^{(n)}, \quad \frac{\partial\mathbf{T}^{(n)}}{\partial y} = \frac{\partial\bar{\mathbf{F}}}{\partial y}\bar{\mathbf{F}}^{-1}\mathbf{T}^{(n)}$$

and

$$\frac{\partial^2\mathbf{w}^{(n)}}{\partial x^2} = \frac{\partial\bar{\mathbf{F}}}{\partial x}\bar{\mathbf{F}}^{-1}\left(\frac{\partial\mathbf{w}^{(n)}}{\partial x}\right), \quad \frac{\partial^2\mathbf{w}^{(n)}}{\partial y^2} = \frac{\partial\bar{\mathbf{F}}}{\partial y}\bar{\mathbf{F}}^{-1}\left(\frac{\partial\mathbf{w}^{(n)}}{\partial y}\right) \quad (4.117)$$

$$\frac{\partial^2\mathbf{T}^{(n)}}{\partial x^2} = \frac{\partial\bar{\mathbf{F}}}{\partial x}\bar{\mathbf{F}}^{-1}\left(\frac{\partial\mathbf{T}^{(n)}}{\partial x}\right), \quad \frac{\partial^2\mathbf{T}^{(n)}}{\partial y^2} = \frac{\partial\bar{\mathbf{F}}}{\partial y}\bar{\mathbf{F}}^{-1}\left(\frac{\partial\mathbf{T}^{(n)}}{\partial y}\right).$$

Applying the suitable boundary conditions for ψ , w and T to the systems (4.106)-(4.108) the known and unknown values are passed from one side to another giving algebraic systems

$$\begin{aligned} \mathbf{A}_1 \mathbf{x}_1 &= \mathbf{y}_1 \\ \mathbf{A}_2 \mathbf{x}_2 &= \mathbf{y}_2 \\ \mathbf{A}_3 \mathbf{x}_3 &= \mathbf{y}_3 \end{aligned} \quad (4.118)$$

where \mathbf{y}_i and \mathbf{x}_i ($i = 1, 2, 3$) contain known (obtained n th level) and unknown ($(n + 1)$ th level) values of ψ , q_ψ , w , q_w and T , q_T .

The DRBEM iterative procedure is started by taking initial values of $w^{(n)}$ and $T^{(n)}$ with $n = 0$. Then the stream function $\psi^{(n+1)}$ is solved from (4.106) using $w^{(n)}$. Velocity components u and v are computed using the coordinate matrix \bar{F} . Using the definition (4.98) the vorticity boundary conditions are obtained. Then the right hand side of the vorticity transport equation is computed and system (4.107) is solved for $w^{(n+1)}$. Lastly, the right hand side of the temperature equation is computed and system (4.108) is solved for $T^{(n+1)}$. A stopping criteria is described for all variables, and the solution procedure is continued until it is satisfied.

In this section, the natural convection flow in a cavity under an applied magnetic field is also studied with the differential quadrature method. The governing equations (4.95)-(4.97) are again transformed to Poisson equation and inhomogeneous modified Helmholtz equations (4.99) for stream function and vorticity, temperature equations, respectively. Then these equations are solved by DQM. The discretized equations employing the differential quadrature method (DQM) corresponding to stream function, vorticity and temperature equations (4.99) are

$$\sum_{k=1}^{N_1} b_{ik} \psi_{kj}^{(n+1)} + \sum_{k=1}^{N_2} \bar{b}_{jk} \psi_{ik}^{(n+1)} = -w_{ij}^{(n)} \quad (4.119)$$

$$\sum_{k=1}^{N_1} b_{ik} w_{kj}^{(n+1)} + \sum_{k=1}^{N_2} \bar{b}_{jk} w_{ik}^{(n+1)} - \tau_w^2 w_{ij}^{(n+1)} = b_2 \quad (4.120)$$

$$\sum_{k=1}^{N_1} b_{ik} T_{kj}^{(n+1)} + \sum_{k=1}^{N_2} \bar{b}_{jk} T_{ik}^{(n+1)} - \tau_T^2 T_{ij}^{(n+1)} = b_3 \quad (4.121)$$

where

$$\begin{aligned} b_2 &= -\left(\frac{1 - \theta_w}{\theta_w}\right) \left(\sum_{k=1}^{N_1} b_{ik} w_{kj}^{(n)} + \sum_{k=1}^{N_2} \bar{b}_{jk} w_{ik}^{(n)} \right) \\ &\quad - \tau_w^2 w_{ij}^{(n)} + \frac{1}{Pr\theta_w} \left(\sum_{k=1}^{N_2} \bar{a}_{jk} \psi_{ik}^{(n+1)} \sum_{k=1}^{N_1} a_{ik} w_{kj}^{(n)} - \sum_{k=1}^{N_1} a_{ik} \psi_{kj}^{(n+1)} \sum_{k=1}^{N_2} \bar{a}_{jk} w_{ik}^{(n)} \right) \\ &\quad - \frac{Ha^2}{\theta_w} \sum_{k=1}^{N_1} b_{ik} \psi_{kj}^{(n+1)} - \frac{Ra}{\theta_w} \sum_{k=1}^N a_{ik} T_{kj}^{(n)} \end{aligned} \quad (4.122)$$

and

$$\begin{aligned}
b_3 &= -\left(\frac{1-\theta_T}{\theta_T}\right)\left(\sum_{k=1}^{N_1} b_{ik}T_{kj}^{(n)} + \sum_{k=1}^{N_2} \bar{b}_{jk}T_{ik}^{(n)}\right) \\
&\quad -\tau_T^2 T_{ij}^{(n)} + \frac{1}{\theta_T}\left(\sum_{k=1}^{N_2} \bar{a}_{jk}\psi_{ik}^{(n+1)} \sum_{k=1}^{N_1} a_{ik}T_{kj}^{(n)} - \sum_{k=1}^{N_1} a_{ik}\psi_{kj}^{(n+1)} \sum_{k=1}^{N_2} \bar{a}_{jk}T_{ik}^{(n)}\right).
\end{aligned} \tag{4.123}$$

Here, $i = 1, \dots, N_1$, $j = 1, \dots, N_2$, and N_1 and N_2 represent the total number of grid points in x - and y -directions, respectively. For the DQ method, a non-uniform grid point distribution (GCL) is used which is expressed as [62].

$$\begin{aligned}
x_i &= \frac{\cos \frac{\pi}{2n} - \cos \frac{(2i-1)\pi}{2n}}{\cos \frac{\pi}{2n} - \cos \frac{(2n-1)\pi}{2n}} L_x \\
y_i &= \frac{\cos \frac{\pi}{2n} - \cos \frac{(2j-1)\pi}{2n}}{\cos \frac{\pi}{2n} - \cos \frac{(2n-1)\pi}{2n}} L_y
\end{aligned} \tag{4.124}$$

for $i = 1, \dots, N_1$ and $j = 1, \dots, N_2$ where L_x and L_y are the lengths in the x - and y -directions. The Dirichlet type boundary conditions for the stream function which are zero due to the no-slip condition for velocity are inserted to the equation (4.119) directly as

$$\psi_{1j} = 0, \quad \psi_{N_1j} = 0, \quad \psi_{i1} = 0, \quad \psi_{iN_2} = 0, \tag{4.125}$$

for $i = 1, \dots, N_1$ and $j = 1, \dots, N_2$. The boundary conditions for the vorticity can be obtained from (4.98) and can also be approximated by the DQ method as follows

$$\begin{aligned}
w_{1j}^{(n+1)} &= \sum_{k=1}^{N_1} a_{1k}v_{kj}^{(n+1)} - \sum_{k=1}^{N_2} \bar{a}_{jk}u_{1k}^{(n+1)}, \\
w_{N_1j}^{(n+1)} &= \sum_{k=1}^{N_1} a_{N_1k}v_{kj}^{(n+1)} - \sum_{k=1}^{N_2} \bar{a}_{jk}u_{N_1k}^{(n+1)}, \\
w_{i1}^{(n+1)} &= \sum_{k=1}^{N_1} a_{ik}v_{k1}^{(n+1)} - \sum_{k=1}^{N_2} \bar{a}_{1k}u_{ik}^{(n+1)}, \\
w_{iN_2}^{(n+1)} &= \sum_{k=1}^{N_1} a_{ik}v_{kN_2}^{(n+1)} - \sum_{k=1}^{N_2} \bar{a}_{N_2k}u_{ik}^{(n+1)},
\end{aligned} \tag{4.126}$$

where $j = 1, \dots, N_2$, $i = 2, \dots, N_1 - 1$, and the velocity components are also obtained from (4.98), with their DQ approximations

$$\begin{aligned}
u_{ik}^{(n+1)} &= \sum_{k=1}^{N_2} \bar{a}_{jk}\psi_{ik}^{(n+1)}, \\
v_{ik}^{(n+1)} &= -\sum_{k=1}^{N_1} a_{ik}\psi_{kj}^{(n+1)}
\end{aligned} \tag{4.127}$$

and then these equations are added to the equation (4.120). Similarly, Dirichlet type temperature boundary conditions can be directly inserted to the equation (4.121), but Neumann

type boundary conditions are also approximated using the DQM, and added to the equation (4.121).

These system of equations are solved iteratively and iterative solution procedure starts by taking $w^{(0)}$ at the right hand side of the stream function equation.

4.4.1 Numerical Results

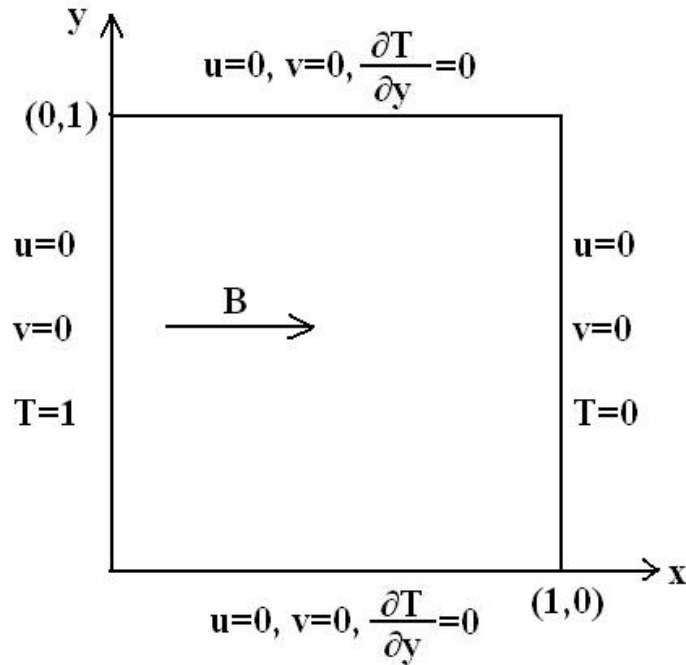


Figure 4.29: Natural convection flow in a square cavity under a magnetic field

We simulated natural convection flow under a magnetic field in a square cavity $\Omega = [0, 1] \times [0, 1]$ with the related boundary conditions in Figure 4.29. The no-slip boundary conditions of the velocity at the boundary walls are assumed. Temperature has Dirichlet type boundary conditions as 1 and 0 (walls are heated and cooled, respectively) at the left and right walls of the cavity, whereas adiabatic boundary conditions $\frac{\partial T}{\partial y} = 0$ are imposed on the top and bottom walls [7]. Boundary conditions for stream function are taken as zero at the walls due to the no-slip wall conditions of velocities, and the vorticity boundary conditions are obtained from the discretization of $w = \frac{\partial v}{\partial x} - \frac{\partial u}{\partial y}$ using DRBEM coordinate matrix or DQM.

The governing equations are discretized by using DRBEM first and then DQM. These numerical algorithms are applied to determine the stream function, vorticity and temperature

variations with the given initial values $w = T = 0$ iteratively. The pre-assigned accuracy for reaching steady-state is taken as $\varepsilon = 10^{-4}$. The DRBEM and DQM results are obtained for $Ra = 10^3$ - 10^6 and $Ha \leq 300$. All the computations are carried by taking $Pr = 1$. The radial basis function $f = 1 + r$ is used to approximate b_1 , and $\bar{f} = r^2 \ln r$ or $\bar{f} = 1 + r^2 + r^3 - \tau^2 \left(\frac{r^2}{4} + \frac{r^4}{16} + \frac{r^5}{25} \right)$ is used to approximate b_2 and b_3 .

Table 4.9: Number of iterations with different θ_w and θ_T in DRBEM using $\bar{f} = r^2 \log r$, $Ra = 10^4$.

		θ_w					
θ_T	0.4	0.5	0.6	0.7	0.8	0.9	
0.4	-	-	-	4068	1404	955	
0.5	-	-	1439	736	528	425	
0.6	-	1301	622	424	336	286	
0.7	-	675	413	304	249	219	
0.8	-	498	320	247	205	182	
0.9	693	396	275	218	182	161	

Table 4.10: Number of iterations with different θ_w and θ_T in DQM, $Ra = 10^4$.

		θ_w						
θ_T	0.3	0.4	0.5	0.6	0.7	0.8	0.9	
0.3	-	-	-	-	-	5543	2165	
0.4	-	-	15556	1601	896	652	527	
0.5	-	1915	867	551	412	340	294	
0.6	-	735	474	341	267	236	208	
0.7	-	485	339	257	214	188	183	
0.8	840	387	276	213	188	187	182	
0.9	513	333	242	198	189	187	181	

Table 4.9 and Table 4.10 show the iteration numbers for reaching steady-state in DRBEM and DQM solutions of the problem, for $Ra = 10^4$ and $Ha = 0$. In the DRBEM application we use $K = 68$ constant boundary elements with $\Delta t = 5.10^{-2}$, and in the DQM applications we use 21×21 GCL grid distribution with $\Delta t = 10^{-3}$. It is noticed that in both of the numerical algorithms relaxation parameters (θ_w, θ_T) for vorticity and temperature can take values close to one, which means quite small number of iterations are required for reaching steady-state solution. These values of relaxation parameters indicate that more contribution is used from the newly obtained solutions. This is the main advantage of writing the equation in the form of modified Helmholtz equations after the discretization of time derivatives, and using relaxation parameters between two consecutive iterations. Also, quite large time increment Δt can be used, since $\tau_w^2 = \frac{1}{Pr\Delta t\theta_w}$ and $\tau_T^2 = \frac{1}{\Delta t\theta_T}$ are still very large for these values of Δt and θ_w, θ_T , so that $K_0(x) \rightarrow 0$ for large x in the DRBEM.

As Ra or Ha increases we need to take more boundary elements in DRBEM and more grid

points in DQM, and smaller Δt in both of them. For a fixed $Ra = 10^3$, Ha varies from 10 to 100 and 300, and requires Δt values 10^{-1} , 10^{-2} , 10^{-3} and $K = 60, 76, 92$, respectively, in DRBEM. Similarly, in DQM, $Ha = 10, 100, 300$ require $\Delta t = 10^{-2}, 10^{-3}, 10^{-4}$, and $20 \times 20, 23 \times 23, 27 \times 27$ grid points, respectively. For a fixed $Ha = 100$, K (number of boundary elements) varies from 76, 84, 116, to 148 as Ra varies from $10^3, 10^4, 10^5$ and 10^6 , respectively, again with decreasing Δt 's.

Table 4.11: Δt values in DRBEM using $\bar{f} = r^2 \log r$ and $\bar{f} = 1 + r^2 + r^3 - \tau^2(\frac{r^2}{4} + \frac{r^4}{16} + \frac{r^5}{25})$ for $Ha = 50$.

	$Ra = 10^3$	$Ra = 10^4$	$Ra = 10^5$
$\bar{f} = r^2 \ln r$	0.05	0.01	0.005
$\bar{f} = 1 + r^2 + r^3 - \tau^2(\frac{r^2}{4} + \frac{r^4}{16} + \frac{r^5}{25})$	0.1	0.05	0.01

In Table 4.11 we present the use of two radial basis functions in approximating the inhomogeneities in modified Helmholtz equations for vorticity and temperature. As it can be noticed that radial basis function containing the constant parameter τ in the equation requires even much larger time increments. Thus, it is more advantageous.

In Figures 4.30-4.31, the effect of the Hartmann number on isotherms, vorticity contours and streamlines is given with Rayleigh number 10^5 for both DRBEM and DQM solutions. From these figures, we can say that the intensity of the convection is decreased because of the drag force of the magnetic field. The vortex of streamlines is in circular pattern for small Ha . The circular vortex of the streamlines is elongated vertically with the increase of Hartmann number. This process continues until this vortex finally breaks up in two secondary vortices.

As Ha increases, at the center of the cavity, the vorticity contours are separated into two cells and one of them approaches the top wall and another one approaches the bottom wall. Also, the vorticity values near the walls decrease and form boundary layers. The central region of the cavity is almost stationary as Ha increases. In addition, for high Hartmann numbers, the isotherms are almost parallel to the vertical walls. This means that, the heat transfer process approaches the pure conduction limit. Therefore we can conclude that the magnetic field suppressed the heat transfer between the hot and cold walls.

In Figures 4.32-4.33, isotherms, vorticity contours and streamlines are given at $Ha = 50$ and for various values of Rayleigh number in both DRBEM and DQM solutions. From the figures one can say that, for low Rayleigh number due to the effect of the Lorentz force, the isotherms are almost parallel to the vertical walls. In addition, thin boundary layers for vorticity and straight form of the streamlines already occur, although the Rayleigh number is very low. But for high Rayleigh number, the effect of the magnetic field is very weak for all variables.

Thus, one can conclude for both methods that, when Hartmann number is increased the conduction heat transfer mechanism becomes dominant. Boundary layers are formed for vorticity and streamlines. For increasing values of Rayleigh number the effect of the magnetic field is weaker which is expected behavior reported in [7, 16]

In obtaining the solutions presented in Figures 4.30-4.31 and 4.32-4.33, $f = 1 + r$ and

$\bar{f} = r^2 \log r$ radial basis functions are used for stream function, and vorticity, temperature equations, respectively. When the radial basis function $\bar{f} = 1 + r^2 + r^3 - \tau^2(\frac{r^2}{4} + \frac{r^4}{16} + \frac{r^5}{25})$ is used for modified Helmholtz equation we obtain the solution up to $Ra = 10^5$ with the same accuracy obtained with $\bar{f} = r^2 \ln r$ by using much larger Δt . These results are given in Figure 4.34.

The comparison of the two methods (DQM and DRBEM) is carried in terms of horizontal and vertical velocity profiles at the mid-plane of the cavity in Figure 4.35. $u(\frac{1}{2}, y)$ and $v(x, \frac{1}{2})$ obtained from DQM and DRBEM are plotted on the same graphs to show the well agreement. The external magnetic field in x-direction produces a force opposite to the flow direction which decreases the horizontal velocity at the centerline.

Table 4.12: The comparison of maximum value of the stream function in magnitude and its location for $Ha = 100$.

Ra		Ψ_{min}	Vortex Center (x,y)	$W_{V.C.}$
10^3	DQM	-0.01245	(0.5, 0.28)	-0.16389
	DRBEM	-0.01312	(0.5, 0.24)	-0.28938
10^4	DQM	-0.12442	(0.5, 0.72)	-1.63795
	DRBEM	-0.13036	(0.5, 0.76)	-1.70420
10^5	DQM	-1.15044	(0.5, 0.72)	-15.57319
	DRBEM	-1.19336	(0.5, 0.76)	-14.90651
10^6	DQM	-6.23678	(0.5, 0.5)	-39.91785
	DRBEM	-6.98622	(0.5, 0.5)	-38.58250

Table 4.13: The comparison of maximum value of the stream function in magnitude and its location for $Ra = 10^4$.

Ha		Ψ_{min}	Vortex Center (x,y)	$W_{V.C.}$
0	DQM	-5.10128	(0.5, 0.5)	-98.37708
	DRBEM	-5.19924	(0.5, 0.5)	-100.12940
50	DQM	-0.47037	(0.5, 0.35)	-6.91643
	DRBEM	-0.49372	(0.5, 0.35)	-7.02472
100	DQM	-0.12442	(0.5, 0.72)	-1.63795
	DRBEM	-0.13036	(0.5, 0.76)	-2.70420
200	DQM	-0.03193	(0.5, 0.84)	-1.76551
	DRBEM	-0.03296	(0.5, 0.81)	-1.22764
300	DQM	-0.01428	(0.5, 0.84)	-0.39429
	DRBEM	-0.01412	(0.5, 0.81)	-0.41955

Figures 4.36 and 4.37 present variations of horizontal and vertical velocity profiles at the mid-planes for increasing values of Hartmann number, respectively for DRBEM and DQM results. It is also observed that an increase in Ha decreases the magnitudes of both horizontal and ver-

tical velocities. This is the well-known characteristic of MHD flow which is the flattening tendency of the velocity as Ha increases. These mid-plane velocity profiles are in agreement with the ones given [7].

In order to compare DRBEM and DQM, we also consider maximum value of stream function in magnitude and the vorticity value at the vortex center, for various Ra and Ha in Tables 4.12 and 4.13, respectively. As Ra increases Ψ_{min} and $W_{V.C.}$ both decrease and the vortex center moves on $x = \frac{1}{2}$ line settling down at the center of the cavity for large Ra as 10^6 . An increase in Ha results in an increase both in Ψ_{min} and w at the vortex center which moves through the bottom and top walls due to the boundary layers formed for large Ha . The differences in w vortex values obtained from DRBEM and DQM arise from the different mesh points used.

Since DQM is based on interpolation of solution and its derivatives by polynomials, it is quite simple considering the construction of the system of ordinary differential equations in time. Although, DQM is preferred and found to be simple in terms of computation, DRBEM especially with polynomial radial basis functions can use larger time increment than DQM to advance the solution to the steady-state faster. Other than this, the two methods give the same accuracy for solving natural convection flow under a magnetic field.

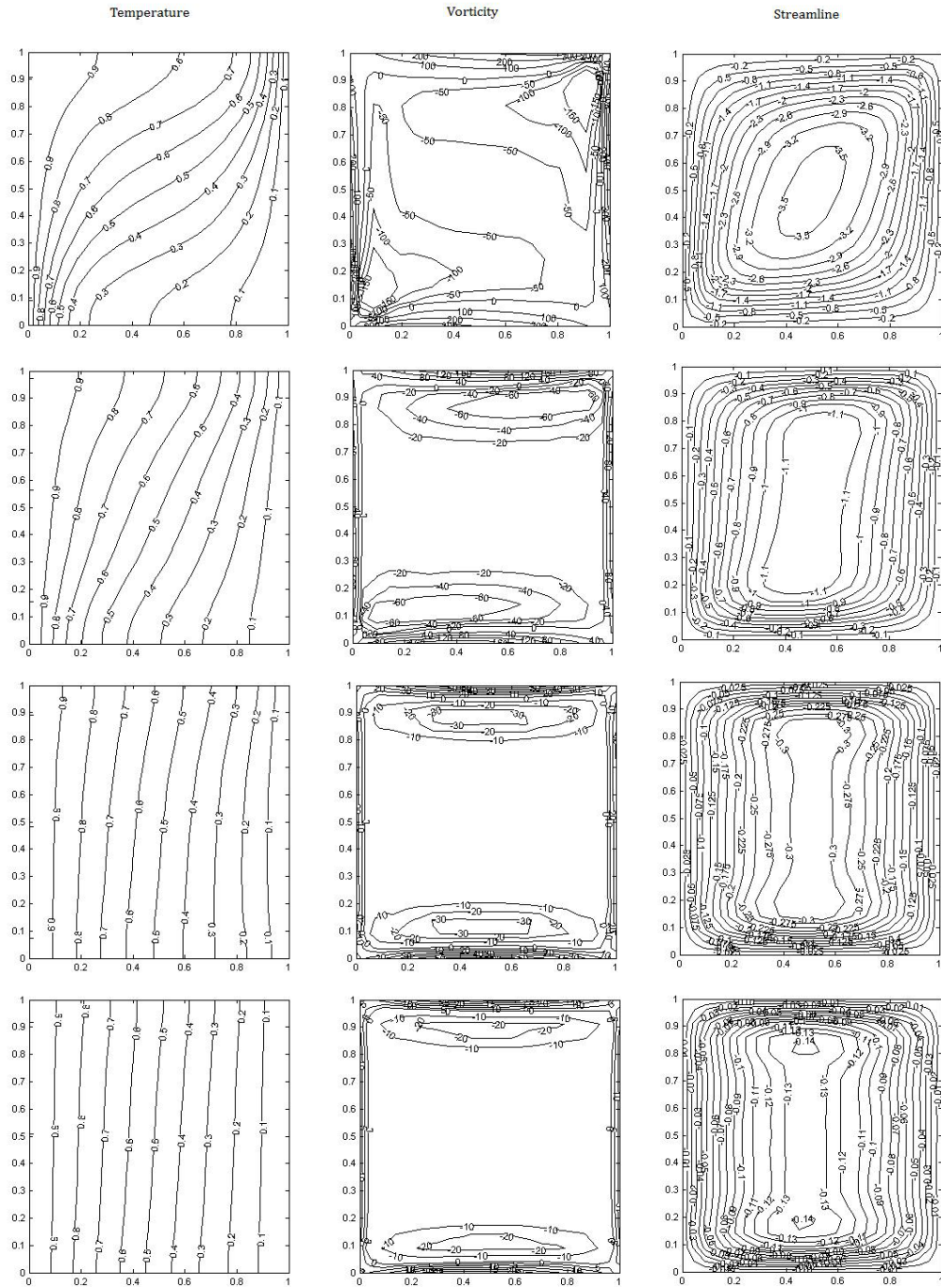


Figure 4.30: Temperature, vorticity and streamline contours with DRBEM using $\bar{f} = r^2 \log r$ for $Ha = 50, 100, 200, 300$ from top to bottom with $Ra = 10^5$.

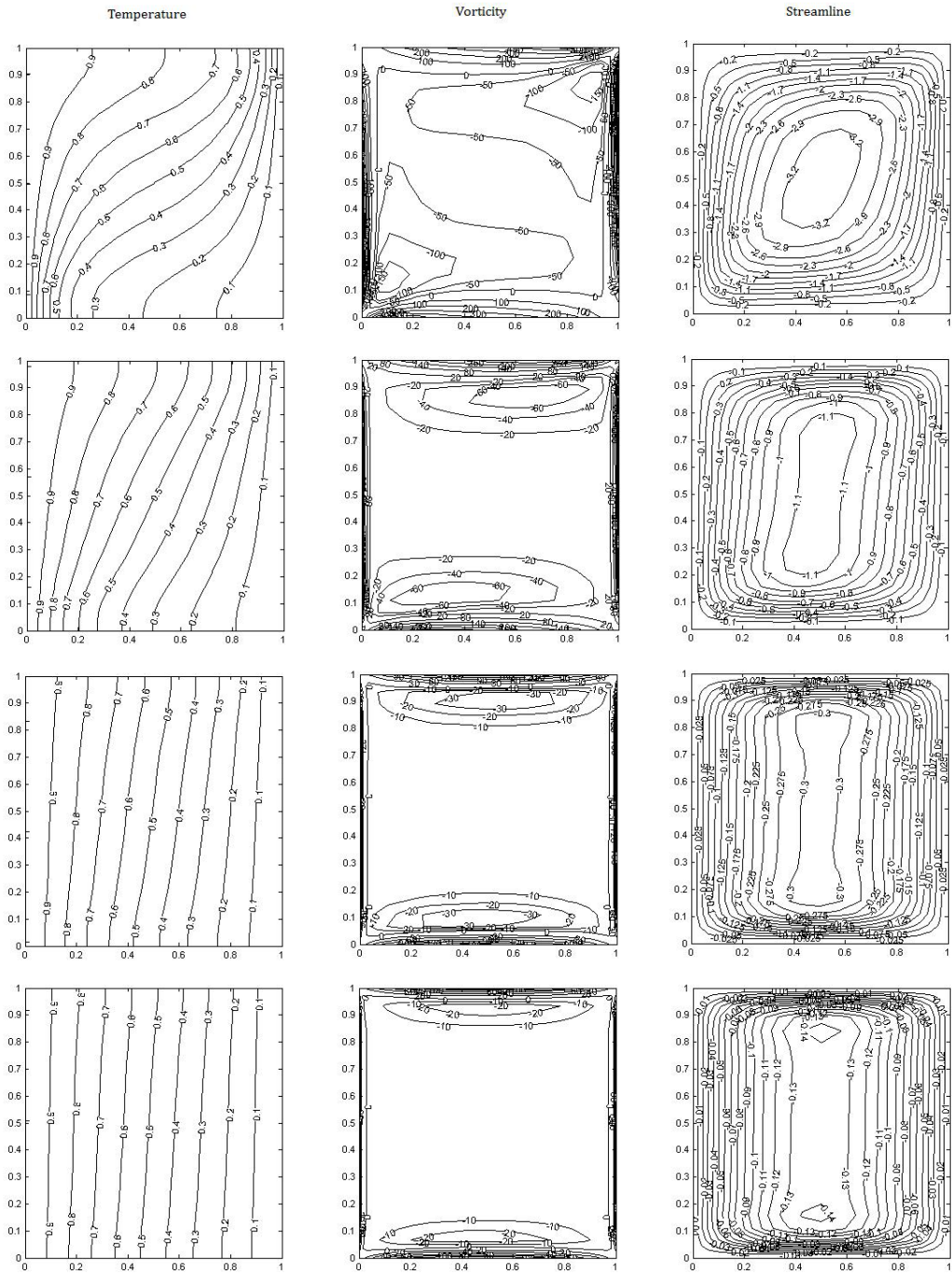


Figure 4.31: Temperature, vorticity and streamline contours with DQM for $Ha = 50, 100, 200, 300$ from top to bottom with $Ra = 10^5$.

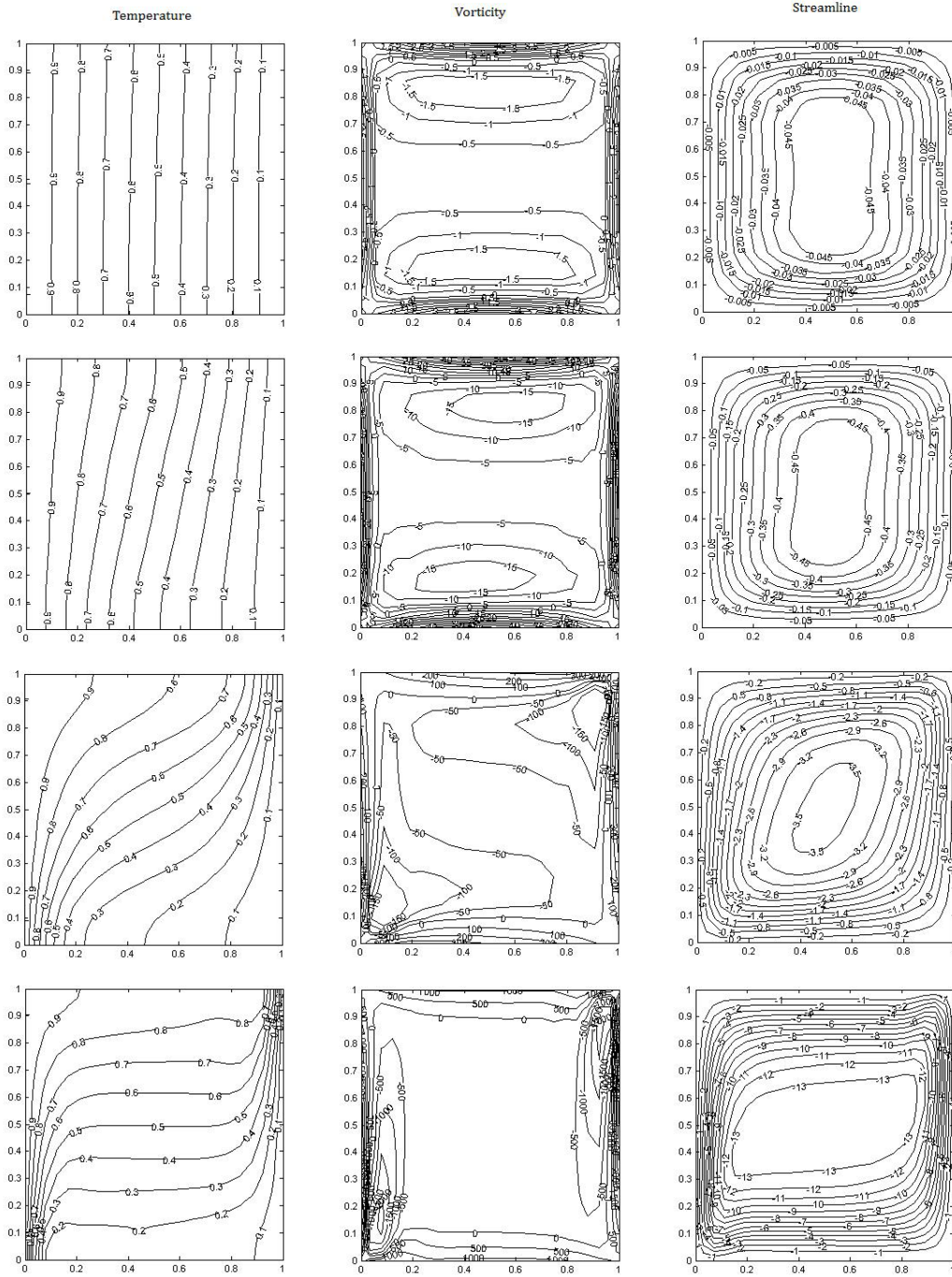


Figure 4.32: Temperature, vorticity and streamline contours with DRBEM using $\bar{f} = r^2 \log r$ for $Ra = 10^3, 10^4, 10^5, 10^6$ from top to bottom with $Ha = 50$.

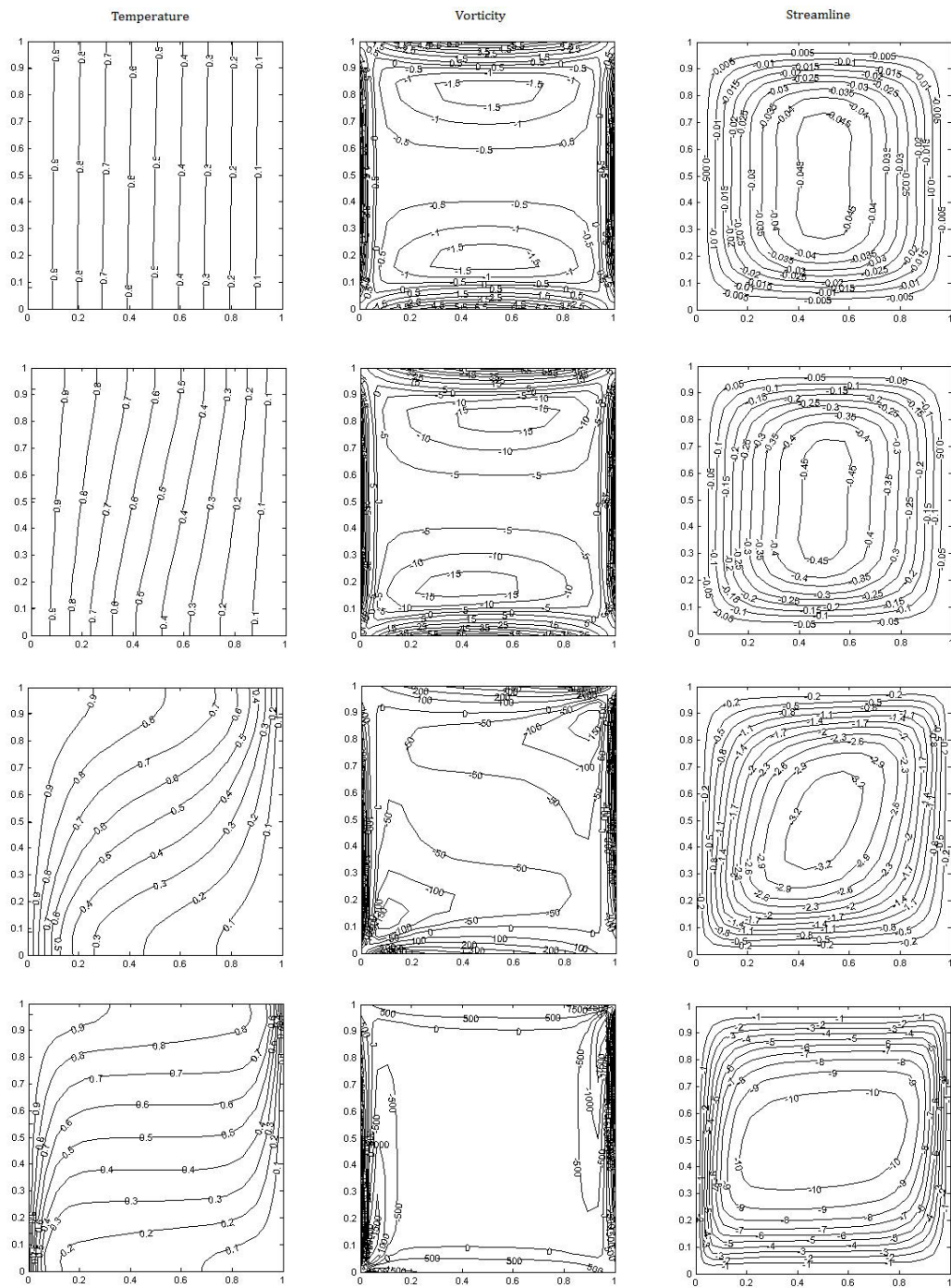


Figure 4.33: Temperature, vorticity and streamline contours with DQM for $Ra = 10^3, 10^4, 10^5, 10^6$ from top to bottom with $Ha = 50$.

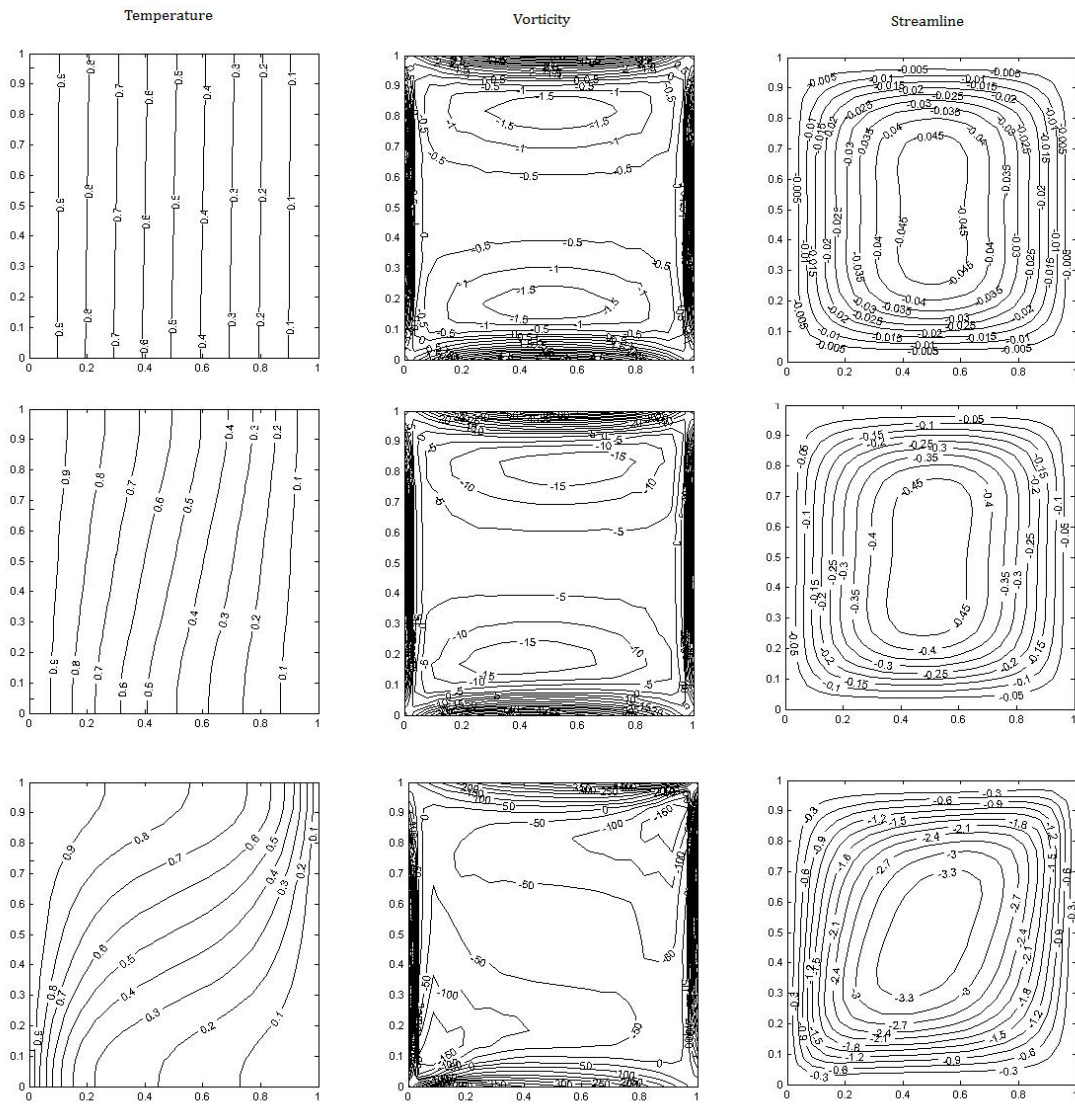


Figure 4.34: Temperature, vorticity and streamline contours with DRBEM using $\bar{f} = 1 + r^2 + r + 3 - \tau^2(\frac{r^2}{4} + \frac{r^4}{16} + \frac{r^5}{25})$ for $Ra = 10^3, 10^4, 10^5$, from top to bottom with $Ha = 50$.

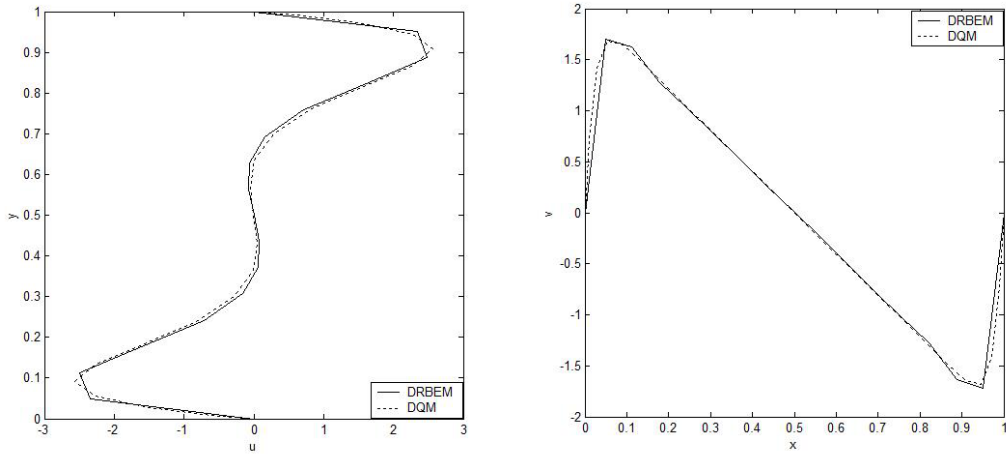


Figure 4.35: Horizontal and vertical velocity profiles at the mid-plane of the cavity for $Ra = 10^4$ and $Ha = 50$.

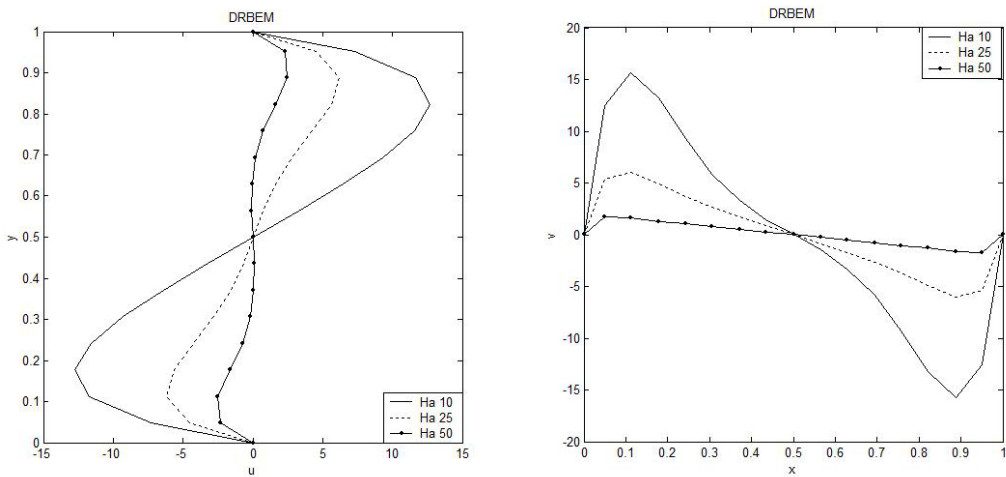


Figure 4.36: Horizontal and vertical velocity profiles at the mid-plane of the cavity for $Ra = 10^4$.

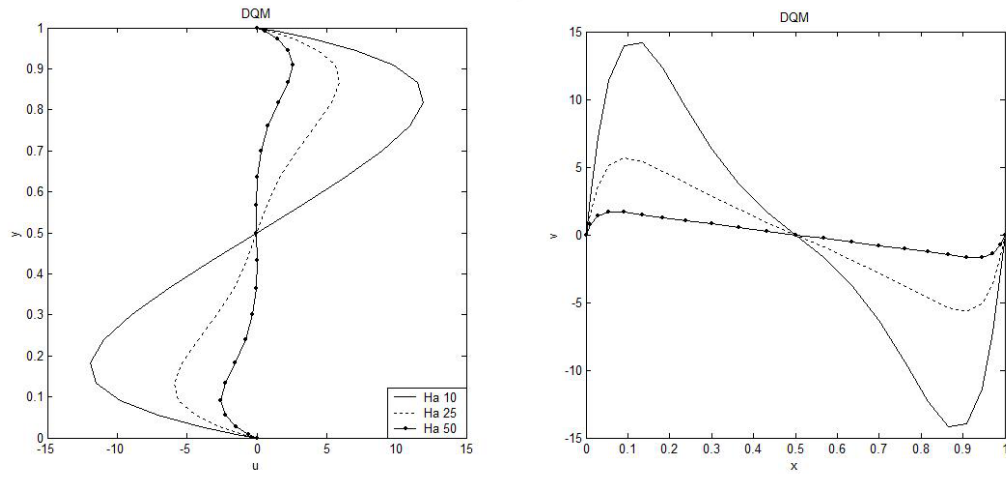


Figure 4.37: Horizontal and vertical velocity profiles at the mid-plane of the cavity for $Ra = 10^4$.

4.5 Application of DRBEM for the Inverse Problems

4.5.1 Natural Convection Flow under a Magnetic Field

In this section, the mathematical direct and inverse formulations of natural magneto-convection flow in a square cavity are given. The DRBEM solution procedure for the direct problem was given in Section 4.4, and in this section it is briefly described for an inverse problem. Together with the velocity-vorticity form of vorticity transport equation, the governing equations are given in non-dimensional form in terms of stream function ψ , vorticity w and temperature T as

$$\nabla^2 \psi = -w, \quad (4.128)$$

$$Pr \nabla^2 w = \frac{\partial w}{\partial t} + u \frac{\partial w}{\partial x} + v \frac{\partial w}{\partial y} + Ha^2 Pr \frac{\partial v}{\partial x} - Ra Pr \frac{\partial T}{\partial x}, \quad (4.129)$$

$$\nabla^2 T = \frac{\partial T}{\partial t} + u \frac{\partial T}{\partial x} + v \frac{\partial T}{\partial y}, \quad (4.130)$$

with the same relations for u , v and w given in (4.98). Pr , Ra and Ha are the Prandtl, Rayleigh and Hartmann numbers, respectively described in Chapter 1.

Approximating the time derivatives using the forward difference approximation, and using relaxation parameters θ_w and θ_T for vorticity and temperature, governing equations take the same form (4.99)

$$\nabla^2 \psi^{(n+1)} = -w^{(n)} \quad (4.131)$$

$$\begin{aligned} \nabla^2 w^{(n+1)} - \tau_w^2 w^{(n+1)} &= -\frac{(1 - \theta_w)}{\theta_w} \nabla^2 w^{(n)} - \tau_w^2 w^{(n)} \\ &+ \frac{1}{Pr \theta_w} \left(\frac{\partial \psi^{(n+1)}}{\partial y} \frac{\partial w^{(n)}}{\partial x} - \frac{\partial \psi^{(n+1)}}{\partial x} \frac{\partial w^{(n)}}{\partial y} \right) \end{aligned} \quad (4.132)$$

$$\begin{aligned} \nabla^2 T^{(n+1)} - \tau_T^2 T^{(n+1)} &= -\frac{(1 - \theta_T)}{\theta_T} \nabla^2 T^{(n)} - \tau_T^2 T^{(n)} \\ &+ \frac{Ha^2}{\theta_w} \frac{\partial^2 \psi^{(n+1)}}{\partial x^2} - \frac{Ra}{\theta_w} \frac{\partial T^{(n)}}{\partial x}, \end{aligned} \quad (4.133)$$

$$+ \frac{1}{\theta_T} \left(\frac{\partial \psi^{(n+1)}}{\partial y} \frac{\partial T^{(n)}}{\partial x} - \frac{\partial \psi^{(n+1)}}{\partial x} \frac{\partial T^{(n)}}{\partial y} \right),$$

where

$$\tau_w^2 = \frac{1}{Pr \Delta t \theta_w}, \quad \tau_T^2 = \frac{1}{\Delta t \theta_T}. \quad (4.134)$$

The DRBEM discretization of the equations (4.131)-(4.133) for both direct and inverse problems is the same which is developed in Section 4.4 resulting in the systems of equations (4.106)-(4.111). In the DRBEM application procedure there is no difference between direct and inverse problems. In the inverse problem, overprescribed boundary conditions are imposed on one boundary while underprescribed boundary conditions are imposed on the other boundary. So, the resulting linearized system of equations is ill-conditioned due to the boundary conditions imposed, and for its stable numerical solution we use a classical Tikhonov regularization [76] with regularization parameter $\lambda > 0$.

4.5.2 Numerical Results

4.5.2.1 Example 1

As a first example, we consider the schematic of the physical situation shown in Figure 4.38 with the same boundary conditions as those previously investigated by Li [61] for an inverse natural convection problem in the absence of the magnetic field. The boundary conditions are

$$\psi(0, y, t) = \psi(1, y, t) = \psi(x, 0, t) = \psi(x, 1, t) = 0, \quad (4.135)$$

$$\frac{\partial \psi}{\partial x}(0, y, t) = \frac{\partial \psi}{\partial x}(1, y, t) = \frac{\partial \psi}{\partial y}(x, 0, t) = \frac{\partial \psi}{\partial y}(x, 1, t) = 0, \quad (4.136)$$

$$\frac{\partial T}{\partial x}(1, y, t) = \frac{\partial T}{\partial y}(x, 0, t) = \frac{\partial T}{\partial y}(x, 1, t) = 0, \quad (4.137)$$

$$\frac{\partial T}{\partial x}(0, y, t) = q(y, t), \quad (4.138)$$

for $x, y \in (0, 1), t > 0$, where $q(y, t) = Q(y, t)/Q_{ref}$ is an unknown non-dimensional heat flux at $x = 0$. The initial conditions are uniform and taken to be zero,

$$u(x, y, 0) = v(x, y, 0) = T(x, y, 0) = 0 \quad , \quad (x, y) \in [0, 1] \times [0, 1]. \quad (4.139)$$

Vorticity boundary conditions are not known but they can be obtained from the vorticity definition (4.98) by using coordinate matrix.

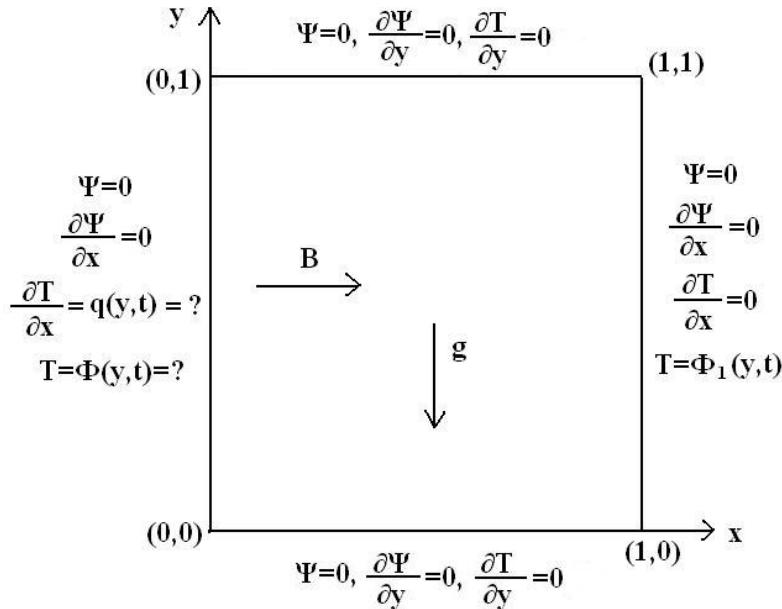


Figure 4.38: Inverse problem for the natural convection flow in a square cavity under a magnetic field.

In the direct problem, the heat flux $q(y, t)$ on the left wall $x = 0$ is considered as prescribed, but in the inverse problem it will be regarded as unknown. Instead, the missing boundary condition at $x = 0$ is compensated for by obtaining (it is obtained from the results of the direct problem at $x = 1$) the boundary temperature at the right wall $x = 1$ as

$$T(1, y, t) = \phi_1(y, t), \quad y \in (0, 1), \quad t > 0. \quad (4.140)$$

At the right wall $x = 1$ we know both the values of the temperature (4.140) and heat flux (4.137) but at the left wall $x = 0$ there is no condition on either temperature, heat flux or a combination of them. Generally, it is expected that such an inverse formulation will lead to the ill-posedness of the problem, e.g. in our case although the solution may be unique, it may not exist if the data (4.140) is prescribed arbitrarily. In addition, the solution is unstable in the sense that small measurement errors into the data (4.140) will lead to large errors in the computed solution for

$$T(0, y, t) = \phi(y, t) = ?, \quad y \in (0, 1), \quad t > 0, \quad (4.141)$$

$$\frac{\partial T}{\partial x}(0, y, t) = q(y, t) = ?, \quad y \in (0, 1), \quad t > 0. \quad (4.142)$$

Consequently, classical methods of inversion are not adequate and instead regularization methods are necessary to be employed in order to obtain a stable numerical solution [76].

As a heat flux (4.142), a triangular time-dependent function independent of y is taken as in [61]

$$q(y, t) \equiv q(t) = \begin{cases} 0, & 0 \leq t < t_0 \\ \frac{t - t_0}{t_1 - t_0}, & t_0 \leq t < t_1 \\ \frac{t_2 - t}{t_2 - t_1}, & t_1 \leq t < t_2 \\ 0, & t_2 \leq t \leq t_3 \end{cases} \quad (4.143)$$

with $t_0 = 10\Delta t_{ref}$, $t_1 = 30\Delta t_{ref}$, $t_2 = 50\Delta t_{ref}$ and $t_3 = 60\Delta t_{ref}$, where $\Delta t_{ref} = 0.0133$. In the time-marching procedure, $\Delta t = \frac{\Delta t_{ref}}{\Lambda_{time}}$ is taken as computational time step and some numerical investigation is performed by changing Λ_{time} .

The iterative computational procedure for solving the inverse problem can be summarized as follows:

1. $w^{(0)} = 0$, $T^{(0)} = 0$ are taken at the zero time level ($n = 0$).
2. Solve the discretized equations for direct problem inserting boundary conditions (4.135)-(4.138), taking definition of $q(y, t)$ from equation (4.143) for using the DRBEM, and compute ψ , w and T .
3. Use the temperature values obtained from the direct problem at $x = 1$ (equation (4.140)) as the input data for the inverse problem.
4. Solve the discretized stream function equation from (4.131), to obtain $\psi^{(n+1)}$ by using $w^{(n)}$.

5. Obtain the velocity components $u^{(n+1)}$ and $v^{(n+1)}$ from the relationship with ψ and compute the unknown vorticity boundary values using (4.98) using the DRBEM idea with coordinate matrix \overline{F} .
6. Approximate the space derivatives of the stream function, $\psi^{(n+1)}$, temperature, $T^{(n)}$, and vorticity, $w^{(n)}$, by using corresponding coordinate matrices.
7. Solve the discretized form of vorticity transport equation (4.132), to obtain $w^{(n+1)}$ by using $w^{(n)}$ and the partial derivatives of $w^{(n)}$, $\psi^{(n+1)}$ and $T^{(n)}$.
8. Solve the discretized form of energy equation (4.133), to obtain $T^{(n+1)}$ and the flux $q(y, t)$ by using $T^{(n)}$, and the partial derivatives of $\psi^{(n+1)}$ and $T^{(n)}$.
9. Update $w^{(n)}$ and $T^{(n)}$ values for the iteration procedure.
10. Continue the steps 4-9 to the next time levels until the required values of the flux $q(y, t)$ at the left wall are obtained.

In the DRBEM, we use as radial basis functions $1 + r$ in the stream function equation (4.131) and thin plate splines $r^2 \ln r$ in the vorticity and energy equations (4.132) and (4.133), where r is the radial distance. All computations are carried with $Pr = 1$.

At the beginning of the numerical study, the convergence of the DRBEM for the direct problem is analyzed by using various numbers of boundary elements K and internal nodes L_1 . The numerical isotherms at the time $t = 30\Delta t_{ref}$, i.e., after 6000 time steps $\Delta t = \frac{\Delta t_{ref}}{200}$, in the absence of the magnetic field, i.e., $Ha = 0$, and $Ra = 5 \times 10^2$ (conduction dominating), $Ra = 5 \times 10^3$ (mild convection) and $Ra = 5 \times 10^5$ (strong convection), obtained with $K \in \{44, 84, 164\}$ boundary elements and $L_1 \in \{25, 100, 400\}$ internal nodes, are shown in Figures 4.39-4.41, respectively. By comparing these figures it can be seen that the mesh in Figure 4.39 is too coarse, whilst the results in Figures 4.40 and 4.41, by almost coinciding with each other show that the convergence of the numerical method has been achieved. The middle mesh $K = 84$ and $L_1 = 100$ in Figure 4.40 is sufficiently fine to ensure that any further increase in it, such as the mesh $K = 164$ and $L_1 = 400$ in Figure 4.41, does not significantly affect the accuracy of the numerical results. Therefore, in the next two Figures 4.42 and 4.43 we present the results for the boundary temperatures $T(0, y, t)$ and $T(1, y, t)$, respectively, for this mesh only.

In the inverse problem which is next investigated, Figures 4.43 represent the input additional boundary temperature data (4.140) at the "friendly" wall $x = 1$, whilst Figures 4.42 represent the desired output of the boundary temperature (4.141) at the "hostile" wall $x = 0$.

We solve the inverse problem with the same conditions as in Li [61] in order to show some comparison between the methods. Note that in [61] only the natural convection problem with the absent magnetic field was addressed and thus we initially take $Ha = 0$. Furthermore, in order to avoid committing on inverse crime the inverse problem is solved using a number of internal nodes $L_2 = 90$ different from $L_1 = 100$ which was used in the direct problem to generate the numerically simulated input data of Figures 4.43. We also include regularization with a regularization parameter $\lambda = 10^{-6}$ with the note that for $\lambda = 0$ the problem is too ill-posed for the computational program to even run.

Figures 4.44 and 4.45 show the numerical results for the internal isotherms and heat flux at $x = 0$, respectively. By comparing Figures 4.40 and 4.44 it can be seen that the internal isotherms at the time $t = 30\Delta t_{ref}$ obtained by solving the direct and inverse problems are in good agreement with each other. We also report that the results obtained in Figure 4.44 are in good agreement with the results presented in Figure 6 of [61] who used the sequential function specification method combined with a control-volume approach. Further, Figure 4.45 shows that the numerical results are in good agreement with the piecewise linear heat flux (4.143).

The DRBEM is applied by transforming the differential equations to boundary integrals based on the fundamental solutions of Laplace's and modified Helmholtz equations which is rather simple compared to the original system of nonlinear partial differential equations. The use of the Bessel function $K_0(r)$ as the fundamental solution for the modified Helmholtz equation in the DRBEM makes it possible to use larger time steps. Before this, when the governing equations (4.131)-(4.133) are constructed, the forward finite difference approximations are used for the time derivatives. So we need smaller time increment in our computations and $\Delta t = \frac{\Delta t_{ref}}{\Lambda_{time}}$ is used as a time step. To achieve suitable time steps, the calculations are performed by using several values of Δt and the results are presented in Figure 4.46. From the figure it can be seen that the accuracy of the numerical results improves as the time step Δt decreases. Although we have better results when smaller time steps are used, since it takes too long computational time we prefer to use $\Delta t = \frac{\Delta t_{ref}}{200}$ in all other computations which gives good results too, as seen in Figure 4.45.

In practice, temperature measurements are obviously affected by noisy errors. We take this into account by perturbing the boundary temperature $T(1, y, t)$ obtained from the direct problem and shown in Figures 4.43 as

$$T^{\text{noise}}(1, y, t) = T^{\text{direct problem}}(1, y, t)(1 + \chi\rho), \quad y \in (0, 1), \quad t \in (t_0, t_3], \quad (4.144)$$

where ρ represents the percentage of noise and χ is a random variable in the interval $[-1, 1]$.

In the analysis of the results under noisy input data, it is considered that there is no noise in the boundary temperature $T(1, y, t)$ up to $t = t_0$ and the noisy data is introduced only after $t = t_0$. The effects of the noisy errors on boundary temperature and heat flux at $x = 0$ for various percentages of noise $\rho \in \{0, 2\%, 4\%\}$ are given in Figures 4.47 and 4.48, respectively. Both figures show good accuracy and stability against noise. The numerical results become less accurate, especially for the heat flux $q(0.5, t)$ in Figure 4.48, as t approaches the final time $t_3 = 60\Delta t_{ref} = 0.8$. This is to be expected since in the inverse problem we use the additional data (4.140) is only up to $t = t_3$ and this information at the right wall $x = 1$ over the time interval $[0, t_3]$ can restore the information at the left wall $x = 0$ only on a shorter time interval $[0, t_3 - \delta]$, for some $\delta > 0$. This phenomenon is commonly encountered in inverse heat conduction problems, see [18] and [38].

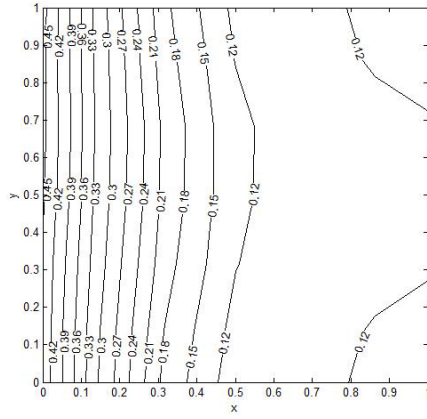
The effect of the Tikhonov's regulation parameter λ is analyzed within the range $\lambda = 10^{-12}$ to 10^{-1} and the results are presented in the Figure 4.49. From this figure it can be seen that the regularization parameter λ has little influence on the stability of the numerical results which is a little surprising. However, it seems that regularization is achieved through DRBEM smoothing and by stopping the iterative process once the semi-convergence of the algorithm is observed, i.e. before the instability of the numerical solution starts to manifest through highly oscillatory and unbounded behavior.

Isotherm patterns at $t = 30\Delta t_{ref}$ and $t = 60\Delta t_{ref}$ with $Ra = 500$, $Ha = 0$ are illustrated to show the effect of noise in Figures 4.50 and 4.51, respectively, in comparison with the direct problem solution. From these figures it can be seen that the largest inaccuracies occur, as expected, at the left wall $x = 0$ which represents the region which is farthest from the right wall $x = 1$ where the Cauchy data are prescribed. The inaccuracies near the right wall $x = 1$ are only apparent because it is at that end where we impose the noisy errors as in (4.144).

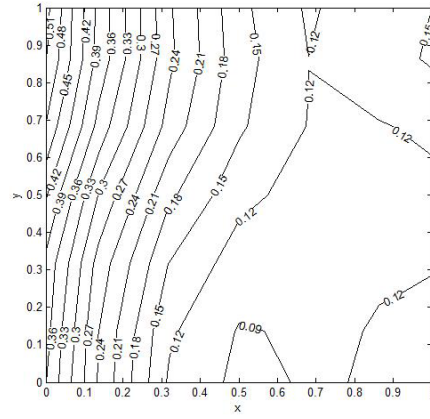
To investigate the effect the magnetic field has on the heat flux, numerical calculations are carried out for various values of $Ha \in \{50, 100, 200\}$ and the results are illustrated in Figure 4.52. As it can be seen from this figure, the results show good agreement with the exact heat flux (4.143) for all values of Ha .

Figure 4.53 shows the isotherms, streamlines and vorticity lines at the various $Ha \in \{50, 100, 200\}$ and $Ra = 500$. This figure clearly illustrates the significant effect that the magnetic field has on the fluid flow though this effect is much less significant on the temperature field.

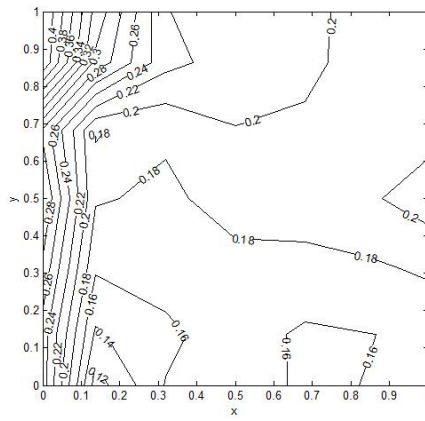
Finally, the effect of noisy error $\rho \in \{0, 2\%, 4\%\}$ on the heat flux is analyzed in Figure 4.54 for mild convection $Ra = 5000$ and magnetic field $Ha = 100$. From this figure it can be seen that the numerical results are quite insensitive to noise for times up to $t = t_1$ after which they start to deviate from each other as the percentage of noise ρ increases.



(a) $Ra = 5 \times 10^2$

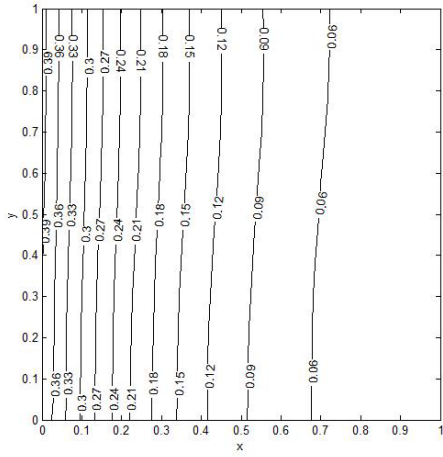


(b) $Ra = 5 \times 10^3$

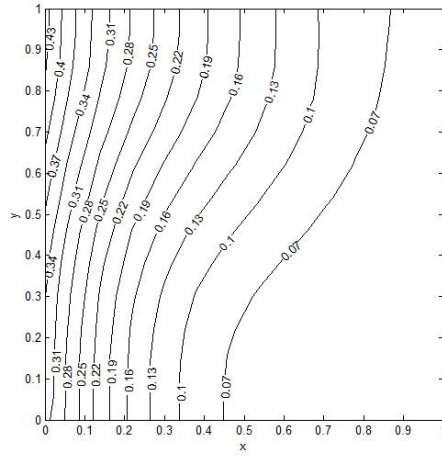


(c) $Ra = 5 \times 10^5$

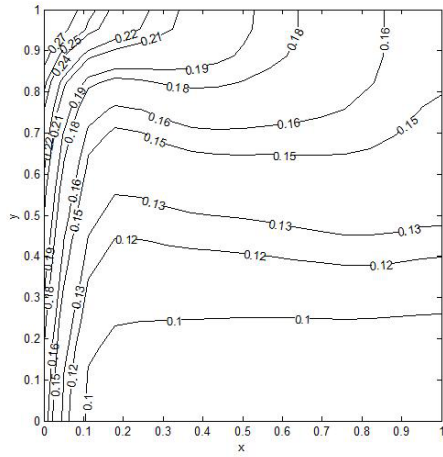
Figure 4.39: Isotherm patterns at the time $t = 30\Delta t_{ref}$ for the direct problem with $Ha = 0$, $\Delta t = \frac{\Delta t_{ref}}{200}$, $K = 44$ and $L_1 = 25$.



(a) $Ra = 5 \times 10^2$

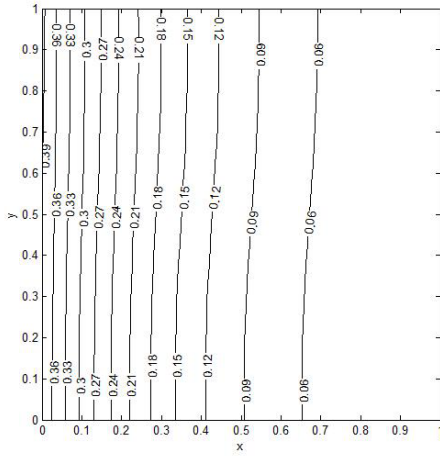


(b) $Ra = 5 \times 10^3$

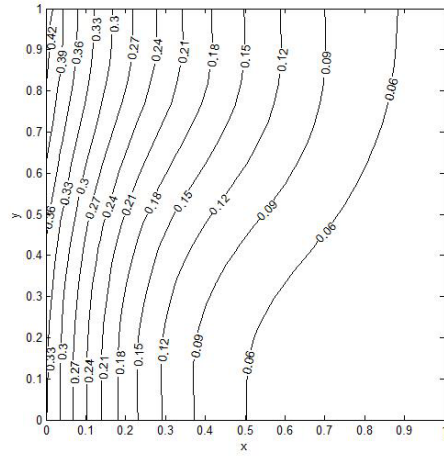


(c) $Ra = 5 \times 10^5$

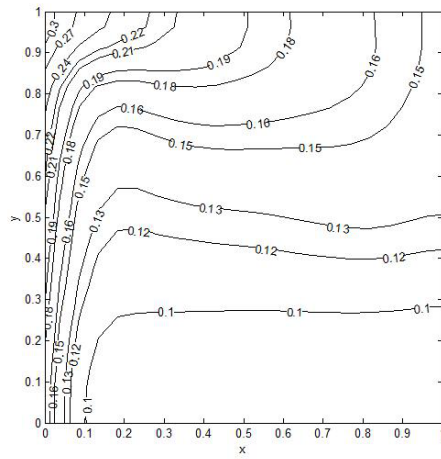
Figure 4.40: Isotherm patterns at the time $t = 30\Delta t_{ref}$ for the direct problem with $Ha = 0$, $\Delta t = \frac{\Delta t_{ref}}{200}$, $K = 84$ and $L_1 = 100$.



(a) $Ra = 5 \times 10^2$

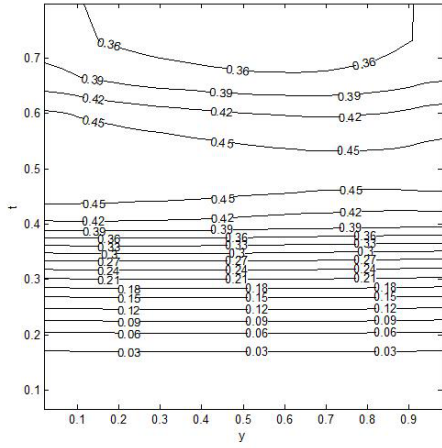


(b) $Ra = 5 \times 10^3$

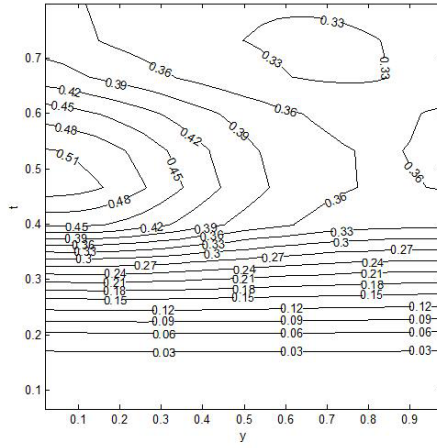


(c) $Ra = 5 \times 10^5$

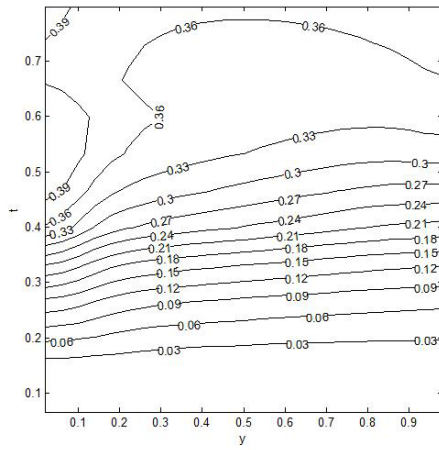
Figure 4.41: Isotherm patterns at the time $t = 30\Delta t_{ref}$ for the direct problem with $Ha = 0$, $\Delta t = \frac{\Delta t_{ref}}{200}$, $K = 164$ and $L_1 = 400$.



(a) $Ra = 5 \times 10^2$

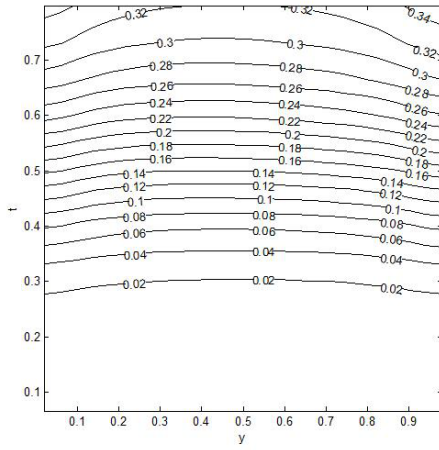


(b) $Ra = 5 \times 10^3$

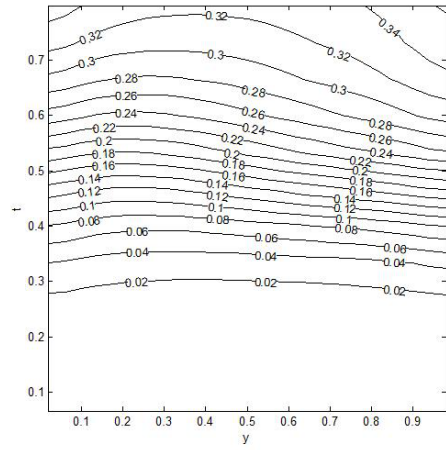


(c) $Ra = 5 \times 10^5$

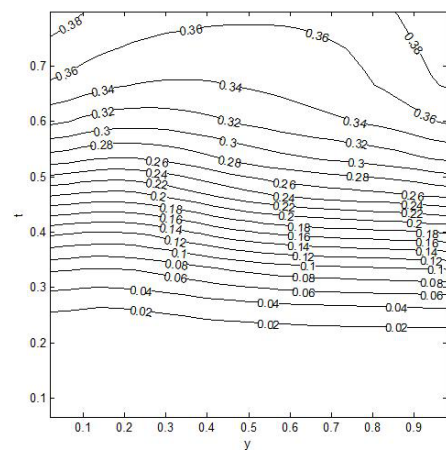
Figure 4.42: Isotherms at boundary $x = 0$ for the direct problem with $Ha = 0$, $\Delta t = \frac{\Delta t_{ref}}{200}$, $K = 84$ and $L_1 = 100$.



(a) $Ra = 5 \times 10^2$

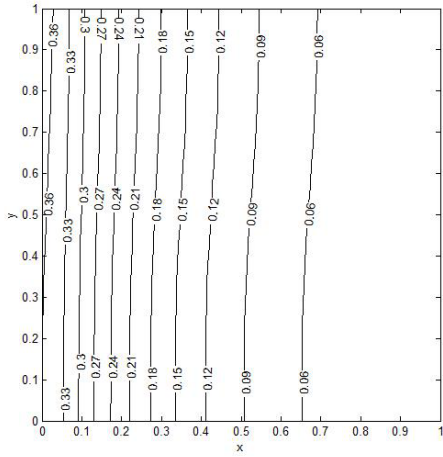


(b) $Ra = 5 \times 10^3$

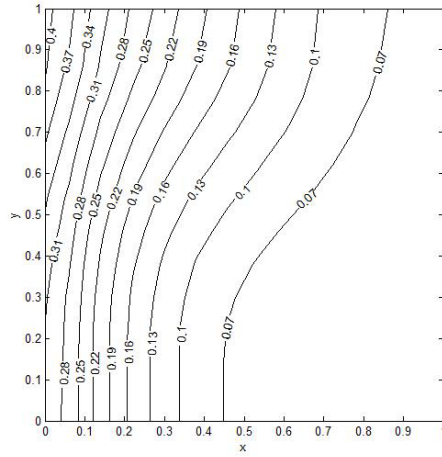


(c) $Ra = 5 \times 10^5$

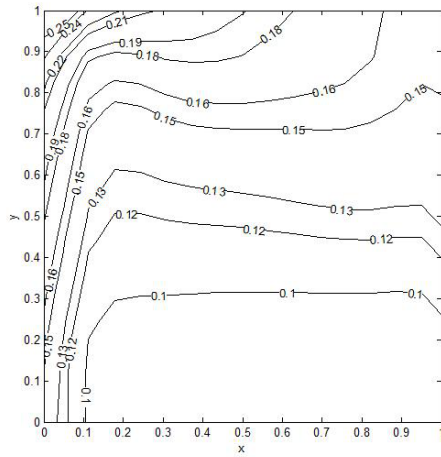
Figure 4.43: Isotherms at boundary $x = 1$ for the direct problem with $Ha = 0$, $\Delta t = \frac{\Delta t_{ref}}{200}$, $K = 84$ and $L_1 = 100$.



(a) $Ra = 5 \times 10^2$



(b) $Ra = 5 \times 10^3$



(c) $Ra = 5 \times 10^5$

Figure 4.44: Isotherm patterns at the time $t = 30\Delta t_{ref}$ for the inverse problem with $Ha = 0$, $\lambda = 10^{-6}$, $\Delta t = \frac{\Delta t_{ref}}{200}$, $K = 84$ and $L_2 = 90$.

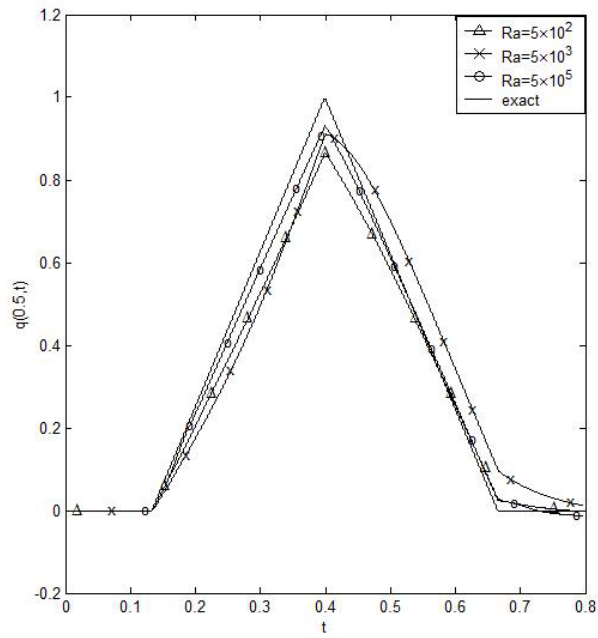


Figure 4.45: Effect of the Rayleigh number on the heat flux $q(0.5, t)$ for $Ha = 0$, $K = 84$, $L_2 = 90$, $\lambda = 10^{-6}$, and $\Delta t = \frac{\Delta t_{ref}}{200}$.

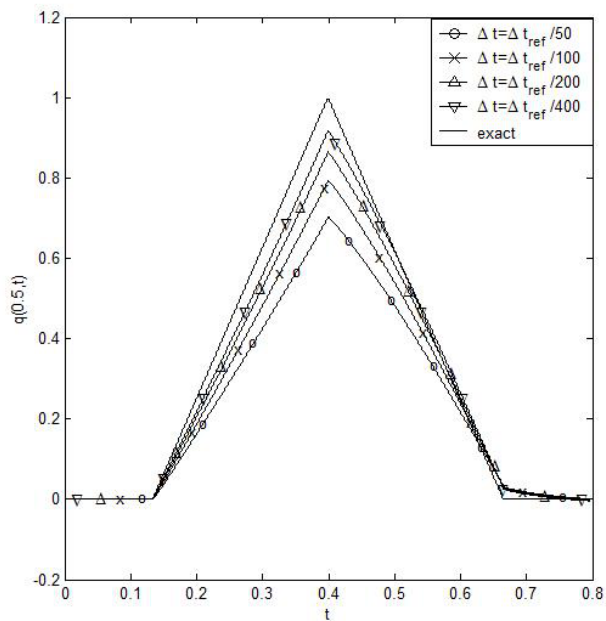


Figure 4.46: Effect of the time step on the heat flux $q(0.5, t)$ for $Ra = 500$, $Ha = 0$, $K = 84$, $L_2 = 90$ and $\lambda = 10^{-6}$.

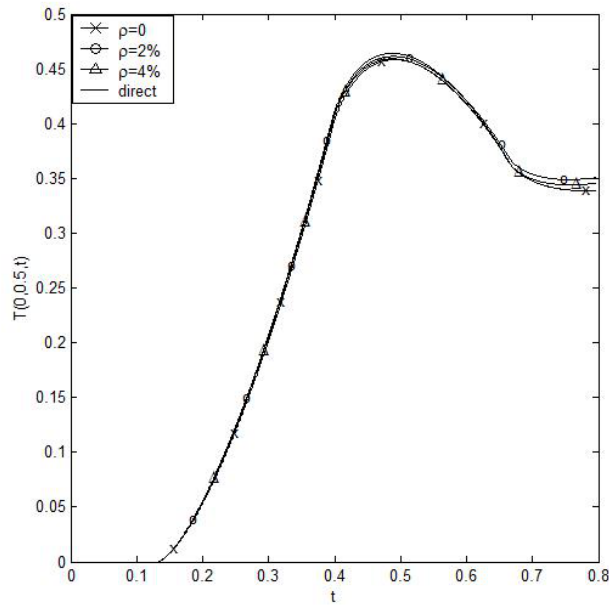


Figure 4.47: Effect of noise on the boundary temperature $T(0, 0.5, t)$ for $Ra = 500$, $Ha = 0$, $K = 84$, $L_2 = 90$, $\lambda = 10^{-6}$ and $\Delta t = \frac{\Delta t_{ref}}{200}$.

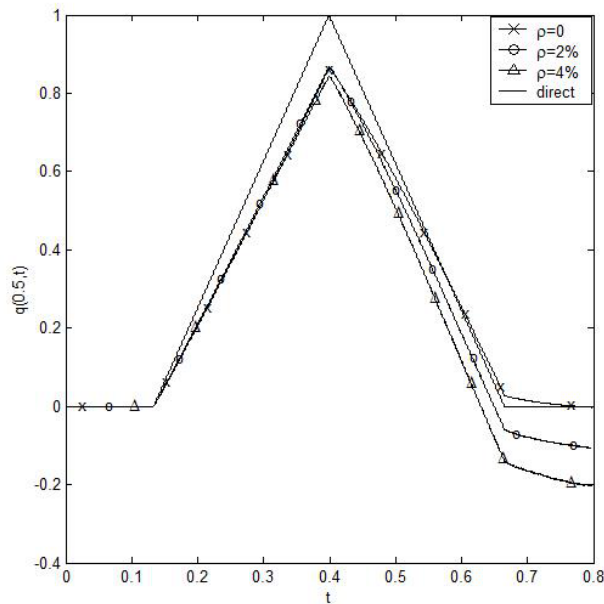


Figure 4.48: Effect of noise on the heat flux $q(0.5, t)$ for $Ra = 500$, $Ha = 0$, $K = 84$, $L_1 = 100$, $L_2 = 90$, $\lambda = 10^{-6}$ and $\Delta t = \frac{\Delta t_{ref}}{200}$.

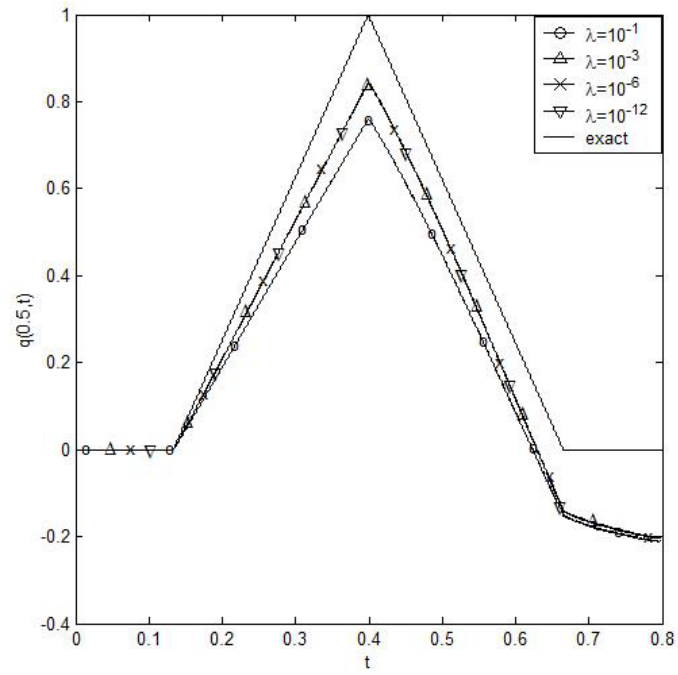
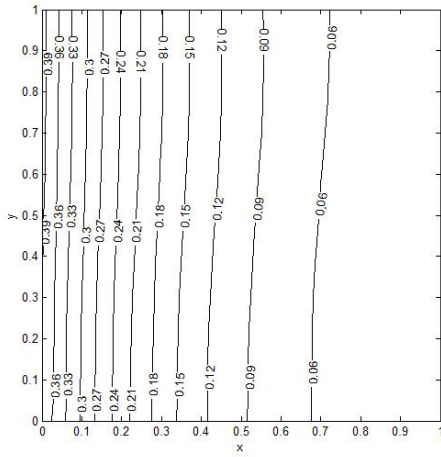
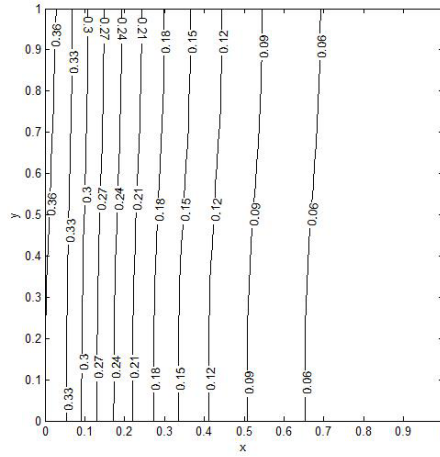


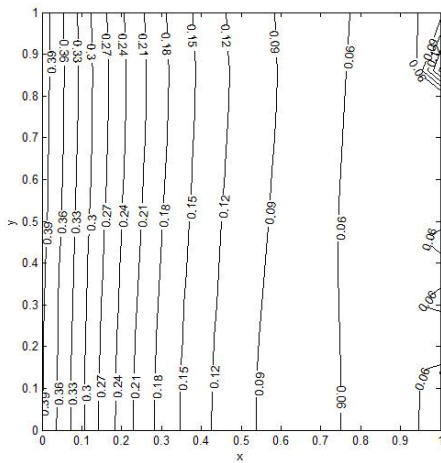
Figure 4.49: Effect of regularization parameter λ on the heat flux $q(0.5, t)$ for $Ra = 500$, $K = 84$, $L_1 = 100$, $L_2 = 90$, $\rho = 4\%$ and $\Delta t = \frac{\Delta t_{ref}}{200}$.



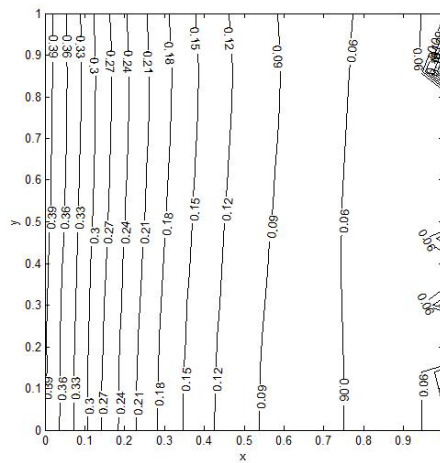
(a) direct



(b) inverse, $\rho = 0$

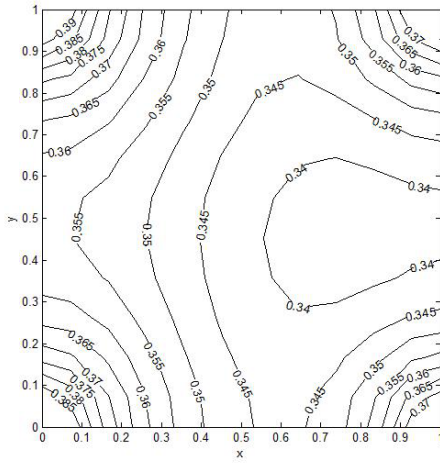


(c) inverse, $\rho = 2\%$

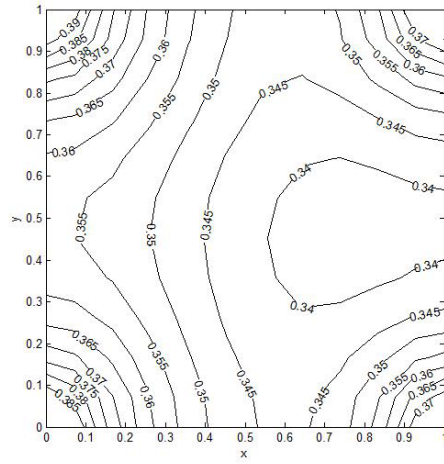


(d) inverse, $\rho = 4\%$

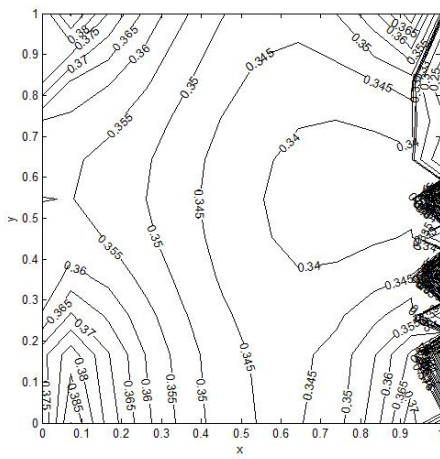
Figure 4.50: Isotherm patterns at the time $t = 30\Delta t_{ref}$ for the direct and inverse ($\lambda = 10^{-6}$) problems with $Ra = 500$, $Ha = 0$, $\Delta t = \frac{\Delta t_{ref}}{200}$, $K = 84$, $L_1 = 100$ and $L_2 = 90$.



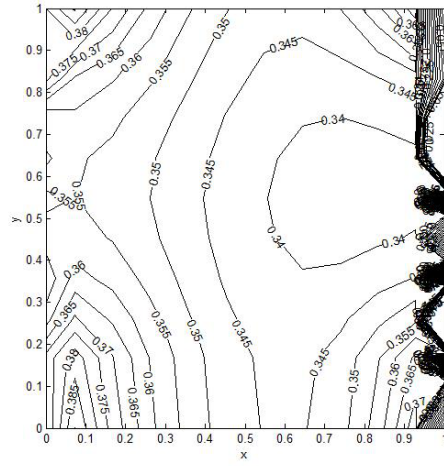
(a) direct



(b) inverse, $\rho = 0$



(c) inverse, $\rho = 2\%$



(d) inverse, $\rho = 4\%$

Figure 4.51: Isotherm patterns at the time $t = 60\Delta t_{ref}$ for the direct and inverse ($\lambda = 10^{-6}$) problems with $Ra = 500$, $Ha = 0$, $\Delta t = \frac{\Delta t_{ref}}{200}$, $K = 84$, $L_1 = 100$ and $L_2 = 90$.

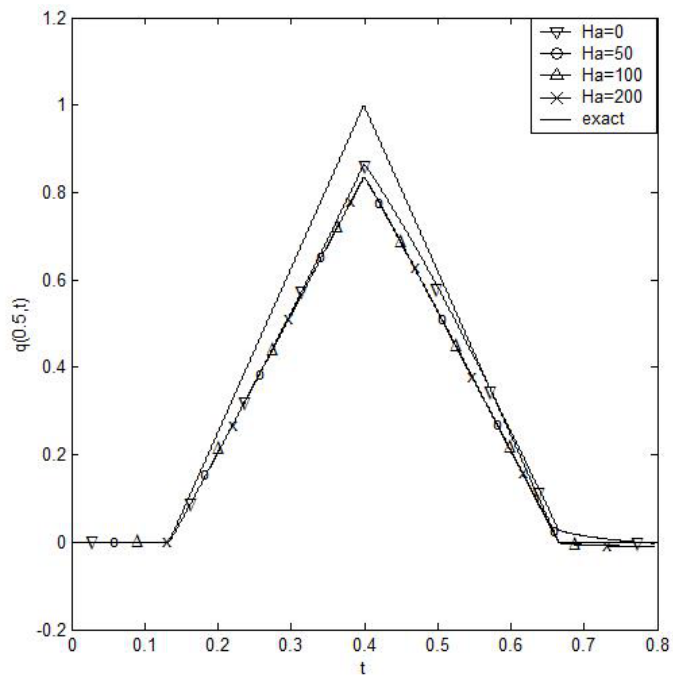


Figure 4.52: Effect of the Hartmann number on the heat flux $q(0.5, t)$ for $Ra = 500$, $K = 84$, $L_2 = 90$, $\lambda = 10^{-6}$, $\rho = 0$ and $\Delta t = \frac{\Delta t_{ref}}{200}$.

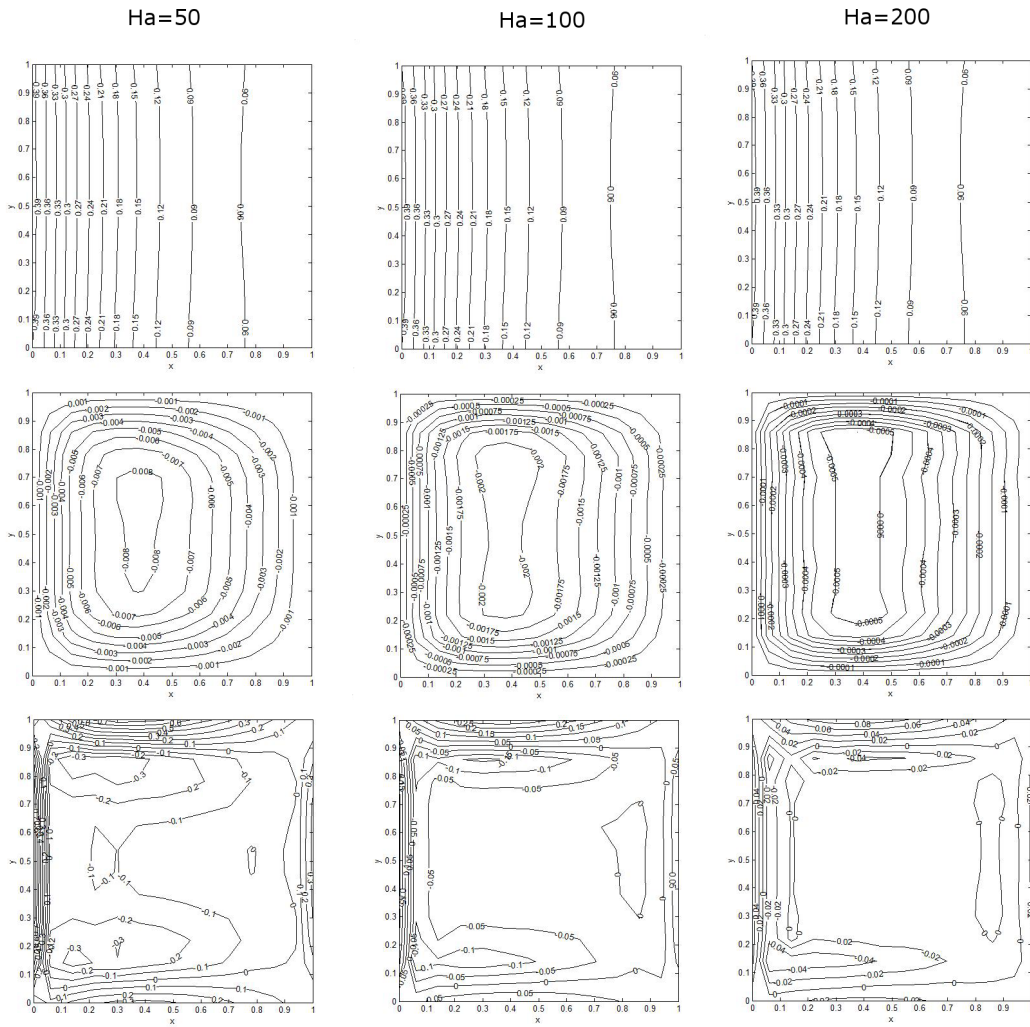


Figure 4.53: Isotherms (top row), streamlines (middle row) and vorticity lines (bottom row) at the time $t = 30\Delta t_{ref}$ for the inverse problem with $Ra = 500$, $\lambda = 10^{-6}$, $\rho = 0$, $\Delta t = \frac{\Delta t_{ref}}{200}$, $K = 84$ and $L_2 = 90$.

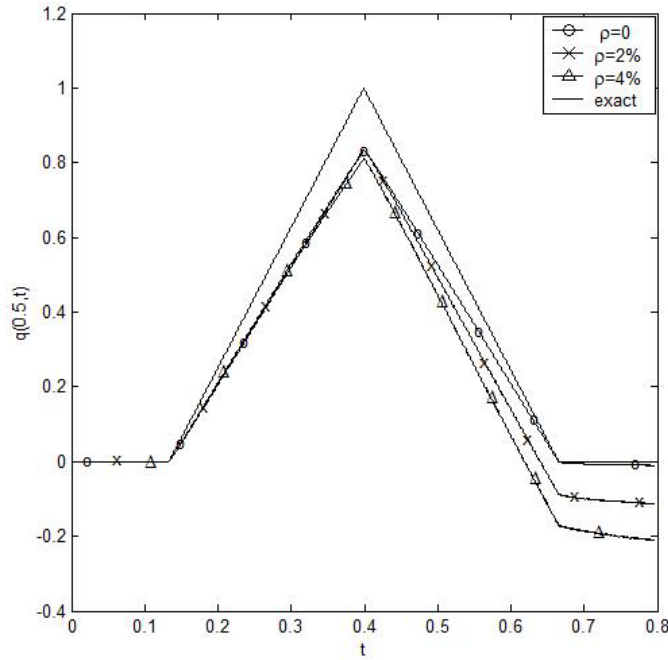


Figure 4.54: Effect of noise on the heat flux $q(0.5, t)$ for $Ra = 500$, $Ha = 100$, $K = 84$, $L_2 = 90$, $\lambda = 10^{-6}$, and $\Delta t = \frac{\Delta t_{ref}}{200}$.

4.5.2.2 Example 2

As a second example, we consider the laminar natural convection flow under a magnetic field in a square cavity (enclosure) with thermal boundary conditions involving an isothermal vertical wall $x = 1$ and adiabatic horizontal walls $y = 0$ and $y = 1$. The wall $x = 0$ may or may not be isothermally heated, see the direct problem numerical simulations of [82] and [71], respectively. On all walls, the no-slip boundary condition on the fluid velocity is imposed. The schematic of the physical problem with the boundary conditions is depicted in Figure 4.55. In this case the boundary conditions (4.135) and (4.136) remain unchanged, but (4.137) and (4.138) change to

$$T(1, y, t) = \frac{\partial T}{\partial y}(x, 0, t) = \frac{\partial T}{\partial y}(x, 1, t) = 0, \quad (4.145)$$

$$T(0, y, t) = \phi(y, t), \quad (4.146)$$

for $x, y \in (0, 1), t > 0$.

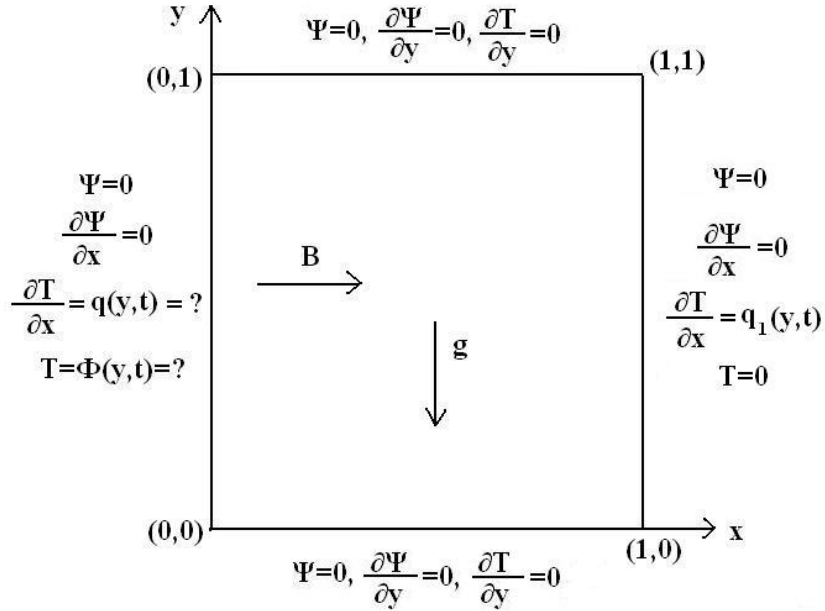


Figure 4.55: Inverse problem for the natural convection flow under a magnetic field with isothermal vertical walls

For a prescribed isothermal boundary temperature $\phi(y, t) \equiv 1$, the direct natural magneto-convection problem in a square enclosure heated and cooled on adjacent walls $x = 0$ and $x = 1$, respectively, given by equations (4.128)-(4.130), (4.135), (4.136), (4.139), (4.145) and (4.146) has recently been investigated at length in Alsoy-Akgün and Tezer-Sezgin [10] where isotherms, streamlines and vorticity lines were illustrated and thoroughly discussed for various $Ra \in \{10^3, 10^4, 10^5, 10^6\}$ and $Ha \in \{50, 100, 200, 300\}$. Therefore, in Figures 4.56 and 4.57 we only present the numerical results for the heat flux at the boundaries $x = 1$ and $x = 0$ which in the inverse analysis will become input data and output desired data, respectively, for strong convection $Ra = 10^5$ and various magnetic fields with $Ha \in \{100, 200, 300\}$.

Next the numerical results of Figure 4.56 given by the heat flux

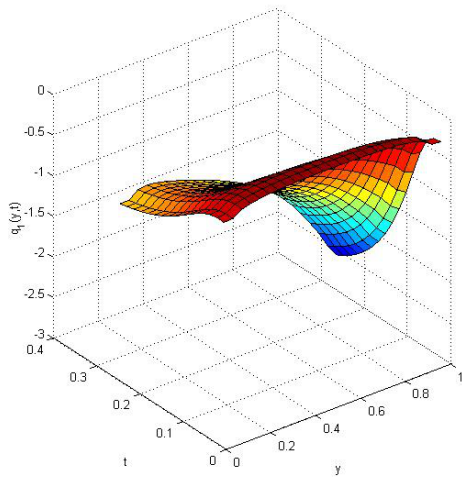
$$\frac{\partial T}{\partial x}(1, y, t) = q_1(y, t), \quad (4.147)$$

perturbed by $\rho = 2\%$ noise as

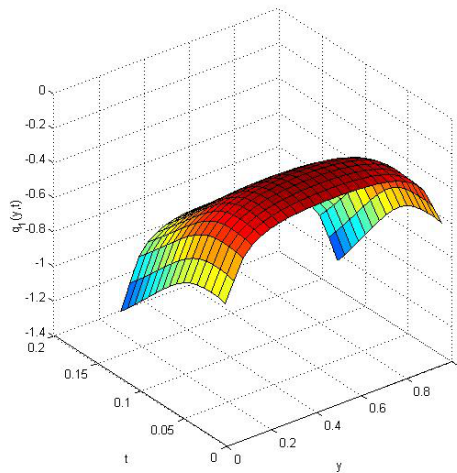
$$q_1^{\text{noise}}(y, t) = q_1^{\text{direct problem}}(1 + \chi\rho), \quad y \in (0, 1), \quad t > 0, \quad (4.148)$$

are used as input in the inverse problem given by equations (4.128)-(4.130), (4.135), (4.136), (4.139), (4.145) and (4.147) where χ is the random variable in $[-1, 1]$. The desired output is represented by the boundary temperature (4.146) with $\phi = 1$ and the heat flux illustrated in Figure 4.57. The numerical retrieved results for $\rho = 2\%$ noise are shown in Figures 4.58 and 4.59. Figure 4.58 shows that the numerically retrieved boundary temperature $T(0, y, t)$ is a good approximation of the exact solution which is equal to unity. Finally, by comparing Fig-

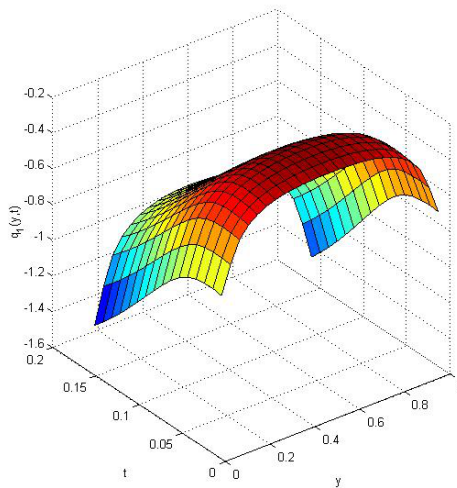
ures 4.57 and 4.59 it can be seen that the numerical results represent a stable and reasonably accurate approximation to the desired direct problem heat flux output.



(a) Ha=100

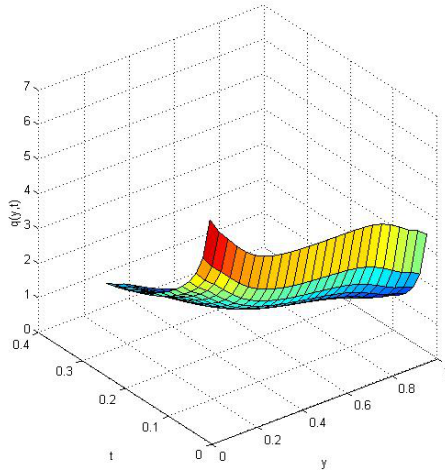


(b) Ha=200

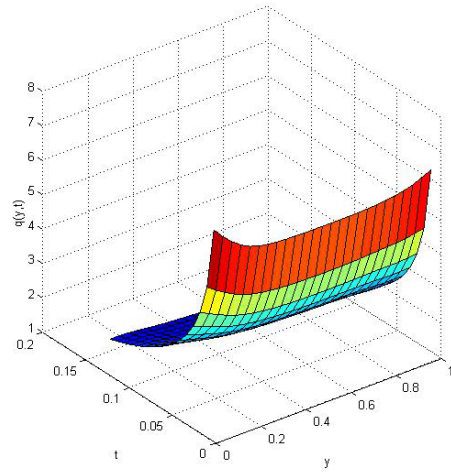


(c) Ha=300

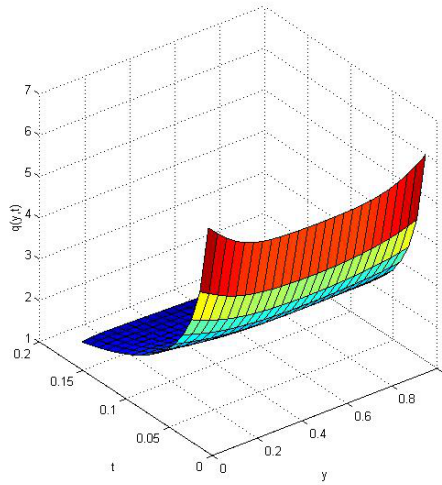
Figure 4.56: The heat flux $q_1(y, t) := \frac{\partial T}{\partial x}(1, y, t)$ at the boundary $x = 1$ for the direct problem with $Ra = 10^5$, $K = 84$, $L_1 = 100$ and $\Delta t \in \{2 \times 10^{-3}, 5 \times 10^{-4}, 3 \times 10^{-4}\}$ for $Ha \in \{100, 200, 300\}$, respectively.



(a) $Ha=100$

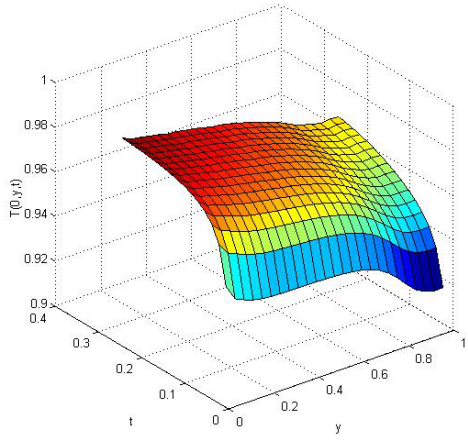


(b) $Ha=200$

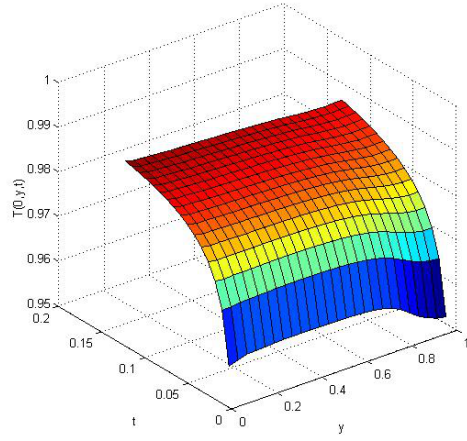


(c) $Ha=300$

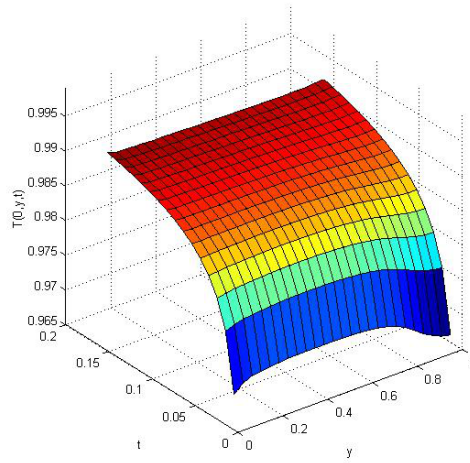
Figure 4.57: The heat flux $q(y, t) := \frac{\partial T}{\partial x}(0, y, t)$ at the boundary $x = 0$ for the direct problem with $Ra = 10^5$, $K = 84$, $L_1 = 100$ and $\Delta t \in \{2 \times 10^{-3}, 5 \times 10^{-4}, 3 \times 10^{-4}\}$ for $Ha \in \{100, 200, 300\}$, respectively.



(a) $Ha=100$

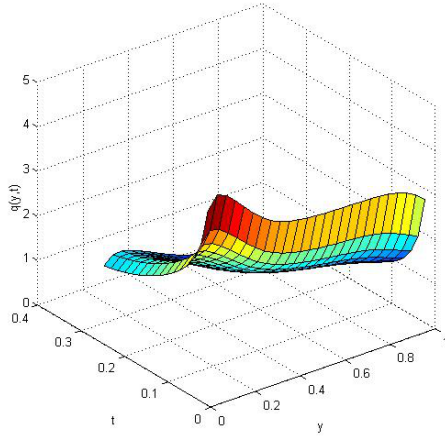


(b) $Ha=200$

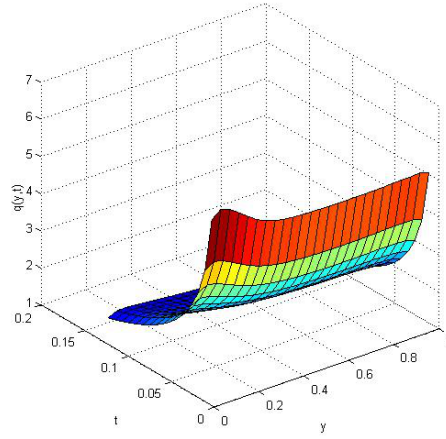


(c) $Ha=300$

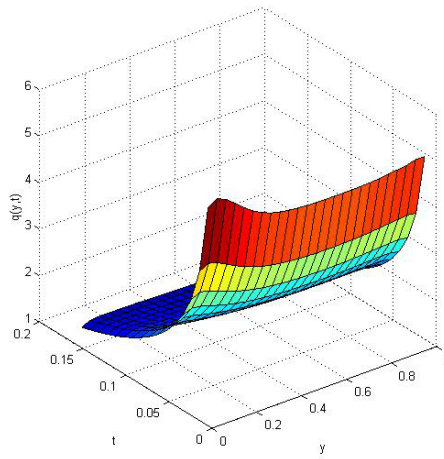
Figure 4.58: The numerically retrieved temperature $T(0, y, t)$ at the boundary $x = 0$ for the inverse problem with $Ra = 10^5$, $K = 84$, $L_2 = 90$, $\lambda = 10^{-6}$, $\rho = 2\%$ and $\Delta t \in \{2 \times 10^{-3}, 5 \times 10^{-4}, 3 \times 10^{-4}\}$ for $Ha \in \{100, 200, 300\}$, respectively.



(a) Ha=100



(b) Ha=200



(c) Ha=300

Figure 4.59: The numerically retrieved temperature $q(y,t)$ at the boundary $x = 0$ for the inverse problem with $Ra = 10^5$, $K = 84$, $L_2 = 90$, $\lambda = 10^{-6}$, $\rho = 2\%$ and $\Delta t \in \{2 \times 10^{-3}, 5 \times 10^{-4}, 3 \times 10^{-4}\}$ for $Ha \in \{100, 200, 300\}$, respectively.

CHAPTER 5

CONCLUSION

This thesis is devoted to the dual reciprocity boundary element solution of inhomogeneous Helmholtz-type equations which are the transformed form of some time-dependent fluid dynamics problems. All the physical problems are considered two-dimensional, laminar, viscous, incompressible and unsteady fluid flow problems. Some of them include temperature and concentration variations, and one includes external magnetic field. The stream function-vorticity formulation of Navier-Stokes equations is basically used in the governing equations. Adding the energy and concentration equations to the Navier-Stokes equations, natural convection and double diffusive mixed convection flows are defined in enclosures, and also the case of applied external magnetic field on natural convection flow is considered.

For the time derivatives, the forward time discretization with a relaxation parameter is inserted at the beginning of the process for obtaining modified Helmholtz equations which eliminates the need of another time integration scheme and the stability problems. The relaxation parameter has an important role in accelerating the convergence of the solution. DRBEM formulations are given for Poisson and inhomogeneous modified Helmholtz equations with their corresponding fundamental solutions. The right hand side functions are approximated by using several coordinate (radial basis) functions. For the case of modified Helmholtz equation, two different coordinate functions are derived which are the thin plate splines and polynomial form, containing the wave number of the modified Helmholtz equation. Corresponding particular solutions of modified Helmholtz equation are derived using annihilator method.

The DRBEM applications are carried out for fluid flow problems with the fundamental solution of Laplace equation for the stream function equation, and with the fundamental solution of modified Helmholtz equation for the vorticity, energy and concentration equations using constant boundary elements. The inhomogeneities are approximated by using coordinate functions $f = 1 + r$ in stream function equation and $\bar{f} = r^2 \ln r$ in the vorticity, temperature and concentration equations. Furthermore, natural convection flow under a magnetic field problem is solved with DRBEM with the coordinate function $\bar{f} = 1 + r^2 + r^3 + \tau^2 \left(\frac{r^2}{4} + \frac{r^4}{16} + \frac{r^5}{25} \right)$ for the vorticity and temperature equations.

The DRBEM applications are given first for the lid-driven flow in a square cavity, and natural convection flow in enclosures. The solutions are obtained for Reynolds number up to 2000, and Rayleigh number values between 10^2 and 10^6 , respectively. The solution procedure needs considerably small number of iterations, and large time increments with suitable values of relaxation parameters which occur in the argument of Bessel function $K_0(x)$. The application of DRBEM using fundamental solution of modified Helmholtz equation is extended then to two-dimensional double diffusive mixed convection flow problem. Three test problems are

solved for different physical domains which are lid-driven cavity, lid-driven cavity with a square blockage at the bottom wall, and horizontal channel with backward-facing step. Computations are carried for several values of Richardson number, buoyancy ratio, and Reynolds number. When the temperature and solutal concentration boundary conditions are changed, the thermal and solutal buoyancy forces can oppose or aid each other. In lid-driven cavity problem, when both Ri and N increase in positive direction, the thermal and solutal buoyancy forces over the fixed inertial force of the fluid become dominant. It is an expected behavior since the walls of the cavity are cooled and are subjected to low concentration, or are heated and are subjected to high concentration. However, in the second problem, at the top lid and square blockage, the opposite boundary conditions are imposed for temperature and concentration. Thus, when the buoyancy ratio is negative, temperature and concentration aid each other while for positive buoyancy ratio they oppose each other. In backward facing step problem, again due to the opposite temperature and solutal concentration boundary conditions assumed on the channel walls, the buoyancy forces aid each other for negative values of N , and oppose each other for positive values of N .

The two-dimensional natural convection flow in a square cavity under an externally applied magnetic field is solved by using DRBEM and DQM. DRBEM is used when forcing terms of vorticity and energy equations are approximated with the coordinate functions $\bar{f} = r^2 \ln r$ or $\bar{f} = 1 + r^2 + r^3 + \tau^2 \left(\frac{r^2}{4} + \frac{r^4}{16} + \frac{r^5}{25} \right)$. DQM is also applied by using nonuniform grid points (Gauss-Chebyshev-Lobatto) which cluster through the end points. In the procedure, together with the stream function equation, obtained modified Helmholtz form of the vorticity and temperature equations are discretized by DQM inserting Dirichlet boundary conditions but discretizing also normal boundary conditions. The solution can be obtained with both DQM and DRBEM for highly large Ra and Ha values up to 10^6 and 300. The use of $K_0(r)$ as fundamental solution in DRBEM application makes possible to use larger time increments. Although DQM is a domain discretization method it gives very accurate results using considerably small number of the mesh points. Also, it is based on interpolation of solution and its derivatives by polynomials, making the construction of the system of ordinary differential equations in time quite simple.

Finally, the DRBEM solution of a two-dimensional transient inverse natural magneto-convection problem is given where it has been done for the first time. Accurate and stable numerical results at various convective Rayleigh and magnetic Hartman numbers are presented obtaining discontinuous time-varying step heat flux in the first problem, and uniform boundary temperature in the second problem. DRBEM interpolation seems to have a stabilizing effect on the inverse problem solution. The presence of natural convection characterized by high Ra affects the accuracy of the numerical solution, but the magnetic field has less influence.

The dual reciprocity boundary element method, when it is applied for solving direct or inverse time-dependent fluid dynamics problems in the form of inhomogeneous modified Helmholtz equations, gives very accurate results since it can extract more information from the governing equations formulated in Poisson equation. As a future study, further investigations could be concentrated on using DRBEM with the differential operator containing Laplace, reaction and convection terms as an extension to modified Helmholtz equation. This requires obtaining fundamental solution and corresponding particular solutions for radial basis functions used in the approximation of the inhomogeneity. Even variable coefficient convection terms should be considered. The physical fluid dynamics problems solved by direct DRBEM in the thesis can be also formulated and solved for the inverse problem formulation.

REFERENCES

- [1] Abramowitz M. and Stegun I.A., *Handbook of Mathematical Functions with Formulas, Graphs, and Mathematical Tables*, Dover Publications, Inc., 1972.
- [2] Abu-Hijleh B. , *Convection Heat Transfer from a Laminar Flow over a 2-D Backward Facing Step with Asymmetric and Orthotropic Porous Floor Segments*, Numerical Heat Transfer, Part A, **31**, 325-335, 1997.
- [3] Abu-Mulaweh H.I., *A Review of Research on Laminar Mixed Convection Flow over Backward- and Forward-facing Steps*, International Journal of Thermal Sciences, **42**, 897-909, 2003.
- [4] Abu-Nada E., Al-Sarkhi A., Akash B. and Al-Hinti I., *Heat Transfer and Fluid Flow Characteristics of Separated Flows Encountered in a Backward-facing Step under the Effect of Suction and Blowing*, Journal of Heat Transfer (ASME), **129**, 1517-1528, 2007.
- [5] Al-Amiri A.M., Khanafer K. M. and Pop I., *Numerical Simulation of Combined Thermal and Mass Transport in a Square Lid-driven Cavity*, International Journal of Thermal Sciences, **46**, 662-671, 2007.
- [6] Alleborn N., Raszillier H. and Durst F., *Lid-driven Cavity with Heat and Mass Transport*, International Journal of Heat and Mass Transfer, **42** 833-853, 1999.
- [7] Al-Najem N.M., Khanafer K.M. and El-Refae M.M., *Numerical Study of Laminar Natural Convection in Tilted Enclosure with Transverse Magnetic Field*, International Journal of Numerical Methods for Heat Fluid Flow, **8**, 651-672, 1998.
- [8] Alsoy-Akçiın N. and Lesnic D., *A Numerical Solution for an Inverse Natural Magneto-Convection Problem*, Numerical Heat Transfer, Part B, **63**, 115-138, 2013.
- [9] Alsoy-Akçiın N. and Tezer-Sezgin M., *DRBEM Solution of Natural Convection and Lid-driven Flow Problems in Cavities*, Proc. of the Eighth UK Conference on Boundary Integral Methods (UKBIM8), Univ. of Leeds, UK, 65-72, July 4-5, 2011.
- [10] Alsoy-Akçiın N. and Tezer-Sezgin M., *DRBEM and DQM Solution of Natural Convection Flow in Cavity Under a Magnetic Field*, Progress in Computational Fluid Dynamics, (in press).
- [11] Alsoy-Akçiın N. and Tezer-Sezgin M., *DRBEM Solution of the Thermo-Solutal Buoyancy Induced Mixed Convection Flow Problems*, Engineering Analysis with Boundary Elements, **37**, 513-526, 2013.
- [12] Alsoy-Akçiın N. and Tezer-Sezgin M., *DRBEM Solution of Double Diffusive Mixed Convection in a Lid-Driven Square Cavity with a Square Blockage Placed at the Bottom Wall*, Proc. of World Congress on Engineering 2012 (WCE 2012), The 2012 Int. Conf. of App. and Eng. Math. (ICAEM), Imperial College London, London, UK, 252-257, 4-6 July, 2012.

- [13] Aydin O., *Aiding and Opposing Mechanisms of Mixed Convection in a Shear- and Buoyancy-driven Cavity*, International Communications in Heat and Mass Transfer, **26**, 1019-1028, 1999.
- [14] Aydin O., Unal A. and Ayhan T., *A Numerical Study on Boyancy-Driven Flow in an Inclined Square Enclosure Heated and Cooled on Adjacent Walls*, Numerical Heat Transfer, Part A, **36**, 585-599, 1999.
- [15] Aydin O., Unal A. and Ayhan T., *Natural Convection in Rectangular Enclosures Heated from One Side and Cooled from the Ceiling*, International Journal of Heat and Mass Transfer, **42**, 2345-2355, 1999.
- [16] Barakos G., Mitsoulis E. and Assimacopoulos D., *Natural Convection Flow in a Square Cavity Revisited: Laminar and Turbulent Models with Wall Functions*, International Journal of Numerical Methods in Fluids, **18**, 695-719, 1994.
- [17] Barletta A., Nobile E., Pinto F., Rossi di Schio E and Zanchini E., *Natural Convection in a 2D-cavity with Vertical Isothermal Walls: Cross-Validation of Two Numerical Solutions*, International Journal of Thermal Science, **45**, 917-922, 2006.
- [18] Beck J.V., Blackwell B., and St. Clair C.R., *Inverse Heat Conduction Ill-Posed Problem*, Wiley, New York, 1985.
- [19] Bejan A., *Heat Transfer*, Wiley, Canada, 1993.
- [20] Bejan A. and Tien C.L., *Laminar Natural Convection Heat Transfer in a Horizontal Cavity with Different End Temperatures*, Journal of Heat Transfer, **100**, 641-647, 1978.
- [21] Bellman R.E. and Casti J., *Differential Quadrature and Long-term Integration*, Journal of Mathematical Analysis and Applications, **34**, 235-238, 1971.
- [22] Brebbia C.A., *The Boundary Element Method for Engineers*, Pentech Press, London, 1978.
- [23] Brebbia C.A. and Dominguez J., *Boundary Elements: An Introductory Course*, Computational Mechanics Publications, McGraw-Hill Book Company, Southampton, New York, 1989.
- [24] Brebbia C.A., Telles J.C.F. and Wrobel L.C., *Boundary Element Techniques*, Springer-Verlag, Berlin and New York, 1984.
- [25] Brown N.M. and Lai F.C., *Correlations for Combined Heat and Mass Transfer from an Open Cavity in a Horizontal Channel*, International Communications in Heat and Mass Transfer, **32**, 1000-1008, 2005.
- [26] Bozkaya C. and Tezer-Sezgin M., *Solution to Transient Navier-Stokes Equations by the Coupling of Differential Quadrature Time Integration Scheme with Dual Reciprocity Boundary Element Method*, International Journal for Numerical Methods in Fluids, **59**, 215-234, 2009.
- [27] Chen W. and Hon Y.C., *Numerical Investigation on Convergence of Boundary Knot Method in the Analysis of Homogeneous Helmholtz, Modified Helmholtz, and Convection-Diffusion Problems*, Computational Methods in Applied Mechanics and Engineering, **192**, 1859-1875, 2003.

- [28] Chen C.S. and Rashed Y.F., *Evaluation of Thin Plate Spline Based Particular Solutions for Helmholtz-type Operators for DRB*, Mechanics Research Communications, **25**, 195-201, 1998.
- [29] Chen S., Tölke J. and Krafczyk M., *A New Method for the Numerical Solution of Vorticity-Stream Function Formulations*, Computational Methods Applied Mechanic Engineering, **198**, 367-376, 2008.
- [30] Chen X.B., Yu P., Winoto S.H. and Low H.T., *Forced Convection over a Backward-Facing Step with a Porous Floor Segment*, Numerical Heat Transfer, Part A, **53**, 1211-1230, 2008.
- [31] Chen W. and Tanaka M., *Solution of Some Heat Conduction Problems by the Dynamic Programming Filter and BEM*, Inverse Problems in Engineering Mechanics III, Elsevier Science, 2000.
- [32] Cheng-Wen Z., Jian-Fei X., Cong-Shan Z., Sheng-Wei X. and Da-Chuan Y., *Simulation of Natural Convection under High Magnetic Field by Means of the Thermal Lattice Boltzmann Method*, Chinese Physics Society and IOP Publishing Limited, **18**, 1674-1056, 2009.
- [33] Choi C.Y. and Balaras E., *A Dual Reciprocity Boundary Element Formulation Using the Fractional Step Method for the Incompressible Navier-stokes Equations*, Engineering Analysis with Boundary Elements, **33**, 741-749, 2009.
- [34] De Vahl Davis G., *Laminar Natural Convection in an Enclosed Rectangular Cavity*, International Journal of Heat and Mass Transfer, **11**, 1675-1693, 1968.
- [35] De Vahl Davis G., *Natural Convection of Air in a Square Cavity: A Benchmark Numerical Solution*, International Journal for Numerical Methods in Fluids, **3**, 249-264, 1983.
- [36] De Vahl Davis G. and Jones I.P., *Natural Convection in a Square Cavity: A Comparison Exercise*, International Journal for Numerical Methods in Fluids, **3**, 227-248, 1983.
- [37] Deng Q.H., Zhou J., Mei C. and Shen Y.M., *Fluid Heat and Contaminant Transport Structures of Laminar Double-diffusive Mixed Convection in a Two-dimensional Ventilated Enclosure*, International Journal of Heat and Mass Transfer, **47**, 5257-5269, 2004.
- [38] Dinh Nho Hao, *Methods for Inverse Heat Conduction Problems*, Peter Lang, Frankfurt, 1998.
- [39] Ece M.C. and Buyuk E., *Natural Convection Flow under a Magnetic Field in an Inclined Rectangular Enclosure Heated and Cooled on Adjacent Walls*, Fluid Dynamics Research, **38**, 564-590, 2006.
- [40] Erturk E., *Discussions on Driven Cavity Flow*, International Journal for Numerical Methods in Fluids, **60**, 275-294, 2009.
- [41] Florez W.F. and Power H., *Comparison Between Continuous and Discontinuous Boundary Elements in Multi-domain Dual Reciprocity Method for the Solution of the Two-dimensional Navier-Stokes Equations*, Engineering Analysis with Boundary Elements, **25**, 57-69, 2001.

- [42] Florez W.F., Power H. and Chejne F., *Multi-domain Dual Reciprocity BEM Approach for the Navier-Stokes System of Equations*, Communications in Numerical Methods in Engineering, **16**, 671-681, 2000.
- [43] Fusegi T. and Hyun J.M., *Laminar and Transitional Natural Convection in an Enclosure with Complex and Realistic Conditions*, International Journal of Heat and Fluid Flow, **15**, 258-268, 1994.
- [44] Ganzarolli M. M. and Milanez L. F., *Natural Convection in Rectangular Enclosures Heated from Below a Symmetrically Cooled from the Sides*, International Journal of Heat and Mass Transfer, **38**, 1063-1073, 1995.
- [45] Ghadimi P. and Dashtimanesh A., *Solution of 2D Navier-Stokes Equation by Coupled Finite Difference-Dual Reciprocity Boundary Element Method*, **35**, 2110-2121, 2011.
- [46] Golberg M.A., Chen C.S. and Rashed Y.F., *The Annihilator Method for Computing Particular Solutions to Partial Differential Equations*, Engineering Analysis with Boundary Elements, **23**, 275-279, 1999.
- [47] Guo K.L. and Wu S.T., *Numerical Study of Flow and Temperature Stratifications in a Liquid Thermal Storage Tank*, Journal of Solar Energy Engineering, **107**, 15-20, 1985.
- [48] Gümğüm S. and Tezer-Sezgin M., *DRBEM Solution of Natural Convection Flow of Nanofluids with a Heat Source*, Engineering Analysis with Boundary Elements, **34**, 727-737, 2010.
- [49] Gümğüm S. and Tezer-Sezgin M., *DRBEM Solution of Natural Convective Flow of Micropolar Fluids*, Numerical Heat Transfer, Part A, **57**, 777-798, 2010.
- [50] Hansen P.C., *Rank-Deficient and Discrete Ill-Posed Problems: Numerical Aspect of Linear Inversion*, SIAM, Philadelphia, 1998.
- [51] Huang C.H. and Ozisik M.N., *Inverse Problem of Determining Unknown Wall Heat Flux in Laminar Flow through a Parallel Plate Duct*, Numerical Heat Transfer, Part A, **21**, 55-70, 1992.
- [52] Incropera F.P. and DeWitt D.P., *Introduction to Heat Transfer*, Wiley, 1996.
- [53] Kimura S. and Bejan A., *Natural Convection in a Differentially Heated Corner Region*, Physics of Fluids, **28**, 2980-2989, 1985.
- [54] Kumar D.S., Murugesan K. and Gupta A., *Numerical Analysis of Interaction Between Inertial and Thermosolutal Buoyancy Forces on Convective Heat Transfer in Lid-driven Cavity*, Journal of Heat Transfer, **132**, 112501/1-112501/11, 2010.
- [55] Kumar D.S., Murugesan K. and Gupta A., *Effect of Thermo-solutal Stratification on Recirculation Flow Patterns in a Backward-facing Step Channel Flow*, International Journal for Numerical Methods in Fluids, **64**, 163-186, 2010.
- [56] Kumar D.S., Murugesan K. and Gupta A., *Thermo-solutal Buoyancy Induced Mixed Convection in a Backward Facing Step Channel Using Velocity-Vorticity Formulation*, Numerical Heat Transfer, Part A, **56**, 604-630, 2009.

- [57] Kumar D.S., Murugesan K. and Thomas H. R., *Numerical Simulation of Double Diffusive Mixed Convection in a Lid-driven Square Cavity Using Velocity-Vorticity Formulation*, Numerical Heat Transfer, Part A, **54**, 837-865, 2008.
- [58] Kumar D.S., Murugesan K. and Thomas H. R., *Effect of Aspect Ratio of a Heated Block on the Interaction Between Inertial and Thermosolutal Buoyancy Forces in a Lid-driven Cavity*, Numerical Heat Transfer, Part A, **60**, 604-628, 2011.
- [59] Lesnic D. and Wake G. C., *A Mollified Method for the Solution of the Cauchy Problem for the Convection-diffusion Equation*, Inverse Problems in Science and Engineering, **15**, 293-302, 2007.
- [60] Lesnic D., *The Decomposition Method for Cauchy Advection-diffusion Problems*, Computers & Mathematics with Applications, **49**, 525-537, 2005.
- [61] Li Z. R., Prud'homme M. and Nguyen T. H., *A Numerical Solution for the Inverse Natural-convection Problem*, Numerical Heat Transfer, Part B, **28**, 307-321, 1995.
- [62] Lo D. C., Young D. L. and Tsai C. C., *High Resolution of 2D Natural Convection in a Cavity by the DQ Method*, Journal of Computational and Applied Mathematics, **203**, 219-236, 2007.
- [63] Luke Y.L., *Integrals of Bessel Functions*, McGraw-Hill, 1962.
- [64] Maiti D.K., Gupta A.S. and Bhattacharyya S., *Stable/Unstable Stratification in Thermosolutal Convection in a Square Cavity*, Journal of Heat Transfer, **130**, 122001/1-122001/10, 2008.
- [65] Marin L., Elliott L., Heggs P.J., Ingham D.B., Lesnic D., and Wen X., *Dual Reciprocity Boundary Element Method Solution of the Cauchy Problem for Helmholtz-type Equations with Variable Coefficients*, Journal of Sound and Vibration, **297**, 89-105, 2006.
- [66] Moshkin N.P., *Numerical Model to Study Natural Convection in a Rectangular Enclosure Filled with Two Immiscible Fluids*, International Journal of Heat and Fluid Flow, **23**, 373-379, 2002.
- [67] Moutsoglou A., *An Inverse Convection Problem*, ASME Journal of Heat Transfer, **111**, 37-43, 1989.
- [68] Muleshkov A.S., Golberg M.A. and Chen C.S., *Particular Solution of Helmholtz-type Operators using Higher Order Polyharmonic Splines*, Computational Mechanics, **23**, 411-419, 1999.
- [69] Nardini D. and Brebbia C.A., *A New Approach to Free Vibration Analysis Using Boundary Elements*, Applied Mathematical Modelling, **7**, 157-162, 1983.
- [70] November M. and Nansteel M.W., *Natural Convection in Rectangular Enclosures Heated from Below and Cooled along One Side*, International Journal of Heat and Mass Transfer, **30**, 2433-2440, 1987.
- [71] Oztop H.F., Oztop M. and Varol Y., *Numerical Simulation of Magnetohydrodynamic Buoyancy-induced Flow in a Non-isothermally Heated Square Enclosure*, Communications in Nonlinear Science and Numerical Simulation, **14**, 770-778, 2009.

- [72] Partridge P.W. and Brebbia C.A., *Computer Implementation of the BEM Dual Reciprocity Method for the Solution of General Field Equations*, Communications in Applied Numerical Methods, **6**, 83-92, 1990.
- [73] Partridge P.W., Brebbia C.A. and Wrobel L.C., *The Dual Reciprocity Boundary Element Method*, Computational Mechanics Publications, Southampton Boston, 1992.
- [74] Partridge P.W. and Wrobel L.C., *The Dual Reciprocity Boundary Element Method for Spontaneous Ignition*, International Journal for Numerical Methods in Engineering, **30**, 953-963, 1990.
- [75] Partridge P.W. and Sensale B., *The Method of Fundamental Solutions with Dual Reciprocity Boundary Element Method for Diffusion and Convection-diffusion using Subdomains*, Engineering Analysis with Boundary Elements, **24**, 633-641, 2000.
- [76] Philips D.L., *A Technique for the Numerical Solution of Certain Integral Equations of the First Kind*, Journal of the Association of Computational Machinery, **9**, 84-97, 1962.
- [77] Power H. and Mingo R., *The DRM Subdomain Decomposition Approach to Solve the Two-dimensional Navier-Stokes System of Equation*, Engineering Analysis with Boundary Elements, **24**, 107-119, 2000.
- [78] Ramm A.G., *Inverse Problems, Mathematical and Analytical Techniques with Applications to Engineering*, Springer, 2005.
- [79] Ramsak M. and Skerget L., *Mixed Boundary Elements for Laminar Flows*, International Journal for Numerical Methods in Fluids, **31**, 861-877, 1999.
- [80] Ranjbar Z. and Elden L., *Numerical Analysis of an Ill-posed Cauchy Problem for a Convection-diffusion*, Inverse Problems in Science and Engineering, **15**, 191-211, 2007.
- [81] Rap A., Elliott L., Ingham D. B., Lesnic D., and Wen X., *DRBEM for Cauchy Convection-Diffusion Problems with Variable Coefficients*, Engineering Analysis with Boundary Elements, **28**, 1321-1333, 2004.
- [82] Rudraiah N., Barron R. M., Venkatachalappa M. and Subbaraya C.K., *Effect of a Magnetic Field on Free Convection in a Rectangular Enclosure*, International Journal of Engineering Science, **33**, 1075-1084, 1995.
- [83] Sahin M. and Owens R.G., *A Novel Fully Implicit Finite Volume Method Applied to the Lid-driven Cavity Problem-Part I: High Reynolds Number Flow Calculations*, International Journal for Numerical Methods in Fluids, **42**, 57-77, 2003.
- [84] Sarler B. and Kuhn G., *Primitive Variable Dual Reciprocity Boundary Element Method Solution of Incompressible Navier-Stokes Equations*, Engineering Analysis with Boundary Elements, **23**, 443-455, 1999.
- [85] Sarler B., Perko J., Gobin D., Goyeau B., and Power H., *Dual Reciprocity Boundary Element Method Solution of Natural Convection in Darcy-Brinkman Porous Media*, Engineering Analysis with Boundary Elements, **28**, 23-41, 2004.
- [86] Skerget L., Hribersek M. and Kuhn G., *Computational Fluid Dynamics by Boundary-domain Integral Method*, International Journal for Numerical Methods in Engineering, **46**, 1291-1311, 1999.

- [87] Sheikhzadeh G.A., Babaei M.R., Rahmany V. and Mehrabian M.A., *The Effect of an Imposed Magnetic Field on Natural Convection in Tilted Cavity with Partially Active Vertical Walls*, International Journal of Engineering Transactions A: Basics, **23**, 65-78, 2010.
- [88] Shu C., *Differential Quadrature and Its Application in Engineering*, Springer-Verlag, London, 2000.
- [89] Teamah M. A., Dawood M.M.K. and Elfeky K., *Numerical Simulation for Double Diffusive Mixed Convection with Aiding and Opposing Flow in Vertical Tubes*, European Journal of Scientific Research, **60**, 396-414, 2011.
- [90] Thompson M.C., *An Adaptive Multigrid Technique for the Incompressible Navier-Stokes Equations*, Journal of Computational Physics, **82**, 94-121, 1989.
- [91] Tanaka M. and Singh K. M., *Application of DRBEM and Iterative Regularization to Inverse Heat Conduction*, Inverse Problems in Engineering Mechanics II, Elsevier Science, 2000.
- [92] Tezer-Sezgin M., *Boundary Element Method Solution of MHD Flow in a Rectangular Duct*, International Journal For Numerical Methods in Fluids, **18**, 937-952, 1994.
- [93] Tikhonov A.N. and Arsenin V.Y., *Solution of Ill-Posed Problems*, Winstonedsons, Washington, 1977.
- [94] Velazquez A., Arias J.R. and Mendez B., *Laminar Heat Transfer Enhancement Downstream of a Backward Facing Step by Using a Pulsating Flow*, International Journal of Heat and Mass Transfer, **51**, 2075-2089, 2008.
- [95] Volgin V.M., Volgina O.V., Bograchev D.A. and Davydov A.D., *Simulation of Ion Transfer under Conditions of Natural Convection by the Finite Difference Method*, Journal of Electroanalytical Chemistry, **546**, 15-22, 2003.
- [96] White F.M., *Viscous Fluid Flow*, McGraw-Hill, 2006.
- [97] Wong J.C.F. and Chan M.K.H., *A Consistent Splitting Scheme for Unsteady Incompressible Viscous Flows I. Dirichlet Boundary Condition and Applications*, International Journal for Numerical Methods in Fluids, **51**, 385-424, 2006.
- [98] Wu J.S. and Shao Y.L., *Simulation of Lid-driven Cavity Flows by Parallel Lattice Boltzmann Method Using Multi-relaxation-time Scheme*, International Journal for Numerical Methods in Fluids, **46**, 921-937, 2004.
- [99] Yun-Xin Z. and Yong-Ji T., *Meshless Schemes for Unsteady Navier-Stokes Equations in Vorticity Formulation Using Radial Basis Functions*, Journal of Computational and Applied Mathematics, **192**, 328-338, 2006.
- [100] Zheng R., Coleman C. J. and Phan-Thein N., *A Boundary Element Approach for Non-homogeneous Potential Problems*, Computational Mechanics, **7**, 279-288, 1974.

CURRICULUM VITAE

PERSONAL INFORMATION

Surname, Name : Alsoy-Akgün, Nagehan
Nationality : Turkish (T. C.)
Date and Place of Birth : 29 March 1981, Samsun
Marital Status : Married
email : nalsoy@metu.edu.tr

EDUCATION

Degree	Institution	Year of Graduation
MS	Eskişehir Osmangazi University, Mathematics Education	2004
BS	Eskişehir Osmangazi University, Mathematics	2003
High School	Samsun Tülay Başaran Anatolian High School	1998

FOREIGN INSTITUTE EXPERIENCE

Institution	Year
University of Leeds Faculty of Mathematics and Physical Sciences , UK	2012

AWARDS

- **The Scientific and Technical Research Council of Turkey (TUBITAK)**
 - The Integrated Ph.D. Scholarship, 2008-2010
- Certificate of Merit (Student) for The 2012 International Conference of Applied and Engineering Mathematics (ICAEM).

WORK EXPERIENCE

Year	Place	Enrollment
2005-present	METU, Mathematics Department	Research Assistant

NUMERICAL METHODS

- Boundary Element Method (BEM)
- Dual Boundary Element Method (DRBEM)
- Differential Quadrature Method (DQM)
- Finite Element Method (FEM)
- Finite Difference Method (FDM)

PROGRAMING LANGUAGES

Fortran, Matlab

FOREIGN LANGUAGES

English (fluent)

PUBLICATIONS

1. N. Alsoy-Akgün, M. Tezer-Sezgin, “DRBEM and DQM Solutions of Natural Convection Flow in a Cavity Under a Magnetic Field” in *Progress in Computational Fluid Dynamics*, in press.
2. N. Alsoy-Akgün, M. Tezer-Sezgin, “DRBEM Solution of the Thermo-Solutal Buoyancy Induced Mixed Convection Flow Problems” in *Engineering Analysis with Boundary Elements*, vol.37, pp.513-526, 2013.
3. N. Alsoy-Akgün, D. Lesnic, “A Numerical Solution for an Inverse Natural Magneto-Convection Problem” in *Numerical Heat Transfer, Part B*, vol.63, pp.115-138, 2013.

CONFERENCE PAPERS

1. N. Alsoy-Akgün, M. Tezer-Sezgin, *DRBEM Solution of Natural Convection and Lid-Driven Flow Problems in Cavities*, Proc. of the Eighth UK Conference on Boundary Integral Methods (UKBIM8), Univ. of Leeds, UK, 4-5 July, 2011, p:65-72.
2. N. Alsoy-Akgün, M. Tezer-Sezgin, *DRBEM Solution of Double Diffusive Mixed Convection in a Lid-Driven Square Cavity with a Square Blockage Placed at the Bottom Wall*, Proc. of World Congress on Engineering 2012 (WCE 2012), The 2012 Int. Conf. of App. and Eng. Math. (ICAEM), Imperial Collage London, London, UK, 4-6 July, 2012, p:252-257.

CONFERENCE PRESENTATION

1. N. Alsoy-Akgün, M. Tezer-Sezgin, *DRBEM and DQM Solutions of Natural Convection Flow in a Cavity Under a Magnetic Field*, 24th Biennial Conf. on Numerical Analy. (NACONF 2011), Glasgow, Scotland, UK, 28 June-1 July, 2011.

2. N. Alsoy-Akgün, M. Tezer-Sezgin, *Differential Quadrature Solution of 2D Natural Convection in a Cavity Under a Magnetic Field*, Inter. School on MHD and Fusion Applic. (ISMFA 2011), Marmaris, Turunç, Turkey, 9-16 September, 2011.
3. N. Alsoy-Akgün, M. Tezer-Sezgin, *Dual Reciprocity Boundary Element Solution of Mixed Convective Heat and Solutal Transport*, 3rd European Seminar on Computing (ESCO 2012), Pilsen, Czech Republic, 25-29 June, 2012, p:26.

PARTICIPATION OF NATIONAL CONFERENCES

1. EM2010, Study Group with Industry, Karadeniz Technical University, Oct. 2010, Trabzon, Turkey.
2. N. Alsoy-Akgün, M. Tezer-Sezgin, *DRBEM Solution of the Thermo-Solutal Buoyancy Induced Mixed Convection Flow Problem*, Workshop on Finite and Boundary Element Methods, IAM, 25 May, 2012.